

وزارة التعليم العالي و البحث العلمي

BADJI MOKHTAR UNIVERSITY- ANNABA

UNIVERSITE BADJI MOKHTAR - ANNABA



جامعة باجي مختار - عنابة

FACULTE DE TECHNOLOGIE

DEPARTEMENT DE GENIE CIVIL

Année : 2022

## THESE

Présentée en vue de l'obtention du diplôme de DOCTORAT en Génie Civil

Thème

Strengthening steel beams with web openings using fiber reinforced polymer

Par

GUEDAOURA Hamda

Directeur de Thèse:

Mr. HADIDANE Yazid

MCA

Université de Badji Mokhtar, Annaba

Devant le jury:

Président:

Mr. OUCIEF Hocine

Pr.

Univ. BADJI Mokhtar ANNABA

Examineurs:

Mr. NAFAA Zahreddine

Pr.

Univ. GUELMA

Mme KOUIDER Nadia

Dr.

Univ. BADJI Mokhtar ANNABA

## ACKNOWLEDGEMENTS

Firstly, I would like to thank Allah for granting me the perseverance, and time to finish this work.

I want to personally thank my supervisor, **Dr. Hadidane Yazid**, for his professional oversight, guidance, encouragement, and insightful assistance throughout all stages of the study effort.

I would also want to extend my sincere appreciation to **my parents**, and **my wife** for their tolerance, motivation, and unending support.

Last but not least, I want to express my gratitude to my friends for supporting me and trusting in me, particularly Dr. Mohammad Jassem Altaee, Dr. Benzerara Mohammed, and Dr. Kouider Nadia.

## ABSTARCT

In modern building development a smart home is a practical house setup where machines and equipment can be controlled remotely from any place using a smartphone or other network resource. The installation of instrument cabling and connections through web openings in steel beams is preferred by architectural and civil engineers for superior aesthetics and for a variety of other advantages. These web-openings can massively increase a condition of instability and decrease the beams' capacities for shear and bending performance. Steel plates are frequently welded onto the area near the apertures to strengthen and stiffen the beams. While in addition to handling difficulties, this also leads to residual stresses that reduce the section's resistance to fatigue. The purpose of this study is to investigate if externally bonded fiber reinforced polymer FRP composites can be used as an alternative method of strengthening for steel beams with web opening and to suggest a new method of reinforcement to gather more details about the use of FRP laminates to stiffen this category of steel beams and progress to a stage where regulations and codes can be created assisting experts in the application and design of such approach .

**Key words :** Strengthening , fiber reinforced polymer ,Web openings , Finite Element Modelling , Bond behavior .

## RESUME

Dans le développement de bâtiments modernes, une maison intelligente est une configuration de maison pratique où les machines et les équipements peuvent être contrôlés à distance depuis n'importe quel endroit à l'aide d'un smartphone ou d'une autre ressource réseau. L'installation de câblage d'instruments et de connexions à travers des ouvertures d'âme dans des poutres en acier est préférée par les ingénieurs architectes et civils pour une esthétique supérieure et pour une variété d'autres avantages. Ces ouvertures d'âme peuvent augmenter massivement une condition d'instabilité et diminuer les capacités des poutres en cisaillement et en flexion. Des plaques d'acier sont souvent soudées sur la zone proche des ouvertures pour renforcer et rigidifier les poutres. Outre les difficultés de manutention, cela entraîne également des contraintes résiduelles qui réduisent la résistance à la fatigue de la section. Le but de cette étude est d'étudier si les composites PRF (polymères renforcés de fibres) peuvent être utilisés comme méthode alternative de renforcement pour les poutres en acier avec une ouverture d'âme et de suggérer une nouvelle méthode de renforcement pour recueillir plus de détails sur l'utilisation des stratifiés FRP pour renforcer cette catégorie de poutres en acier et passer à un stade où des réglementations et des codes peuvent être créés en aidant les experts dans l'application et la conception d'une telle approche.

**Mots clef :** Renforcement, polymère renforcé de fibres, Ouverture d'âme, modélisation élément finis, comportement de liaison.



## ملخص

في تطوير المباني الحديثة، يعد المنزل الذكي إعدادًا عمليًا للمنزل حيث يمكن التحكم في الآلات والمعدات عن بُعد من أي مكان باستخدام هاتف ذكي أو مصدر شبكة آخر. يفضل المهندسين المعماريين والمدنيين تركيب كابلات الأجهزة والوصلات من خلال فتحات الويب في العوارض الفولاذية للحصول على جماليات فائقة ولمجموعة متنوعة من المزايا الأخرى. يمكن أن تؤدي فتحات الويب هذه إلى زيادة حالة عدم الاستقرار بشكل كبير وتقليل قدرات العارضة لأداء القص والانحناء. كثيرًا ما يتم لحام الألواح الفولاذية في المنطقة القريبة من الفتحات لتقوية وتدعيم هذه الروافد. بالإضافة إلى صعوبة التعامل، يؤدي هذا أيضًا إلى ضغوط متبقية تقلل من المقاومة للإرهاق. الغرض من هذه الدراسة هو التحقق إذا ما كان يمكن استخدام مركبات FRP المصنوعة من البوليمر المقوى بالألياف المترابطة كطريقة بديلة لتقوية الروافد الفولاذية مع فتح الويب واقتراح طريقة جديدة للتدعيم لجمع المزيد من التفاصيل حول استخدام شرائح FRP من أجل تشديد هذه الفئة من الكمرات الفولاذية والتقدم إلى مرحلة يمكن فيها إنشاء الاكواد والقوانين الهندسية لمساعدة الخبراء في تطبيق وتصميم مثل هذا النهج.

**الكلمات المفتاحية: التدعيم، البوليمر المقوى بالألياف، فتحات العصب، نموذج FE ، أداء الرابطة.**

# TABLE OF CONTENTS

<b>TABLE OF CONTENTS .....</b>	<b>VI</b>
<b>LIST OF TABLES.....</b>	<b>X</b>
<b>LIST OF FIGURES.....</b>	<b>XI</b>
<b>NOTATIONS.....</b>	<b>XVI</b>
<b>GENERAL INTRODUCTION.....</b>	<b>01</b>

## **Chapter I: Literature**

<b>I.1. Steel beams with web openings.....</b>	<b>01</b>
<b>I.2.Manufacturing process of steel beams with web openings .....</b>	<b>01</b>
<b>I.3.Prior design recommendations.....</b>	<b>03</b>
<b>I.4.Cellular beams.....</b>	<b>04</b>
I.4.1.Solid webbed beams and cellular beams comparison.....	04
I.4.2.Comparison of cellular and castellated beams.....	04
I.4.3.Potential failure scenarios for steel beams with multiple web openings.....	05
I.4.3.1.Pure bending.....	05
I.4.3.2.Vierndeel mechanism.....	05
I.4.3.3.Weld joints rupture.....	06
I.4.3.4.Lateral torsional buckling .....	06
I.4.3.5.Web post-buckling.....	07
I.4.3.6.Local failures under compression.....	08
I.4.4.Previous research for cellular and castellated beams.....	08
<b>I.5. Steel beams with single web openings.....</b>	<b>10</b>
I.5.1.Potential failure mode for steel beams with single web openings.....	10
I.5.1.1.Vierndeel failure.....	10
I.5.1.2.Flexural failure.....	11
I.5.2..Previous research for steel beams with single web opening.....	11
<b>I.6. Steel structure strengthening and FRP Material .....</b>	<b>13</b>
<b>I.7.The primary processes in rehabilitating existing steel buildings.....</b>	<b>14</b>
<b>I.8.Initial examination.....</b>	<b>14</b>
<b>I.9.Evaluating present circumstances and reinforcement methods.....</b>	<b>14</b>
I.9.1.Techniques of strengthening.....	15
I.9.2.Estimating the loading capacity of existing structures.....	15
I.9.3.Connections capacity improvement.....	16
I.9.4. Flexural strength enhancement of floor framing elements.....	16
I.9.5.Columns' axial load capability improvement .....	16
I.9.6.Handling Weldability Problems.....	16
I.9.7.Adding a novel frame to an existing frame.....	17

I.9.8.Strengthening web openings of steel beams.....	17
I.9.8.1.Existing methods for strengthening the web opening.....	17
I.9.8.1.1.The Hicks and Lawson strategy.....	17
I.9.8.1.2.The Darwin method .....	17
I.9.8.2.Previous studies on strengthening steel beams with web openings using welded steel stiffeners .....	17
<b>I. Fiber reinforced polymer .....</b>	<b>19</b>
I.10.1.Carbon and Glass Fibers.....	21
I.10.2.FRP-strengthening of metallic structures.....	22
I.10.3.Previous studies on FRP strengthening of steel bridges and structures beams.....	22
I. 10.3.1.FRP Strengthening of Bridges’ Girders.....	22
I.10.3.2.FRP Previous studies on strengthening solid steel structures.....	23
I.10.3.3.FRP Previous studies on FRP strengthening of steel beams with web openings .....	26
<b>I.11. Behavior of FRP and steel bonds.....</b>	<b>33</b>
<b>I.12.Bond failure.....</b>	<b>33</b>
<b>I.13.Bond performance.....</b>	<b>35</b>
I.13.1.Strength of the bond.....	36
I.13.2.Bond-slip concept.....	38
<b>I.14.Theoretical model for FRP—Steel glued joints.....</b>	<b>39</b>
I.14.1.Interfacial fracture energy.....	39
<b>I.15.FRP-to-Steel bonded interface bond-slip models.....</b>	<b>40</b>
I.15.1.Linear Adhesives.....	40
I.15.2.Non Linear Adhesives.....	41
<b>I.16.Performance of FRP-Steel glued junctions over the entire set.....</b>	<b>42</b>
I.16.1.Linear Glues: An Analytical Approach.....	44
I.16.2.Nonlinear Glues: An Analytical solution.....	44
<b>I.17.The formula of bond strength.....</b>	<b>45</b>

## **Chapter II : Description of finite element model and validation .**

<b>II.1.Material modeling.....</b>	<b>47</b>
II.1.1. Steel modeling.....	47
II.1.2. FRP modeling.....	48
II.1.2.1. Composite material behavior.....	48
II.1.2.1.1 Elastic behavior.....	48
II.1.2.1.2.FRP failure behavior.....	48
II.1.2.1.3.FRP failure criteria.....	49
<b>II.1.3.Adhesive modeling.....</b>	<b>50</b>
II.1.3.1. Cohesive surfaces process.....	50
II.1.3.2. Cohesive element process.....	51
II.1.3.3.Adhesive damage modeling.....	51
II.1.3.3.1.Damage initiation.....	52
II.1.3.3.2.Damage evolution.....	53

<b>II.2.Solver type.....</b>	<b>53</b>
<b>II.3. Finite element model validation.....</b>	<b>55</b>
II.3.1. Experimental test conducted by Okeil and al.....	56
II.3.1.1. Numerical model.....	57
II.3.1.2. Results and discussion.....	58
II.3.2. Experimental Test conducted by Lucas and al.....;	59
II.3.2.1. Numerical model.....	61
II.3.2.2. Results and discussion .....	62
II.3.3. Experimental Test conducted by M .Altaee and al.....	66
II.3.3.1.Numerical model.....	70
II.3.3.2. Results and discussion .....	71

## **Chapter III : Strengthening web post buckling of cellular beams using FRP .**

<b>III.1.Preliminary investigation of web post buckling strengthening using CFRP.....</b>	<b>77</b>
III.1.1.Results and Discussions.....	79
III.1.1.1.CFRP plate strengthening.....	79
III.1.1.2.CFRP Pultruded T section strengthening.....	86
<b>III.2.Strengthening web post buckling if cellular beams using pultruded carbon profiles.....</b>	<b>88</b>
III.2.1.Results and discussion.....	90
III.2.1.1.T section strengthening.....	90
III.2.1.2.U section strengthening.....	96
<b>III.2.2.How the FRP process strengthening of cellular beam web posts works.....</b>	<b>99</b>
<b>III.3.Strengthening web post buckling of cellular beams using GFRP .....</b>	<b>100</b>
III.3.1.Results and Discussions.....	101
III.3.1.1.Pultruded GFRP T section strengthening.....	101
III.3.1.2.Pultruded GFRP U section strengthening.....	107
III.3.1.3.Pultruded GFRP Angle section strengthening.....	108
<b>III.3.2. Process of GFRP stiffener breakdown at the adhesive interface.....</b>	<b>111</b>
<b>III.3.3.Effect of different GFRP profile dimensions on bond behavior and strength enhancement.....</b>	<b>113</b>
III.3.3.1.Results and discussion.....	115
III.3.3.2.Validation of results on other GFRP profile shape.....	117
<b>III.4.Summary .....</b>	<b>117</b>

## **Chapter IV: Strengthening steel beams with single web openings using FRP**

<b>IV.1.Strengthening steel beams with single rectangular web openings using NM CFRP.....</b>	<b>119</b>
IV.1.1.Model description and material properties.....	119

IV.1.2.Results and discussion .....	121
IV.1.2.1.Mid span opening position.....	121
IV.1.2.1.1.Strength enhancement and failure mode comparison.....	121
IV.1.2.1.2.Bond behavior.....	122
IV.1.2.1.3.CFRP plate strain dispersion.....	124
IV.1.2.1.4.The optimum NM CFRP plate thickness in mid span.....	126
IV.1.2.2.Shear zone opening position.....	128
IV.2.2.1.Strength enhancement and failure mode comparison.....	128
IV.2.2.2.Bond behavior.....	129
IV.2.2.3.CFRP plate strain dispersion.....	130
IV.2.2.4.The optimum NM CFRP plate thickness in shear zone.....	131
<b>IV.2.Strengthening steel beams with single rectangular web opening using GFRP.....</b>	<b>134</b>
IV.2.1.Results and discussion.....	136
IV.2.1.1Mid span position results.....	136
IV.2.1.1.1.GFRP laminates of 3mm thicknesses.....	136
IV.2.1.1.2.GFRP laminates of 6mm thicknesses.....	139
IV.2.1.1.3.GFRP laminates of 10 mm thicknesses.....	141
IV.2.1.2.Shear zone position results.....	144
IV.2.1.2.1.GFRP laminates of 3mm thicknesses.....	144
IV.2.1.2.2.GFRP laminates of 6mm thicknesses.....	144
IV.2.1.2.3.GFRP laminates of 10 mm thicknesses.....	148
<b>IV.2.2.Summary.....</b>	<b>150</b>
<b>IV.3.Strengthening steel beam with different web opening shapes and dimensions using GFRP.....</b>	<b>151</b>
IV.3.1.Case study.....	151
IV.3.1.1.Boundary conditions, material modelling and meshing.....	154
IV.3.2.Results and discussion.....	155
IV.3.2.1.Mid span position .....	155
IV.3.2.1.1.Effect of web opening shape and size on steel beam performance and capacity.....	155
IV.3.2.1.2.Force mid-span deflection reaction.....	159
IV.3.2.1.3.Adhesive degradation and failure mechanism.....	171
IV.3.1.2.Shear zone position.....	178
IV.3.1.2.1.Effect of web opening shape and size on steel beam performance and capacity.....	178
IV.3.1.2.2.Forcemidspandeflectionreaction.....	184
IV.3.1.2.2.Adhesivedegradationandfailure mechanism.....	194
IV.3.3.Summary.....	201

## General Conclusion

## LIST OF TABLES

<b>Table 1-1</b> : Details about the two studies carried out by M Altaee and Al khfaji.....	<b>29</b>
<b>Table 1-2</b> : Details about the two studies carried out by Hamood and S Mustafa.....	<b>30</b>
<b>Table 1-3</b> : Details about the two studies carried out by M Altaee and S Mustafa.....	<b>31</b>
<b>Table 1-4</b> : Details about the two studies carried out by Ezzat and M Khadim.....	<b>32</b>
<b>Table 2-1</b> : Pultruded GFRP T section Mechanical properties.....	<b>57</b>
<b>Table 2-2</b> : Epoxy mechanical properties.....	<b>57</b>
<b>Table 2-3</b> : Specimens dimensions and mechanical properties.....	<b>59</b>
<b>Table 2-4</b> : Experimental and finite element ultimate load .....	<b>62</b>
<b>Table 2-5</b> : Adhesive mechanical properties.....	<b>68</b>
<b>Table 2-6</b> : Carbon FRP mechanical properties.....	<b>69</b>
<b>Table 3-1</b> : CFRP mechanical properties.....	<b>77</b>
<b>Table 3-2</b> : Adhesive mechanical properties.....	<b>77</b>
<b>Table 3-3</b> : The three proposed strengthening configuration.....	<b>77</b>
<b>Table 3-4</b> : Results of all strengthened cellular beams using CFRP plate.....	<b>83</b>
<b>Table 3-5</b> : Results of all strengthened cellular beams with pultruded T section.....	<b>84</b>
<b>Table 3-6</b> : Pultruded carbon T section and U section profiles dimensions.....	<b>87</b>
<b>Table 3-7</b> : CFRP mechanical properties.....	<b>88</b>
<b>Table 3-8</b> : T section strengthening ultimate load enhancement.....	<b>92</b>
<b>Table 3-9</b> : T section strengthening bond behavior and failure mode.....	<b>93</b>
<b>Table 3-10</b> : U section strengthening ultimate load enhancement.....	<b>97</b>
<b>Table 3-11</b> : U section strengthening bond behavior and failure mode.....	<b>98</b>
<b>Table 3-12</b> : GFRP mechanical properties.....	<b>100</b>
<b>Table 3-13</b> : Mechanical properties of adhesives: Adhesive 1 -Adhesive 2.....	<b>100</b>
<b>Table 3-14</b> : Results of all strengthened steel beams using T GFRP section.....	<b>103</b>
<b>Table 3-15</b> : Results of all strengthened steel beams using U GFRP section.....	<b>109</b>
<b>Table 3-16</b> : Results of all strengthened steel beams using angle GFRP section.....	<b>110</b>
<b>Table 3-17</b> : Diffèrent GFRP T section dimensions.....	<b>113</b>
<b>Table 3-18</b> : Peak load and horizontal displacement findings.....	<b>114</b>
<b>Table 3-19</b> : Bond behavior and failure mode.....	<b>115</b>
<b>Table 4-1</b> : Mechanical properties of NM CFRP (127 MPa).....	<b>120</b>
<b>Table 4-2</b> : Mechanical properties of NM CFRP (167 MPa).....	<b>120</b>
<b>Table 4-3</b> : The Proposed GFRP strengthening configurations.....	<b>135</b>
<b>Table 7-4</b> : The different openings shapes dimensions in mid span position.....	<b>153</b>
<b>Table 7-5</b> : The different openings shapes dimensions in shear zone position.....	<b>153</b>
<b>Table 7-6</b> : Strength enhancement percentage for specimens with rectangular opening.....	<b>162</b>
<b>Table 7-7</b> : Strength enhancement percentage for specimens with trapezoidal opening.....	<b>162</b>
<b>Table 7-8</b> : Strength enhancement percentage for specimens with reversed trapezoidal opening.....	<b>163</b>
<b>Table 7-9</b> : Strength enhancement percentage for specimens with parallelogram opening.....	<b>163</b>
<b>Table 7-10</b> : Strength enhancement percentage for specimens with ellipsoidal opening.....	<b>163</b>
<b>Table 7-11</b> : Strength enhancement percentage for specimens with rectangular opening.....	<b>184</b>
<b>Table 7-12</b> : Strength enhancement percentage for specimens with trapezoidal opening.....	<b>185</b>
<b>Table 7-13</b> : Strength enhancement percentage for specimens with reversed trapezoidal opening.....	<b>185</b>
<b>Table 7-14</b> : Strength enhancement percentage for specimens with parallelogram opening.....	<b>185</b>
<b>Table 7-15</b> : Strength enhancement percentage for specimens with ellipsoidal opening.....	<b>186</b>

## LIST OF FIGURES

- Figure 1-1:** Introduction of services and lines through cellular beams.
- Figure 1-2:** (a) Castellated beam from hot-rolled profile –(b) cellular beam from hot-rolled profile - (c) Cellular beam from steel plates.
- Figure 1-3:** Flexure mechanism of castellated beam.
- Figure 1-4:** Vierndeel failure mode of castellated beam.
- Figure 1-5:** Weld joints rupture failure mode of castellated beam.
- Figure 1-6:** Lateral-torsional buckling failure mode of castellated beam.
- Figure 1-7:** Web post-buckling failure mode of cellular beam.
- Figure 1-8:** Compressive stress web buckling.
- Figure 1-9:** Vierndeel failure mode of single rectangular web opening.
- Figure 1-10:** Perforated section aperture positions.
- Figure 1-11:** Strengthening steel elements by addition of steel material.
- Figure 1-12:** Reinforced beams examples.
- Figure 1-13:** Examples of reinforced columns.
- Figure 1-14:** Experimental test details conducted by Hayder W.
- Figure 1-15:** Fiber reinforced polymer.
- Figure 1-16:** Fiber reinforced polymer products: (a) plate – (b) sheet –(c) pultruded sections.
- Figure 1-17:** Experimental test conducted by Colombi and Poggi.
- Figure 1-18:** (a) un-strengthened specimen, (b) CFRP on the outside, (c) CFRP on the inside , (d) Both sides have CFRP.
- Figure 1-19:** Strengthening arrangement used by Mohammed H.
- Figure 1-20:** FRP –Steel bond failure.
- Figure 1-21:** single-shear pull-off test for FRP-steel glued connection.
- Figure 2-1:** composition of composite laminates.
- Figure 2-2:** simple bilinear traction-separation law.
- Figure 2-3:** Exponential damage evolution in a traction-separation law.
- Figure 2-4:** Criteria of damage initiation.
- Figure 2-5:** Cost of computation in comparison.
- Figure 2-6:** Reference and reinforced specimens OB1 and OB2.
- Figure 2-7 :** Bilinear steel stress-strain curve .
- Figure 2-8:** The control specimen OB1 failure mode.
- Figure 2-9:** The strengthened specimen OB2 failure mode.
- Figure 2-10 :** Tested specimens dimensions.
- Figure 2-11 :** Vertical and lateral displacement measurement.
- Figure 2-12 :** Loading and boundary conditions.
- Figure 2-13 :** FE model mesh situations.
- Figure 2-14:** Experimental and FE load-vertical displacement for specimen A2.
- Figure 2-15:** Experimental and FE load-vertical displacement for specimen A5.
- Figure 2-16:** Experimental and FE load-vertical displacement for specimen B2.
- Figure 2-17:** Experimental and FE load-vertical displacement for specimen B5.
- Figure 2-18:** Experimental and FE load-horizontal displacement for specimen A2.
- Figure 2-19:** Experimental and FE failure mode of specimen A2.
- Figure 2-20:** Experimental and FE failure mode of specimen A5.
- Figure 2-21:** Experimental and FE failure mode of specimen B2.
- Figure 2-22:** Experimental and FE failure mode of specimen B5.
- Figure 2-23 :** Specimen B1-R0 strengthening arrangement .
- Figure 2-24 :** Specimen B2-R0 strengthening arrangement .
- Figure 2-25 :** Specimen B3-R0 strengthening arrangement .

**Figure 2-26 :** Experimental test dimensions and arrangement .

**Figure 2-27 :** Tensile stress-stain curve from coupon tests of the flange.

**Figure 2-28 :** Tensile stress-stain curve from coupon tests of the web.

**Figure 2-29 :** Numerical model loading and boundary conditions.

**Figure 2-30:** Finite element and experimental load-deflection curve for specimen B0.

**Figure 2-31:** Finite element and experimental load-deflection curve for specimen B1-R0.

**Figure 2-32:** Finite element and experimental load-deflection curve for specimen B2-R0.

**Figure 2-33:** Finite element and experimental load-deflection curve for specimen B3-R0.

**Figure 2-34 :** Finite element and experimental failure mode for specimen B0 .

**Figure 2-35 :** Finite element and experimental failure mode for specimen B1-R0 .

**Figure 2-36 :** Finite element and experimental failure mode for specimen B2-R0 .

**Figure 2-37 :** Finite element and experimental failure mode for specimen B3-R0 .

**Figure 2-38 :** Bond behavior checking for specimen B1-R0.

**Figure 3-1 :** Web post buckling of the cellular beam A2 .

**Figure 3-2 :** Horizontal displacement measurement points .

**Figure 3-3 :** One side CFRP plate strengthening load-displacement curve (S1) .

**Figure 3-4:** Two sides CFRP plate strengthening in single web post load-deflection curves (S2) .

**Figure 3-5 :** Two sides CFRP plate strengthening in the two web posts load-deflection curves (S3) .

**Figure 3-6:** Horizontal displacements for control beam A2.

**Figure 3-7:** Horizontal displacements for specimen A2-S1-1.

**Figure 3-8 :** CFRP plate debonding.

**Figure 3-9 :** No adhesive layer damage on S1 strengthening pattern.

**Figure 3-10:** Adhesive layer deletion of S2 strengthening pattern.

**Figure 3-11 :** Load –vertical displacement curves of 3 mm T section CFRP reinforcement.

**Figure 3-12 :** Horizontal displacement of beam A2-PS3.

**Figure 3-13:** Vierendeel failure of A2-TS3.

**Figure 3-14 :** CFRP pultruded profiles : (a) U section –(b) T section.

**Figure 3-15 :** Strengthening configuration and bonding positions: PS1 and PS2 configurations.

**Figure 3-16 :** Pultruded carbon T section and U section profiles dimensions .

**Figure 3-17 :** CFRP T section strengthening .

**Figure 3-18 :** Load -deflection curves of T section strengthening specimen A2.

**Figure 3-19:** Load -deflection curves of T section strengthening specimen B2.

**Figure 3-20:** Load -deflection curves of T section strengthening specimen A5.

**Figure 3-21:** Load -deflection curves of T section strengthening specimen B5.

**Figure 3-22:** Vierendeel failure mode for specimen : A2 -PS1-3.

**Figure 3-23:** Web post-buckling failure mode and profile debonding for specimen: A5-PS2-6.

**Figure 3-24:** Checking bond behavior using SDEG parameter and adhesive layer deletion for specimen: B2 -PS1-3.

**Figure 3-25:** Load -deflection curves of U section strengthening specimen A2 .

**Figure 3-26:** Load -deflection curves of U section strengthening specimen B2 .

**Figure 3-27:** Load -deflection curves of U section strengthening specimen A5.

**Figure 3-28:** Load -deflection curves of U section strengthening specimen B5 .

**Figure 3-29:** Pultruded CFRP U section debonding for specimen B2 -PS1-3.

**Figure 3-30 :** FRP pultruded element out-of-plane stiffness.

**Figure 3-31:** Pultruded glass FRP profiles : (a) U section –(b) Angle section – (c) T section.

**Figure 3-32:** GFRP T section strengthening .

**Figure 3-33 :** Load-deflection curves of PS1 strengthening configuration .

**Figure 3-34:** Load-deflection curves of PS2 strengthening configuration using adhesive 1.

**Figure 3-35:** Load-deflection curves of PS2 strengthening configuration using adhesive 2.

**Figure 3-36:** Load-deflection curves of PS3 strengthening configuration using adhesive 1.

**Figure 3-37:** Load-deflection curves of PS3 strengthening configuration using adhesive 2.



**Figure 3-38:** Change of web post buckling position.

**Figure 3-39:** End debonding of the GFRP T section.

**Figure 3-40:** Vierendeel failure of A2-PS2-1S.

**Figure 3-41:** Pultruded GFRP angle section strengthening technique.

**Figure 3-42:** Process of FRP stiffener breakdown at the adhesive interface.

**Figure 3-43 :** Strengthening arrangement :(a) PS1 – (b) PS2.

**Figure 3-44 :** Pultruded GFRP T section dimensions.

**Figure 3-45 :** A2-G7-PS2 Failure mode.

**Figure 3-46 :**GFRP U section ( $H = 387$  , $B = 50$  , $b = 51$ ).

**Figure 3-47 :**Load deflection curves of GFRP U validation .

**Figure 3-48 :** A2-G8-PS2 Failure mode.

**Figure 4-1 :**Details and dimensions of HM CFRP strengthened specimen B1-R0.

**Figure 4-2 :**Details and dimensions of HM CFRP strengthened specimen B2-R0.

**Figure 4-3 :** Normal modulus CFRP Strengthening model .

**Figure 4-4:** Load-deflection curves of HM CFRP and NM CFRP strengthening .

**Figure 4-5 :** Failure mode of specimen B1-R0-127.

**Figure 4-6 :** Failure mode of specimen B1-R0-167.

**Figure 4-7 :** Adhesive damage parameter, SDEG at failure of specimen B1-R0-127.

**Figure 4-8:** Adhesive damage parameter, SDEG at failure of specimen B1-R0-167.

**Figure 4-9 :** Strain distribution on high modulus CFRP plates at the peak load B1-R0 beam .

**Figure 4-10 :** Strain distribution on normal modulus CFRP167 plates at the peak load B1-R0 beam.

**Figure 4-11 :** Strain distribution on normal modulus CFRP 127plates at the peak load B1-R0 beam.

**Figure 4-12 :** Load deflection curves of different NM CFRP 167 MPa plate thicknesses .

**Figure 4-13 :** Load deflection curves of different NM CFRP 127 MPa plate thicknesses .

**Figure 4-14 :** Failure mode of specimen B1-R0-167-1.

**Figure 4-15 :** Failure mode of specimen B1-R0-127-1.

**Figure 4-16 :** Load-deflection curves of shear zone HM and NM CFRP web opening strengthening .

**Figure 4-17 :** Bond behavior checking for NM CFRP strengthening .

**Figure 4-18 :** Strain distribution on normal modulus CFRP 167 plates at the peak load B2-R0 beam.

**Figure 4-19 :** Strain distribution on normal modulus CFRP 127 plates at the peak load B2-R0 beam.

**Figure 4-20 :** Strain distribution on normal modulus CFRP 200 plates at the peak load B2-R0 beam.

**Figure 4-21 :** Load deflection curves of different NM CFRP 167 MPa plate thicknesses for shear zone opening position .

**Figure 4-22 :** Load deflection curves of different NM CFRP 127 MPa plate thicknesses for shear zone opening position .

**Figure 4-23 :** Failure mode of specimen B2-R0-167-2.

**Figure 4-24 :** Failure mode of specimen B2-R0-127-1.

**Figure 4-25:** Pultruded GFRP :(a) plate-(b) U section –(c) T section –(d) Angle section .

**Figure 4-26 :** Strengthening specimen B1-U0 using (R4) GFRP technique .

**Figure 4-27 :** Load-deflection curves of 3mm GFRP laminates strengthening.

**Figure 4-28 :**Mid span lateral buckling of specimen B1-R3-3 .

**Figure 4-29 :** Mid span lateral buckling of specimen B1-R4-3 .

**Figure 4-30 :** Bond behavior for specimen B1-R3-3.

**Figure 4-31 :** Load deflection curves of specimen B1-UO strengthened using 6 mm GFRP laminates thicknesses .

**Figure 4-32 :** Failure mode of specimen B1-R4-6.

**Figure 4-33 :** Failure mode of specimen B1-R3-6 .

**Figure 4-34 :** Bond behavior of specimen B1-R2-6.

**Figure 4-35:** Bond behavior of specimen B1-R3-6.

**Figure 4-36:** Load deflection curves of specimen B1-UO strengthened using 10 mm GFRP laminates thicknesses.

**Figure 4-37:** Failure mode of specimen B1-R1-10.  
**Figure 4-38:** Failure mode of specimen B1-R4-10.  
**Figure 4-39:** Bond behavior of specimen B1-R1-10.  
**Figure 4-40:** Load deflection curves of specimen B2-UO strengthened using 3 mm GFRP laminates thicknesses.  
**Figure 4-41:** Failure mode for specimen B2-R4-3.  
**Figure 4-42 :** Failure mode for specimen B2-R2-3.  
**Figure 4-43:** Bond behavior for specimen B2-R2-3.  
**Figure 4-44:** Load deflection curves of specimen B2-UO strengthened using 6 mm GFRP laminates thicknesses.  
**Figure 4-45:** Failure mode for specimen B2-R2-6.  
**Figure 4-46:** Bond behavior for specimen B2-R2-6.  
**Figure 4-47 :** Load deflection curves of specimen B2-UO strengthened using 10 mm GFRP laminates thicknesses.  
**Figure 4-48 :** Failure mode of specimen B2-R4-10.  
**Figure 4-49 :** Bond behavior for specimen B2-R1-10.  
**Figure 7-50 :** Details of tested specimen.  
**Figure 7-51 :** Web opening shapes used in this investigation and there dimensions.  
**Figure 7-52 :** Steel stress-strain curve employed in the simulation.  
**Figure 7-53 :** GFRP strengthening technique.  
**Figure 7-54 :** Boundary conditions.  
**Figure 7-55 :** The chosen mesh distribution.  
**Figure 7-56 :** Load deflection curves of unstrengthened specimens with mid span rectangular web openings .  
**Figure 7-57 :** Failure mode of unstrengthened specimens with mid span rectangular web openings.  
**Figure 7-58 :** Load deflection curves of unstrengthened specimens with mid span trapezoidal web openings .  
**Figure 7-59 :** Failure mode of unstrengthened specimens with mid span Trapezoidal web openings.  
**Figure 7-60 :** Load deflection curves of unstrengthened specimens with mid span reversed trapezoidal web openings .  
**Figure 7-61 :** Failure mode of unstrengthened specimens with mid span reversed Trapezoidal web openings.  
**Figure 7-62 :** Load deflection curves of unstrengthened specimens with mid span parallelogram web openings.  
**Figure 7-63 :** Failure mode of unstrengthened specimens with mid span Parallelogram web openings.  
**Figure 7-64 :** Load deflection curves of unstrengthened specimens with mid span ellipsoidal web openings .  
**Figure 7-65 :** Failure mode of unstrengthened specimens with mid span ellipsoidal web openings.  
**Figure 7-66 :** Load-mid span deflection curves for strengthened specimen U0-Rec-1.  
**Figure 7-67 :** Load-mid span deflection curves for strengthened specimen U0-Rec-2.  
**Figure 7-68 :** Load-mid span deflection curves for strengthened specimen U0-Rec-3.  
**Figure 7-69 :** Load-mid span deflection curves for strengthened specimen U0-Rec-4.  
**Figure 7-70 :** Load-mid span deflection curves for strengthened specimen U1-Trap-1.  
**Figure 7-71 :** Load-mid span deflection curves for strengthened specimen U1-Trap-2.  
**Figure 7-72 :** Load-mid span deflection curves for strengthened specimen U1-Trap-3.  
**Figure 7-73 :** Load-mid span deflection curves for strengthened specimen U2-Traprv-1.  
**Figure 7-74 :** Load-mid span deflection curves for strengthened specimen U2-Traprv-2.  
**Figure 7-75 :** Load-mid span deflection curves for strengthened specimen U2-Traprv-3.  
**Figure 7-76 :** Load-mid span deflection curves for strengthened specimen U2-Parall-1.  
**Figure 7-77 :** Load-mid span deflection curves for strengthened specimen U2-Parall-2.  
**Figure 7-78 :** Load-mid span deflection curves for strengthened specimen U2-Parall-3.

**Figure 7-79** : Load-mid span deflection curves for strengthened specimen U4-Elli-1.  
**Figure 7-80** : Load-mid span deflection curves for strengthened specimen U4-Elli-2.  
**Figure 7-81** : Load-mid span deflection curves for strengthened specimen U4-Elli-3.  
**Figure 7-82** : Failure mode of strengthened specimens with mid span rectangular opening .  
**Figure 7-83** : Failure mode of strengthened specimens with mid span trapezoidal opening .  
**Figure 7-84** : Failure mode of strengthened specimens with mid span reversed trapezoidal opening .  
**Figure 7-85** : Failure mode of strengthened specimens with mid span parallelogram opening .  
**Figure 7-86** : Failure mode of strengthened specimens with mid span ellipsoidal opening .  
**Figure 7-87** : Bond behavior for specimen U0-Rec-1-10.  
**Figure 7-88** : Bond behavior for specimen U0-Trap-1-3.  
**Figure 7-89** : Bond behavior for specimen U2-Traprv-1-6.  
**Figure 7-90** : Load deflection curves of unstrengthened specimens with shear zone rectangular web openings .  
**Figure 7-91** : Failure mode of unstrengthened specimens with shear zone rectangular web opening.  
**Figure 7-92** : Load deflection curves of unstrengthened specimens with shear zone trapezoidal web opening.  
**Figure 7-93** : Load deflection curves of unstrengthened specimens with shear zone reversed trapezoidal web opening.  
**Figure 7-94** : Failure mode of unstrengthened specimens with shear zone trapezoidal web opening.  
**Figure 7-95** : Failure mode of unstrengthened specimens with shear zone reversed trapezoidal web opening.  
**Figure 7-96** : Load deflection curves of unstrengthened specimens with shear zone parallelogram web opening.  
**Figure 7-97** : Failure mode of unstrengthened specimens with shear zone parallelogram web opening.  
**Figure 7-98** : Load deflection curves of unstrengthened specimens with shear zone ellipsoidal web opening.  
**Figure 7-99** : Failure mode of unstrengthened specimens with shear zone ellipsoidal web opening.  
**Figure 7-100** : Load-mid span deflection curves for strengthened specimen U0-SZRec-1.  
**Figure 7-101** : Load-mid span deflection curves for strengthened specimen U0-SZRec-2.  
**Figure 7-102** : Load-mid span deflection curves for strengthened specimen U0-SZRec-3.  
**Figure 7-103** : Load-mid span deflection curves for strengthened specimen U0-SZRec-4.  
**Figure 7-104** : Load-mid span deflection curves for strengthened specimen U1-SZTrap-1.  
**Figure 7-105** : Load-mid span deflection curves for strengthened specimen U1-SZTrap-2.  
**Figure 7-106** : Load-mid span deflection curves for strengthened specimen U1-SZTrap-3.  
**Figure 7-107** : Load-mid span deflection curves for strengthened specimen U1-SZTraprv-1.  
**Figure 7-108** : Load-mid span deflection curves for strengthened specimen U1-SZTraprv-2.  
**Figure 7-109** : Load-mid span deflection curves for strengthened specimen U1-SZTraprv-3.  
**Figure 7-110** : Load-mid span deflection curves for strengthened specimen U3-SZParall-1.  
**Figure 7-111** : Load-mid span deflection curves for strengthened specimen U3-SZParall-2.  
**Figure 7-112** : Load-mid span deflection curves for strengthened specimen U3-SZParall-3.  
**Figure 7-113** : Load-mid span deflection curves for strengthened specimen U4-SZElli-1.  
**Figure 7-114** : Load-mid span deflection curves for strengthened specimen U4-SZElli-2.  
**Figure 7-115** : Load-mid span deflection curves for strengthened specimen U4-SZElli-3.  
**Figure 7-116** : Failure mode of strengthened specimens with shear zone rectangular opening .  
**Figure 7-117** : Failure mode of strengthened specimens with shear zone trapezoidal opening .  
**Figure 7-118** : Failure mode of strengthened specimens with shear zone reversed trapezoidal opening .  
**Figure 7-119** : Failure mode of strengthened specimens with shear zone parallelogram opening .  
**Figure 7-120** : Failure mode of strengthened specimens with shear zone elliptical opening .  
**Figure 7-121** : Bond behavior for specimen U0-SZRec-1-3 .  
**Figure 7-122** : Bond behavior for specimen U0-SZRec-2-3 .  
**Figure 7-123** : Bond behavior for specimen U2-SZTraprv-1-3 .

## NOTATIONS

PFRP: Pultruded fiber reinforced polymer.

CFRP: Carbon fiber reinforced polymer.

GFRP: Glass fiber reinforced polymer.

$h$ : Height of profile.

$b_f$  : Width of flange.

$t_f$ : Thickness of flange.

$t_w$  : Thickness of web.

$d_w$ : Height of web.

$d_0$ : Web opening diameter.

$S_0$  : Web post width.

$S$  : Opening diameter and web post width

$L$ : Length of the beam.

$f_y$ : The yield strength of steel.

$E$ : Young's modulus.

$t_n$ ,  $t_s$  and  $t_t$ : Peak values of the nominal stress.

$\partial_{max}$  : Tensile strength of the adhesive.

$\tau_{max}$ : Shear strength of the adhesive.

$D$  : The scalar damage variable.

$\delta_m^{max}$ : The maximum effective relative displacement attained during the loading history.

$\delta_m^0$  and  $\delta_m^f$ : The effective relative displacement at the initiation and end of failure respectively.

$\lambda$ : Web post slenderness.

$l_m$ : The strut length.

$P_u$  : Ultimate load.

SDEG : Stress degradation parameter.

WPB : Web post-buckling failure mode.

V: Vierendeel failure mode.

DEB: CFRP profile debonding.

TFY: Top flange yielding.

LTB: Lateral torsional buckling.

$\varepsilon_{true}$  : True strain.

$\varepsilon_{Nominal}$  : Nominal strain.

$\sigma_{true}$  : True stress.

$\sigma_{nominal}$  : Nominal stress.

$E_x$  : Elastic modulus in the fiber direction.

$E_y$ ,  $E_z$ : Elastic modulus in the transverse direction.

$G_{xy}$ : In-plane shear modulus.

$G_{xz}$ ,  $G_{yz}$  : Shear modulus in the transverse direction.

$\nu$  : Poisson ratio.

$K_{nn}$ : The adhesive elastic stiffness in the normal direction, which is equal to the initial slope of the bond separation model for mode-I loading.

$K_{ss}$  and  $K_{tt}$ : The adhesive elastic stiffness in the shear directions.

$E_a$  : Elastic modulus of the adhesive layer.  
 $G_a$  : The shear module of the adhesive layer.  
 $G_f$ : Energy of interfacial fracture.  
 $T_a$  : Thickness of the adhesive layer.  
R: is the adhesive's tensile strain energy.  
f : Natural frequency of the member  
HM CFRP : High modulus carbon fiber reinforced polymer.  
NM CFRP : Normal modulus carbon fiber reinforced polymer.  
QUADSCT: criteria of Quad damage stress.  
S: Shear strength longitudinal.  
TFY: The yielding of top flange.  
VF: Vierndeel failure mode .  
 $X_c$ : compressive longitudinal strength.  
 $X_t$ : Tensile strength along the length.  
 $Y_c$ : Strength in the transverse direction.  
 $Y_t$ : Tensile strength transversely.  
 $\delta$  : Separation/ Slip.  
 $\delta_1$ : Separation at maximum bond stress /Slip.  
 $\delta_2$ : Slip at the start of softening.  
 $b_p$ : The breadth of the FRP plate .  
 $t_p$  : The thickness of FRP plate .  
 $b_{st}$  : Steel plate width .  
 $t_{st}$  : Steel plate thickness .  
 $\tau$ : the glue layer's shear stress.  
 $\sigma_p$ : is the FRP plate's axial stress.  
 $\sigma_{st}$ : is the steel plate's axial stress.  
 $P_u$ : Peak load / strength of the bond .  
 $E_p$ : A plate's tensile elastic modulus

## GENERAL INTRODUCTION

Currently, steel beams with web openings and cellular beams are commonly employed in innovative steel structures buildings to allow services and instrumentation cables. Despite the fact that this notion provides a superior visual aspect as well as other additional benefits, the existence of web holes generates a condition of instability and various failure modes in cellular beams. In addition, the insertion of web openings in existing solid beams reduces the strength capacity and stiffness of the beams dramatically.

The sole method of reinforcing and stiffening steel beams with web openings under all design guidelines is to weld additional steel plates around the openings; this not only presents practical problems but can also lead to residual stresses that influence the fatigue performance of the section.

Researchers have extensively explored and applied structural strengthening with Fiber Reinforced Polymer (FRP) composites in the field. FRP composites provide a number of advantages over traditional structural materials, the most notable advantage of FRP composites is their enhanced mechanical properties.

The purpose of this research is to determine if externally bonded fiber-reinforced polymer composites materials (FRP) can be used as an alternative to welding techniques to strengthen web-post instability in cellular beams and restore the flexural capacity of steel beams after the creation of web holes.

The influence of strengthening configuration, FRP material types, and FRP laminate thicknesses were explored after a numerical investigation to establish the most effective structurally efficient arrangement of FRP strengthening in order to acquire more sufficient information about the use of FRP laminates to strengthen steel beams with web openings and achieve an advanced phase in which guidelines and codes can be developed to assist engineers in the design and application of such systems.

Using a validated non-linear finite element approach the research started by testing the effects of strengthening web post-buckling in cellular beams with pultruded plates and profiles of carbon fiber reinforced polymer composites (CFRP) .Then pultruded glass fiber reinforced polymer composites (GFRP) were investigated also to enhance the stiffness and the stability of cellular beams. It was found that this novel technique was able to prevent the web post instability or delay it to a grater load with a considerable strength enhancement comparable to control beams.

Further numerical modeling was also performed to assess the ability of pultruded NM CFRP and GFRP laminates to recover the flexural and shear strength of steel beams after the creation of single rectangular opening shapes in mid-span and high shear zone positions and compare results with previous experimental test conducted previously on strengthening the same tested beams with single rectangular opening in shear zone and mid span position using HM CFRP.

It was also found that GFRP pultruded profiles were able to restore the strength and the stiffness of tested beams using the optimum strengthening configuration with better economical technique in comparison to previous HM CFRP.

The most effective GFRP reinforcement system found was used then to strengthen steel beams with various single web-opening shapes of different opening sizes in the two positions along the span (mid span and shear zone). The most efficient GFRP laminates thicknesses was found for every opening geometry and location and the ability of low cost GFRP in comparison to HM CFRP to reinforce steel beams after the creation of web apertures was confirmed.

➤ **The purpose of this research:**

The objective of this project is to create an efficient reinforcement configuration using the most effective FRP laminates that could recover the strength and stiffness of steel beams after the introduction of web openings and reinstate the stiffness of slender steel beams with multiple web holes in order to make recommendations and reach an important stage in which regulations and guidelines can be created to aid designers in the conception and application of such relatively new reinforcement schemes.

➤ **Thesis organization :**

- Chapter one: This section reviews the existing reinforcement methods for steel constructions as well as various types of steel beams with web holes. Additionally, a thorough review of the bond behavior between steel and FRP will be given along with a description of FRP composite materials.
- Chapter two: A thorough explanation of the suggested finite element model will be presented in this chapter, along with a validation using various prior experimental test findings and key circumstances. This will give the trust to utilize the established numerical model to strengthen the web post-buckling of cellular beams and increase the strength of steel beams just and after creation of a single web opening.
- Chapter Three : The numerical examination in this section focuses on reinforcing web post buckling of cellular beams utilizing various reinforcement configurations and factors, such as the kind of FRP laminate, multiple kinds of adhesive, the slenderness of the web post and many other parameters .
- Chapter Four : In this segment, the FRP reinforcement scheme will be explored to strengthen the same specimen that was before utilized in an experimental test with a single rectangular web opening in the shear zone position and mid span position. The findings of

NM CFRP strengthening will be compared to earlier findings, and the same specimen was reinforced with various GFRP reinforcement topologies. In addition, other specimens with various opening shapes and sizes in the two positions along the span were strengthened using the most efficient GFRP reinforcement found previously.

- Finally, many judgments and suggestions with regard to this innovative method were made as a general conclusion.



## CHAPTER I: LITERATURE

### I.1. Steel beams with web openings:

With the remarkable progress of modern technology in all daily uses, home automation trends have gathered important advancements. New houses use an automated process to automatically control the building's operation including lighting, ventilation, water supply, PC system, security, and other systems to ensure a high quality of comfort.

Certainly, the idea of converting an existing home to a smart home can be easier for homeowners than buying a new one. However, the addition of devices requires engineers and major companies to create openings in the web of existing steel beams for the placement of services and the laying lines and cables (**Figure 1-1**). Several experts have been doing investigations since 1940 to identify advanced methods to accomplish economy in steel buildings. During World War II, steel beams with web holes were initially employed in constructions to reduce the price of metal structures. The extra strong qualities of structural steel cannot always be utilized to their full potential. As a result, several approaches have been developed to enhance the hardness of steel parts without increasing the mass of the steel.

The ability to integrate technical services via the web holes of the beam is a significant benefit in steel constructions. As a result, steel beams having web apertures, including castellated and cellular beams, have been frequently employed. When opposed to the typical technique, in which the services are put underneath the beams, this decreases the height of the building since the open area between the roof and the floor is reduced.

When opposed to the typical technique, where the pipes and lines are put just below beams, this minimizes the building height since the open area between the roof and the base is reduced. Benefits of up to 0.5 m per floor are possible. As a result, there is a more reasonable, compact, and expense manner of building.

The production procedure of the aforementioned perforated beams is critical since it influences the price and structural system of the final structural element.

### I.2. Manufacturing process of steel beams with web openings:

Steel beams with web holes can be manufactured in three different ways (**Figure 1-2**):

- Individual holes are cut into the web of a hot-rolled section. The form of the metal section is symmetric. So for steel beams with isolated web apertures, this procedure is applied.

- Three I-section plates are welded together to produce a manufactured component. The web is cut into perforations either before or after the I-section creation .This approach may be utilized for both single and regularly spaced multiple apertures.
- To create a series of uniform openings in a deeper section, a hot rolled portion is reshaped along the web, then replaced and re-welded. The castellated beam was the initial of its kind previously, although current building employs circular aperture beams which is labeled as cellular beams .
- This segment may be made asymmetric by cutting the Tee from distinct I-sections. This approach is only suitable for apertures with equal spacing.

Due to the absence of a massive amount of the web, large perforations reduce beam shear resistance significantly, but only slightly reduce the flexural resistance. Shear transfer over sections with wide holes is a major technical issue, and wide apertures should be located away from the high shear region of the beams to reduce their influence. Shear transmission over big apertures is accomplished by flexing the web flange 'Tee' portions above and below the aperture. The edges of the aperture will be led by this. Longitudinal stiffener plates increase the local resistance of the Tees, which improves shear transmission.



**Figure 1-1: Introduction of services and lines through cellular beams**

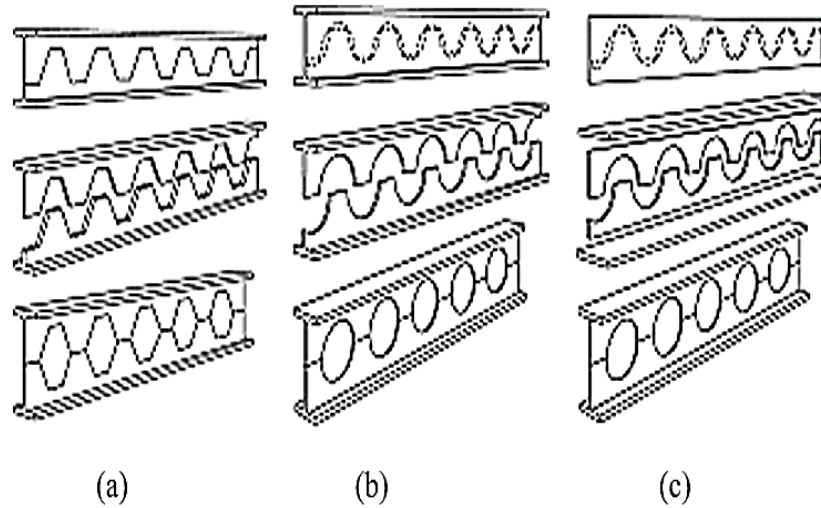


**Figure 1-2 : (a) Castellated beam from hot-rolled profile –(b) cellular beam from hot-rolled profile - (c) Cellular beam from steel plates**

Slender webs in prefabricated beams (cellular beams) may necessitate transverse stiffening to prevent buckling of the web at the aperture. Nevertheless, by adopting a thicker web and carefully positioning the openings away from force places, the requirement for these kind of stiffening can be reduced, leading in a much more cost-effective arrangement.

### **I.3. Prior design recommendations:**

A design technique for hot-rolled metal beams with discrete apertures was provided in the SCI article design of steel beams with webs perforations , which was established in 1988[1] . The approach was validated using tests performed at WARWICK University on steel beams of ten meter span with web openings of rectangular shapes [2] .

The current design and manufacturing of steel beams with web holes varies markedly from the SCI article and the variations tested at WARWICK in several ways :

- In terms of the proportion of the lower to upper flange regions, steel sections are frequently very asymmetric.
- Because the webs are generally thin, the impact of local buckling is amplified.
- In regards of their dimensions ratio, apertures are frequently rather long.
- Inside the depth of the portion, apertures are frequently asymmetric and mostly near to one of the flanges.
- The "web-post" spanning consecutive circular holes is typically removed to create elongated apertures.

Because of these changes in practice, the SCI publication has been re-evaluated. As a result, such recommendation can be applied to a large variety of situations for manufactured and hot-rolled steel sections. Nevertheless, it is impossible to provide clear recommendations in all circumstances, and conventional structural design basics must still be followed.

In addition, the adoption of Eurocodes necessitates that design techniques correspond to the main principles and applicability guidelines for Eurocode 3 and Eurocode 4, accordingly for steel and composite elements. A draught modification to Annex N of the pre-standard ENV 1993-1-1:1992 / A2:1998 addressing the design of beams having perforations in the web was initiated but never released, neither included in the official Eurocode[3]. In the United States, there is further international guidelines on beams having large web apertures[4]. However, this does not applicable to cellular or equally spaced aperture beams.

### **I.4. Cellular beams :**

Cellular beams were invented and patented by Westok Structural Service [5]. They were first presented in 1987 for architectural applications in which circular holes in uncovered steel structures were deemed visually attractive. Traditionally, a round was burned into the web segment to create circular web apertures. To manufacture cellular beams as castellated beams, a double cut procedure was designed along the profile.

Castellated beams were designed largely to increase the structural performance of rolled I beams, and could be considered the predecessor of cellular beams. HE Horton of the Chicago Bridge was the first to employ Castellated beams in 1910 [5].

#### **I.4.1. Solid webbed beams and cellular beams comparison :**

Cellular beams offer various benefits across solid beams. The improvement flexural rigidity caused by the expansion phase is proportional to the rise in height. When opposed to a solid beam exposed to the same stress with the same span, there is a weight savings using cellular beam. The web apertures can also serve as services tunnels, lowering the floor elevation. As a result of this, the height of multistory structures is greatly reduced.

#### **I.4.2 Comparison of cellular and castellated beams :**

The circular holes of cellular beams are much more attractive than hexagonal apertures in castellated beams in terms of aesthetics. For cellular beams, the double cut manufacturing technique loses a minor quantity of material, while the single cut procedure for castellated beams spends nothing. The topology of cellular beams is significantly greater versatile than that of castellated beams. With cellular beams, the final depth, hole diameter, and aperture frequency are all adjustable, but in castellated beams, the completed depth and aperture spacing are fixed by the opening altitude. As a result, this type of beams are often lighter than even the effective castellated beams. It is possible to configure cellular beam design to minimize the requirement for infill plates,

which significantly raise production costs. For castellated beams, infill plates are utilized in places of strong shear near the ends of the beam or at locations with stresses concentration. By arranging the apertures to produce large web posts, a cellular beam may be constructed to provide a good resistance to shear stresses. In contrast, bending moments are dominant when a section is minimally loaded. To reach the optimum moment of inertia, a cellular beam with the greatest depth and densely packed holes will be preferred. In addition to that a cellular beam with the maximum depth and closely packed perforations will be favored to achieve the optimal moment of inertia. Rather than the infill panels used on castellated beams, perforations can be reinforced using a circle stiffener. This has the benefit of preserving the apertures for servicing access.

#### **I.4.3.Potential failure scenarios for steel beams with multiple web openings:**

Experiments on Steel beams with multiple web apertures have revealed six failure mechanisms [6]. These modes of failure are linked with geometry of the beam, slenderness of the web, opening shape, type of Loading, and availability of lateral supports. Failure is likely to take place in one of the following types when lateral or coupled loads are imposed:

**I.4.3.1.Pure bending :** So when beam is exposed to stressful bending with limited vertical shear, this failure mechanism occurs. Toprac and Cook [7] and Halleux [8] both observed this failure mode in their research. They came to the conclusion that the yielding of a steel beam's with multiple web openings tee portions upper and lower the apertures was identical to that of a solid beam under flexural pressures (**Figure 1-3**).

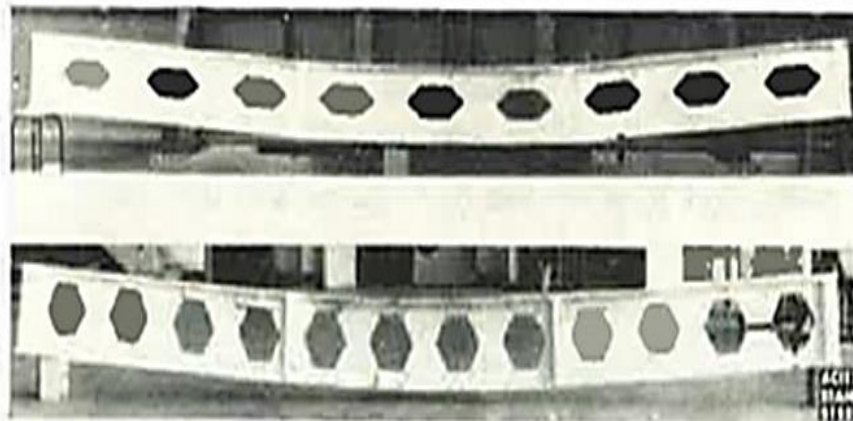


**Figure 1-3 : Flexure mechanism of castellated beam**

**I.4.3.2.Vierendeel mechanism:** When the beam is exposed to a substantial vertically shear stress, this failure involves. Primary bending and shear is applied to the tee portions upper and lower the apertures. They're additionally susceptible to a supplementary Vierendeel moment, which is created by the shearing force applied across the length of the tee. The hole distorts into a parallelogram, compressing or ripping the weak zone (**Figure 1-4**).

**I.4.3.3.Weld joints rupture :**The weld joint of the web post between two adjacent perforations can fail when lateral shear stresses overcome the yield strength of the welded connection joint. In addition to that this kind of failure is influenced by the length of the welded joint .The weld in the web-post becomes much more sensitive to fail in this form if the horizontal length is decreased to minimize secondary moments. However, from the other side. When the lateral yield stress is surpassed, smaller weld lengths are subject to failure by the welded joints rupture (**Figure 1-5**) .

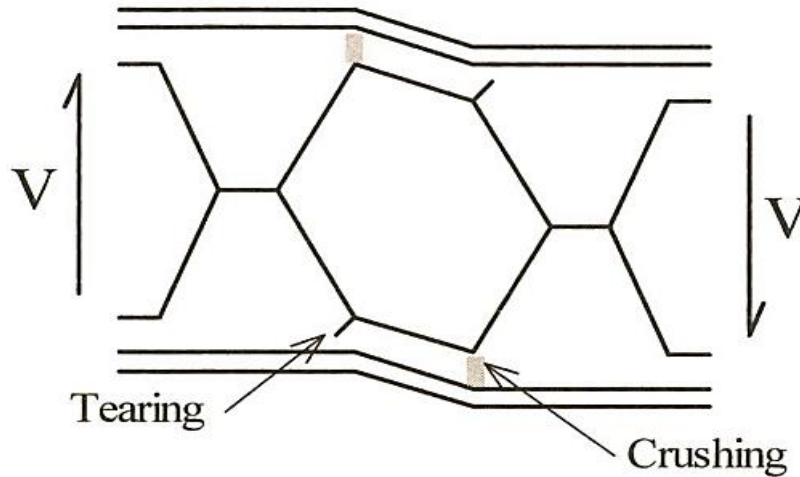


**Figure 1-4 :Vierendeel failure mode of castellated beam**

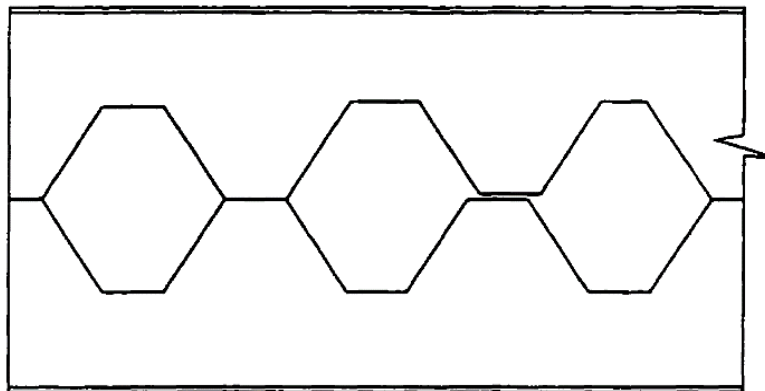


**Figure 1-5: Weld joints rupture failure mode of castellated beam**

**I.4.3.4.Lateral torsional buckling :**

This type of failure is described by out of plane mobility even without any web distortions, just like in plain web beams. When it comes to lateral torsional buckling, cellular beams behave similarly to castellated beams. This buckling mechanism is caused by the web's decreased rigidity as a consequence of its considerably deeper and thinner section characteristics. The existence of



web holes had no discernible impact on the lateral-torsional buckling performance on this type of beams (**Figure 1-6**).

**I.4.3.5. Web post-buckling :**The horizontal shear stress in the web-post is caused by dual fold curvature twisting over the elevation of the post. One sloped border of the aperture will be pressured in tension, while the opposing border will be pressed in compression, causing the web post to buckle along its depth. It should be noted that the web post-buckling is one of the major failure mode in steel beams with several web perforations (**Figure 1-7**).

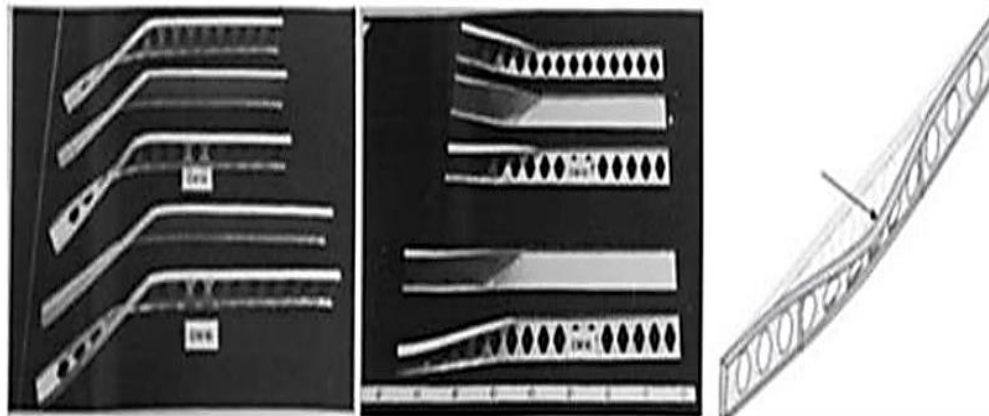


**Figure 1-6: Lateral-torsional buckling failure mode of castellated beam**

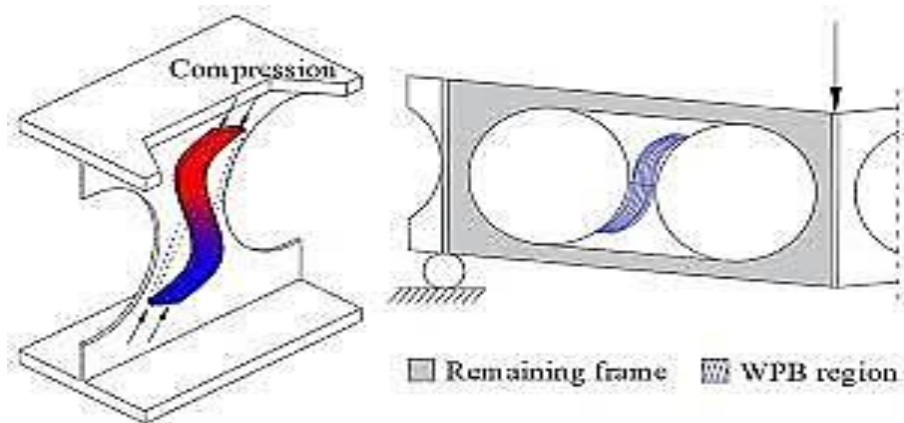


**Figure 1-7 : Web post-buckling failure mode of cellular beam**

**I.4.3.6. Local failures under compression:** This failure mechanism is caused by a concentrated load placed directly above the web-post. Buckling of the web post with compressive stresses does not result in post distortion, as it would with shearing stress. Thus, a failure mechanism could be avoided if enough web strengthening reinforcements are given (**Figure 1-8**).

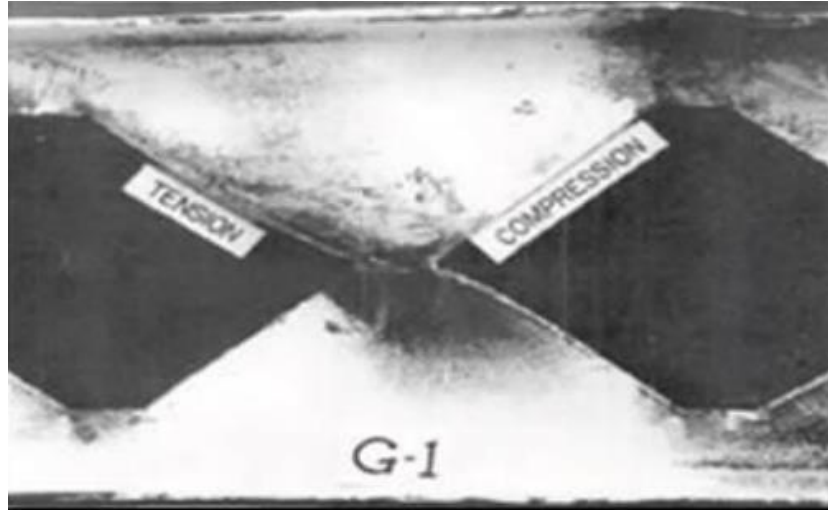


**Figure 1-8 :Compressive stress web buckling**

#### **I.4.4.Prévious research for cellular and castellated beams:**

Sherbourne and Van Oostrom [9] created a numerical program for analyzing castellated beams that took into account either elastic and plastic deformations by employing actual reduced limit equations for moment, shear, and axial load coupling of plasticity.

In non-composite symmetric and asymmetric cellular beams, Panedpojaman [10] provided analytical model for the shear resistance of web-post buckling failure mode .A finite element model of the web-post is utilized in the parametric analysis to explore buckling actions and process in order to create the design process. The novel design formulas make it easier to construct cellular beams that are both cost - effective.

Aminian et al [11] introduced novel design equations for determining the strength capacity of castellated beams employing linear genetic program and effective search algorithms. It was discovered that using a computational model to assess the failure force of castellated beams is an efficient approach.

Redwood and Mc Cutcheon [12] conducted severe experiments on wide-flange metal beams having varied shear-to-moment proportions, with the holes cut out by a flying cutter. The plastic collapse moment was calculated by plotting the deflections along the beams at every stress increase against the moment at the aperture. Nine specimens with circular opening shape , four with single aperture , and five pairs of opening were examined. Three of the five specimens having pairs of apertures had apertures that were near together and two of them had apertures that were widely



separated .In the sections having singular apertures exposed to shear, a Vierendeel failure mode was seen .Instead of defined plastic hinges, a diffused yielding of the web around the aperture was observed. The yielding of the web was moved to the hole stress side. specimens with pairs of apertures that were exposed to minor shear collapsed at the hole closest to the force in the same way as single opening beams .The web post buckled as a result of the increased shear, and the couple of apertures collapsed as a single unit. The researchers came to the conclusion that the existence of shear decreased the specimens flexural capacity, but that beams with couples of holes were not weaker than those with individual perforations. The existence of round web holes was shown to decrease the beam's flexural capacity by 64 to 72 percent, based on the shear-to-moment proportion.

Wang et al. [13] has published a parameterized research on the high vertical displacement evaluation of castellated beams at elevated temperatures. They calculated the increase of the end resultant force, mid span vertical displacement, and flexure moment at vulnerable regions of castellated beams using the finite element approach. To investigate the influence of web perforations, the findings were compared to those of similar solid beams.

Ravinger and LaScekova [14] tested thin-webbed plate girders having round perforations. We looked at both non-strengthened and strengthened apertures. Due to the general extremely thin webs, the non-reinforced apertures collapsed by the web buckling surrounding the opening. Since universal segments' webs are significantly thicker, cellular beams are unlikely to drop in this failure mechanism .As a result, it was suggested that the holes should be strengthened. Unfortunately, this is costly and must be prevented in cellular beams if feasible.

Menkulasi et al [15] evaluated the endurance of castellated beams to concentrating pressures with and without stiffeners by analyzing 30 prototypes of castellated beams exposed to point load with varying cross sections and load locations. The nonlinear finite element analysis approach was used to conduct the research.

Kim et al. [16] provided an empirical investigation on the web shear impacts on the horizontal buckling of castellated beams subject to pure flexural and evenly speared load. They carried out their research utilizing the classical theory of minimal energy potential. They also stated that in order to improve the precision of the crucial moments' quantity and forces, the average torsional invariant of the entire and decreased sections should be used in calculations rather than directly taking the average of the crucial moments or loads.

To estimate the flexural ratio of unrestrained castellated beams, Showkati[17] proposed numerous empirical formulae. His findings were compared to previously published data from other investigations. The findings shows that the section parameters influence the elastic-flexural capabilities of castellated beams exposed to spaced loads on the upper flange face.

Morkhade and Gupta [18] investigated the influence of web hole diameters and placements, as well as stiffener positions surrounding the openings, on the performance of a perforated steel I

beam with rectangular geometry web perforations. The researchers reported that the placement of the perforations affects the load bearing capability of the beam. In this work, experimental and finite element analytic approaches were used. ANSYS software was used to perform the nonlinear finite element simulation.

Soltani et al [19] explored the effect of substance and geometrical nonlinearity on castellated beam failure mechanism prediction. Their research was carried out utilizing MSC/NASTRAN program to calculate flexural moments and shearing load capacity, which were then verified to those available in the literature.

Zaarour and Redwood [20] tested twelve castellated beams with simple supports and a concentrate load applicated at the mid-span, resulting in a low moment-to-shear proportion. It revealed the ability of web posts twisting between web apertures occurring. Buckling forces were calculated using a nonlinear finite element simulation that took into consideration plastic deformation. A comparison was performed between their findings and the results of earlier investigations.

### **I.5. Steel beams with web openings:**

For hot-rolled steel beams having single web apertures rectangular web holes were frequently created with ratio in the range between 1.0 and 3.0, whereas the opening height was generally fixed to around 50% of the entire portion height,  $h$ . Due to the ease of maintenance of water piping, circular web apertures were very common in structures with high construction service criteria.

#### **I.5.1.Potential failure mode for steel beams with single web openings:**

Steel beams with single web apertures have two fundamental mechanisms of failure in the lack of global instability with lateral torsional buckling. So according on the shape and placement of the web hole along the span:

##### **I.5.1.1 Vierendeel failure:**

Strong shear stresses pressing on the beam generate four plastic hinges at the aperture corners, forcing the perforated portion to distort into a parallelogram, resulting in this mechanism of failure [21] (**Figure 1-9**).

##### **I.5.1.2 Flexural failure:**

The upper T-section above the hole is subject to buckling failure due to significant compressive pressures when an opening is introduced in the ultimate bending zone of a simply supported beam.



**Figure 1-9: Vierendeel failure mode of single rectangular web opening**

#### **I.5.2. Previous research for steel beams with single web opening:**

Lately, scientists have begun to investigate the behavior and load capacities of several varieties of web perforated steel beams under dispersed and concentrated forces.

Liu and Chung [22] investigated shear-moment correlation and failure mechanism using a numerical research on steel beams with distinct sizes and forms of web holes. All simply supported specimens with a span of 12m were subjected to equally distributed force. The web apertures were concentric to the section's mid-depth and positioned at various points along the beam's span. The web opening at position 1 of the beam was in pure shear stresses with no global moment. In contrast to location 4, the correlation of global shear force and moment was considerable at places 2 and 3, as seen in **Figure 1-10**. The yield characteristics were discovered to represent typical failure mechanisms for all steel beams, and the distance of the T-sections upper and lower the web hole was shown to be the greatest relevant factor in analyzing the structural behavior of perforated steel beams because it regulates the size of the localized Vierendeel moments operating on T-sections. Additionally, the global shear-moment interaction curves have a the same format, therefore empirical shear-moment association curves can be derived to estimate the load capabilities of all steel beams with web apertures of varied forms and sizes.

Congdon and Redwood [23] estimated the strength of specimens with strengthened rectangular apertures supposing fully plastic behavior by testing a beam with a single web reinforced rectangular aperture. Furthermore, they calculated the surface of reinforcement necessary to reach the section's ultimate shear bearing capacity.

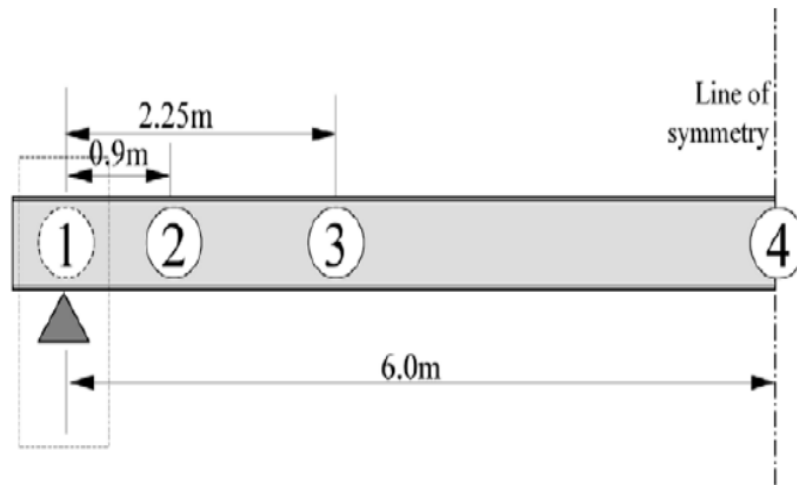


**Figure 1-10: Perforated section aperture positions**

Sixteen simply supported steel beams of W12x45 section and A36 steel material were tested experimentally by Cooper and Snell [24]. The tested specimens were subjected to a concentrated force at mid-span under several moment-to-shear ratios to determine the elastic stresses at web holes. They discovered that the vierendeel technique of analysis used to predict the normal stresses at the pierced portion was in excellent accordance with the experimental normal stresses. The lateral shear stresses predicted by this approach did not agree with the experimentally reported one.

Lupien and Redwood [25] investigated an experimental research on six simply supported specimen with mid depth rectangular web apertures. The apertures were strengthened laterally in one side of the specimen web that was assumed slender. They evaluated the specimens at several moment-to-shear proportions to examine the effectiveness and influence of one-sided strengthening for the opportunity to benefit from its economy in welding and operating. They evaluated the specimens at several moment-to-shear proportions to examine the effectiveness and influence of one-sided strengthening for the opportunity to benefit from its economy in welding and operating. They discovered that in certain cases, the strengthening applied only on one side of the web hole could be exploited. They additionally discovered that the required anchoring distance of the reinforcement is often longer than for the same size symmetrically positioned.

Redwood and Cho SH. [26] established a comprehensive technique of evaluation for the design of web perforation in steel beams. They studied the behavior of steel and composite beams having web holes, developing an approach for predicting maximum strength, and linked it to current design aids.

Prakash et al. [27] used ANSYS software to conduct a finite element study on steel beams with unstrengthened and strengthened central single web aperture. Their research focuses on the aspect ratio for apertures, deformation properties, load bearing capacity, and vierendeel processes. They

discovered that web apertures in the lower shear and high moment area function better than web openings in the extreme shear and reduced moment zone. They also noticed a significant decrease in strains and deflections by raising the level of reinforcement of the web aperture.

Thevendran studied the influence of web apertures in slender beams and Shanmugam [28]. The existence of web holes affects both the maximum strength and the lateral buckling ability of beams. Depending on the energy theory, a computational technique for predicting the maximum lateral-buckling stresses of slender, doubly symmetric beams with unstrengthened web holes was proposed. The numerically calculated critical values are compared to the empirically determined results. The study found a high level of correlation for both experimental and numerical data.

*Although earlier studies used different parameters in terms of:*

*Opening geometries, opening dimensions, single and multiple openings or failure mechanisms, neither of them explored the feasibility of preserving beam strength, rigidity and stability utilizing FRP plates or sections.*

### **I.6. Steel structure strengthening and FRP material:**

Attributable to the increasing deterioration of existing steel structures and bridge constructions during their useful service lives, the replacement of buildings is required for full operation capacities, but in certain cases, the expense of replacement is not feasible. Therefore the strengthening and reinforcing procedures which provide cost-effective and realistic solutions for renovating older and failing infrastructures have been required since the late twentieth century due to numerous types of deterioration to consider like corrosion, looseness in assembly, fatigue effort, introduction of web perforation, overload, fire or seismic effects.

Steel structures are increasingly being upgraded rather than demolished and rebuilt, for economical and environmental reasons. Experts evaluating constructions for higher or unusual loadings are discovering that novel methods of study, like as computer simulations, are uncovering flaws under operational and extreme circumstances. In such cases, a mechanism must be created to make the structure up to the needed quality. There are a variety of procedures that can be employed on constructions, but one should consider the fact that disturbance to regular phase should be kept to a minimum while work is being done. Existing buildings must be evaluated and strengthened using a practical and logical design concept. Generally, when increased load bearing capacity is needed of an existing structure, experts have the decision of strengthening the existing frame or installing new frames to repair or replace the current.

### **I.7. The primary processes in rehabilitating existing steel buildings:**

Estimating the bearing capacity of existing constructions is a difficult task. One of the crucial factors is the engineer's experience. In the first phase, the specialist must thoroughly evaluate the structure and provide some rudimentary estimations based on simple and efficient analytical methodologies, as well as a statement regarding the building's technical condition. Figure 2-1 depicts the basic processes in the appraisal of existing buildings.

### **I.8.Initial examination:**

When it is decided to reinforce certain portions of an existing structure or a particular part, a number of criteria impact the design concept:

- Data on important present situations, which is frequently scarce.
- Once the structure to be reinforced is frequently covered or hindered by traditional architectural or structural services systems that are expensive or difficult to eliminate.
- As structural rehabilitation, work is often hampered by the necessity for building activities to continue.
- The existing structure's ductility can restrict its capacity.
- The sensitivity of existing flanges to local buckling, and the absence of connections ductility.

Because non-structural expenses frequently surpass operational expenses, the number of work places mostly limits the real costs of a retrofit project rather than the quantity of work performed in each place, and this impacts structural design and analysis considerations.

The typical strategy of strengthening existing structures involves the following factors:

- Risk evaluation and vulnerability structure analysis.
- Critical preliminary examination.
- The importance of connections and their design specifications.

The overall objective is to:

- Critical structural members must be safeguarded.
- Offer structural systems durability.
- Make a certain portion of the construction stronger.

### **I.9.Evaluating present circumstances and reinforcement methods:**

A site inspection must also be made to assess the structure, when evaluating the current state of a steel structure, take note of the following: frame degradation, visible corrosion, Indications that structural changes may have been made without engineering evaluation, unexpected deformation in floor framework; fractures in slabs that are maintained; indications of foundation settlement; indications for novel roofing instrumentation; Suspended piping charges that are hefty; scaffolding or other hanging loads introduced without sufficient engineering evaluation.

The preceding are the several types of strengthening strategies:

- Passive techniques versus Active approaches.
- Techniques of Strengthening.

#### **I.9.1. Techniques of strengthening:**

- Cleaning and painting: Firstly, Protection of corroded sections is done by sweeping and compressed air cleaning or by aspiration in accessible and inaccessible places, in the next step painting has traditionally been employed as a method of surface protection. It's the most common method of steel corrosion prevention.



- Addition of steel material: A metal structure can be reinforced by increasing the section of its weakest components by adding steel profiles or plates (**Figure 1-11**), to enhance the load capacities and performance of deficient structures. Welding, riveting, or bolting are all choices for this technique. Bolting is a technique that may be employed in a variety of situations while welding is seen to be the most flexible and effective. It's a type of assembly that uses the local fusion phenomena to assure the metal continuity of two parts. For example, to avoid buckling of the flange or web panels, metal girders can be reinforced with horizontal or vertical steel stiffeners.



**Figure 1-11: Strengthening steel elements by addition of steel material**

- Strengthening connections: by angles that are seated; end-plate with partial depth; Framing; using high-strength fasteners instead ;Placing angles or plates to modify single-shear connections to double-shear links, installing a web stiffener plate; including steel covering plates.
- Span reduction: by including beams, columns, and girders; insert diagonally braces; include a steel-braced framework; improving the strength and flexibility of bracing systems.
- Adding combined acts: by partially or completely concrete encasing steel; shear connectors.
- Beam and connector post-tensioning.
- Member replacement: This may be cost-effective in some cases.
- Column reinforcement
- Modify the gravitational frame into a moment-resisting frame.

### **I.9.2. Estimating the loading capacity of existing structures:**

The yielding strength of the employed structure steel must be known in order to calculate the load capacity. As a result, tests shall be carried out to determine and validate the exact yield stress. One method is to analyze the steel to ascertain its real yield stress in the expectation that it is greater than the quantity utilized in the initial design.

### **I.9.3. Connections capacity improvement :**

The approach for strengthening existing moment and shear connections is just restricted by the expert's inventiveness. Following that, several methodologies will be discussed, depending on well-established but also new research results collected from multiple computational studies and experimental efforts. It is important to note that when current framing is modified or new capacity is desired, the capabilities of existing connections should be assessed.

### **I.9.4.Flexural strength enhancement of floor framing elements:**

Extant flooring structures can be strengthened in two ways to withstand greater loads:

- Add new frame to compliment the current framing.
- Strengthen current girders, connections and beams.
- The simplest option is generally to reinforce the old structural parts, assuming that the floor slab is strong enough to support the forces. The suitable method is to weld high strength Steels to the flanges (**Figure 1-12**).

#### **I.9.5.Columns' axial load capability improvement :**

In evaluating the vertical load capacity of columns, the buckle limitation condition and its changeable slenderness must be calculated. Column reinforcement decreases slenderness by raising the radius of gyration of the portion, and also stresses. Column buckles is a process that occurs at mid-height, hence raising column rigidity between both supports, rather than at the supports, is necessary to enhance column ability. Both procedures shown in **Figure 1-13** are beneficial, however the technique on the left improves the strong axis stiffness of an H-shaped section more efficiently.

#### **I.9.6.Handling Weld ability Problems:**

Chemical and mechanical tests are used to ensure weld quality. The former assesses suppleness, whereas the latter calculates the carbon relative value.

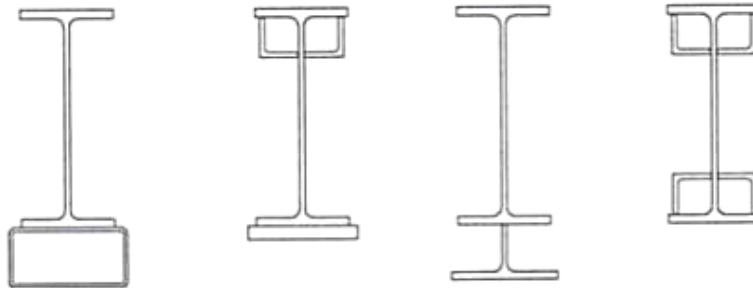


**Figure 1-12:Reinforced beams examples**



**Figure 1-13: Examples of reinforced columns**



### **I.9.7.Adding a novel frame to an existing frame:**

As with the interactions, there are several methods to link novel frame to old one. Welding additional steel elements to current members is a simple method that involves less accuracy than bolting, which needs piercing new holes into existing steel and fastening in the area.

### **I.9.8.Strengthening web openings of steel beams :**

#### **I.9.8.1.Existing methods for strengthening the web opening:**

##### **I.9.8.1.1.The Hicks and Lawson strategy:**

The sole approach used to reinforce the web aperture in steel beams is the use of a steel welded stiffener. A design rule based on transverse stiffeners made from steel plates and welded around the holes on one or two sides was proposed in SCI paper [1, 2] .This approach can assist in transferring stresses over apertures and preventing local web buckling.

##### **I.9.8.1.2.The Darwin method :**

The American Institute of Steel Fabrication evaluates the capacity of a structural member using web holes in bending moment rather than giving stiffening geometric elements [4] .The disadvantage of this technique is that it lacks data on stiffener form, as with anchoring length and stiffener location, making it hard to utilize as a practical reference when opposed to the Hicks & Lawson Technique[1].

#### **I.9.8.2Previous studies on strengthening steel beams with web openings using welded steel stiffeners :**

Hayder Wafi Ali Al-Thabhawee[29] investigated an experimental study on strengthening four steel beams under concentrated point load, The first was a plain web that served as the original case study, creating a round aperture in the web of specimens with and without steel ring reinforcements was used to examine the three other cases. All dimensions of tested specimens are detailed in **Figure 1-14**.The testing findings show that creating a hole in a web reduces the ULC and stiffness of steel I-beams greatly, the percentage loss in ultimate load potential of specimen with web aperture compared to identical steel I-beam without opening was 37.0 %.The maximum stress and plastic hinge were generated at the mid-span in the failure mechanism of the controlling beam, whereas the highest stress was dispersed surrounding hole for the steel beam with web hole , and the plastic hinges evolved at the openings location.

A steel ring with two distinct thickness values ( $t=6\text{mm}$  and  $t=8\text{mm}$ ) was welded along the perimeter of the web apertures to recover the ultimate load capacity and stiffness response lost Figure 2-6.Results were compared to a similar beam with a solid web. The Steel's behavior of I beams with aperture strengthening webs utilizing metal rings was found to be in good agreement with the performance of metal I beams with original webs. So when compared to the specimen without reinforced hole, the maximum load capacity obtained with strengthening hole utilizing metal ring of 8 mm and 6 mm thicknesses were enhanced by a rate of (47.8%) and (41.4%) correspondingly.

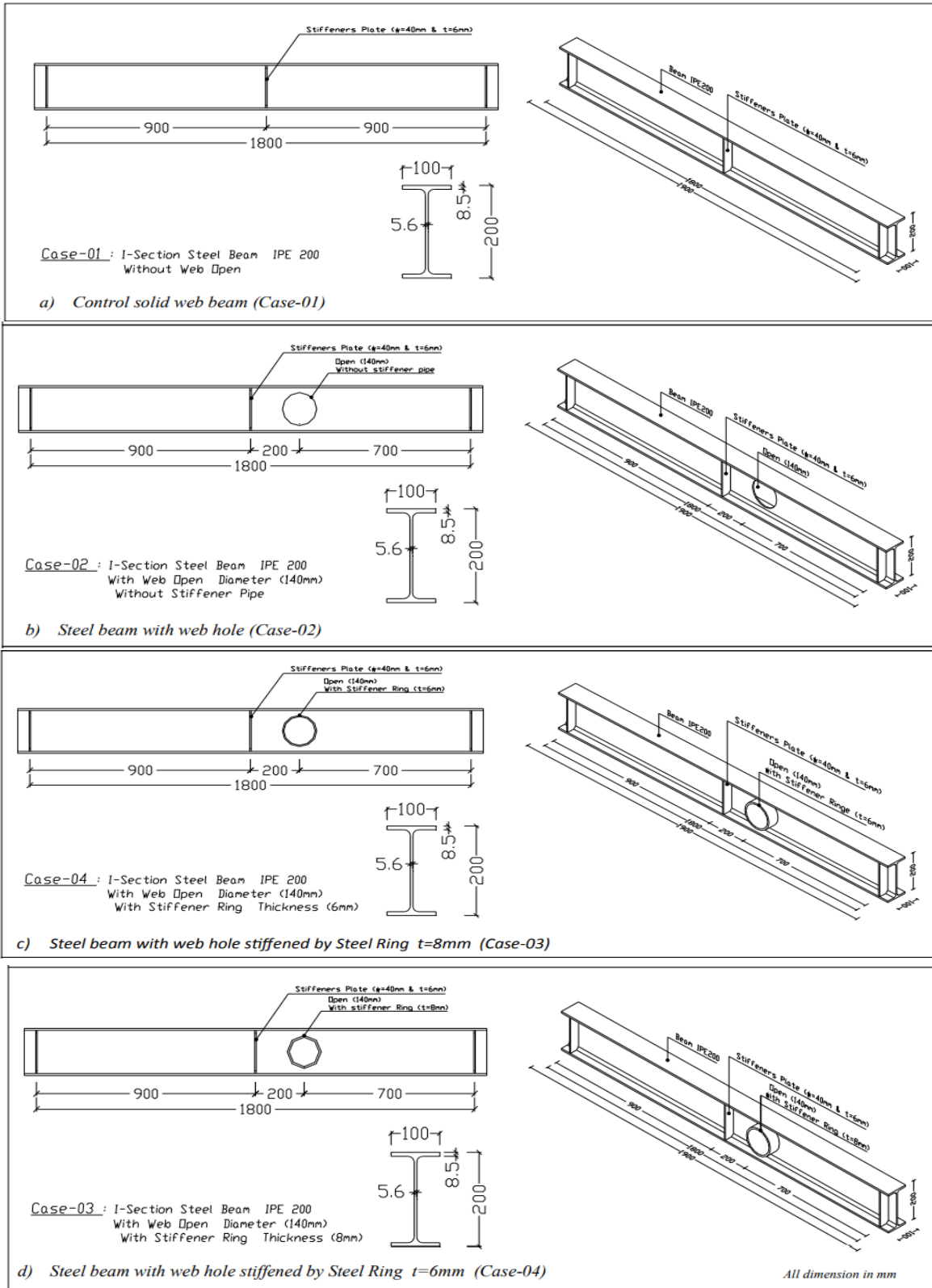


Figure 1-14: Experimental test details conducted by Hayder W [29]

K. Tsavdaridis and G. Galiatsatos [31] conducted a parametric FE analysis to evaluate the web-post buckling resistance of cellular beams with dual transversal stiffeners across the two faces of the web. The web aperture space ( $S/d$ ) proportion, web and stiffener thickness ( $t_w$ ) were the factors that were varied. In summary, welded transverse stiffeners were shown to be extremely successful in preventing out-of-plane buckling for up to  $S/D = 1,3$ .

M. F. Shaker and M. Shahat [32] did a numerical research on reinforcing non-compact steel girders web apertures, to be able to increase the beam's peak load capacity, this research tested the effectiveness of several varieties of reinforcements soldered at holes areas according to shape, size, and placement of the opening with regard to beam length. The most efficient method of strengthening to compensate for the beam's strength loss at the perforated part is the use of two long horizontal stiffeners upper and lower the aperture. Since it distributes shear stress along the gap to the nearby areas.

A numerical study was conducted also by Samadhan G. Morkhade and all [33] on castellated beams of different opening shapes: Circular, Square, Hexagonal and Octagonal and different opening sizes according to the beam depth:  $0.5 H$ ,  $0.625H$  and  $0.75 H$ . As per to the findings, Stiffener's around apertures of castellated beams boost the strength by 36 percent on average over unreinforced openings.

These traditional strengthening procedures, on the other hand, have a number of drawbacks, welded heavy steel plates adds large amount of dead weight to the structure and change its original property which can result in a disastrous collapse, the Mississippi River Bridge collapsed as a result of dead load expansion. The increase in dead load happened as a result of the placement of more components to the original building during maintenance. According to the National Transportation Safety Board study, the gap across the line of rivets in the viaduct's gusset plate was created by the excess weight on the bridge [34]. Besides to that the excellence of field procedure which is frequently criticized and fatigue sensitivity of repaired systems owing to the concentration of stresses caused by bolting and welding technique, in addition to that difficulty of repairing and installing heavy steel plates and the considerable period of service interruption during the installation time. All these drawbacks of traditional strengthening techniques encouraged researchers to find an alternative method of strengthening steel structures.

Recently materials that are made up of several different components, such as fiber Reinforced Polymer, have become more common in structural strengthening applications due to their better characteristics. FRP materials are lightweight and simple to work with. In comparison to other building and retrofitting materials, they are non-corrosive, durable, and less susceptible to environmental conditions. They have a high resistance to corrosion and fatigue, and their endurance is disproportionately strong in comparison to their weight [35].

### **I.10.FIBER REINFORCED-POLYMER :**

FRP is a composite material made up of two parts: fiber reinforcement and polymeric resin which is labeled as the matrix (**Figure 1-15**). The fibers improve the FRP composites' stiffness and strength, while the matrix permits load transmission between the fibers and protects them from mechanical and environmental degradation.

The matrix and fiber characteristics, as well as the fiber volume ratio and fiber orientation, all influence the characteristics of the FRP composite. Fiber-reinforced polymers are perfect for any design project that requires weight reduction, precise engineering, tight tolerances, and part simplicity in both manufacturing and operating. A polymer product is less expensive, quicker, and easier to make than an aluminum or steel product, with equivalent or better specifications and material strengths sometimes. Since World War II, modern composite fibers have been in use. In the last twenty years, these sorts of fibers have been used in the aerospace & defense sectors. Advanced composite materials were slowly introduced into the building industry in the early 1980s.

Glass fiber reinforced polymer and carbon fiber-reinforced polymer composites are the most often utilized among FRP composites in structural engineering they are used as pultruded plates, profiles, and sheets. (Figure 1-16), whereas aramid and basalt fiber reinforced polymer composites are less common.

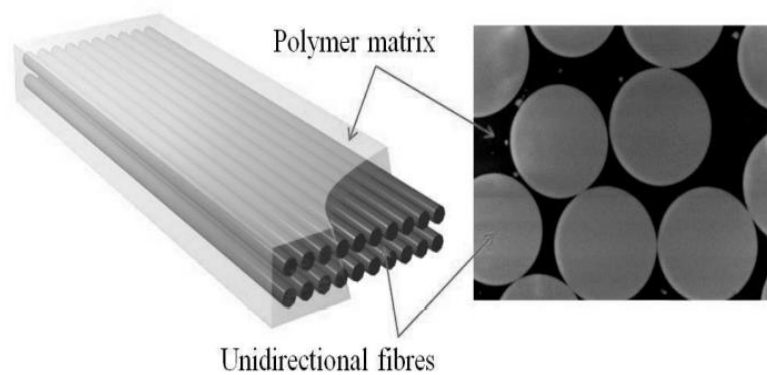
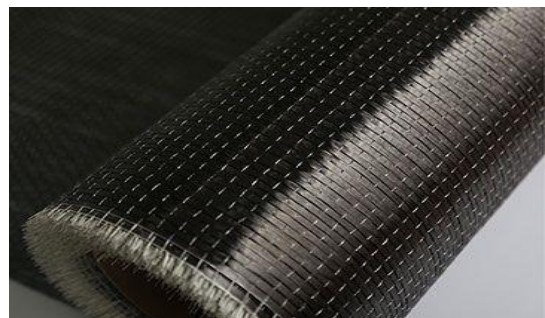


Figure 1-15:Fiber reinforced polymer



(a)



(b)



(c)

**Figure 1-16: Fiber reinforced polymer products: (a) plate – (b) sheet –(c) pultruded sections.**

### **L.10.1. Carbon and Glass Fibers :**

In practice, fibers are made by squeezing raw materials (in various stages) through small pores, then solidifying them (under various circumstances) and drawing them out (permits molecules to be arranged across the fiber orientation). In the industry, There are several different types of natural (animal, mineral fibers and cellulosic/plant) and man-made (inorganic and organic) fibers. However, inorganic synthetic fibers such as glass and carbon are the most commonly employed fibers for producing superior efficiency FRP composites.

Carbon fibers are carbonized fibers with a diameter of 5–10  $\mu$ m. The most extensively used materials for the production of Carbon fibers are viscose rayon, mesophase pitch, PAN fiber, and petroleum wastes (in a controlled environment). The primary properties of carbon fibers are: strong stiffness and tensile strength, lightweight, , fatigue resistance, Superior chemical/corrosion endurance, large temperature constancy ,effective vibration damping, electrical conductivity, and low coefficient of thermal expansion have made it incredibly populara wide range of construction applications. However, when compared to glass fibers, the main disadvantage of Carbon fibers is their massive price.

Glass fibers are now recognized as one of the most versatile production materials available. They're simple to make out of raw materials, which come in an almost limitless quantity. There are numerous types of glass fibers (GFs) that are often used in GFRP composites, based on the quantity materials utilized. The Glass fibers qualities immediately transferred onto the fibers are chemical stability, tensile strength and Young's Modulus [36].

As previously stated, the overall cost of project strengthening using FRP materials and their advantages has become available several prospects for FRP composites in both retrofitting existing buildings and new structures, besides to that in certain cases, FRP composites are the main viable material of reinforcing, particularly in locations where heavy machinery access is restricted or facility shutdown is difficult.

### **I.10.2. FRP-strengthening of metallic structures:**

The success of FRP composites in several domains motivated engineers to employ them for concrete and steel structural strengthening instead of traditional steel strengthening techniques which eliminates the need for large scaffolding and heavy lifting for welding. An overview of the usage of FRP composites for steel structural reinforcement is provided below.

### **I.10.3. Previous studies on FRP strengthening of steel bridges and structures beams:**

Several metallic girders in bridges and other structures have been reinforced using FRP composites across the world to raise the load-carrying capacity, stiffness, fatigue life, and required expansions

#### **I.10.3.1. FRP Strengthening of Bridges' Girders:**

Researchers are working harder to comprehend the dynamic and structural actions of metallic bridges reinforced with fiber-reinforced polymers (FRPs). The Kingdom United, the United States, Italy, Canada and Japan are among countries that originated this retrofit approach, as well as its study and execution. This could be seen in the following examples:

In Japan, UHM-CFRP plates were used to reinforce the Takiguchi Bridge in Tokyo. The bridge girders were reinforced by bonding 4mm thick laminates to the bottom lower flange, resulting in a optimum laminate thickness at mid-span of 14 mm [37]. Two bridges in the United States, I-704 and I-95 were reinforced with normal modulus CFRP plates [38]. The measured strain in the steel girder's tension flange was decreased by 15% after refurbishment, while the girder rigidity was raised by 12%. The King Street Railway Bridge in Mold was reinforced with 360GPa HM-CFRP strips, which served to strengthen six cast-iron girders, allowing 40-tonne trucks to pass through. Besides to that the Hythe Bridge in the United Kingdom was reinforced using normal modulus CFRP plates to enhance the load-carrying capacity to 40 tonnes [39]. These previous studies have shown that this approach can recover the elastic rigidity of deteriorated parts and maximum capacity to values equivalent to the unharmed girders and if significant stiffness improvements are sought, the utilization of a high modulus CFRP is advised..

D.Ke-wei and Z. Xu-ping [40] conducted a comparative study on the reinforcement and repairing effect girders with CFRP and GFRP, it was found that the use of carbon and glass fiber reinforced polymer can increase the steel girders' bearing capacity however, the reinforcement impact differs.

A normal modulus CFRP strip was attached to an aluminum honeycomb core to reinforce the Sauvie Island Bridge in Washington by Mossallam A [41]. The aluminum component was applied to enhance the distance among the CFRP strip and the steel beam's neutral axis, hence enhancing the member's stiffness.

Miller [42] assessed four more full-scale damaged steel bridge girders that had been modified with pultruded CFRP strips. The bottom flanges were judged to have degraded between 13 and 32 percent of their original state. The maximum failure force for both beams was enhanced 17 percent and 25% above the predicted capacities of deteriorating girders once pultruded CFRP laminates were attached to the upper and lower surface of tension flanges. These two beams' stiffnesses grew by 10% and 37%, respectively, from their starting stiffnesses.



Under static loads, Tavakkolizadeh and Saadatmanesh [43] examined the performance of composite steel girders reinforced with carbon fiber reinforced polymer. Consist of three specimens, made up by section profile W355x13.6 with A36 steel material connected to concrete slabs of 910-mm wide and 75-mm thick. The tested composite beams were reinforced with sheets of CFRP with varied thicknesses and numbers of layers joined to the bottom flange.

The sheets were bonded together with a 2 different viscous epoxy. Four point flexural test was used to evaluate the tested beams, the authors came at a conclusions:

- (1) The maximum load of the reinforced girders enhanced by 44, 51 and 76 percent for 1, 3, and 5 layers of carbon fiber reinforced polymer sheets, respectively.
- (2) As the number of layers reduced, the effectiveness of using the CFRP sheet rose, and stresses in the CFRP sheet reached 42 percent of maximum stress for the five-layer arrangement and 75 percent for the one-layer configuration at failure.
- (3) The numerical simulations produced conservative findings in projecting the enhanced girder's ultimate bearing capacity.

The findings of an experimental study on the performance of CFRP reinforced metallic girders were given by Al-Saidy and al [44]. The Carbon FRP plates were attached to the lower flange and in certain cases the web of the specimen. The influence of stiffness was investigated using two different kinds of Carbon fiber reinforced polymer plates of different tensile modulus. It was determined that the usage of CFRP plates can provide up to 45 % reinforcement and ductility was somewhat decreased by the insertion of CFRP plates.

#### **I.10.3.2. FRP Previous studies on strengthening solid steel structures :**

To evaluate the behavior of steel I beams reinforced by CFRP pultruded laminates, Colombi and Poggi [45] used a numerical and experimental approach. Four beams were used in the study, one un-strengthened and three CFRP-strengthened. A 2500 mm in length HEA 140 steel beam served as the reference beam named TR0. Both specimens TR1 and TR2 beams had a single layer CFRP strips with a width of 60 mm wide and thickness of 1.4 mm glued to the bottom flange using the epoxies Sikadur30 and SikadurR330. the bottom flange of the 3<sup>rd</sup> reinforced specimen, TR3, was bonded with 2 layers of CFRP strips utilizing epoxy resin Sikadur R30. Mechanical characteristics of the two epoxies were different. SikadurR30's elastic modulus and tensile strength were 4500 and 24.8 MPa, respectively, whereas SikadurR330's were 3800 and 30 MPa. Using the test platform indicated in **Figure 1-17**, three-point bending tests were conducted. Lateral supports were added to the TR0, TR2, and TR3 specimens to avoid lateral-torsional buckling, which happened when specimen TR1 was tested without one.

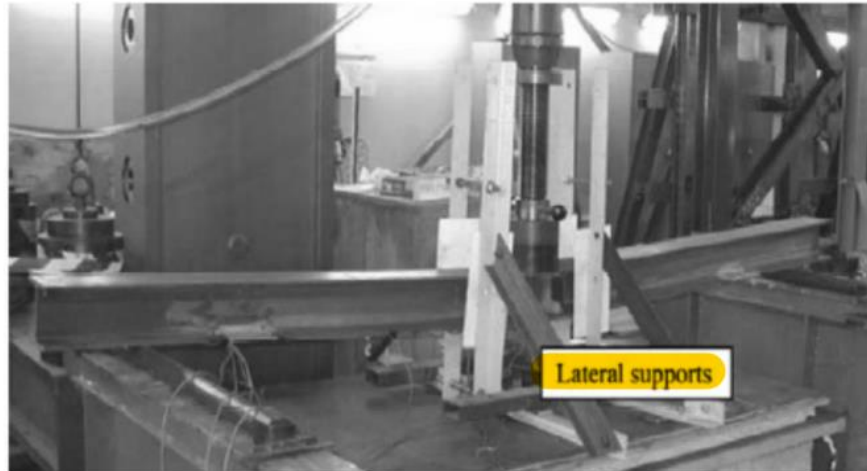


**Figure 1-17: Experimental test conducted by Colombi and Poggi[45]**

The CFRP-strengthened beams, TR1, TR2, and TR3, had ultimate loads that were 14 %, 31%, and 40% higher than the control specimen, TR0. Because of the transverse support and the use of distinct epoxy adhesive, specimen TR2 had a twofold increase ratio in peak load in comparison to TR1.

Galal and al. [46] bonded Carbon FRP plates and sheets to the lower flange of intentionally damaged steel specimen to reinforce them. In damaged areas, 5 layers of Carbon FRP sheets bonded using two distinct epoxies and anchored CFRP plates without bonding were placed. Debonding at the steel to CFRP junction and at the CFRP plates rupture were also found as failure mechanisms. In comparison to the purposely degraded specimens, the strength improvement was 25%. A method of anchoring was also studied. It didn't increase the bending capacity of the degraded steel beams, but it did have flexible and ductile response similar to a system bonded with epoxy

The glued pultruded CFRP laminate was used at the beam web for shear reinforcement of steel I-beams. To study this, Narmashiri and al [47] conducted FE analysis and experimental studies. Five specimens, a control reference specimen, and four strengthened beams in various locations were tested in a four point bending test. The shear region was 200 mm and 130 mm width and depth, and was bordered by two partial height stiffeners and two flanges close the supports. A 1.3 m in span length, 150 mm deep with a 6.6 mm web thickness, and 100 mm broad with 10 mm thick flanges were used in all prototypes. The experiment findings indicate that the increased force capacity of the strengthened specimens, which used three and two Carbon FRP strips on the two sides of the web, was roughly 52 %, compared to the reference specimen, while the increased maximum loads of the strengthened beams, which used 2 and 3 strips on one side of the web, were 43 % and 35 %, respectively, relative to the control beam. The control specimen failed due to flange buckling and web crippling, according to the researchers. In terms of failure mode, the results revealed that in the reinforced examples, both longitudinal delamination of the Carbon FRP laminates in the region near the impact loading or debonding of the Carbon FRP strips was initiated. Finally, the Carbon FRP reinforcement was able to reduce the web's shear buckling. This research shows the importance of bonding CFRP strips to both sides of the web compared to only reinforcing one side.



Vatonec and al. [49] evaluated the performance of metal tubes reinforced using pultruded Carbon FRP strips in various patterns. The Carbon FRP laminates were bonded to the upper, bottom, and both upper and lower sides of the steel pipes. Two un-strengthened metal pipes and eight CFRP-reinforced steel tubes were studied. CFRP sheets have a young's modulus of 165 GPa and maximum strengths of 2800 MPa .The CFRP mobilization capability was inhibited over the first two beams due to localized flange buckling. To minimize flange local buckling, the eight specimens' center lengths were packed with conventional concrete. A four-point loading mechanism was used to examine all beams. Compared to the unreinforced beams, the specimen with the single upper CFRP sheet displayed a lesser increase of 6% in flexural strength, while the specimen with the single top and double bottom sheets demonstrated an increase of 26%.Moreover, all of the reinforced pipes CFRP laminates débonded, and the upper sheets debonded before the bottom ones in every circumstance.

Zao and Al-Mahaidi [50] evaluated the influence of CFRP-reinforcement on the web-buckling capacities of steel beams. The experiment included seven reference beams as well as twenty-one CFRP-strengthened specimens, all of which were examined under compressive force. The web slenderness proportions of the seven reference specimens, ranged from 62.5 to 125. For every type, three different strengthening procedures were applied. The CFRP plates with unidirectional fiber were applied with the proper glue adhered to their webs on the upper, inner or either side. The test findings demonstrated an improvement in the peak load in each pattern when compared to the un-strengthened beams. The peak loads of the reinforced beams were enhanced by 40 percent to 200 percent when CFRP laminates were used on the external surface of the web while the ultimate loads were developed by 140 percent to 300 percent when CFRP was used on the bottom edge of the web, besides to that the maximum loads of the strengthened specimens were enhanced by 250 % to 500 % when CFRP laminates were used on the two sides of the web. Delamination of CFRP was a prominent mode of failure for all forms of strengthening (Figure 1-18).These findings show that employing CFRP on the to sides of the web to reinforce it is much more significant than using it simply on one side.

Fawzia and al.[52] looked into the performance of VHS circular steel tubes reinforced with Carbon FRP and exposed to tensile stress [12]. The strengthening method included the use of high-strength epoxy resins (Araldite 420). The strain distribution was investigated along the length of the CFRP joint and layer thickness. So when it came to retrofitting steel tubes, HMCFRP outperformed normal modulus CFRP. The adequate length of the bond was discovered to be roughly 50 mm for steel tubes bonded with the High modulus Carbon FRP technique and 75 mm for normal modulus Carbon FRP, it was also observed that the strain distribution reduced from the bottom of the CFRP sheet to the top .

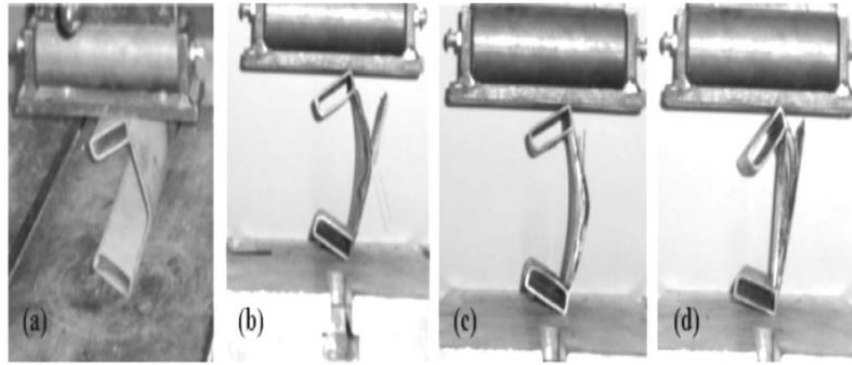


**Figure 1-18: (a) un-strengthened specimen , (b) CFRP on the outside , (c) CFRP on the inside , (d) Both sides have CFRP**

### **L.10.3.3. FRP Previous studies on FRP strengthening of steel beams with web openings :**

From the very few researches ,Al-khafajian and Al-abbas [53] used non-linear computer simulation to analyze the performance of steel beams with web holes enhanced by Carbon FRP laminates .The influence of forms, the positions of web holes, and the quantity of layers were the characteristics considered in this investigation. For the parameterized investigation, an IPE 300 section profile beam with simple supports and a span of 2200 mm in length was employed utilizing the four-point flexural test. One and two web aperture was created with round, square, and rectangular forms in the mid span and shear regions, accordingly. With the reinforcing procedure, the specimens lower load bearing capability by 38 percent was raised by 15-36 percent. There was also remarked a reduction in the specimens deflection. Despite the fact that using Carbon FRP plates surrounding bending zone apertures did not improve force capability, In the shear zone, a rise of 4 to 14 percent for one layer carbon FRP and 15 to 36 percent for 3 layers carbon FRP was found.

S. Mustafa and al.[54] did a numerical study to identify the proper Carbon FRP plate length of placed upper and lower the web holes as in straight line. To evaluate the impact of varying aperture forms and positions of web openings reinforcement utilizing Carbon FRP laminates , the researchers used the specimen of the experimental investigation conducted by Deng and Lee [55] .For both the flexural and shear zones, individual circular and rectangular holes were introduced. For every perforation, the CFRP plate's length that assisted in recovering the original beam's load capacity was determined, and referred as adequate length. Different acceptable lengths of Carbon FRP strengthening were found:

- The effective CFRP length for circular perforation in the shear region:  $9,6D$ .
- The effective CFRP length for circular perforation in the mid span region:  $3,6D$ .
- The effective CFRP length for rectangular opening in the shear region:  $5,25L$ .
- The effective CFRP length for rectangular opening in the mid span:  $1,65L$ .

Where:

D: The circular opening's diameter.

L: is the rectangular opening's length.

Enhancing the carbon FRP plate length beyond what was necessary did not improve the maximum load and properties of the tested specimen since the added length were mostly removed from the highly stressed concentration area surrounding the aperture.

M. Altaee and al [56] conducted the first full scale experimental investigation to determine the performance of steel beams with rectangular web holes reinforced using Carbon FRP plates'. A six-point bending test with lateral restraint was adapted to a simply supported specimen to avoid lateral-torsional buckling. There were three instances in this experiment:

- Specimen with single aperture in the middle of the span referred as :( B1-RO).
- Specimen with twin mid span holes referred as : (B3-RO) .
- Specimen with a unique aperture in the coupled bending and shear zone referred as: (B2-RO).

The lower faces of the upper and bottom flanges, as well as the two sides of the web, were covered with Carbon FRP plate's laminates .All carbon FRP plates were mounted longitudinally, aligned to the specimen's horizontal axis.

The testing revealed that B1-RO enhanced load ability by 20% over original beam B0 and was the strongest of the 3 reinforcement methods. In comparison to solid beams also, the ultimate load of B2-RO and B3-RO increased by 5% and 10%, respectively. This experiment concluded that carbon FRP reinforcement not only enabled to restore the initial capacity of the solid steel beam but also exceeded its hardness .The researchers came to the conclusion that CFRP reinforcement improved the strength, rigidity, reliability, and maximum state performance of the steel beam with web hole.

Mohammed H [57] and colleagues performed shear-loading tests on seven steel-plated girders having web openings. Four of these specimens are reinforced, while the remaining other three are control girders. The latter one has a square web aperture shape; another has a diamond web hole, while the third has no entrance at all. To assess the most efficient reinforcement technique, the webs of the reinforced beams were adhesively bonded to CFRP of varied designs, as illustrated in **Figure 1-19**.

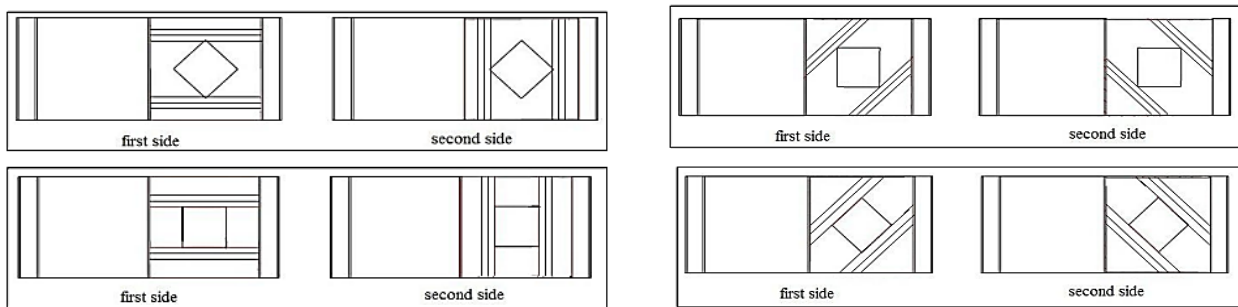


**Figure 1-19: Strengthening arrangement used by Mohammed H [57].**

It then investigates the percentage gain in maximum shear ability of perforated beams with a given size and position, wherein the latter is equivalent to 40 percent of the total depth of the web .Initially, the maximum shear load of the CFRP-reinforced specimens wit having square web

openings is greater than the unreinforced specimen with a square web opening shape, varying from 8.7 percent to 15.7 percent. Furthermore, a range of 9.8 percent to 21.5 percent, the peak shear force of the CFRP-reinforced girders having a diamond web hole is greater than the corresponding control girder. The following tables (From **Table 1-1** to **Table 1-4**) resumes the very few researches conducted on strengthening steel beams with web openings using FRP materials and their conclusions.

The few studies that have been done are limited to recover the flexural strength of steel beams after the creation of web openings using FRP plates or sheets without a consideration of the bond behavior between steel and FRP except the experimental test conducted by M. Altaee [56]. Many aspects are yet to be investigated. *In this study, a novel technique on strengthening web post-buckling of cellular beams using FRP products will be suggested and novel strengthening configurations will also be proposed for the strengthening of single rectangular web opening in different location along the span in order to acquire more sufficient information about the use of FRP laminates to strength steel beams with web openings and achieve an advanced phase in which guidelines and codes can be developed to assist engineers in the design and application of such system.*

M. Altaee[56]	Al khfaji and Al Abass[53]	Authors
Experimental	Numerical	Research type
305x102x25 UKB section of 3000 mm clear span	IPE 300 section of 2200 mm clear span	Beam details
CFRP	CFRP	FRP type
Static flexural test of 6-points	Static flexural test of 4-points	Load type
/	Web opening shape ,position and number of CFRP layers	Parameters
Rectangular	Square, circular and rectangular	Opening shape
Mid span/Shear zone	Mid span/ Shear zone	Opening position
One and Two	One and Two	Openings number
Longitudinal plates at the lower face of the tension and compression flanges, as well as the web upper and below the aperture	Bonded all over the opening	FRP configuration
When a web hole is inserted, CFRP reinforcement improves the beam's strength, rigidity, service life, and peak state behavior (s).	Reinforcing the web aperture with CFRP plate decreased the deflection of the specimen as well as the amount of layers, raising the load performance by 15 to 36 %.	Conclusion

Table 1-1 : Details about the two studies carried out by M Altaee [56] and Al khfaji[53]

Hamood and al [57]	S. Mustafa and al [54]	Authors
Experimental	Numerical	Research type
620 X 125 I-section of 1220 mm clear span	127x76 Ub section of 1200 clear span	Beam details
CFRP	CFRP	FRP type
Static flexural test of 4-points	Static flexural test of 3-points and 4-points	Load type
/	CFRP laminates length and thickness	Parameters
Square, diamond	Circular , Rectangular	Opening shape
Shear zone	Mid span ,Shear zone	Opening position
One	One	Openings number
Longitudinal, perpendicular, and diagonal CFRP plates at the web opening's border	longitudinal plates bonded upper and lower the web perforation	FRP configuration
With suitable CFRP reinforcement. Shear force increases by 8.7-15.7 percent and 9.8-21.5 percent for rectangle and diamond apertures, accordingly.	By ensuring an appropriate length of CFRP, the reduction of load capacity of steel beam was improved.	Conclusion

Table 1-2 : Details about the two studies carried out by Hamood [57] and S Mustafa [54]

M. Altaee and al [59]	S. Mustafa and al [58]	Authors
Numerical	Numerical	Research type
305 X 102 X 25 UKB section of 3000 mm clear span	127X76 UB of 1200 clear span	Beam details
CFRP	CFRP BFRP	FRP type
Static flexural test of 6-points	Cyclic loading	Load type
/	FRP plate length	Parameters
Rectangular	Circular, rectangular	Opening shape
Mid span, shear zone	Mid span, shear zone	Opening position
One, two	One	Openings number
Longitudinal plates bonded to the tension and compression flanges, as well as the web upper and below the aperture	Patterns of longitudinal plates , longitudinal and vertical plates, and curving over apertures	FRP configuration
An improvement in load carrying capacity by using CFRP plates, if the aperture was in the flexural zone or the high shear area, CFRP plates can compare with standard steel plate reinforcement.	The introduction of CFRP plates aided in the recovery of beam force nevertheless resulted in a loss in ductility. For cyclic loads, BFRP plates with greater lengths provided the same force recovery as CFRP plates	Conclusion

Table 1-3 : Details about the two studies carried out by M Altaee [59] and S Mustafa [58]

Ezzat and al [61]	M. A. Kadhim and al [60]	Authors
Experimental and Numerical	Experimental	Research type
120 X 65 I-section of 1500 mm clear span	512 X 120 I section of 2300 mm clear span	Beam details
CFRP	CFRP	FRP type
Static flexural test of 4-points	Static flexural test of 3-points	Load type
CFRP configuration	CFRP configuration	Parameters
Circular, rectangular	Circular, square	Opening shape
Shear zone	Shear zone	Opening position
Four, Six	Two	Openings number
A perpendicular plate in the web, a transverse plate at the lower face of the tension flange, or a combination of the two preceding configurations	Horizontal, vertical, and diagonal arrangements	FRP configuration
Since there were web apertures in shear zones, the most successful technique was to use CFRP in shear and tension areas.	Reinforcement with CFRP laminate increased shear load by 52.6 percent and 63 percent for specimens with circular and square apertures, respectively.	Conclusion

Table 1-4 : Details about the two studies carried out by Ezzat [61] and M Khadim [60]



### I.11. Behavior of FRP and steel bonds

This section reviews existing expertise of FRP-strengthened steel structures in which the efficiency of this reinforcing system is dependent on the stress transfer characteristic in FRP-steel junction. The first subsection goes over the different types of FRP-to-steel adhesive joints. The influence of interfacial surface pretreatment on adhesive bonding is discussed. Surface characterization and the impact of surface preparation processes on surface properties are given with special consideration. Surface assessment and the impact of surface preparation processes on surface properties are given with careful attention. Following that, existing research on the performance of FRP-steel glued joints is discussed in order to underline the importance of surface treatment in adhesive bonding.

The functional usage of FRP in conjunction with steel can be classed into two groups, in a similar way to the usage of FRP in concrete constructions:

- **Applications that are bond critical:** In which the adhesive layer's interfacial shear stress transfer function is vital to the structure's performance.
- **Applications that are contact critical:** In which the steel and FRP must keep on interaction for effectiveness interlayer normal stress transmission, that is a key to the fiber reinforcing polymer strengthening performance.

Externally bonded FRP strengthening for bending reinforcement of steel beams and confinement of concrete-filled steel tubular elements using FRP jackets are two applications of FRP in steel structural reinforcement. The contact behavior of FRP and steel in all bond-critical applications is essential in deciding when failure happens and how successfully the FRP is used. Interfacial failure appears inside the concrete element only little inches from the adhesive and the concrete contact in most fiber reinforced concrete structures. Furthermore, because steel has a significantly better tensile strength than glue, failure in the steel substrate is unlikely. As a consequence, interfacial fracture can only proceed inside the adhesive layer which is named cohesion failure or even at the material interfaces which is named adhesion failure between the steel and the glue (**Figure 1-20**). If the capacity of FRP-reinforced steel structures is determined by adherence collapse, therefore the interfacial bond strength is determined by the treatment of the steel and FRP surfaces, and even the adhesive's bond abilities.

Because adhesive breakdown is dependent on surface preparation, and surface maintenance, particularly to steel element which is hard to manage on workplace, the formulation of conceptual models is lot extremely extensive.

### I.12. Bond failure:

Bonding failure can happen at the adhesive and the steel contact or at the adhesive and FRP junction in a FRP-steel glued connection. Bonding problems at the FRP and steel interaction has been rare once the Fiber reinforced polymer is produced and attached to the element on place using the wet lay-up procedure [39]. To achieve a nice and clear FRP interface for bonding when using pultruded FRP strips the peel-ply must be erased before bonding. Whenever a peel ply isn't available, the surface should be sanded and kept clean prior to actually bonding [62].

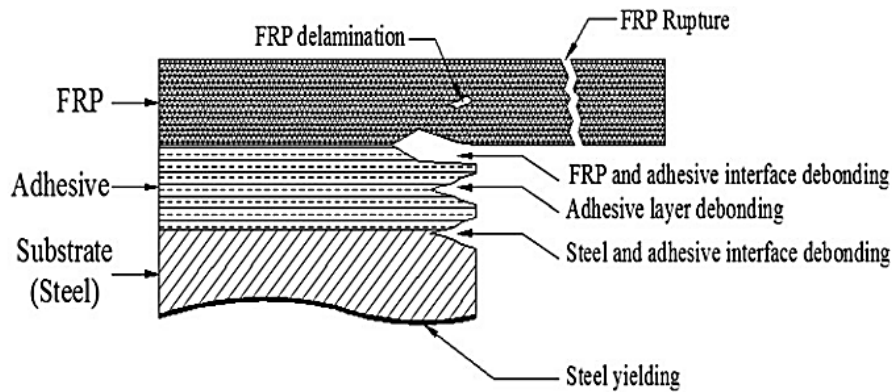


**Figure 1-20 : FRP –Steel bond failure**

The probability of bonding failings at the FRP/adhesive junction can be considerably reduced using these strategies [39]. In the other hand, because damage at the steel and adhesive interaction is far more common, enhancing the steel area for epoxy bonding has attracted researchers' attention [63, 64].

A good interaction between adhesive and steel contact achieves from mechanical and chemical connection between the adherents [63, 65]. The adhesive should be in direct touch with the steel area as the initial and most important prerequisite for forming a strong connection between adhesive and steel. This necessitates an adhesive with a reduced enough viscosity to run freely above the steel substrate as well as covering the pores [66].

If the steel area is polluted, only a low viscosity epoxy will get into touch with the thin pollutant layer, resulting in a poor bonding [63]. As a result, cleaning the steel area before gluing is required. The steel substrate already have a significantly elevated surface energy than the glue, which must also have a low viscosity, in order to spread the adhesive on the steel surface [63]. Chemical bonds are formed when the adhesive and the steel face interacted, so chemical bonding are formed primarily by the chemical components of the metal surfaces and the adhesive, therefore choosing a chemically suitable glue is critical [63]. Despite chemical coupling is responsible for the majority of the good adhesion between adherents, mechanical bonding could also play a role [63].

When porosity are present on the surface, the glue will seep into them and will operate as a restricted interlock when hardened. As a result, bonding is influenced by the epoxy characteristics and also the surface roughness and shape of the metal [65]. Although roughening the area can improve mechanically adhesion, it can also decrease the quantity of interactions among different adherents. As a result, the most important qualities of a metallic surface are:

- Surface power.
- Surface chemical content.
- Surface ruggedness.

which are frequently utilized as essential signs to define a metal surfaces for bonding [67] chemical treatment and mechanical abrasion via sand blasting or even other equipment are two of the most prevalent methods for cleaning a metal surfaces [39].

The initial stage in preparing metal surfaces for bonding agents is solvent treatment, which eliminates oils and other impurities from the surface. Chemical treatment, on the other hand, has only a minimal impact on bonding strength since it does not modify the metal surfaces qualities. It is critical to utilize a volatility solvent such as acetone to reduce the number of impurities and their detrimental effects on bonding strength [68].

Automated sanding roughens the area and eliminates any vulnerable surface layers such as the oxide layer, resulting in a reactive chemical smooth surface for epoxy coating [63]. Grinding with roughness pads and metal brushes, as well as sandpaper, are multiple options of changing the surface, with grit-blasting seems to be the most successful [39]. According to Harris and Beevers [70], sandpaper improves surface power and roughness, which promotes bonding. As a result, many current recommendations propose grit-blasting.

Grit-blasting introduces grit residue, which affects the chemical structure of the area [69]. As a result, it's critical to choose a grit that's available to react with the glue. Although the grain dimensions employed in abrasives can have a substantial impact on the material attributes, Harris and Beevers [70] reported the influence of grit size on bonding tenacity is restricted inside the range of particle sizes investigated in their research. Sandpaper also creates abrasive dust on the face, that can affect bond strength [39]. As a result, following grit-blasting, it's critical to maintain the cleanliness again. Dry-wiping or using a vacuum head to remove fine dust was advised by Hollaway and Cadei 2002 [39] over the cleaning with solvent which only completely clear out the particles and distribute the leftover grains of the region. El Damatty and al [62] on the other hand, proved that by applying a large amount of solvent, the dust could be completely removed and a clear surface generated.

To prevent contamination of the area or the creation of a thin oxide film, the epoxy must be placed quickly as possible just after surface preparation [70]. Cadei and al. [71] proposed that perhaps the time among sand spraying and applying the epoxy must not surpass two hours, whereas Schnerch and al. [64] recommended twenty-four hours. A side from using the proper surface treatment methods, it's crucial to define the area to see if it's suitable for the establishment of an excellent adhesion.

### **I.13. Bond performance:**

Debonding emerge in FRP-reinforced steel constructions in two ways:

- Intermediate debonding : Debonding outward from the extremities of the FRP laminates.
- End debonding: Bond failure begins at the end of FRP laminates.

Large interfacial shear stresses produced by the existence of a fracture or the steel yielding cause a breakdown in the former [72,73]. Large interfacial peeled forces and also inter laminar stresses towards the extremities of the FRP plate cause fracture in [35]. Intermediate debonding

was shown in FRP-reinforced steel beams and sections reinforced to resist to the local buckling [73], Whereas the debonding in the plate end was shown in flexural reinforced steel specimens and steel elements enhanced over end bearing stresses [55] or even other forces that cause buckling in a specific area.

The behavior of simple bonded joints must first be characterized in order to fully comprehend and simulate debonding occurrences. Simple single-lap FRP-to-steel glued junctions can reveal important information on the behavior of FRP-steel glued interface in a beam once intermediate debonding is significant because interfacial shear forces govern intermediate delamination. Furthermore, comprehending the basic FRP-steel glued junction is the initial stage toward appreciating much extremely challenging phenomena of FRP-steel interactions exposed to simultaneous contact shear and peeling forces.

Collapse of the steel element is impossible in connected FRP-to-steel junctions as bonded FRP-to-concrete junctions while failure happens inside the concrete near the concrete/adhesive interface. As a result, whether adhesion collapse at the adhesive and steel interaction or the FRP and adhesive interaction is prevented, steel-FRP linked joints usually fail due to adhesive cohesion failure. Unlike this, the common principles such as interfacial fracture energy that have been created for FRP-to-concrete connected junctions can also be used to FRP-to-steel adhesive junctions.

Various researchers have utilized several test procedures for adhesive joints [35], as well as tests on beams, double-lap shear testing [45], shear-lap tests [62] and pull-off testing on a single lap [74]. Regardless of the methodology utilized, the majority of research has concentrated on the maximum load named the bond-slip relationship and bond strength, which seem to be the principle two characteristics features of junction behavior.

### **I.13.1 Strength of the bond:**

In a bonded joint test, the strength of bond is the maximum tension stress that the FRP plate can withstand prior debonding from the element. Numerous experiments on FRP-to-steel joined connections have found that bond strength doesn't often grow increasing the length of the bond. Any subsequent rise in length of the bond does not result in another rise in strength after the bonding reaches a specified amount of length [74], this was also observed with FRP-concrete bonded junction experiments [75]; So the effective bond length referred as ( $L_e$ ) is defined as the length at which no additional bond force will arise [75]. Predicting bond strength is critical when engineering FRP-to-steel connected junctions. There are two strategies:

- Strength-based methods, that presume that the strength of the bond is achieved once the adhesive's highest stress/strain attains its respective force [76].
- Fracture mechanics strategies, which seem to be comparable to those for FRP-to-concrete glued joints and surmise that the strength of the bond is attributed to the interfacial fracture energy [75].

Steel-to-steel glued junctions have also used strength-based techniques this was observed in the study conducted by Hart-Smith [77] and also the research conducted by Volkersen [78]:

- The maximum shear stress criterion.
- The maximum main stress criterion.
- The maximum shear strain criterion .

Were all employed as fracture mechanics for the bond. When the corresponding strength is attained in these strength-based strategies, collapse is supposed. The first glue cracks means that the ultimate load of the glued junction is attained. Nevertheless, previous research on concrete-FRP glued junctions under pressure has demonstrated that glued junctions with bond lengths greater than ( $L_e$ ) do not always break when the relevant force is reached [79]. Strength-based explanations are inadequate to describe similar behavior. Strength-based techniques, on the other hand, can however provide accurate forecasts for glued joints with reduced length of the bond and if the glued junction fails completely as soon as the first fracture in the glue shows.

An exact estimation of interlayer strain and stress dispersion is necessary for the methods based on strengths to be employed in estimating the endurance of the bond. This crucial problem has sparked a lot of studies [78, 79, and 80]. These investigations include both analytical and finite element (FE) research. The correctness of such analysis, on the other hand, is dependent on the reliability of the premises used to arrive at the results. These introduce neglecting peeling stresses and presuming that their influence is insignificant [78] maintaining a constant stress condition well over glue layer, and idealizing the FRP plate end's border shape as a square end.

These estimates can diverge greatly from truth, leading to severe inaccuracies, according on the junction arrangement and load situation. Zhang and Teng [80] provide a comprehensive overview of contact stress testing. Fracture mechanics strategies are greater than strength-based strategies for estimating the strength properties of concrete-steel and FRP to concrete glued junctions, according to available research. The strength of the bond is largely determined by the interfacial fracture energy rather than the epoxy power, according to fracture mechanics-based approaches. Some theories therefore prove the origin of an adequate bond length, as seen in FRP-to-steel glued junction experiments [74]. Lately, Xia and Teng [74] carried out a number of single shear pull off experiments to greater explain the entire span of behavior of steel-FRP glued junctions. her findings proved that a cracks mechanics based methodology for predicting the strength of the bond of steel-FRP glued junctions can be used. Unfortunately, the impact of adhesive properties and physical features on bond-slip behavior and hence interfacial fracture energy was not taken into account.

### **I.13.2 Bond-slip concept:**

The necessity of an appropriate bond-slip concept in comprehending and modeling the behavior of FRP reinforced concrete structures has been demonstrated in available studies on concrete-FRP attached interactions [81]. In a same way, a precise bond-slip concept is critical for comprehending and simulating the behavior of FRP-reinforced steel structures. The interaction with both localized interfacial shear stress and proportional slip across the adjacent adherents is described by a bond slip theory. As a result, the behavior of the glued interaction under mode-II (shear stresses) is described by a bond-slip theory.

When guessing the bond-slip model experimentally, ensure that the testing meets the pure mode-II stress requirement. Mode-II loading situation could be hard to ascertain with every one of the available bond test set-ups attributable to plate edge ripping pressures. The named single-shear pull-off test near-end supported is actually a great way to investigate the bond-slip behavior of FRP-to-concrete glued junctions [82], in addition, it was used in a previous research conducted by Xia and Teng 2005 [74] on the behavior of steel-FRP glued junctions.

Despite the fact that releasing stresses are confined to a restricted area at end of the plate and hence have no effect on the system's behavior [82]. In these types of bonding tests, there has been no experimental or numerical evidence of purely shear stress.

Lu and al.[81] carried out an evaluation of bond-slip models for FRP-to-concrete glued junctions and suggested new bond slip with two branches features, both comprising a branch that ascends and descends. The geometry of the bond slip model and the corresponding degree of precision varied between them. A bi-linear bond-slip model with acceptable precision is the basic variant of such bond-slip theories. The maximum local bond stress  $\tau_{max}$  and the related slip  $\delta_1$  are the essential factors.  $G_f$  that is the area in the form contained by the bond-slip graph and the horizontal axis. When the local bond stress falls to zero, the slip is called  $\delta_f$ . These variables are frequently linked to the tensile strength of concrete for FRP-concrete glued junctions, as concrete is generally the weakest point in the connection. As a result, the formulations derived for these characteristics should not directly relate to FRP-steel glued junctions, in which the adhesive is typically the missing point. Xia and Teng [74] demonstrated that a bi-linear interact slip concept could well be employed for steel-CFRP bonded junctions with bond slip variables determined by adhesion characteristics. This fact is thought to be applicable exclusively again for brittle adhesives utilized in their research, that exhibited a linear-elastic slope till brittle tensile fracture was reached.

#### **I.14. Theoretical model for FRP—Steel glued joints:**

As mentioned above the bond shear stress and proportionate slipping between pair adherents glued together are depicted in a bond-slip model. Delamination fails in FRP-strengthened steel elements require an appropriate bond-slip concept for the FRP-to-steel interaction, which is critical for correct modeling. Yuan and al.[79] used a bond-slip model for the interface to predict the complete delamination transmission mechanism of a glued junctions. A theoretical model is introduced in this part for estimating the whole debonding transmission procedure of FRP-steel glued junctions. For different loading phases, formulations for the interfacial shear stress propagation and the load-displacement behavior are produced using Yuan and al [79] techniques. During the procedure of creating empirical expression for the complete range behavior of glued junctions using the bond slip approach, the bond strength model is investigated and the notion of the effective bond length is also defined using an equation.

##### **I.14.1 Interfacial fracture energy:**

The bond slip behavior of an interaction and the strength of the bond a glued junction are both determined by the interfacial fracture energy  $G_f$ . As a result, a prototype that can estimate the



fracture energy of the interface of FRP-steel glued junctions based on the basic parameters of the joints is required. Following an experimental research employing linear adhesives, Xia and Teng provided the only formula for estimating  $G_f$  of steel-FRP contacts. Xia and Teng [74] suggested the following formula:

$$G_f = 62 \left( \frac{\sigma_{max}}{G_a} \right)^{0.56} t_a^{0.27} (\text{N/mm}^2 \cdot \text{mm}) \quad (1)$$

Where :

$G_a$ : Shear modulus .

$t_a$ : Adhesive thickness layer .

When the preceding equation estimations of Xia and Teng [74] is verified to the test findings , it was discovered that, despite the suggested formula makes good projections for linear glue, it exceeded the fracture energy of non-linear glue. The findings of the tests revealed that nonlinear adhesives with a reduced young's modulus however a higher deformation capability can have a significantly greater interfacial crack energy than linear adhesives with equivalent or also greater tensile strength. A closer look at the test results, reveals that the interfacial facture energy is relative to the square of the glue tensile strain energy. D. Fernando [83] proposed the strongest equation to estimate  $G_f$  according to the previous information :

$$G_f = 628 t_a^{0.5} R^2 (\text{N/mm}^2 \cdot \text{mm}) \quad (2)$$

Where:

$t_a$ : Adhesive thickness layer.

R: is the adhesive's tensile strain energy

This equation's predictions is also verified to the experimental test findings found by Xia and Teng [74] .The fracture energy interface scores were estimated based on the matching interaction strengths in Xia and Teng [74] test because they were not published. When a tensile stress-strain curve wasn't really supplied for the glue used in Xia and Teng [74], it was considered to be a elastic linear material and it was assumed that the strain energy was:

$$\frac{\sigma_{max}^2}{2E_a}$$

With:

$E_a$ :The adhesive's elastic modulus.

It was found that the proposed equation predicts all given test results with a high degree of accuracy.

## **I.15. FRP-to-Steel bonded interface bond-slip models:**

### **I.15.1. Linear Adhesives:**

The linear adhesive has a roughly bi-linear form with an ascending and descending curve:

- The bond–slip curve's starting rigidity is much higher than the secant stiffness at the maximum peak.
- With increasing slide, the slope of the falling segment falls.

The preceding observations imply the bond-slip trajectory for a FRP-to-steel interaction is quite identical to the bond slip graph for a concrete-FRP contact [81]. Based on the FRP-to-concrete contact models presented by Lu and al. [81]. D. Fernando [83] streamlined it for usage with FRP-to-steel connections. The preceding-mentioned properties of a nonlinear bond slip curve were captured by this approach, as well as the conventional bi-linear prototype. It's worth noting that Lu and al.[81] also presented a rather advanced model depending on their numerical model at the mesoscale. However, the specific model's variables are influenced by the three dimension constitutive behavior of concrete, that differs from that of glue. It's important to note also that Xia and Teng [74] suggested a bilinear bond slip concept for FRP-steel interactions .Lu et al. [81] suggested a simple model that looks like this:

$$\tau = \tau_{max} \sqrt{\frac{\delta}{\delta_1}} \quad \text{if } \delta < \delta_1 \quad (3a)$$

$$\tau = \tau_{max} \exp\left(-\alpha \left(\frac{\delta}{\delta_1} - 1\right)\right) \quad \text{if } \delta > \delta_1 \quad (3b)$$

$$\alpha = \frac{3\tau_{max}\delta_1}{3G_f - 2\tau_{max}\delta_1} \quad (3c)$$

Where:

$\tau$  : The bond shear stress .

$\rho$ : is the slip.

Because of the major discrepancies between FRP-steel glued junctions and FRP-to-concrete glued junctions as described before, the formulations offered by Lu et al. [81] for  $\tau_{max}$ ,  $\delta_1$  and  $G_f$  are not applicable for FRP to steel joints .

Either linear or non-linear glues, maximal bonding shear stress was shown to be distinct of glue thickness and longitudinal stiffness of FRP plate. As a result, regarding the test findings, the following equation was provided by D.Fernando [83] :

$$\tau_{max} = 0.9 \sigma_{max} \quad (4)$$

It's acceptable to assume that  $\delta_1$  is proportional to the rigidity of epoxy layer and the maximum interaction shear stress  $\tau_{max}$  with FRP-to-steel glued junctions with a linearly epoxy. The next formula was derived by D.Fernando [83] as a consequence of the assessment:

$$\delta_1 = 0.3 \left(\frac{t_a}{G_a}\right)^{0.65} \sigma_{max} \quad (5)$$



It's important to keep in mind that Eq (4) applies to linear and non-linear glue, while Eq (5) specifically applies to linear adhesives. In addition, Xia and Teng [74] did not published the test maximum bonding shear stress or even the related slip for their examples. In addition to that Lu et al.[81] proposed a bi-linear bond-slip prototype:

$$\tau = \tau_{max} \frac{\delta}{\delta_1} \quad \text{if} \quad \delta \leq \delta_1 \quad (6a)$$

$$\tau = \tau_{max} \frac{\delta_f - \delta}{\delta_f - \delta_1} \quad \text{if} \quad \delta_1 < \delta \leq \delta_f \quad (6b)$$

$$\tau = 0 \quad \text{if} \quad \delta > \delta_f \quad (6c)$$

$$\delta_f = \frac{2G_f}{\tau_{max}} \quad (7)$$

The bi-linear bond-slip type is defined by three variables:  $G_f, \tau_{max}, \delta_1$

### I.15.2. Non Linear Adhesives:

Experiments on FRP-to-steel glued connections using a non-linear epoxy are scarce. all accessible tests passed by cohesion failure mode. The bond-slip profiles of such interactions have an essentially trapezoidal form, which is very distinctive than those of FRP-to-steel interactions with a linear epoxy, according to these restricted test data. Resulting in limited testing findings, this part outlines a tentative bond-slip concept proposed by D.Fernando [83] anticipating the shape of a trapezoidal curvature which was stated as:

$$\tau = \tau_{max} \frac{\delta}{\delta_1} \quad \text{if} \quad \delta < \delta_1 \quad (8)$$

$$\tau = \tau_{max} \quad \text{if} \quad \delta_1 < \delta < \delta_2 \quad (9)$$

$$\tau = \tau_{max} \frac{\delta_f - \delta}{\delta_f - \delta_2} \quad \text{if} \quad \delta_2 < \delta < \delta_f \quad (10)$$

$$\tau = 0 \quad \text{if} \quad \delta > \delta_f \quad (11)$$

In addition, this trapezoidal bond-slip model requires just two more independent variables to be described. And the following formula can be used to calculate  $\delta_f$  :

$$\delta_f = \frac{\left( G_f - \tau_{max} \left( \delta_2 - \frac{\delta_1}{2} \right) \right)}{\tau_{max}} + \delta_2 \quad (12)$$

Therefore,  $\delta_1$  and  $\delta_2$  are likely to change depending on the epoxy layer's qualities.

### I.16. Performance of FRP-Steel glued junctions over the entire set:

On the basis of a bi-linear bond-slip concept, Yuan and al.[79] proposed an approximate expression for the complete debonding growing cycle for FRP-concrete glued junctions. When

the formulas for the three essential variables :  $G_f$  ,  $\tau_{max}$  ,  $\delta_1$  are substituted with formulas for concrete-to-steel glued interactions, their mathematical expression can be immediately utilized to forecast the entire behavior of FRP-to-steel glued junctions using linear adhesives. This part offer a mathematical formulation proposed by D. Fernando [83] for a typical single-shear pull-off test for FRP-steel glued connection (**Figure 1-21**).

These parts have the same thickness and breadth throughout their span, whereas:

$b_p$ : The breadth of the FRP plate .

$t_p$  : The thickness of FRP plate .

$b_{st}$  : Steel plate width .

$t_{st}$  : Steel plate thickness .

The glue layer's width is represented by  $b_p$ , while it's thickness is marked by  $t_a$  .L is the plate's bonding length.  $E_p$  and  $E_{st}$  are the young's modulus of the FRP plate and the steel plate, respectively.

The epoxy layer is supposed to be mostly exposed to shear strain. It's also supposed that adherents are exposed to equally distribute axial tension, while the epoxy layer is just exposed to regular shear stresses throughout its texture. built on the notion of force balance:

$$\frac{d\sigma_p}{dx} - \frac{\tau}{t_p} = 0 \quad (13)$$

$$\sigma_p t_p b_p + \sigma_{st} t_{st} b_{st} = 0 \quad (14)$$

With:

$\tau$ : the glue layer's shear stress

$\sigma_p$ : is the FRP plate's axial stress

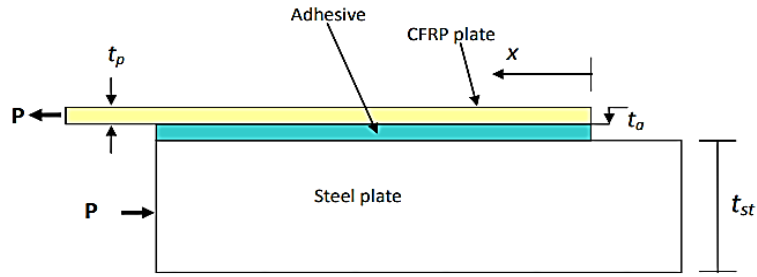
$\sigma_{st}$ : is the steel plate's axial stress.

Given that the two adherents react linearly elastic deformation and the interface shear stress is a factor of the interface slip ( $\delta$ ), the governing equations are as follows:

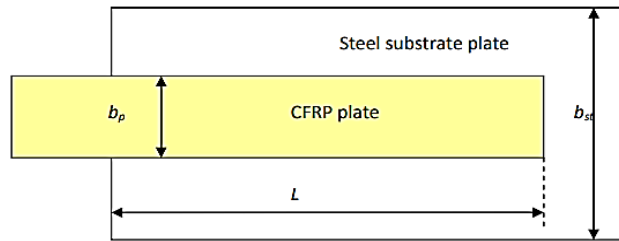
$$\tau = f(\delta) \quad (15)$$

$$\sigma_p = E_p \frac{du_p}{dx} \quad (16)$$

$$\sigma_{st} = E_{st} \frac{du_{st}}{dx} \quad (17)$$



(a) Elevation



(b) Plan

**Figure 1-21: single-shear pull-off test for FRP-steel glued connection**

Where:

$u_p$ : Displacement of FRP plate.

$u_{st}$ : Displacement of steel plate .

$$\delta = u_p - u_{st} \quad (18)$$

$$E_p \frac{du_p}{dx} t_p b_p + E_{st} \frac{du_{st}}{dx} t_{st} b_{st} = 0 \quad (19)$$

$$\frac{d^2 \delta}{dx^2} = E_p t_p \frac{d^2 u_p}{dx^2} \left( \frac{1}{E_p t_p} + \frac{b_p}{E_{st} t_{st} b_{st}} \right) \quad (20)$$

$$\lambda^2 = \frac{\tau_{max}^2}{2G_f} \left( \frac{1}{E_p t_p} + \frac{b_p}{E_{st} t_{st} b_{st}} \right) \quad (21)$$

$$\frac{d^2 \delta}{dx^2} - \frac{2G_f}{\tau_{max}^2} \lambda^2 f(\delta) = 0 \quad (22)$$

Where:

$\tau_{max}$ : is the highest shear stress on a bond.

$G_f$ : is the energy of interfacial fracture.

This present the glued joint's controlling differential equation that can be resolved if the bond-slip concept is specified, which links the interface shear stress towards the slippage.

### I.16.1 Linear Glues: An Analytical Approach

As previously stated, Yuan and al. [79] established a mathematical formulation that may readily be adjusted for FRP-to-steel glued connections using linear glue, due to the fact that they used a bi-linear bond-slip concept. The approach proposed by Yuan and al.[79] comprises statements for various loading phases:

- Stage of elasticity.
- Stage of elastic softening.
- Stages of elasticity, softening, and debonding.
- Stage of softness and debonding.

In the subsequent paragraph, using a trapezoidal bond-slip concept, a mathematical formulation for FRP-to-steel glued junctions with a non-linear glue is provided by D .Fernando [83]. By assuming  $\delta_1 = \delta_2$ , the trapezoidal bond-slip form can be simplified to a bi-linear version. Linear adhesives can benefit from the numerical solutions given in the following subsection. As a result, the mathematical formulation of FRP-to-steel glued connections using linear glue is not included differentially

### I.16.2 Nonlinear Glues: An Analytical solution:

The mathematical formulation of FRP-to-steel glued junctions with a non-linear epoxy is developed by D.Fernando [83] using trapezoidal bond slip concept. The interface shear stress dispersion and force -displacement pattern can be found by solving **Eqn 22** using this bond-slip theory .For the next loading steps, a solution is provided on:

- Stage of elasticity.
- Stage of elasto-plastic.
- Stage of elastoplastic softening.
- Stage of elastoplastic softening and delamination.
- Stage of plastic softening and delamination.
- Stage of softening and delamination.

The six loading steps are only available with glued junctions with a long enough length.

### I.17.The formula of bond strength:

In light of the preceding parts on the analytical approach .The strength of the bond or the peak load  $P_u$  can be determined if the length of the bond is greater than  $L_e$ .

D.Fernando [83] reported the given formula:

$$P_u = \frac{\tau_{max} b_p}{\sqrt{\frac{\tau_{max}^2}{2G_f} \left( \frac{1}{E_p t_p} + \frac{b_p}{E_{st} t_{st} b_{st}} \right)}}$$

Given that the stiffness of the steel plate is significantly greater than of the FRP plate, It's fair to believe:

$$\frac{b_p E_p t_p}{E_{st} t_{st} b_{st}} = 0$$

After that, the preceding formula may be reduced to:

$$P_u = b_p \sqrt{2G_f E_p t_p}$$

It is clear from a comparative study that the suggested approach by D.Fernando [83] accurately predicts the strength of bond of FRP-to-steel glued connections, through both linear and non-linear glues , while using a non-linear epoxy is severely underestimated by Xia and Teng 's [74] approach.

In this study, D.Fernando's [83] proposed approach will be used to predict adhesive strength, mechanical properties, and key data in forecast the presence of debonding failure mode between steel and FRP bond in the strengthening of steel beams with web opening using FRP products.

*The majority of the aforementioned earlier research studies were primarily concerned with the performance of steel beams with web openings, the impact of FRP composite layouts and properties of the material on the shear and bending capacity of solid steel beams, and the bond behavior around steel and FRP. Furthermore, no in-depth computational and experimental investigations were made to reinforce the web aperture of the steel beam or to strengthen the stability of cellular beams, with the exception of the numerical and experimental test performed by M. Altaee[56]. In the upcoming chapters, this thesis will implement this numerically. A full description and validation of the proposed numerical model will be offered in the next chapter since the precision of finite element model outcomes heavily rely on the modelling approach*

## **CHAPTER II: DESCRIPTION OF FINITE ELEMENT MODEL AND VALIDATION**

### **Introduction**

This chapter provides a description of the numerical modeling technique used in the software ABAQUS, including key parameters like solver type and a brief description of the characteristics of the materials, then the mechanical behavior will be discussed with special attention to delamination between steel and FRP composite materials. The ABAQUS simulation and different experimental test results of steel beams with and without strengthening and with and without web opening are then compared in the next chapter of finite element model validation.

### **II.1. Material modeling:**

#### **II.1.1 Steel modeling:**

Modeling steel beams can be done using either shell or solid parts. Due to their better computing performance, shell elements are favored in this case. In ABAQUS, S4 and S4R are two quadrilateral shell components with complete and reduced integration [84]:

S4 has four integration points, while S4R has one.

In this study, it was chosen to use the S4R, which had four nodes and six degrees of freedom, three rotations three translations for each node [84], because the S4 element has much more integration points and hence takes longer to execute the model.

#### **II.1.2 FRP modeling:**

As described in the previous chapter FRP is a structural combination made composed of two phases whose mechanical properties are meant to outperform the component phases individually. The reinforcing fibers for example: carbon, glass, boron, aramid, and many other fiber types are stronger and stiffer than the matrix around them. The matrix core supports and protects the fibers while also conveying local pressures from one fiber to the next. The fibers have a constant direction inside each ply, they are unilateral. This leads to a ply with a fiber orientation represented by an angle related to a specific reference axis. A lamination is made by stacking many plies together in different directions. The lay-up is the organization of the laminate that shows its ply component with distinct fiber orientations. A [0/-45/90/45/0] lay-up is depicted in the illustration below (**Figure 2-1**).

The definition of a lay-up in ABAQUS can be created in two ways: by generating a composite section or by developing a composite lay-up. The composition lay-up method improves the specification of a composite lay-up and is particularly beneficial when only a few portions must be assigned to the composite definition.

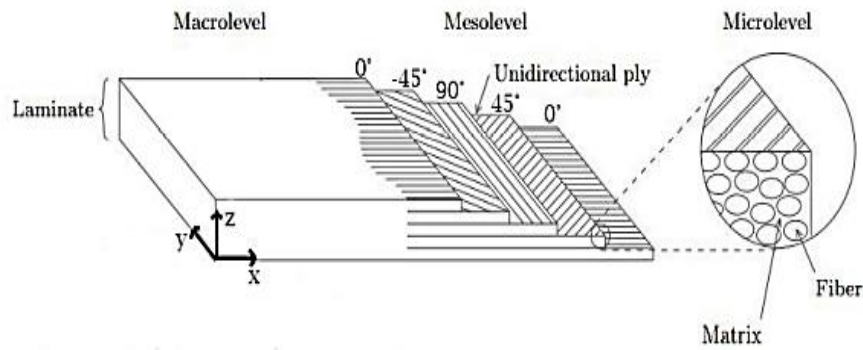


**Figure 2-1 : Composition of composite laminates**

**II.1.2.1 Composite material behavior:**

**II.1.2.1.1 Elastic behavior:**

When the ply is rigid in the fiber orientation and flexible in other directions, the transversely isotropic form of Hooke's law can be used to define the elastic behavior of an orthotropic composite. It's expressed as :

$$\varepsilon = S * \delta$$

Where:

S is the compliance matrix.

The stress-strain relationship is minimized by assuming that the ply is thin, unidirectional, and will be subjected to plane stress conditions ( $\sigma_{33} = 0, \tau_{13} = 0, \text{ and } \tau_{23} = 0$ ), requiring only four elastic parameters ( $E_1, E_2, \nu_{12}, \text{ and } G_{12}$ ) [85]. The subscript specifies the axis in the equation, with one axis indicating the axis in the lengthwise fiber direction and the other two axis indicating are in the lateral direction, orthogonal to the fiber direction.

$$\begin{bmatrix} \varepsilon_{11} \\ \varepsilon_{22} \\ \varepsilon_{12} \end{bmatrix} = \begin{bmatrix} \frac{1}{E_1} & \frac{-\nu_{12}}{E_1} & 0 \\ \frac{-\nu_{12}}{E_1} & \frac{1}{E_1} & 0 \\ 0 & 0 & \frac{1}{G_{12}} \end{bmatrix} \begin{bmatrix} \delta_{11} \\ \delta_{22} \\ \delta_{12} \end{bmatrix}$$

In ABAQUS, this formula is utilized to characterize orthotropic elastic properties under plane stress. The elastic variables  $G_{13}$  and  $G_{23}$  must always be entered since they may be needed to evaluate transverse shear deformations in a ply [86].

**II.1.2.1.2. FRP failure behavior:**

The ideal usage of FRP materials is now being restricted due to the difficulty in predicting both their strength and damage limits. Costly examinations and validations are required to ensure the reliability of a composite material. Today's modern challenge is to develop designs that can perform the function of certain "realistic" tests. Engineers will be able to have much more

latitude in the design stage, as well as making structural or item optimization smoother. Engineers will be able to have much more latitude in the design stage, as well as making structural or item optimization smoother. The difficulty with analyzing laminate damage is that numerous failure processes might happen, resulting in a variety of outcomes. In a composite laminate, three main failure modes can be identified:

- **Matrix fracture:** is the most common nonlinear damage failure in laminates. Crack appears between the fibers, running the length of the ply. Matrix fractures, also known as split fractures, which can occur in the load direction.
- **Delamination:** is caused by the failure of the junction among plies as a result of the load. Because the stress is redistributed across the contact between the plies, stress concentration form at the junction. Unless the stress concentration reaches the interaction layer's power, the surface interaction will detach, and the plies will lose contact with their neighbors.
- **Fiber damage:** is a complicated loss of material since it can generate a variety of other failure mechanisms in the area. When a fiber fails, it can cause transversal matrix fracture if the matrix is fragile and has strong bond with the fibers, or debonding if the contact between both the fiber and matrix is poor and the fibers have a superior ultimate strain. When a fiber breaks, a large amount of conserved energy is released, which might cause the nearby fibers and matrix to failure. Almost all of the time, this will result in the entire composite failing.

**IV.1.2.1.3.FRP failure criteria:**

Many experts have spent decades researching how to formulate failure criteria for composite laminates. The fundamental challenge is: how can we forecast collapse onset due to a specific state of material stress? The factors of failure at the microscale are extremely complicated, and using micromechanical techniques to answer this question would be futile. As a result, several failure criteria, such as average stresses and strains, are dependent on macro variables.

Tsai's study from 1965 was one of the initial contributions to this field. He reasoned that the failure mechanism for a unidirectional laminate has the same mathematical model as an orthotropic plastic material's failure mode. [26][27] The downside of this method was that it didn't take into account for isotropic stresses. Hoffman resolved the issue by incorporating linear stress components into Tsai's criterion.

Tsai and Wu devised the Tsai-Wu criterion previously [87], which is still used nowadays due to its simplicity. For a subject under plane stress, the interaction criterion is expressed as:

$$\sigma_{11} \left( \frac{1}{f_{1t}} - \frac{1}{f_{1c}} \right) + \sigma_{22} \left( \frac{1}{f_{2t}} - \frac{1}{f_{2c}} \right) + \frac{\sigma_{11}^2}{f_{1c}f_{1t}} - \frac{\sigma_{11}\sigma_{22}}{\sqrt{f_{1c}f_{1t}f_{2c}f_{2t}}} + \frac{\sigma_{22}^2}{f_{2c}f_{2t}} + \frac{\tau_{12}^2}{f_{12}^2} = 1 \quad (23)$$

Despite the fact that this seemingly simple equation suited experimental results well, its execution and interpretation resulted in underlying issues. It's due to the fact that FRP composites are made up of phases that are highly different. As a result, failure can manifest itself in a variety of ways. The Tsai-Wu criterion does not allow for all failure mechanisms to



be represented by a single smooth function. That is why Hashin was the first to propose failure initiation criteria for various failure scenarios [88]. Under plane stress conditions, he identified four possible failure processes for a unidirectional composite:

- **Failure of tensile fibers:** Tensile fiber rupture in the fiber direction is crucial when longitudinal tension and shear damage the material reciprocally .

$$\left\{ \frac{\sigma_{11}}{f_{1t}} \right\}^2 + \left\{ \frac{\tau_{12}}{f_{12}} \right\}^2 \begin{cases} < 1 \text{ no failure} \\ = 1 \text{ failure} \end{cases} \quad \text{With } \sigma_{11} > 0 \quad (24)$$

- **Failure of compressive fibers :** Buckling or twisting of the fibers is a common symptom of compression fiber damage. Since the coupling between transverse and longitudinal compression is believed to be insignificant, it results in a simple peak stress criterion.

$$\frac{\sigma_{11}}{f_{1c}} \begin{cases} < 1 \text{ no failure} \\ = 1 \text{ failure} \end{cases} \quad \text{With } \sigma_{11} < 0 \quad (25)$$

- **Tensile matrix damage :** happens if :

$$\left\{ \frac{\sigma_{22}}{f_{2t}} \right\}^2 + \left\{ \frac{\tau_{12}}{f_{12}} \right\}^2 \begin{cases} < 1 \text{ no failure} \\ = 1 \text{ failure} \end{cases} \quad \text{With } \sigma_{22} > 0 \quad (26)$$

- **Compressive matrix damage:** The criterion for compressive matrix rupture seems to be more difficult. The transversely isotropic stresses are thought to have a bigger impact than the uni-axial compressive rupture stress.

$$\left( \frac{\sigma_{22}}{2f_{23}} \right)^2 + \left[ \left( \frac{f_{2c}}{2f_{23}} \right)^2 - 1 \right] \frac{\sigma_{22}}{f_{2c}} + \left( \frac{\tau_{12}}{f_{12}} \right)^2 \begin{cases} < 1 \text{ no failure} \\ = 1 \text{ failure} \end{cases} \quad \text{with } \sigma_{22} > 0 \quad (27)$$

In the numerical model of this study, an S4R shell element was used to model all FRP products.

### II.1.3. Adhesive modeling:

In ABAQUS, two approaches to modeling the adhesive behavior:

Cohesive elements and cohesive surfaces are used to model the steel/adhesive/FRP interaction [86]:

#### II.1.3.1. Cohesive surfaces process:

The surface-based cohesive approach is defined by surface interface parameters generated to a contact pair utilizing the finite sliding, node-to-surface concept. It is preferable to conduct the investigation with the surfaces just near each other on a cohesive surface. As a result, interface

thickness has no effect on cohesive surfaces [84]. Even though surface-based cohesive technique is common, it is only employed in situations when the adhesive thickness is insignificant. Furthermore, the ABAQUS/Explicit solver does not enable it.

**II.1.3.2.Cohesive element process:**

With the ABAQUS/Implicit and ABAQUS/Explicit solvers, ABAQUS [84] provides an alternate technique to defining adhesive connections. Since the nodal coordinates of the cohesive elements are determined depending on the baseline thickness, intrinsic thickness has a significant impact on contact behavior. As a result, features of the adhesive layer, like as stiffness and strength, can be used to represent the cohesion. The tie constraint of the cohesive element, COH3D8, is used to do this, with eight nodes, three degrees of freedom in each node, and surfaces to steel substrate and FRP .Bond failure happens along the layer of cohesive elements, with no deformation of entities that interact. As a result, the cohesive element method can forecast bond behavior from starting loading through damage initiation and then damage evolution.

**II.1.3.3. Adhesive damage modeling:**

Using traction-separation models, the bond's rupture reaction may be modeled in both of the available methods. **Figure 2-2** shows a simple bilinear traction-separation equation that is widely employed in computations, with linear softening after damage beginning.

**Figure 2-3** shows another commonly used theory, in which the softening post damage onset is characterized by an exponential curve. The damage model across both cases is divided into different phases: damage initiation and damage evolution. The traction-separation reaction can be specified to a user-defined damage evolution rule once a damage criterion is reached.

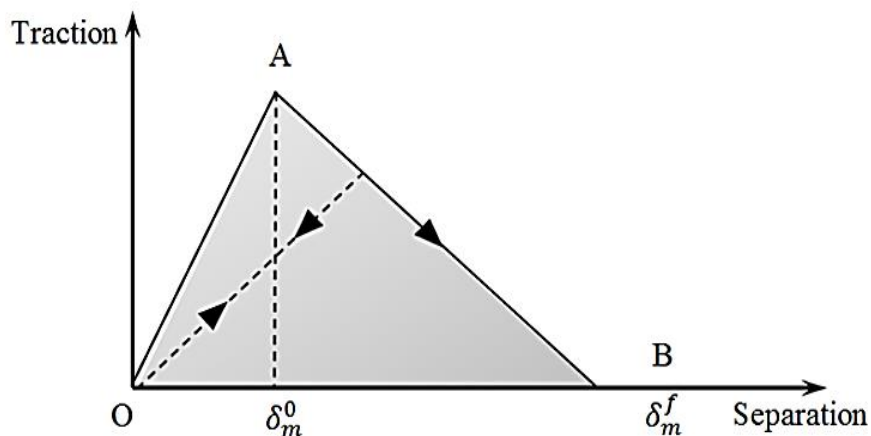


**Figure 2-2: simple bilinear traction-separation law [84]**

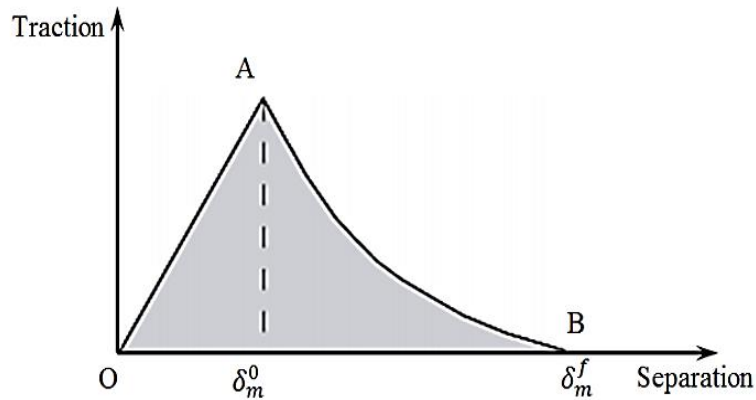


**Figure 2-3: Exponential damage evolution in a traction-separation law [84].**

**II.1.3.3.1 Damage initiation:**

Two of the damage initiation criterion in ABAQUS [84] are focused on stress, but the other two are dependent on separation. The quadratic nominal stress or strain criterion and the maximum nominal stress criteria, maximum nominal strain criterion are all instances of this type of criterion (Figure 2-4).

The damage initiation criteria in this research is the quadratic nominal stress criterion, which can be written as:

$$\left(\frac{\langle t_n \rangle}{\sigma_{max}}\right)^2 + \left(\frac{t_s}{\tau_{max}}\right)^2 + \left(\frac{t_t}{\tau_{max}}\right)^2 = 1 \tag{28}$$

$t_n, t_s$  and  $t_t$  are the nominal stress's peak values.

$\sigma_{max}$  is the adhesive's tensile strength.

$\tau_{max}$  is the adhesive's shear strength. The symbol  $\langle \rangle$  stands for the Macaulay bracket, which indicates that compressive stresses don't really cause damage ( $t_n$  is negative and hence  $\langle t_n \rangle$  is zero).

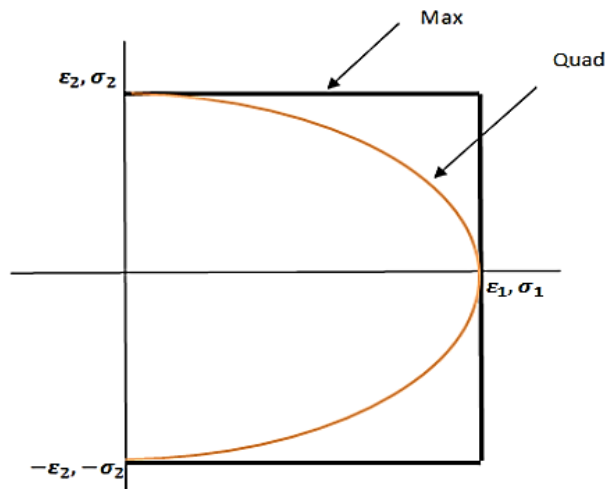


**Figure 2-4: Criteria of damage initiation**

**II.1.3.3.2.Damage evolution:**

A scalar damage parameter D is added as the total damage in the material following damage initiation. D has a range of 0 to 1, where 0 signifying undamaged and 1 denoting entire detachment. Following that, the respective stress components are deteriorated in the following manner:

$$t_n = \begin{cases} \bar{t}_n(1 - D), & \bar{t}_n \geq 0 \\ \bar{t}_n, & \bar{t}_n < 0 \\ t_{t=(1-D)\bar{t}_t} \\ t_{s=(1-D)\bar{t}_s} \end{cases} \quad (29)$$

$\bar{t}_n, \bar{t}_t$  and  $\bar{t}_s$  are the stress components which are anticipated by scaling the original stiffness by the present relative displacements.

The degradation factor D can be stated as follows for the linearly softening law:

$$D = \frac{\delta_m^f(\delta_m^{max} - \delta_m^0)}{\delta_m^{max}(\delta_m^f - \delta_m^0)} \quad (30)$$

$\delta_m^{max}$ : is the greatest relative displacement obtained during the stress period.

$\delta_m^0$  is the effective relative displacement upon the onset of failure.

$\delta_m^f$  is the effective relative displacement at the failure.

The effective relative displacement  $\delta_m^f$  can be expressed in the following manner:

$$\delta_m^f = \sqrt{(\delta_n)^2 + \delta_s^2 + \delta_t^2} \quad (31)$$

**II.2.Solver type:**

ABAQUS/Standard can solve linearly and smooth nonlinear problems in both static and quasi-static situations [86]. In ABAQUS, typical analysis is divided into two perspectives: implicit and explicit. For extremely nonlinear and dynamic phenomena, ABAQUS/Explicit is a good choice [84]. On the other hand, numerous static or quasi-static issues have shown to benefit from ABAQUS/Explicit. In ABAQUS/Standard, these issues usually entail contact or material

complexity that cause convergence issues. Such analyses are computationally intensive in ABAQUS/Standard because they need the solution of a significant number of linear equations.

ABAQUS/Explicit determines the solve of nonlinear issue without incrementing by advancing directly the kinematic state of the preceding iteration, while ABAQUS/Standard must iterate to obtain the solution [84]. Even though ABAQUS/Explicit needs several temporal steps for the same analysis, the explicit technique is much more practical since the implicit approach will take a significant number of repetitions. The resolution is estimated utilizing Newton Raphson technique when adopting the implicit approach and the linear system of equations must be resolved numerous times, this can result in extended CPU times, and for highly nonlinear situations, and convergence is not assured (**Figure 2-5**) [84]. The explicit technique, on the other hand, does not involve any convergence tests, although it does necessitate quite short time increments to preserve the stability restriction. A reliable time step duration must be determined that is less than the minimum time that dilatational wave takes to pass through an element in the model. It is computed using the following formula:

$$\Delta_t \leq l_{element} * \sqrt{\frac{\rho}{E}} \quad (32)$$

Where:

$\Delta_t$ : Is the stable time step.

$l_{element}$ : Is the element's length.

$\rho$ : The material's density.

E: young's modulus.

Semi-automatic mass scalability is included throughout the Dynamic, Explicit model. Massive scaling is a solution for running models in less time while maintaining the correctness of the quasi-static solution. It's a popular and successful strategy for models with low velocities and little kinetic energy in comparison to stored energy [84]. The density of the smallest components is increased to scale up the bulk. As a result, the numerical method of the dynamic model will have a bigger feasible stable time step and, as a result, a reduced CPU time. When utilizing an implicit solver like ABAQUS/Standard to resolve material models with softening and stiffness deterioration, considerable convergence problems are common. These convergence issues are caused by an abrupt change in stiffness at the peak load and consequent adverse softening. The application of viscous normalization of the constitutive equations is a frequently employed numerical stability control approach for overcoming such challenges.

In submitting the explicit dynamic approach to quasi-static problems, several particular criteria are required, to find the solutions in a small space of time with no dynamic influence [84]. Determine the element natural frequency that corresponds to the predicted failure mechanism using frequency analysis.

Utilizing \*AMPLITUDE, DEFINITION=SMOOTH STEP, ABAQUS/Explicit, link each one of the data sets with curvatures whose first and second derivation are smooth and whose sloping are zero at each of the sample points employing the smooth loading amplitude termed SMOOTH STEP.

In this amplitude, just use appropriate time, which you can find by:

$$t = \frac{1}{f} \quad (33)$$

where:

$f$ : Is the targeted failing mode's natural frequency as determined by the frequency analysis .

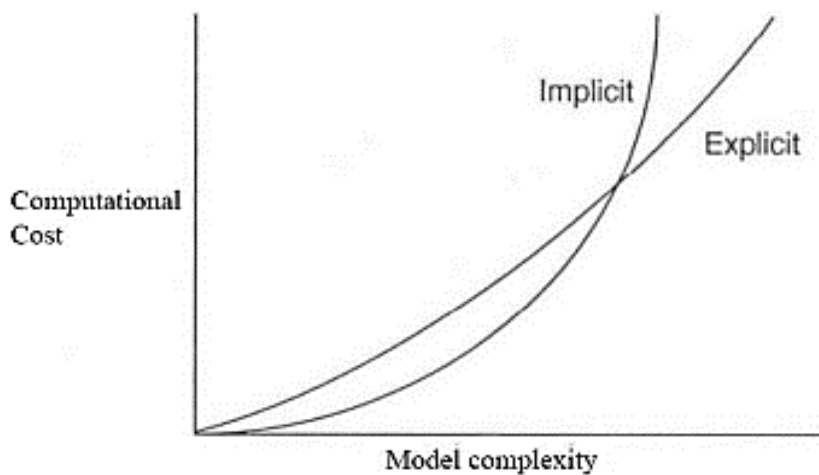


**Figure 2-5: Cost of computation in comparison**

As a result, the explicit solver was used to run 3-D nonlinear FE simulations in this study. In the 3-D FE model nonlinearities of material and geometric were explored to capture massive and local deformation effects ,so by activating the optimum option "NLGEOM" in ABAQUS, the geometric nonlinearity was considered.

### **II.3.Finite element model validation**

Verification of the model provided in the preceding section is required. This will be accomplished in this part by analyzing the accuracy of the obtained results while taking into account the appropriate meshing size and boundary conditions. The reliability of the results will be determined by comparing the relative reaction forces, ultimate loads, failure mode, and

plotting the graphs of load – vertical displacements with previous experimental tests which provides key phenomena of this study including de-bonding to visualize the convergence of results.

**II.3.1. Experimental test conducted by Okeil and al. [94]:**

A study was conducted by Okeil and al [94] on the out-of-plane strengthening using pultruded GFRP section of steel-plate girders that are subject to web buckling, two specimens named OB1 and OB2 which are un-strengthened control beam and GFRP strengthened beam respectively. The GFRP T sections were cut across a pultruded wide-flange section with a table cutter fitted with a concrete knife blade. The beam portion was first cut to the necessary dimensions, and then the flange was cut on one side to create a T-shaped part that would act as the GFRP shear reinforcement.

As illustrated in **Figure 2-6**, the steel-plate girder beam measured 2083 mm in length, 532 mm in depth with a 3.2 mm thick web, and 279 mm wide with 13 mm thick flanges. Because web buckling was the examined mechanism of plate girder failure, all other probable modes of plate girder failure, such as flange buckling were planned to be avoided by dividing four panels using five vertical stiffeners of 9.5 mm thickness on both sides with the same equal spacing 521 mm.

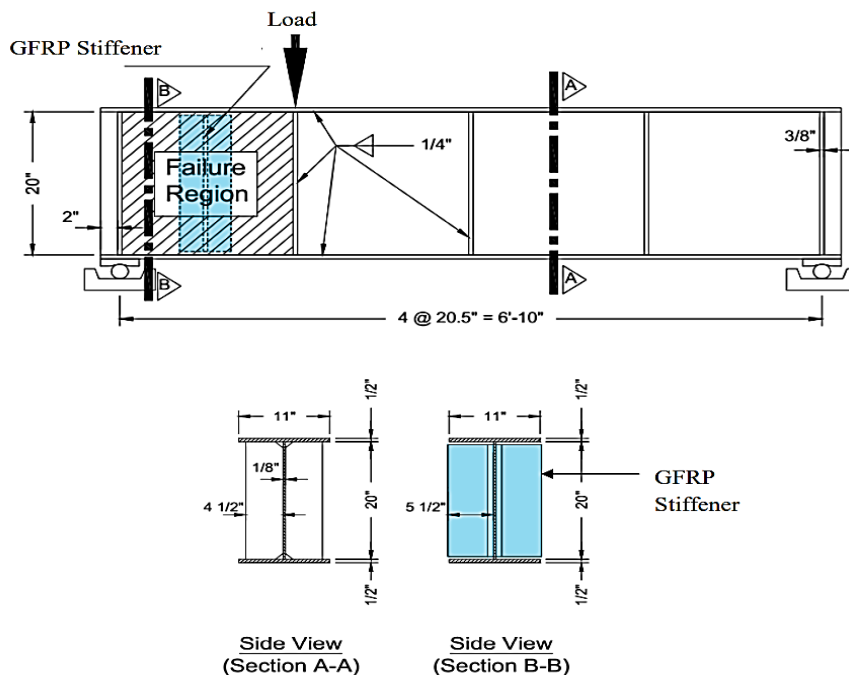


**Figure 2-6 :Reference and reinforced specimens OB1 and OB2**

Throughout the first intermediate stiffener, a point load force was applied. As shown in **Figure 2-6**, this loading pushed the first panel to nearly 3 times the shear load operating on the remainder of the beam.

On the two faces of the web, the two vertical GFRP-pultruded T-sections were mounted to the specimen OB2 at one extremity of the plate girder as further stiffeners and on one end of the

plate girder, a single-point load was applied at the first internal stiffener (**Figure 2-6**) . The GFRP stiffener was added to the reinforced specimen to allow the first segment in opposing its inclination to buckle due to the strong shear pressures.

The goal of this study was to show that low modulus FRP can be used to reinforce steel constructions. The investigation used pultruded glass FRP (GFRP) profile.

### **II.3.1.1 Numerical model:**

The FE models' goal is to provide an acceptable framework for studying this sort of reinforcement strategy. Even material and geometric nonlinearity were taken into consideration in the Numerical model. The loading and boundary conditions were the same as in the experiment. Stiffeners were tied on both sides of the web and both the top and bottom flanges, using the ABAQUS tie option. A buckling analysis was conducted firstly before the nonlinear analysis to find the appropriate failure mode. Any one of the two forms of analysis gives valuable data for this sort of situation. In analysis of structures, eigenvalue is frequently used to reduce complicated behaviors into distinct uncoupled behaviors. Employing eigenvalue analysis, the mode shape matching to every natural frequency can be individually recognized. The eigenvalues represent the forces required to begin buckling in any of the modes. By progressively loading the structure in a way comparable to the laboratory test experiment, the simulation should display the same behavior as that seen experimentally.

As illustrated in **Figure 2-7**, a bi-linear stress-strain curve (elastic hardening) was utilized for the steel while the GFRP and the adhesive were considered to behave linear elastic until failure. The GFRP part was modeled as an orthotropic elastic material, whereas the epoxy resin was treated as an isotropic elastic material .The general-purpose shell element S4R with reduced integration was applied to model the steel part and the GFRP section, while the cohesive element COH3D8 was employed to model the adhesive layer. In the same way as before, the adhesive layer's top and bottom faces were tied to the beam's panel and the GFRP T section flange surface .For the examined specimens, the prior validation mesh size, was investigated with various mesh sizes to find the most efficient mesh, it was also found that The uniform distribution of 20 mm mesh size can benefit in the reduction of computation time with an acceptable convergence of results.



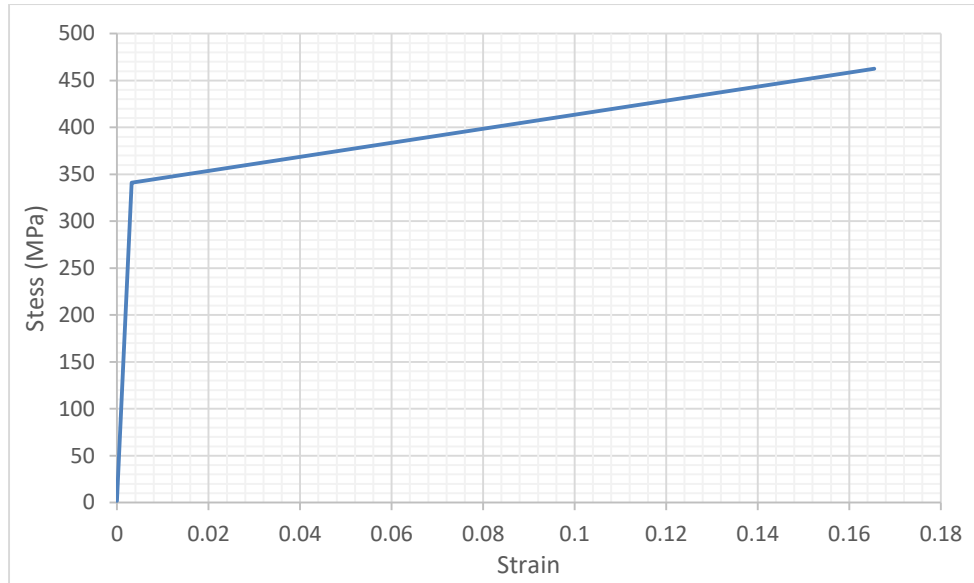


**Figure 2-7: Bilinear steel stress-strain curve**

Tensile Stress	138(MPa)
Flexural Stress	207(MPa)
Modulus of Elasticity	17,200 (MPa)

**Table 2-1: pultruded GFRP T section Mechanical properties**

Tensile Stress	50 (MPa)
Tensile Modulus	3.18 (Gpa)
Flexural Stress	123 (Gpa)
Flexural Modulus	3,120 (Gpa)
Elongation [%]	5.0

**Table 2-2: Epoxy mechanical properties**

**II.3.1.2. Results and discussion:**

The experiment's ultimate load, bond behavior, and failure mode were all retrieved and compared to the FE results. It was found that the maximum load of the GFRP-strengthened specimen in the experimental test, OB2, was 389 kN, which was 40% higher than that of the control specimen OB1 while the ultimate load of OB2 in the numerical model was equal to 393kN which was slightly higher than in the experimental test .The first noticeable web buckling was seen at 389 kN with failure in the GFRP-strengthened specimen and at 249 kN in the un-strengthened specimen, resulting in a 56 % enhancement this was the same strength enhancement obtained in the numerical simulation . **Figure 2-8** depicts the beam conditions before the onset of buckling. The failure mode of the control specimen in the experimental test was the web buckling this was also observed in the finite element model. In the other hand the GFRP-strengthened specimen failure was a fracture of the steel-GFRP bond accompanied with instantaneous web buckling which was also the same failure mechanism in

the numerical simulation **Figure 2-9**. Nevertheless, the majority of the adhesive fractures were hidden behind the GFRP T section, with just a few showing at the borders.

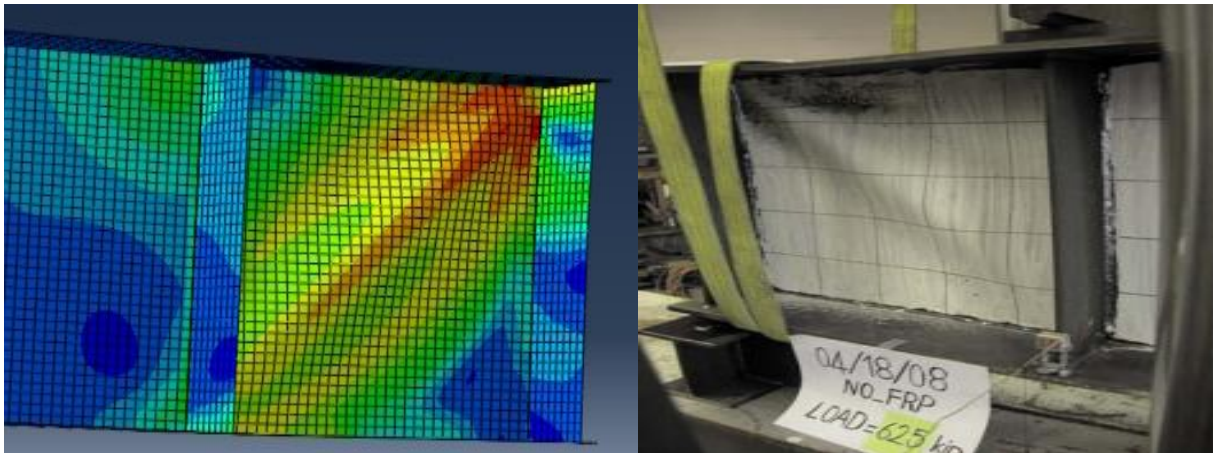


**Figure 2-8: The control specimen OB1 failure mode**

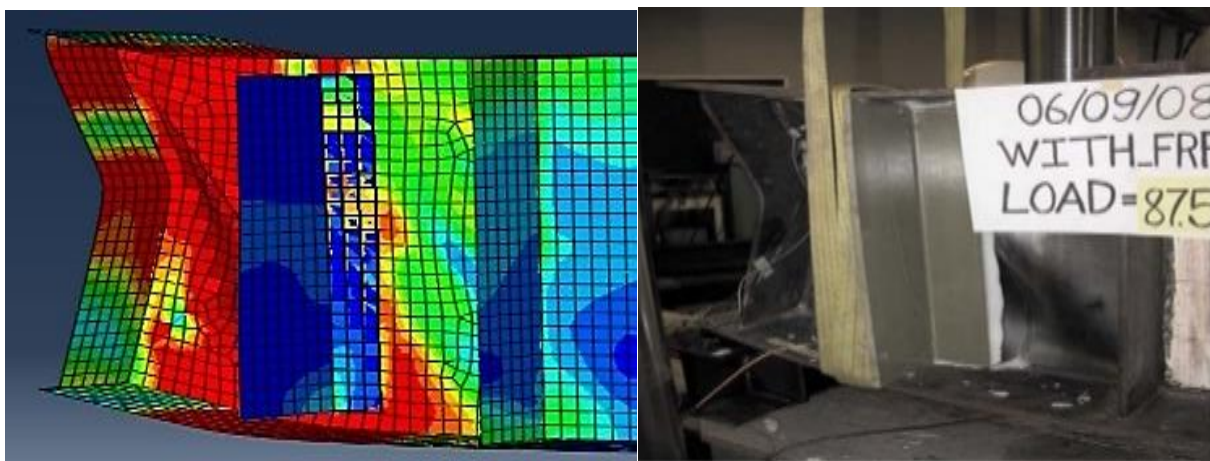


**Figure 2-9: The strengthened specimen OB2 failure mode**

### **II.3.2 Experimental Test conducted by Lucas and al [95]:**

A set of experiments were carried out by Lucas and al [95] on nine cellular beams which were designed to fail by web post buckling the predominant failure mode of this type of beams to present a novel method for calculating cellular beam shear resistance for this situation. **Table 2-3** shows the dimensions of each specimen after production, where L denotes the specimen's length between supports. Because web-post buckling is mostly induced by lateral shear stress, it was decided in this experimental test to explore the phenomena using shorter span specimens. Furthermore, as WPB behavior is strongly reliant on the geometry of the web-post, every prototype was built with a distinct layout and dimension. Tensile coupons were used to determine the yield and extreme stresses of steel ( $f_y$  and  $f_u$ , accordingly) (**Table 2-3**). This simple supported specimen were used in the lab testing, which were pressed using an MTS

hydraulic system that controlled displacement. Steel rollers in fork supports in the two extremities supported the specimens, allowing for unrestrained longitudinal movement. The load was supplied to the top flange, and the specimens were prevented from lateral torsional buckling by an equipment that restricted transverse displacement. The load was applied at an eccentricity of 20 mm of the mid-span to produce buckling on the instrumented side of the beam, as shown in **Figure 2-10**. The DTs that record the horizontal displacements of the web-post (DT-01 to DT-04) were mounted in arms connected to the flanges and web posts (**Figure 2-11**).

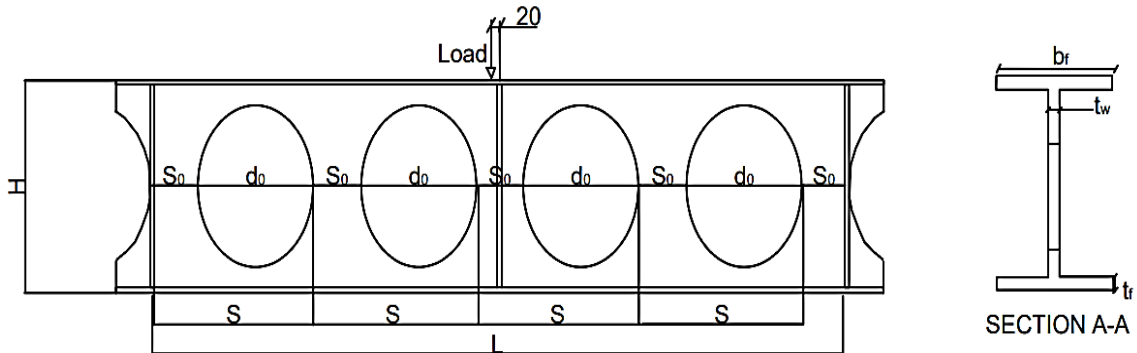


**Figure 2-10 : Tested specimens dimensions**

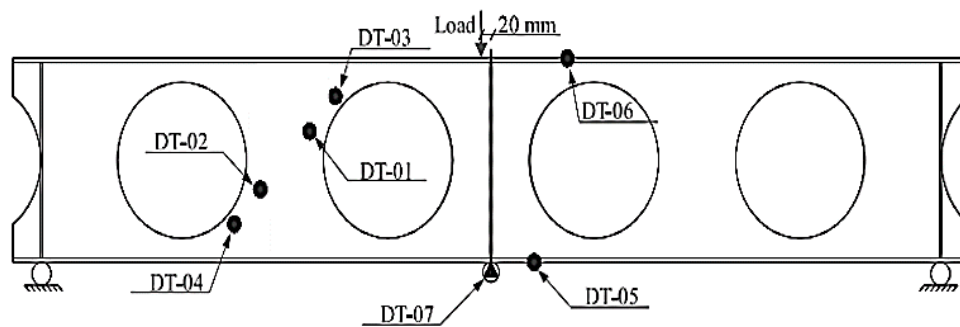


**Figure 2-11 : Vertical and lateral displacement measurement.**

Specimen	$t_w$ (mm)	$t_f$ (mm)	$b_f$ (mm)	s	H	L	$d_0$ (mm)	$f_y$ (MPa)	$f_u$ (MPa)
A2	4.8	5.6	102	445.8	433	1874	342.5	416	480
A5	4.8	6.0	102	325.1	409	1370	248.8	416	480
B2	5.4	9.0	101	458.3	440	1933	352.1	365	422
B5	5.9	9.0	99	318.4	412	1346	243.8	398	511

**Table 2-3 : Specimens dimensions and mechanical properties**

**II.3.2.1. Numerical model:**

ABAQUS was used to simulate all of the specimens evaluated in the laboratory, keeping the defined geometry in the test. The material properties were identically the same as the experiment and a bilinear stress-strain curve was used to represent the steel material with a young modulus of 200 GPa. The Simulations took into account either material and geometric nonlinearity. The specimens were assumed as simply supported, with imposed loads and boundary conditions as illustrated in **Figure 2-12**. On both sides of the web, three full-depth stiffeners were installed. Each one was attached to the upper flange, lower flange, and web using tie option in the software. The Nodes in the mid span top flange was restricted in vertical and horizontal displacement orientation to prevent massive deformation at the applied load location and the lateral torsional buckling. To choose the web-post failure mechanism, the linear buckling analysis was conducted first, followed by the nonlinear analysis. The eigenvalue buckling analysis was used to produce the initial imperfection form used in the simulation . Nevertheless, because this imperfection geometry seems to be identical to the finished form of a buckled web-post, the amplitude of the imposed defects must be reduced in comparison to those evaluated in the experiment [96]. After multiple analyses ,the effective scale factor for geometric imperfection was discovered to be the value of  $H/500$  [10], which, when used in numerical models, produced the best results for all tested specimens. To simulate the steel section, the general-purpose shell element S4R with limited integration was used. Based on mech convergence study, mesh size of 20 mm x 20mm with a regular quadratic pattern exhibited satisfactory convergence with corresponding experimental results (**Figure 2-13**).

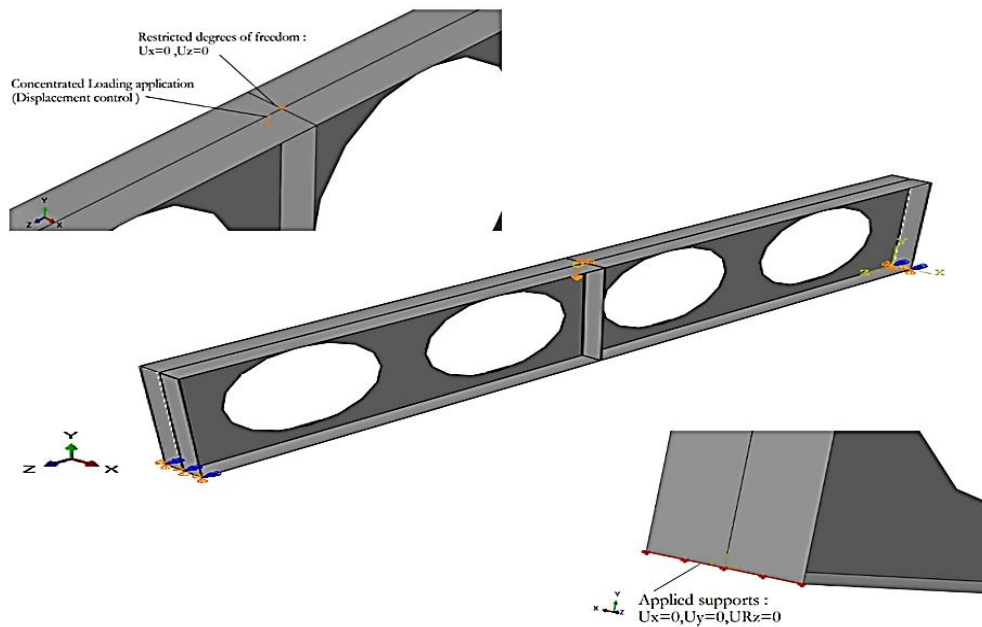


**Figure 2-12 : Loading and boundary conditions**

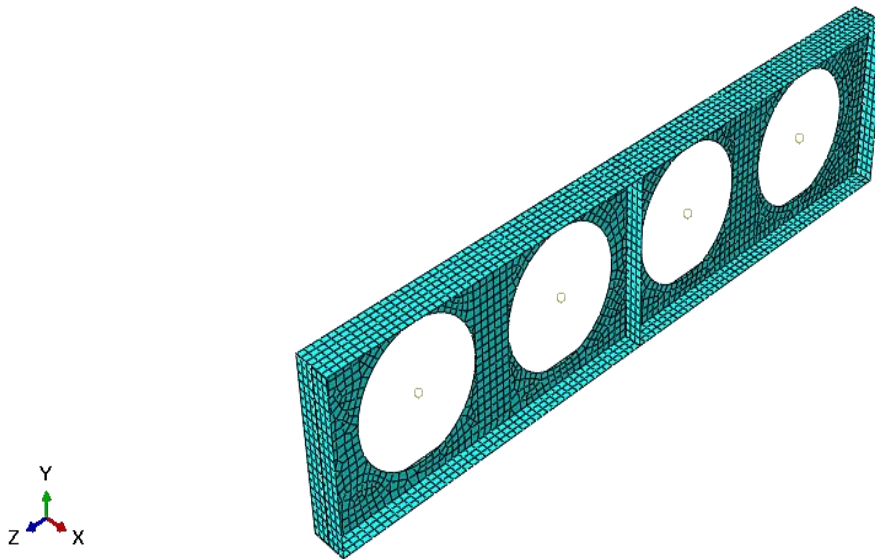


**Figure 2-13: FE model mesh situations.**

### **II.3.2.2 Results and discussion:**

The retrieved experimental findings, which included the maximum load, load-deflection curves, horizontal displacement, and failure mechanism, were compared to FE data. It can be noticed from **Table 2-4** that ultimate loads of tested beams obtained from the developed FE model were compared to their corresponding experiment data.

It can be seen that ultimate load differences do not exceed 6% for all tested beams, and that load- vertical deflection curves of numerical and experimental results were also in good agreement (**Figures 2-14** to **Figure 2-17**). The stiffness derived from the FE analysis was comparable to the experimental test . In addition to that the horizontal displacement measured in points (D2,D2,D3 and D4 ) (**Figure 2-18**) were in good agreement between experimental and FE results confirming the buckling of the web post . Narmashiri and al [97]. were able to attain this degree of reliability between experimental and FE findings .

This little variation might be traced to residual stresses in the beam caused by the production process, which are not accounted in the Finite element model. The failure modes of all cellular beams in FE models were similar with experimental test results, all specimens failed by web post-buckling as shown in **Figure 2-19** to **Figure 2-22** showing the predicted S-shape buckling deformation in the simulation process, which matched the experimental test findings.

Based on the data reported thus far, one may infer that the numerical simulation have been effectively verified, since the results revealed a comparably low error in contrast to the experimental test

Spécimen	$P_u$ (EXP) (kN)	$P_u$ (FE) (kN)	Percental difference (%)	Failure mode
A2	123.7	123.82	-0.09	WPB
A5	198.2	209.63	-5.76	WPB
B2	157.9	151.18	4.25	WPB
B5	276.9	290.77	-5.00	WPB
Average			-1.65	

**Table 2-4 : Experimental and finite element ultimate load**

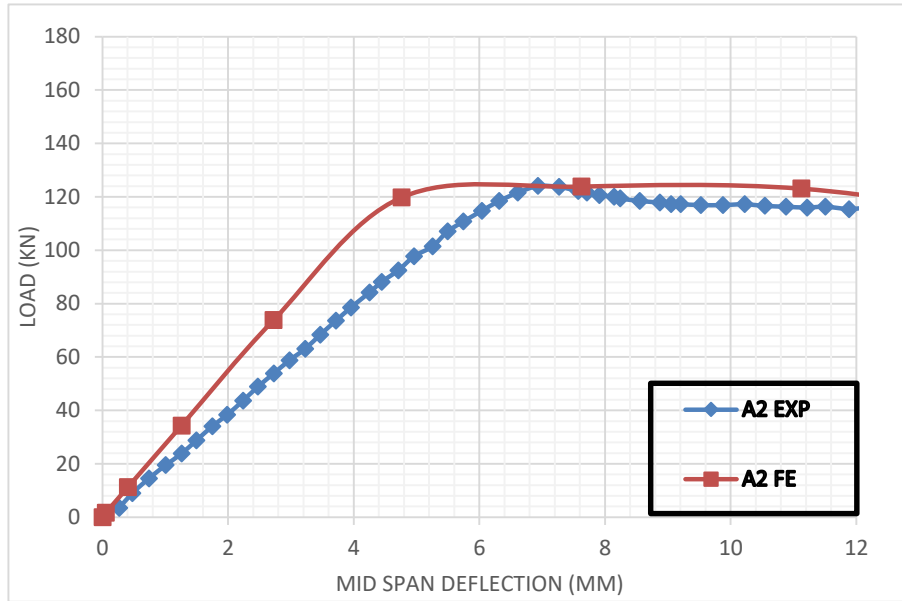


**Figure 2-14: Experimental and FE load-vertical displacement for specimen A2.**

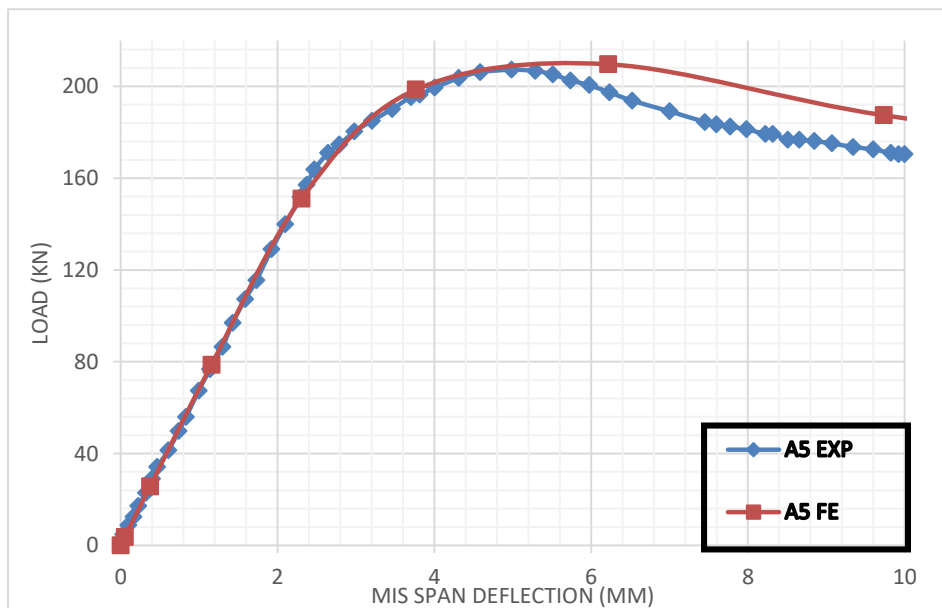


**Figure 2-15: Experimental and FE load-vertical displacement for specimen A5**

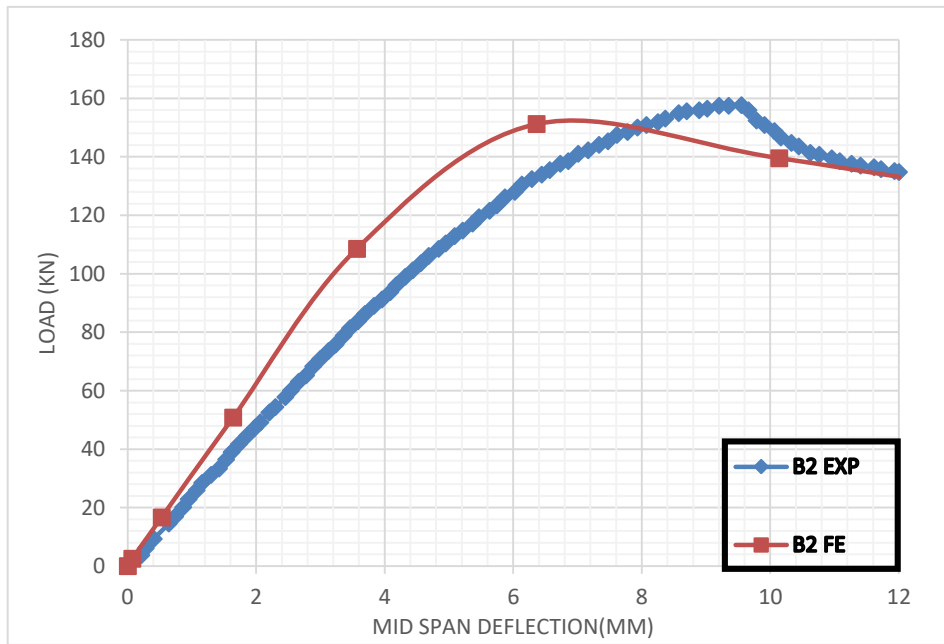


**Figure 2-16: Experimental and FE load-vertical displacement for specimen B2**

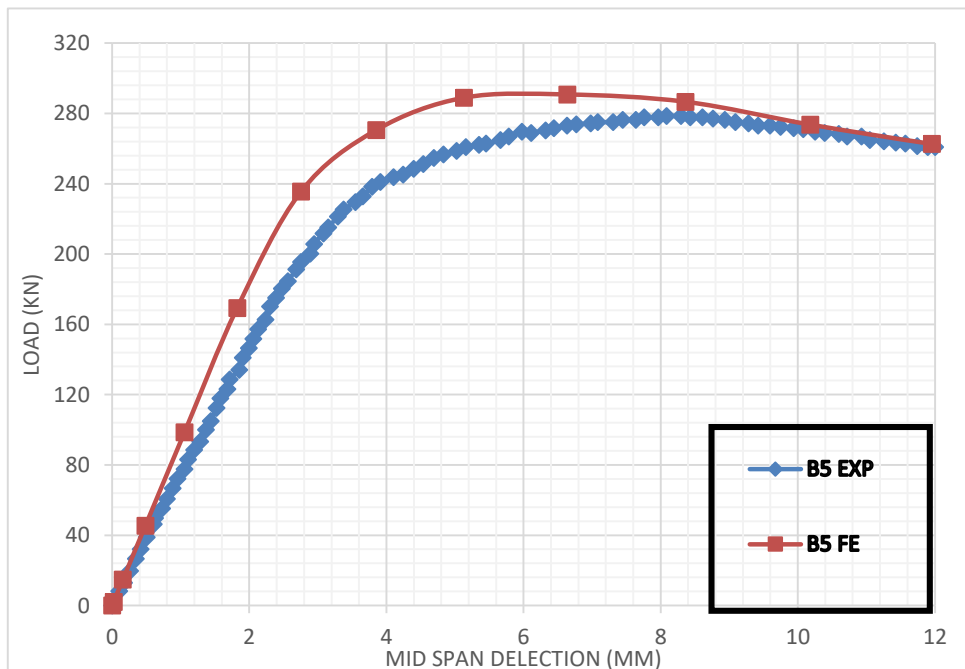


**Figure 2-17: Experimental and FE load-vertical displacement for specimen B5**



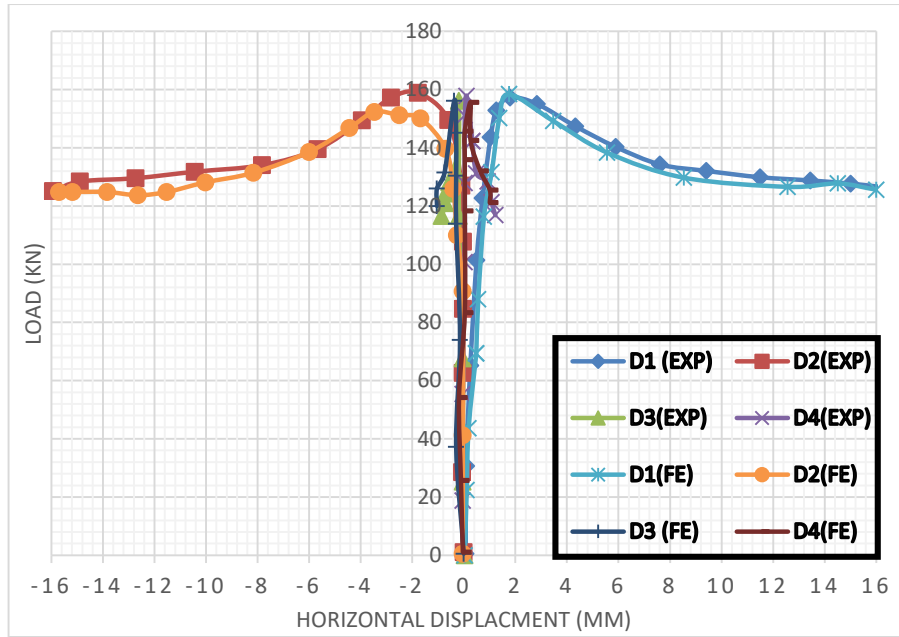


**Figure 2-18: Experimental and FE load-horizontal displacement for specimen A2**

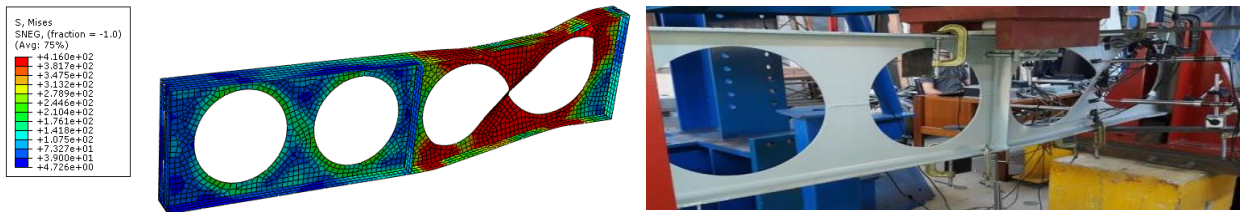


**Figure 2-19: Experimental and FE failure mode of specimen A2**

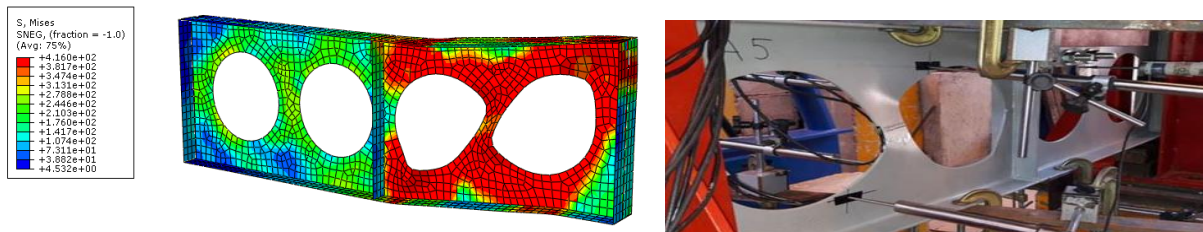


**Figure 2-20: Experimental and FE failure mode of specimen A5**



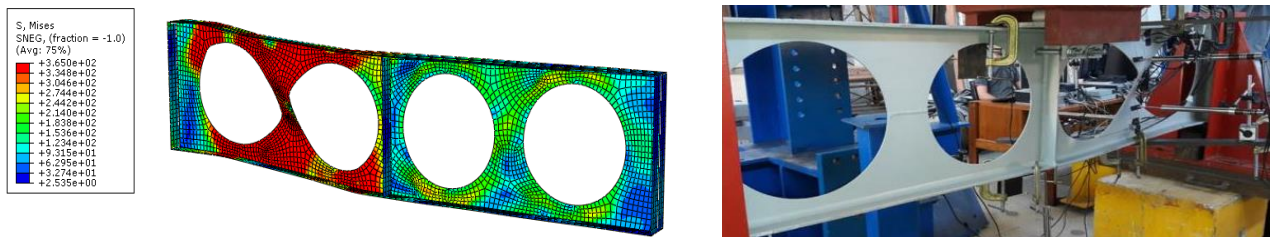


**Figure 2-21: Experimental and FE failure mode of specimen B2**

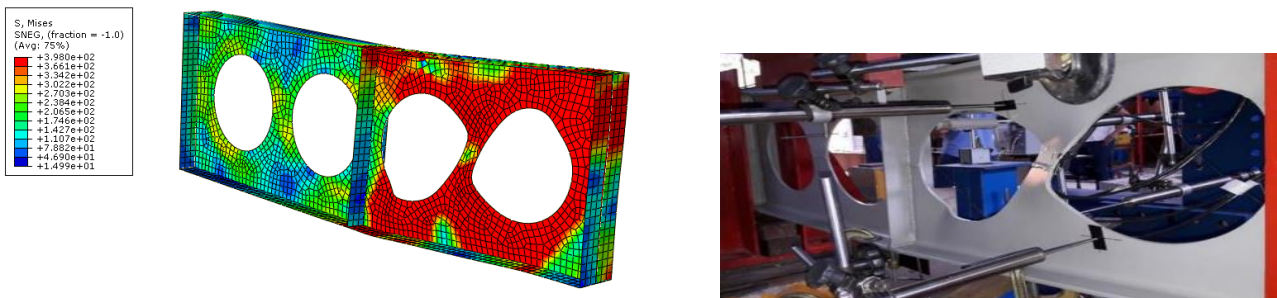


**Figure 2-22: Experimental and FE failure mode of specimen B5**

**II.3.3 Experimental Test conducted by M .Altaee and al [56]:**

The only detailed experimental test on strengthening full scale beams with web openings using FRP materials was conducted by M. Altaee [56] .The experimental prototype had four specimens (305x10x225 UKBs) with a wide span of three meters. The specimen that isn't open was used as a control solid beam named B0 and the three others with rectangular web holes at various places: single opening in the mid span, single opening in the shear zone and two openings in the mid span are named B1-RO, B2-RO and B3-RO respectively. CFRP plates were used to reinforce these beams, as illustrated in **Figures 2-23, 2-24 and 2-25**. To simulate a uniformly spaced load, all beams were evaluated using 6-point bending.

The specimens' ends were supported by two supports vertically restrained the specimen but enabled it to rotate and traverse horizontally .To produce this horizontally movement, a 50mm steel roller was employed at every specimen extremity. To avoid early web stressing and buckling collapse, 130mm broad bearing plates were fitted to the supports. Figure 2-26 describes the characteristics and sizes.

Every tested beam has clear span of 3000mm. Employing an electrical cutter, single or two web apertures of 210 x 185mm dimensions were produced in various locations throughout the specimen length.

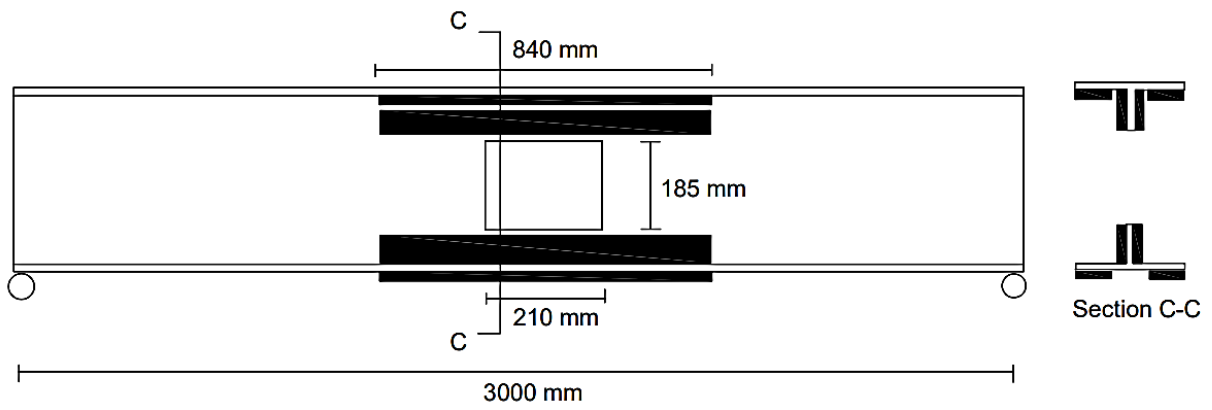


Figure 2-23 : Specimen B1-R0 strengthening arrangement .

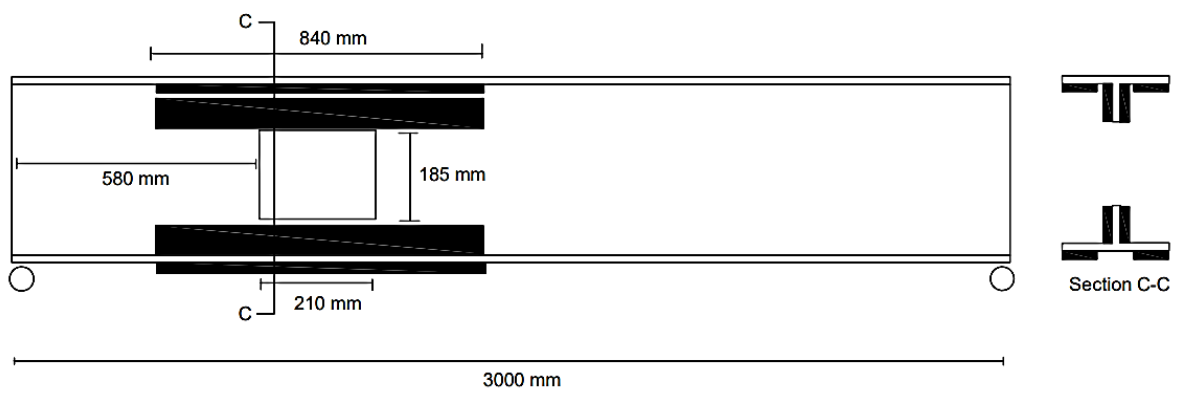


Figure 2-24 : Specimen B2-R0 strengthening arrangement .

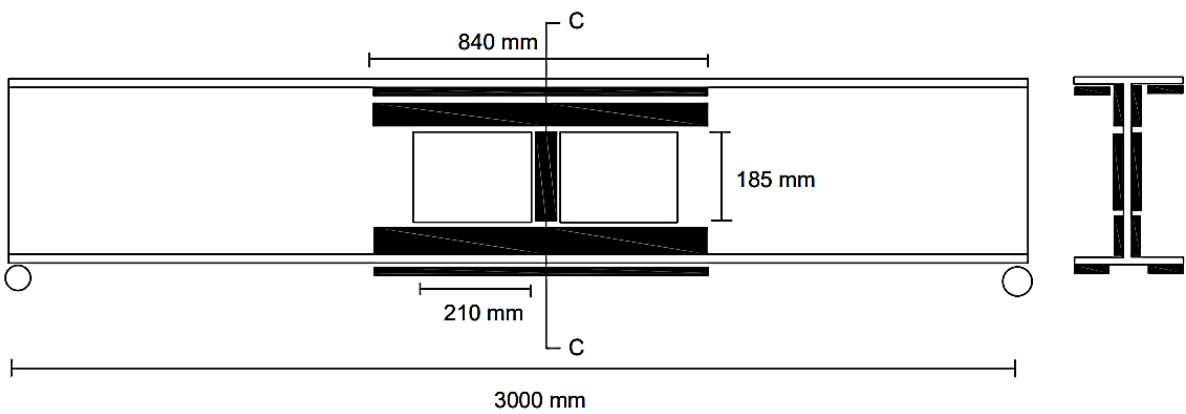
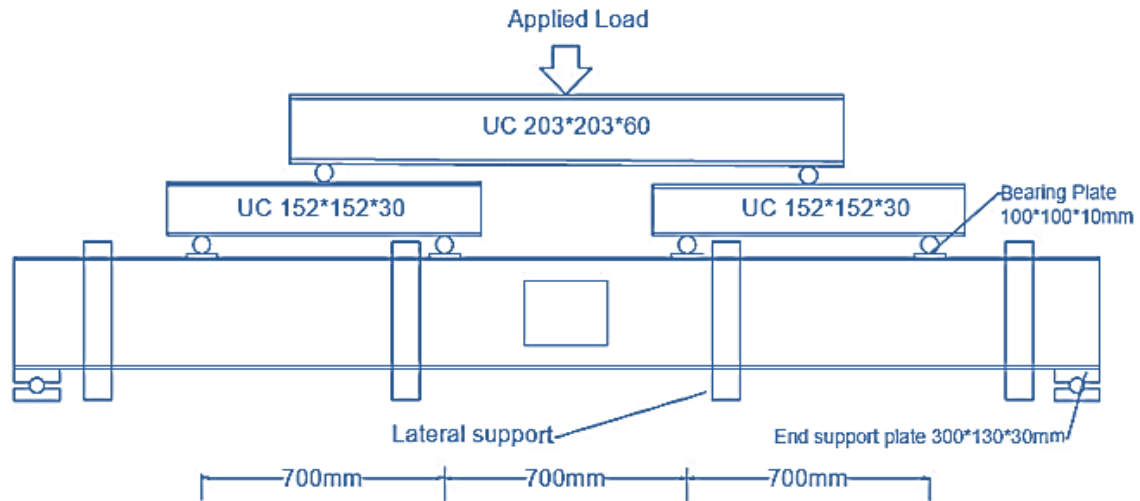
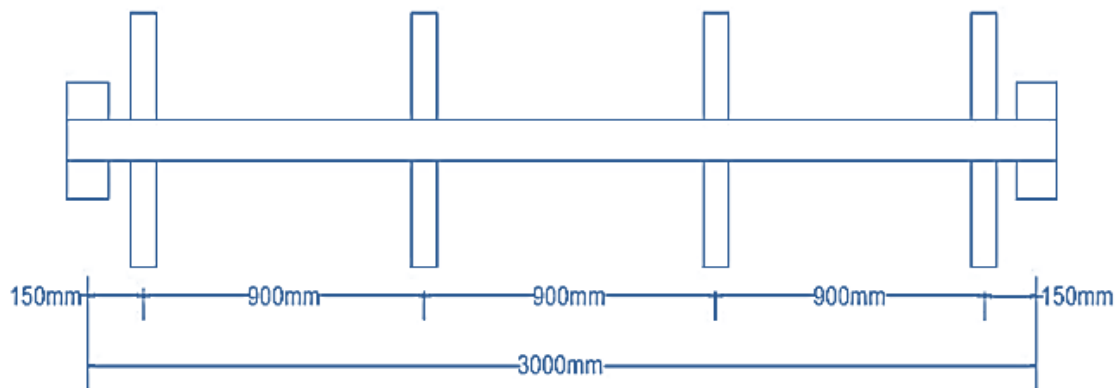


Figure 2-25 : Specimen B3-R0 strengthening arrangement .



(a) Elevation



(b) Plan view

**Figure 2-26 : Experimental test dimensions and arrangement .**

To create lateral constraints, steel frames were manufactured using I-sections (178x102x28 UKB). As illustrated in **Figure 2-26**, they were spread along the span length by 900mm. The steel stress strain curves for the web and the flange was established using tensile coupon tests. Unidirectional CFRP plate of 3 mm thickness, 200 GPa elastic modulus and a tensile strength equal to 2970 MPa, bonded using two parts of epoxy : Araldite 420, Araldite Co .

Mechanical properties of the adhesive were detailed in **Table 2-5** . Mechanical grinding, as detailed in the prior chapter, was utilized to remove the thin oxide layer, resulting in the best possible bond between steel and CFRP. Prior applying the glue and CFRP layers, the area was cleaned to remove any oil or grease. The CFRP plates were bonded to every tested specimen as showed in **Figures 2-23 , 2-24 and 2-25** .

To minimize inadvertent joining, a 10mm metal plate with a PTFE separating film was installed over the CFRP plate locations to avoid any movement or sliding.

Young's Modulus (GPa)	1.5
Ultimate Tensile strength (MPa)	29
Ultimate Shear strength (MPa)	26
Strain at rupture %	4.6

**Table 2-5 :Adhesive mechanical properties**

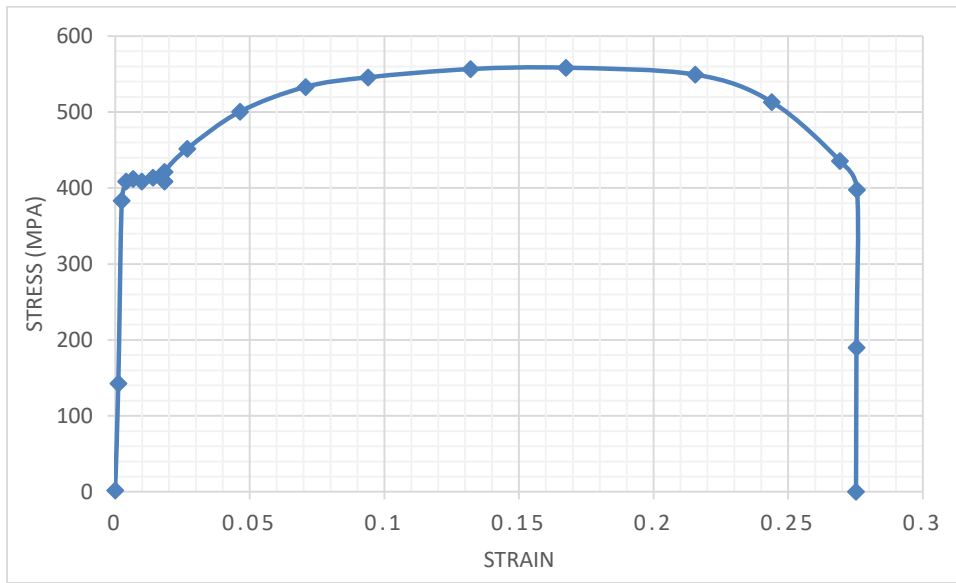


**Figure 2-27 :Tensile stress-stain curve from coupon tests of the flange.**

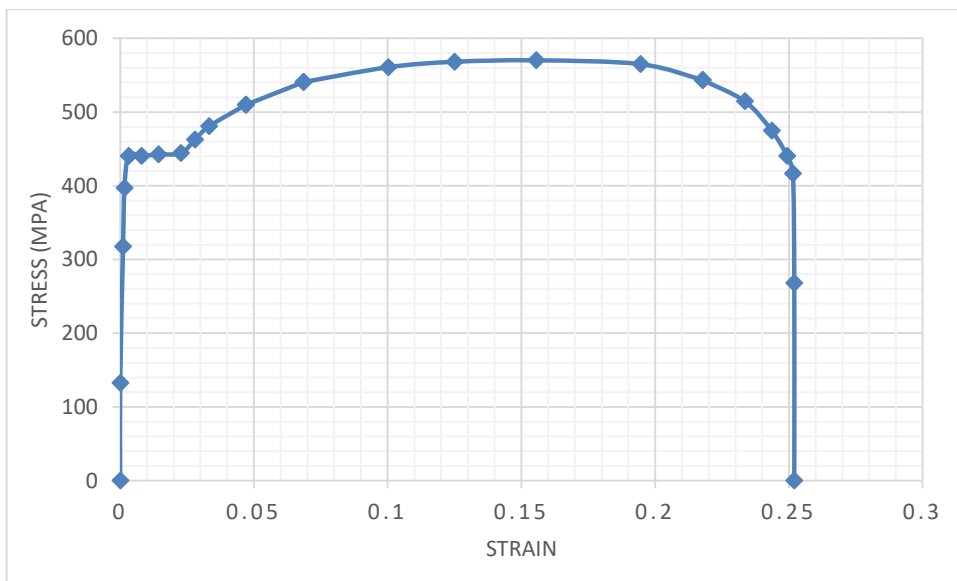


**Figure 2-28 :Tensile stress-stain curve from coupon tests of the web.**

**II.3.3.1.Numerical model :**

The models are evaluated with ABAQUS, following the procedures outlined in previous chapter. The identical loading and boundary conditions that were employed in the test were the same used for all numerical models. The prototypes were supported at the two ends after inserting the bearing plates with the same features as the experiment, and the vertical load was shipped straight to the beam simultaneously as test sites after utilizing the rigid plates. The used contact behavior between these plates and the beam was hard interaction. The friction coefficient used in the support's plates and the specimen's bottom surface was 0.16, while 0.8 has been utilized between the charge plates and the specimens top surface [98]

True stress-strain relationships were employed to convert nominal stress and strain to true stress and strain:

$$\epsilon_{True} = \ln(\epsilon_{nominal} + 1)$$

$$\sigma_{True} = \sigma_{nominal}(\epsilon_{nominal} + 1)$$

The steel was treated as an isotropic material in the simulation while the CFRP plate was designed to be an orthotropic elastic material. As recently described in Chapter 4, the linear response was employed to simulate the CFRP plates in the simulation analysis. A four-node shell element S4R was adopted for both steel and CFRP . As outlined in previous Chapter ,because the CFRP require characteristics in both directions .The previous study conducted by as Abdullah [99] gave the material parameters of CFRP, including tensile strength, elastic modulus, and Poisson ratio in all directions as detailed in **Table 2-6** .

For the aspect of cohesion ,the adhesive substance was modeled using COH3D8, an eight-node three-dimensional cohesive element. The adhesive layer's upper and lower surfaces were tied to the steel and CFRP surfaces, correspondingly. Traction-separation response and appropriate failure criterion were as indicated in the previous section.

Using eigen value analysis, the model includes an initial geometric imperfection based on the first buckling mode. An initial geometric imperfection of H/500 for each beam was employed in the simulation . In regards of stiffness and maximum load, the chosen mesh of 20 mm demonstrated satisfactory agreement with experimental results .

Elastic modulus (MPa)	Poisson ratio	Shear modulus (MPa)
$E_x= 200000$	$\nu_{xy}=0.29$	$G_{xy}=5127.5$
$E_y=14050$	$\nu_{xz}=0.29$	$G_{xz}=5127.5$
$E_z=14050$	$\nu_{yz}=0.6$	$G_{yz}=4390.6$

**Table 2-6 : Carbon FRP mechanical properties .**

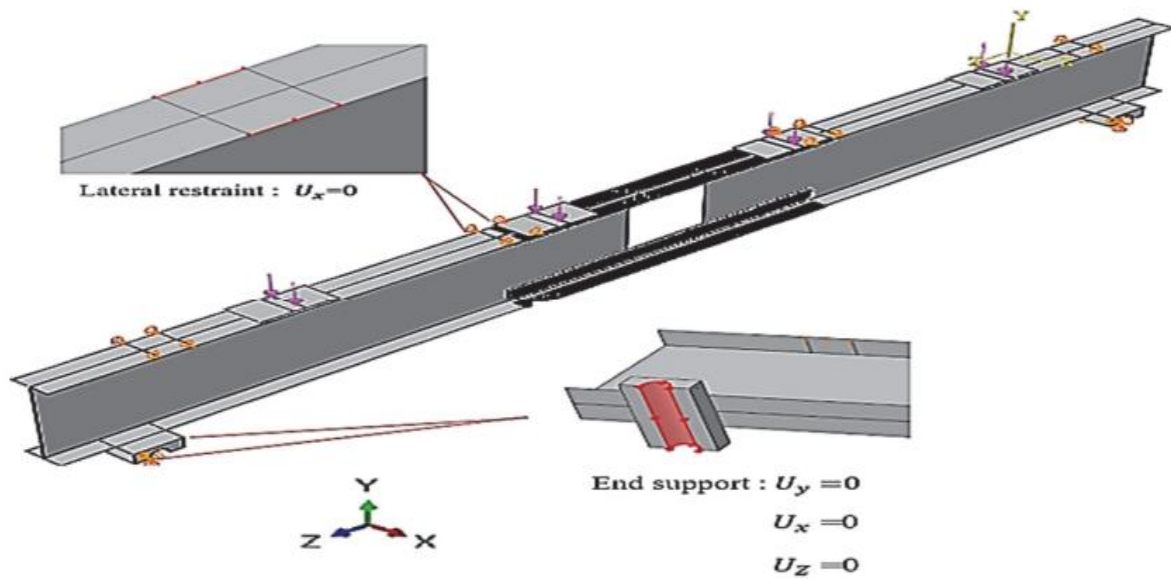


**Figure 2-29 :Numerical model loading and boundary conditions.**

**II.3.3.2. Results and discussion :**

For cost reasons, just the reinforced specimens and the control beam were evaluated experimentally in the test ,so as a means of comparison between experimental findings and numerical model results **Figures 2-30 ,2-31 , 2-32 and 2-33** presents load displacement relationship of specimens B0 and specimens B1-R0 to B3-R0 which are the control solid beam and the strengthened specimens respectively

An elastic range response up to roughly 300 kN was recorded in the early phases of the experiment for the specimen B0, this was also observed in the numerical simulation , further than this level the development of concentrated yield in the inner surface at mid-span was noticed. Finally reaching a an ultimate load of 406kN (**Figure 2-30**) , lateral torsional buckling was detected between the central horizontal constraints (**Figure 2-34**).

The load-displacement behavior of reinforced specimen B1-RO is compared between numerical simulation and experimental test in **Figure 2-31**. Until roughly 440 kN of load, Beam B1-RO showed a very linear pattern in the experimental and numerical simulation . Above this stress level, plastic hinge creation began in the upper flange close to the end of the CFRP plate (**Figure 2-35**) .As a result, lateral buckling started at 478kN of force. The maximum load strength was 500kN; after that the experiment was stopped while in the numerical model the load declined rapidly . However, ,the bond degradation can be predicted utilizing the adhesive damage variable SDEG which has attained a value of 1 at the epoxy edge (**Figure 2-38**).

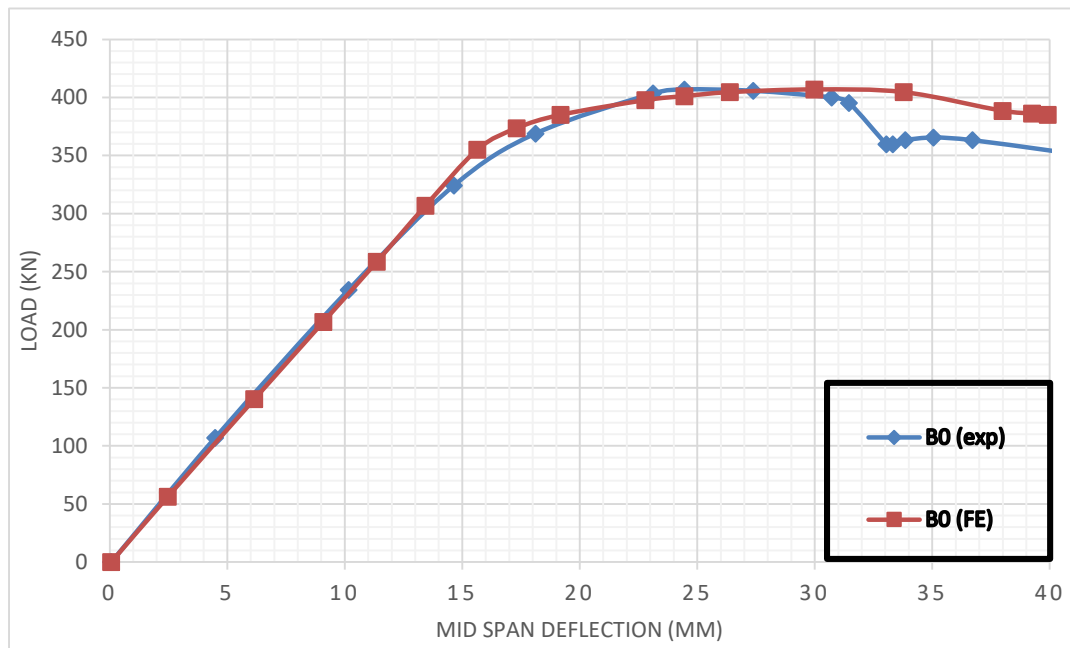


**Figure 2-30: Finite element and experimental load-deflection curve for specimen B0.**

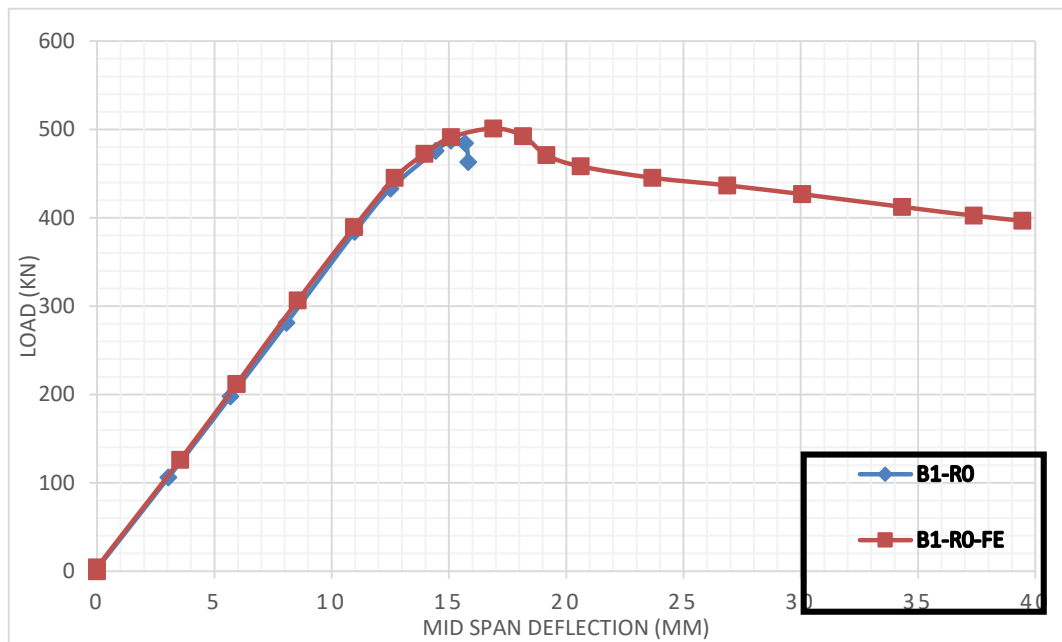


**Figure 2-31: Finite element and experimental load-deflection curve for specimen B1-R0.**

Higher than or equal to 380kN of load, Beam B2-RO likewise showed a line graph, plastic hinge creation started in the upper flange at the mid-span of the specimen beyond this load level (Figure 2-32) . As a result, lateral buckling began between the middle horizontal supports at 396kN of force ,this was also noticed in the numerical model which can clearly be seen in Figure 2-36 .The load was supported by the specimen until it reached 430kN. Lastly, during loading, owing to severe horizontal distortion, a plastic behavior was observed, this was not identified in the test since it was halted immediately load decreasing commenced. The adhesive

had not been affected, as evidenced by the damage parameter SDEG, which had all levels less than one. **Figure 2-33** shows the load deflection at the specimen B3-R0 mid-span which was reasonably linear up to 420 kN of force. Further than stress level, the upper flange at the edge of the CFRP plate began to yield at 448kN of load. As a result, horizontal buckling began at a force of roughly 470 kN, when the load reduced due to plastic lateral distortion. delamination of the CFRP in the inner surface began at this point (**Figure 2-37**).

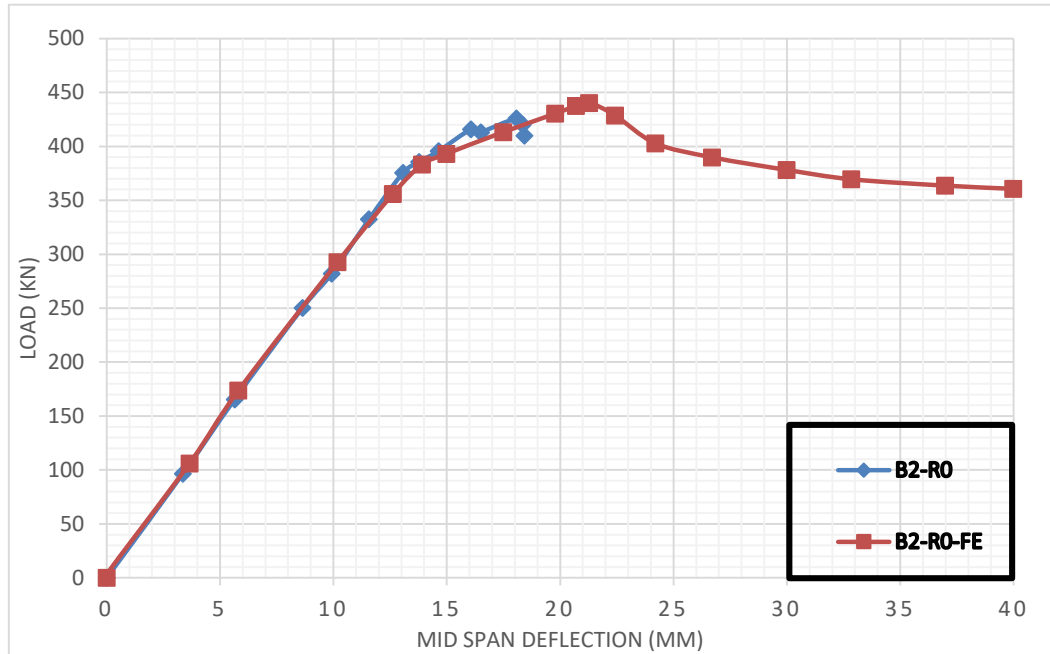


**Figure 2-32: Finite element and experimental load-deflection curve for specimen B2-R0.**

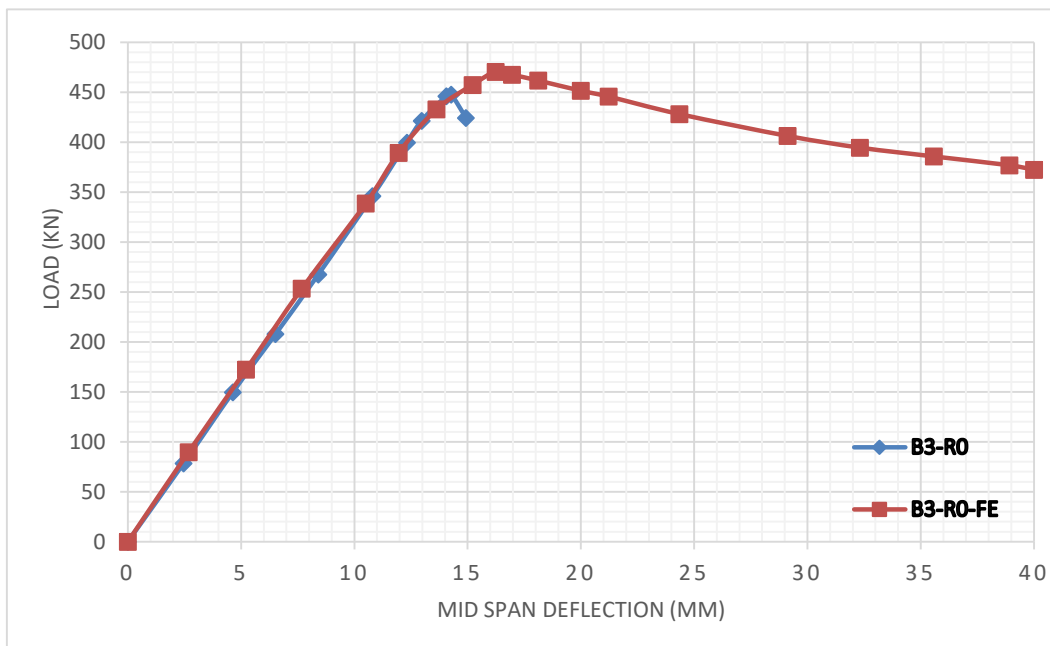


**Figure 2-33: Finite element and experimental load-deflection curve for specimen B3-R0.**



The simulation findings were in excellent accordance with the reported experimental data. In terms of load-displacement correlations, failure mechanism such as the critical occurrence of delamination, these results provides confidence to use the developed numerical model.

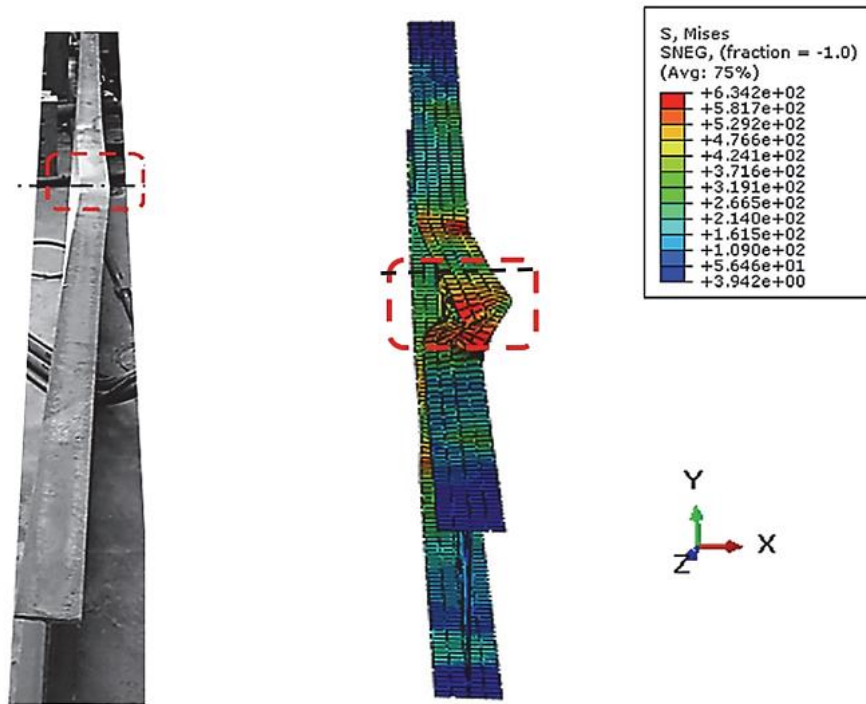


**Figure 2-34 : Finite element and experimental failure mode for specimen B0 .**

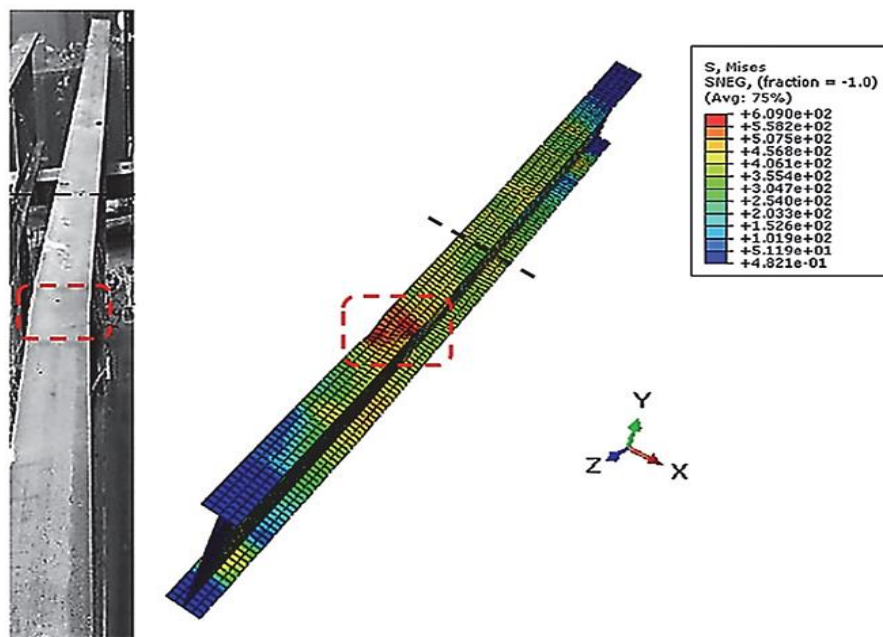


**Figure 2-35 : Finite element and experimental failure mode for specimen B1-R0 .**

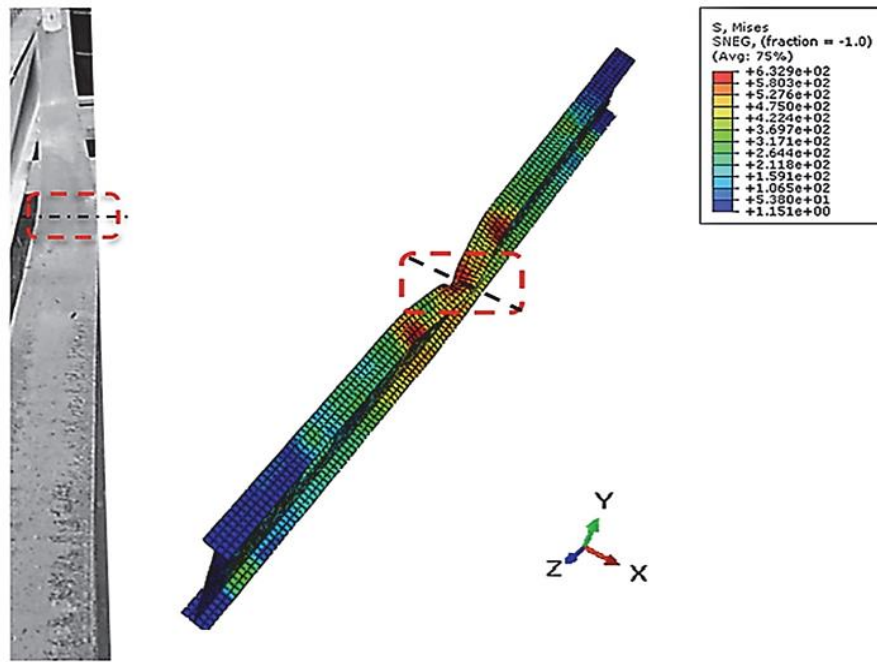


**Figure 2-36 : Finite element and experimental failure mode for specimen B2-R0 .**

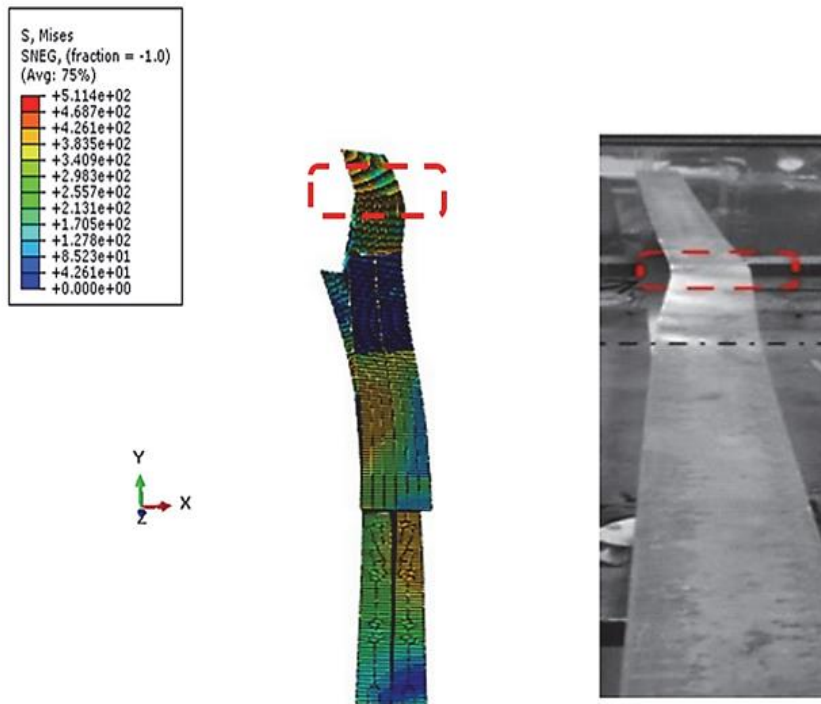


**Figure 2-37 : Finite element and experimental failure mode for specimen B3-R0 .**

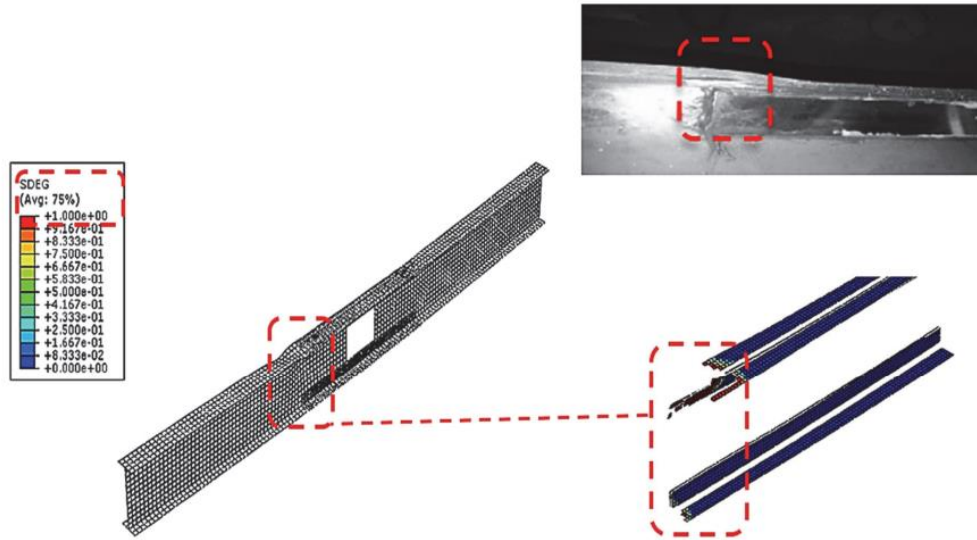


**Figure 2-38 : Bond behavior checking for specimen B1-R0 .**

## **CHAPTER III : STRENGTHENING WEB POST BUCKLING OF CELLULAR BEAMS USING FRP**

### **III.1.Preliminary investigation of web post buckling strengthening using CFRP:**

According to the literature, the most undesirable defect in cellular beams is web post instability. The effectiveness of strengthening web post buckling using CFRP products will be investigated now using the validated numerical model approach described previously. The verified Cellular beam A2 in the study conducted by Lucas and Ricardo 2018 [95] in the previous chapter (**Figure 3-1**) will be strengthened using two type of CFRP products : pultruded T section of :103x387x5mm dimensions and CFRP plate of 103x387 mm dimensions .The CFRP tensile elastic modulus has been taken from a previous study [99]which was equal to 200GPa in the fiber direction and the material properties of other directions are detailed in **Table 3-1**.The tensile elastic modulus of the adhesive was 8GPa with tensile strength 29.7 MPa as seen in **Table 3-2** .

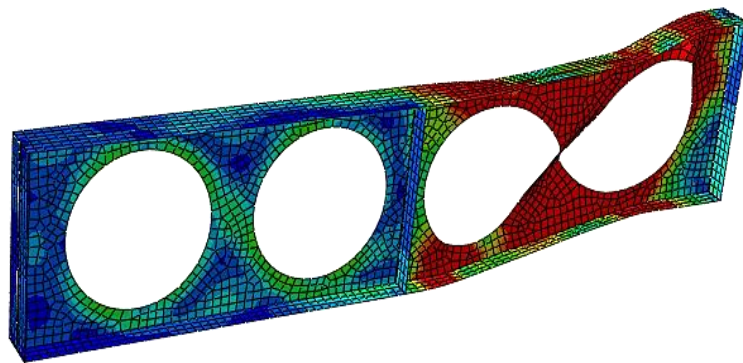


**Figure 3-1 : Web post buckling of the cellular beam A2 .**

Three proposed CFRP strengthening technique positions will be investigated using the pultruded CFRP T section and plate (**Table 3-3**).The S1 strengthening pattern used CFRP laminates only in the failure position and in one side of the web post of the cellular beam A2 while S2 and S3 strengthening technique used CFRP products in the two web posts of the beam in one side and two sides respectively .The effect of different CFRP thicknesses will be included in the case of strengthening by CFRP plate (1mm , 2mm and 3mm ).The CFRP pultruded profile had a fixed thickness equal to 3mm .

The CFRP and the adhesive are assumed to be linear elastic until failure . It should be noted also that both the CFRP plate and the steel section were simulated employing the general-purpose shell element S4R with decreased integration, while the cohesive element COH3D8 was used to model the adhesive layer as described in previous chapter. The upper and lower sides of the adhesive layer were tied to the web post side of the cellular beam and the top of the CFRP plate, respectively. As found previously in the chapter of finite element model validation the mesh size of 20 mm x20 mm was adopted for steel and CFRP . The Discussion of Results will be in term of : load-Vertical displacement ,failure mode, horizontal







displacement measured in point D1,D2,D3and D4 as shown in **Figure 3-2** and bond behavior using the stress degradation parameter SDEG of the adhesive provided by ABAQUS.

Longitudinal modulus of elasticity	200 (GPa)
Transverse modulus of elasticity	20 (GPa)
Major in -plane Passion's ratio	0.3 (GPa)
Out-of-plane Passion's ratio	0.2 (GPa)
In- plane shear modulus	3.7
out-of-plane shear modulus	2.6

**Table 3-1: CFRP mechanical properties**

Elasticity modulus	8 (GPa)
Shear modulus	2.6 (GPa)
Shear strength	26 (Mpa)
Tensile strength	29 (Mpa)

**Table 3-2 :Adhesive mechanical properties**

NAME	CFRP Laminates positions	Strengthened Side
S1		 <b>One side</b>
S2		 <b>One side</b>
S3		 <b>Two sides</b>

**Table 3-3: The three proposed strengthening configuration .**

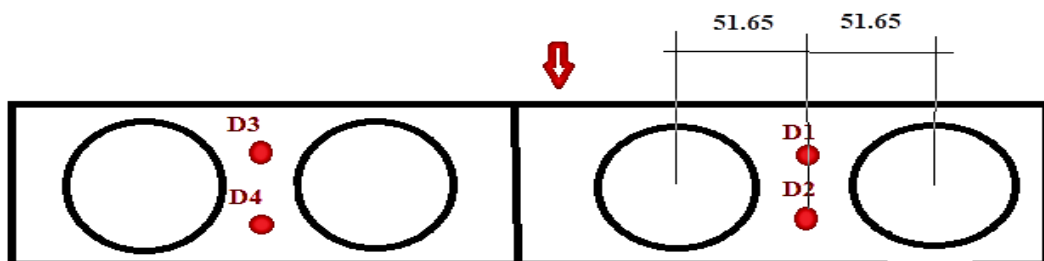


**Figure 3-2 : Horizontal displacement measurement points .**

**III.1.1 Results and Discussions:**

Firstly, for both strengthening types of laminates (CFRP plate-CFRP T section) ,results will be compared to the control beam (Unstrengthened beam A2) and each specimen was given a name: the first character in each specimen designation is the name of the tested beam, followed by the CFRP stiffening configuration (S1 or S2), and finally the CFRP laminate thickness. For example, “A2-S1-3” is the cellular beam “A2” reinforced with bonded CFRP profiles of 3mm in one side of the vulnerable regions.

**III.1.1.1 CFRP plate strengthening :**

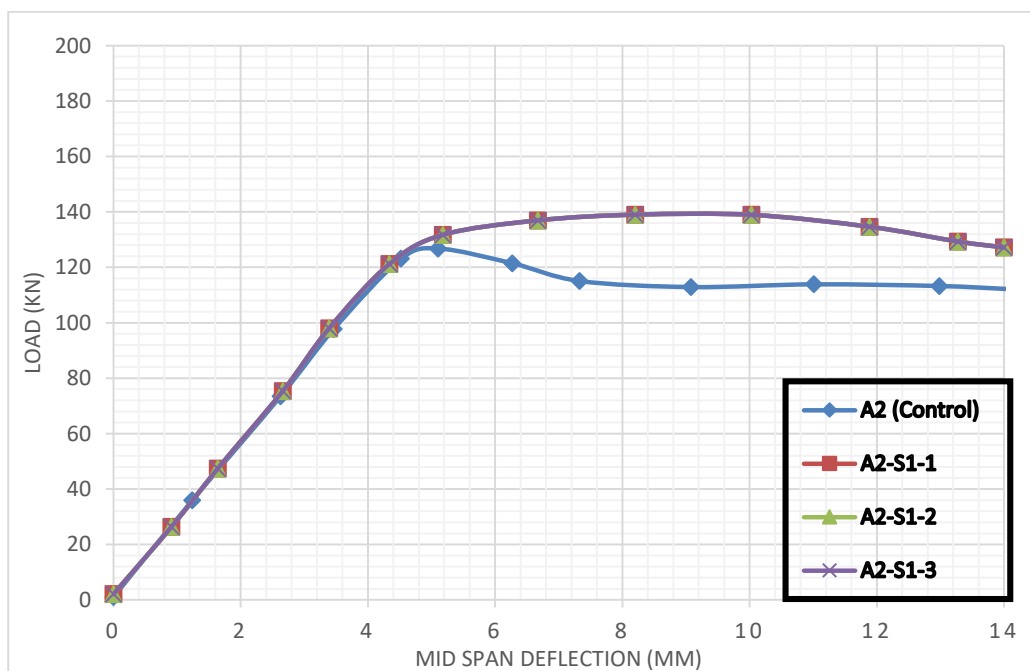


**Figure 3-3 : One side CFRP plate strengthening load-displacement curve (S1) .**

The use of three strengthening configurations, gives different percentages of strength . Positions S1,S2 and S3 have demonstrated significant strength increases ranged from 9.6% and 37.88% compared to the control beam A2 , this can be seen from **Figures 3-4 ,3-5** and **Table 3-4**.

The increase of CFRP plate thickness in these locations did not helped the strength enhancement, for every corresponding configuration, ultimate load ,stiffness and load – displacement response was very similar (Figure 6-4) .The load rose until 125 kN for the control

unstrengthened beam A2, which represented the failure load, after which the force fell, but for the specimens strengthened with CFRP plate, the force increased until 137 kN, at which point web post buckling began.

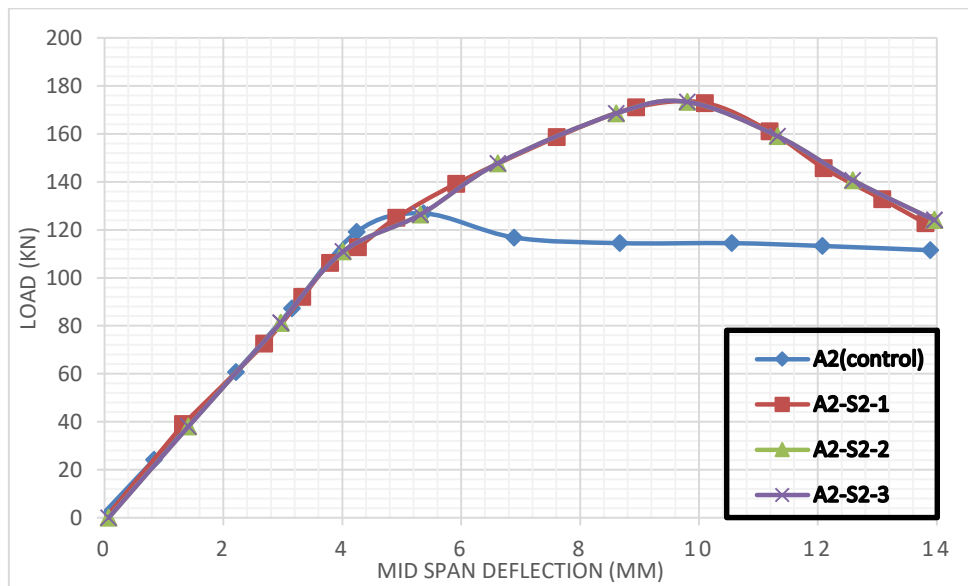


**Figure 3-4: Two sides CFRP plate strengthening in single web post load-deflection curves (S2) .**

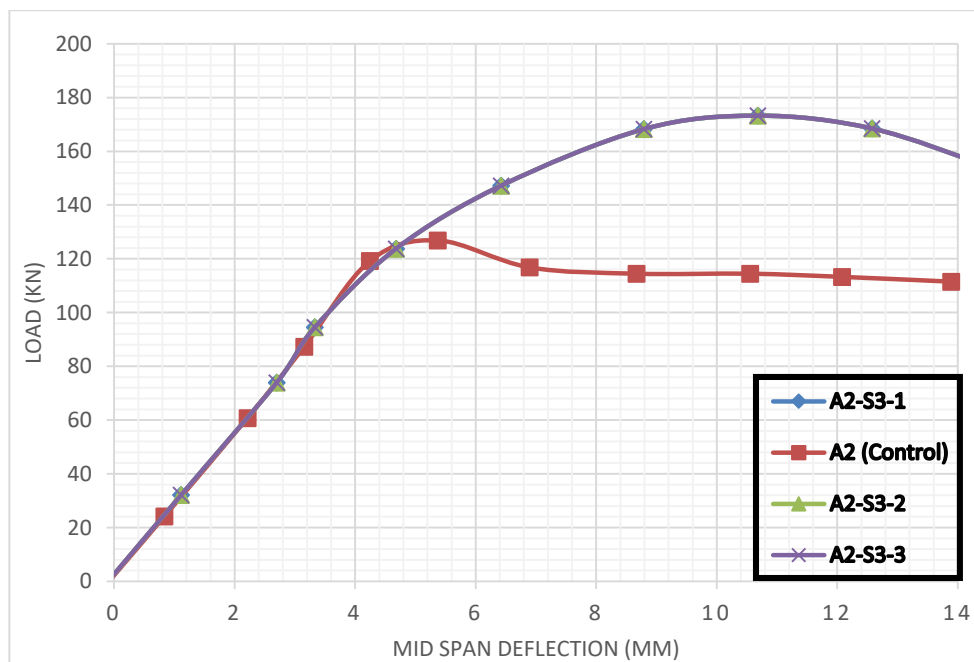


**Figure 3-5 : Two sides CFRP plate strengthening in the two web posts load-deflection curves (S3) .**

Because the failure mechanism of the tested specimens was a local instability phenomenon, and there was no reinforcement in the bottom flange, the vertical displacement was the same for the unreinforced and reinforced instances.



Regarding to **Table 3-4** it can be reported that the CFRP sheet delayed and reduced the horizontal displacement of the web post to a higher load according to configuration type (S2 and S3) and the increasing of CFRP plate thickness. The horizontal displacement was shifted from D1 and D2 measurement points to D3 and D4 measurement points for the three S1 reinforced specimens, indicating that the horizontal displacement was moved from the strengthened web post to the unreinforced one (Figure 3-7). Compared to the control beam, A3-S3-3 given the best stiffer response of the web post displacement among all tested beams.

In this novel technique, in addition to increasing strength and stiffness, the bonding behavior across steel and FRP presents a vital issue that must be considered. The damage of the adhesive layer was investigated using the numerical stress degradation parameter SDEG as explained in the previous chapter of finite element descriptions denoted as D. It can be noticed that no debonding occurred for the S1 strengthening configuration (**Table 3-4**) where the values of damage variable SDEG did not reached 1, this can be explained by the occurrence of failure away from the strengthened area .

Debonding was occurred with S2 configuration (**Table 3-4**), this can be proved by the deletion and damage of the adhesive layer (**Figure 3-10**) which occurred after steel yielding due to an excessive web post buckling (**Figure 3-8**). It can also be observed for S3 strengthening configuration in all cases damage parameter was  $<1$  which indicate that debonding did not occurred despite that it was close to 1 .

Although the strength and stiffness was enhanced for all tested beams. The first configuration S1 failed by web post buckling away from the strengthened area which confirm the change of the stress state of the beam due to the presence of CFRP.

On the other hand the web post buckling failure mode of the S2 configuration was accompanied by slight or end debonding of the CFRP plate .Furthermore ,It can be noticed that despite the strength enhancement of S2 and S3 were closely the same the bond behavior was not identical ,no debonding was occurred for the S3 strengthening arrangement contrary to the S2 technique ,the same failure mode was seen for all tested beams of S3 configuration but no debonding occurred which means that the use of CFRP in both sides of web help in avoiding the bond separation failure mode and the specific position of the CFRP is frequently more important in this novel technique of reinforcement.

Based on these results ,web post buckling was not prevented for all strengthening configurations using CFRP plate .It is logical that by adding CFRP plate thickness to the beam, you may prevent the web post from buckling; but, debonding will be predominant and preliminary; also, in actual design, an economical amount of material to do this must be determined. As said before, de-bonding frequently influences the failure of the reinforcement rather than the capability of the CFRP core.

This will encourage the use of another carbon fiber reinforced polymer product (CFRP), in order to find the best configuration and effective system strengthening. It was decided to use pultruded carbon fiber reinforced polymer profiles bonded as a stiffener to web post buckling. The CFRP T section of 3 mm thicknesses, inspired by typical welded steel plate stiffeners, will now be examined as an alternative to the CFRP plate employed in this part



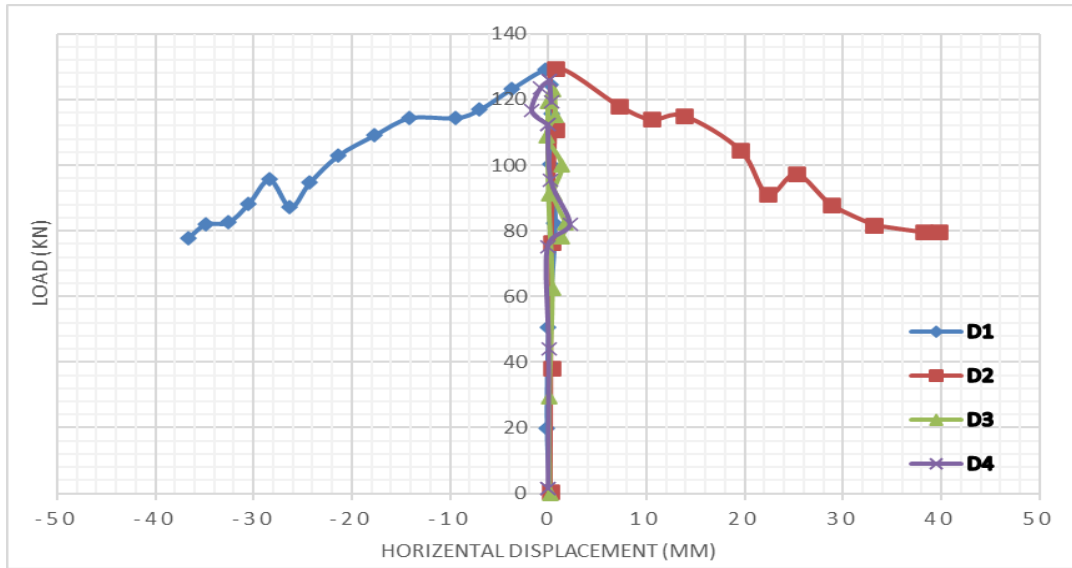


**Figure 3-6:Horizontal displacements for control beamA2**

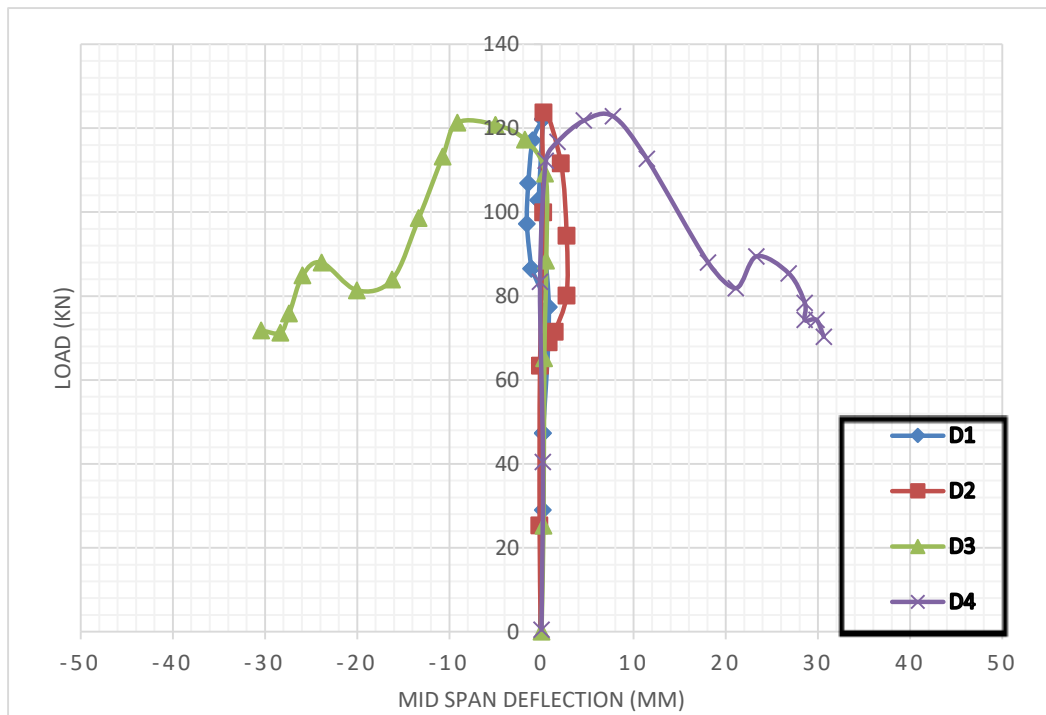


**Figure 3-7 :Horizontal displacements for specimen A2-S1-1.**

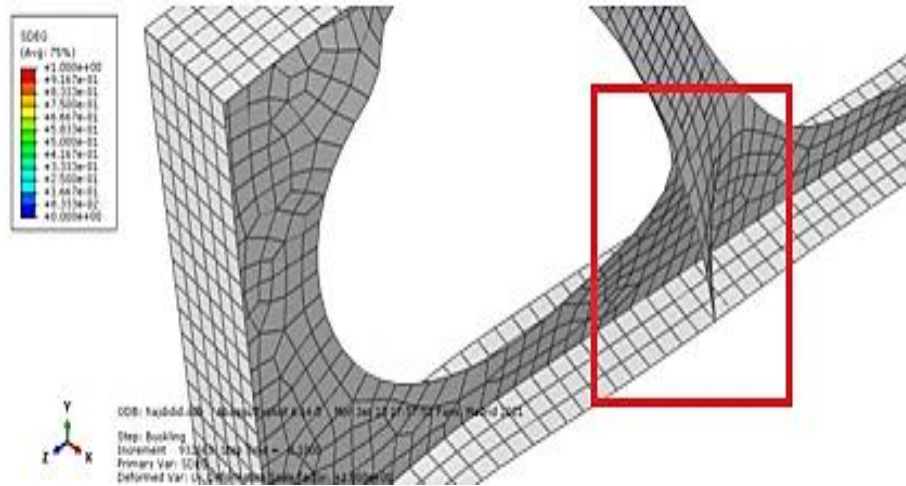


Figure 3-8 :CFRP plate debonding

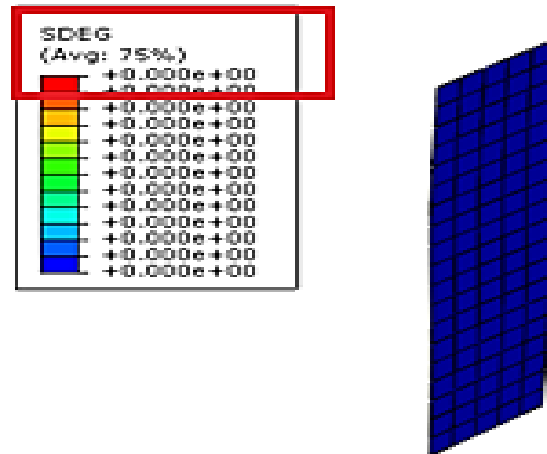


Figure 3-9 : No adhesive layer damage on S1 strengthening pattern

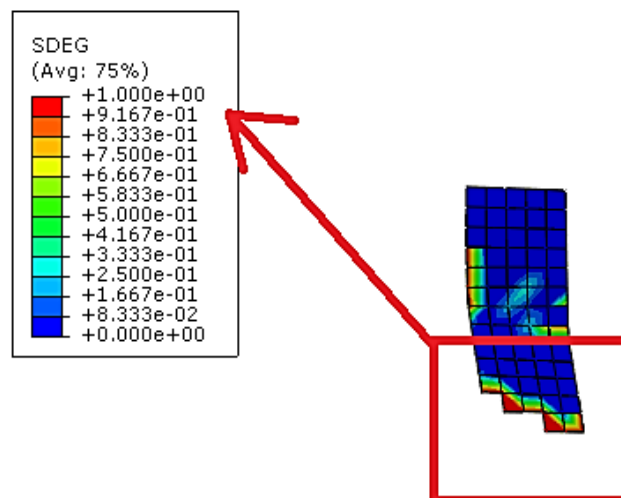


Figure 3-10: Adhesive layer deletion of S2 strengthening pattern.

	<b>BEAM</b>	<b>CFRP Thickness (mm)</b>	<b>Pu(kN)</b>	<b>D1(mm)</b>	<b>D2(mm)</b>	<b>D3(mm)</b>	<b>D4(mm)</b>	<b>SDEG</b>	<b>Failure Mode</b>
Control	A2	-	125.67	38,54	-36,3	3,4	1,32	/	WPB
S1	A2-S1-1	1	137,85	-0,52	2,59	-30,17	30,29	0	WPB
	A2-S1-2	2	137,99	-0,45	2,57	-30,13	30,02	0	WPB
	A2-S1-3	3	138,06	-0,41	2,43	-30,2	30,06	0	WPB
S2	A2-S2-1	1	170,95	-2,2	4,79	-30,43	32,07	1	DB+WPB
	A2-S2-2	2	171,05	-4,61	5,48	-19,35	30,05	1	DB+WPB
	A2-S2-3	3	171,19	3,94	-3,97	-10,69	31,76	1	DB+WPB
S3	A3-S3-1	1	172,91	-18,14	34,25	-11,21	13,35	0.723	WPB
	A3-S3-2	2	173,12	-19,21	31,75	-10,13	13,96	0.808	WPB
	A3-S3-3	3	173,26	-17	25	-8,46	9,18	0.887	WPB

**Table 3-4:Results of all strengthened cellular beams using CFRP plate**

**VI.1.1.2 CFRP Pultruded T section strengthening :**

	<b>BEAM</b>	<b><math>Pu_{(KN)}</math></b>	<b>D1(mm)</b>	<b>D2(mm)</b>	<b>D3(mm)</b>	<b>D4(mm)</b>	<b>SDEG</b>	<b>Failure Mode</b>
Control	A2	125.67	38,54	-36,3	3,4	1,32	/	WPB
TS1	A2-TS1	158,41	-0,125	0,32	27,25	-23,07	0	WPB
TS2	A2-TS2	181,28	2,96	-0,65	0,82	0,43	1	V+DB
TS3	A2-TS3	183,37	1,49	-0,11	0,59	0,19	1	V+DB

**Table 3-5 : Results of all strengthened cellular beams with pultruded T section.**

The numerical results obtained from pultruded profile T section of 3 mm strengthening technique present an increase in the peak load for each strengthening configuration case ,this can be seen in **Figure 3-11** and **Table 3-5**. Compared to control beam ,A2-TS1 gained 26.05% of strength while A2-TS2 and A2-TS3 was nearly the same with 44.25 % and 45.91% of strength enhancement respectively. Furthermore, as compared to the prior CFRP plate strengthening the T section profile gave improved performance and strength augmentation .

The yielding load for the control beam was recorded at 125 kN, at which level instability in the web post was seen and the curve decreased rapidly, but for specimen (A2-TS1), the load was increased to 158 kN, at which point instability in the web post appeared (**Figure 3-11**). The load for specimens (A2-TS2 and A2-TS3), on the other hand, was increased to around 180kN (**Figure 3-11**).

**Table 3-5** shows that the horizontal displacement for specimen A2-TS1 was adjusted from D1 and D2 measurement points to D3 and D4 measurement points as discovered using the S1 reinforcement approach employing CFRP plate. It can also be seen that no horizontal displacement was happened for A2-TS2 and A2-TS3 Due to the presence of pultruded CFRP profile (**Figure 3-12** ),the horizontal displacement measured was nearly zero.

TS1 strengthening configuration gives the same results found with the CFRP plate(S1 strengthening arrangement ), lateral displacement was recorded away from the strengthened area (D3 and D4).

Slight end debonding was observed for beams A2-TS2 and A2-TS3 at load of 153Kn but the CFRP Profile did not detached from the beams until the failure, this can be clearly seen from the scalar damage SDEG in **Table 3-5** which reached the value 1. In the other hand debonding did not observed for TS1 strengthening configuration which can also be explained by the web post buckling which occurred far from the reinforced area .

Compared to the reference beam A2 ,the failure mode of A2-TS2 and A2-TS3 was changed from web post buckling to Vierendeel failure **Figure 3-13** due to the influence of T shaped CFRP section which was able to retain the web post from buckling.

For the beam A2-TS1 which is strengthened with S1 configuration failure mode was the same observed with strengthening by CFRP plate , the Pultruded section changed the stress state of the beam .

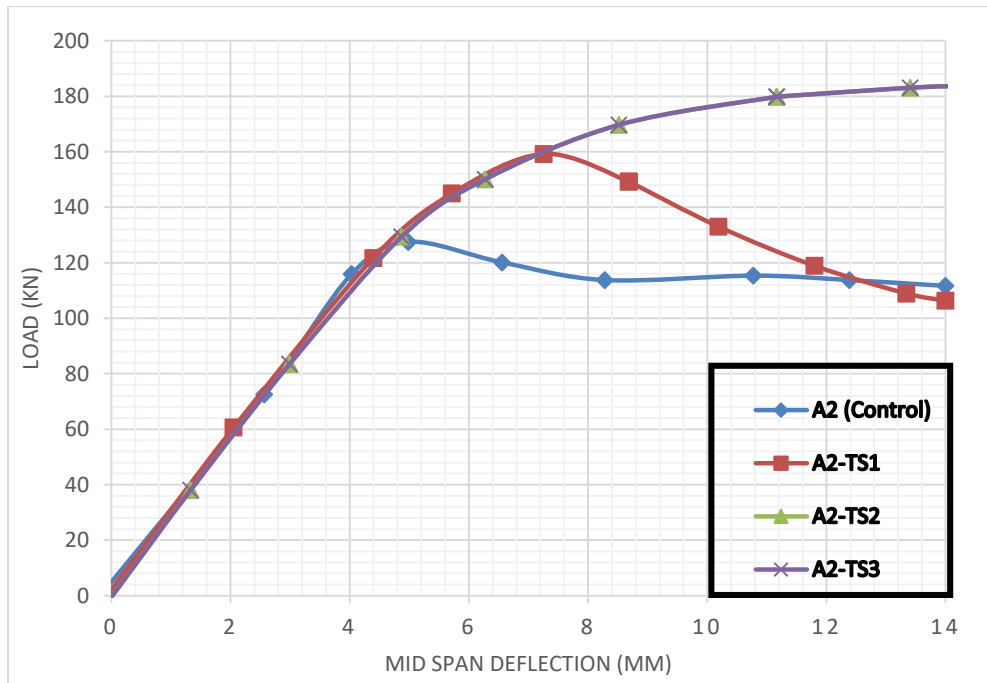


**Figure 3-11 :Load –vertical displacement curves of 3 mm T section CFRP reinforcement**

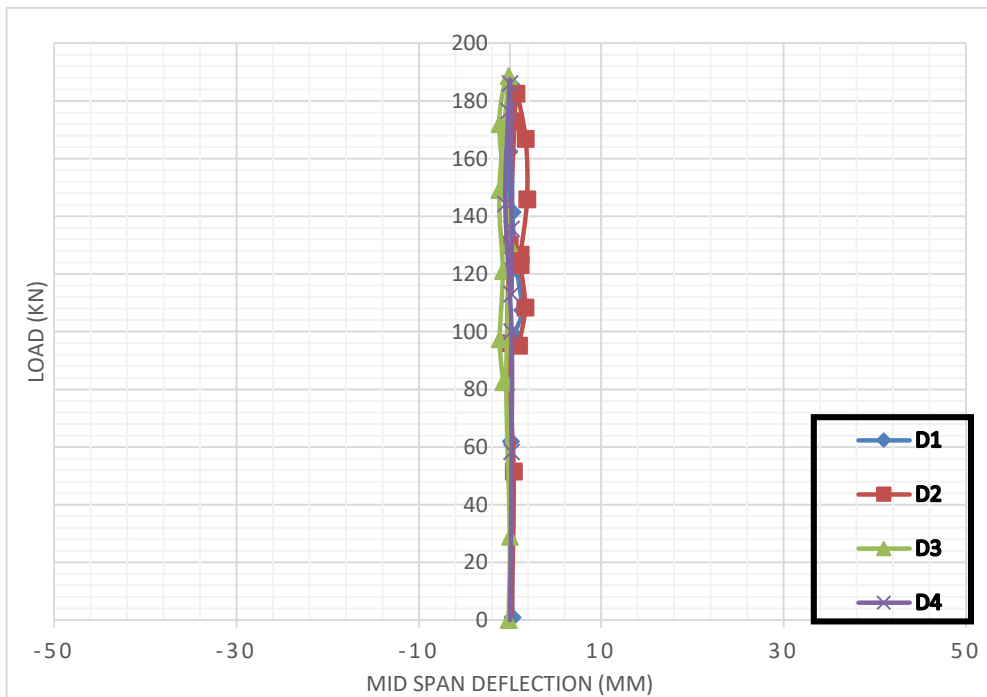


**Figure 3-12 :Horizontal displacement of beam A2-PS3**

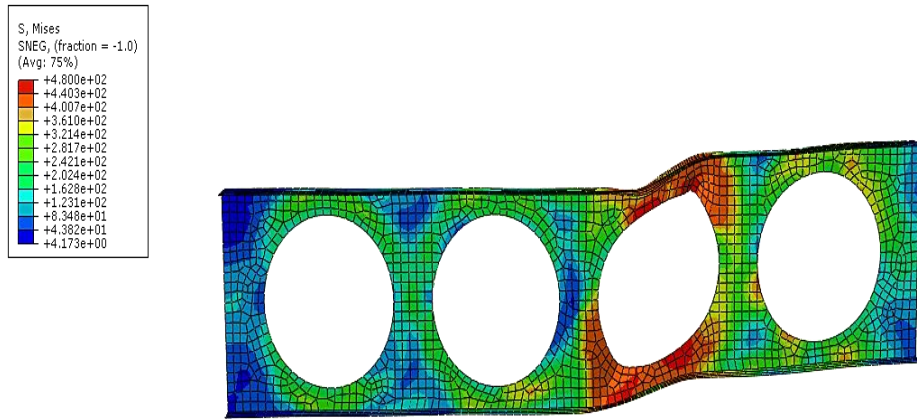


**Figure 3-13:Vierendeel failure of A2-TS3.**

### **III.2.Strengthening web post buckling if cellular beams using pultruded carbon profiles :**

The previous results found in the first part encouraged to investigate the effectiveness of strengthening web post buckling of cellular beams using carbon pultruded profiles .The verified and numerically validated cellular beams in the previous chapter of finite element model validation which were tested in the experimental test conducted by Lucas and Ricardo [95],named: A2, A5, B2, and B5 will be strengthened using two pultruded CFRP profiles sections bonded in the instability regions (**Figure 3-14** and **Figure 3-15**)

- The T shaped section .
- The U shaped section .

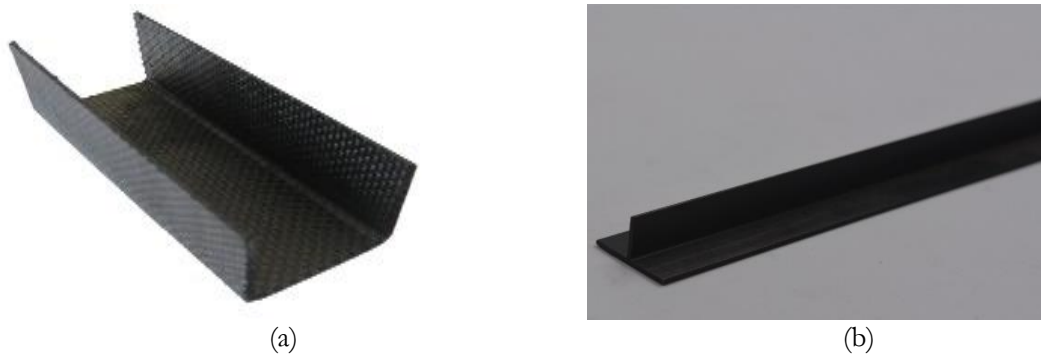


**Figure 3-14 : CFRP pultruded profiles : (a) U section –(b) T section.**

As the selection of an optimum CFRP profile dimension for our case is not specified in any design rule, for all tested specimens the pultruded stiffener’s width was selected to be equal to the web post width while the length was preferred to cover the full depth of the web post and avoid the weld seam , between the web post and the flange for all tested specimens **Table 3-6** and **Figure 3-16** . The impact of bonding pultruded stiffeners in one side and two opposing sides was investigated in this study using two strengthening configurations named PS1 and PS2 respectively, PS1 approach implies bonding pultruded profiles to one side of web posts, whereas PS2 technique offers attaching profiles to both sides of web posts (**Figure 3-15**). The

impact of various CFRP profile thicknesses was also considered. (3mm , 6 mm and 10 mm profile thicknesses ) .The CFRP elastic modulus in the fiber direction was 200 MPA and properties of other directions are detailed in **Table 3-7**.The adhesive's tensile young's modulus was 11.3 GPa with a tensile strength of 22.3 MPa [100]. The effect of web post slenderness on the strengthening technique was also explored, it was calculated using the following mathematical formulations [10,95] :

$$\lambda = \frac{l_m \sqrt{12}}{t_w} \quad (34)$$

$$l_m = 0.5 \sqrt{S^2 - d_0^2} \quad (35)$$

The Discussion of Results will be in terms of : Ultimate load enhancement, load-Vertical displacement response, failure mode and bond behavior.

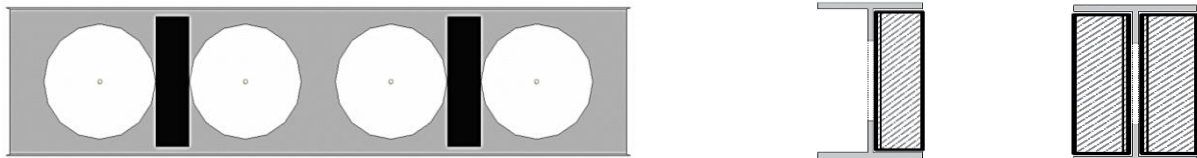


**Figure 3-15 : Strengthening configuration and bonding positions: PS1 and PS2 configurations.**

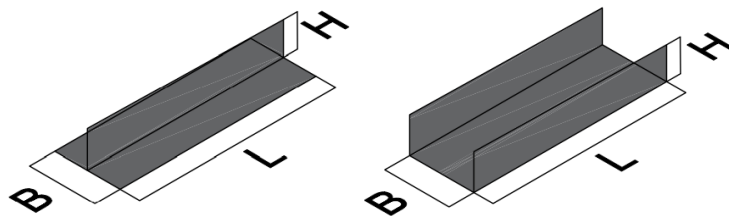


**Figure 3-16 :Pultruded carbon T section and U section profiles dimensions .**

Spécimens	T section dimensions (mm)			U section dimensions (mm)		
	B	L	H	B	L	H
A2	103	419	50	103	419	50
B2	106	423	50	106	423	50
A5	76	396	50	76	396	50
B5	74	393	50	74	393	50

**Table 3-6 : Pultruded carbon T section and U section profiles dimensions.**

Elastic modulus (MPa)	Poisson ratio	Shear modulus (MPa)	Tensile/shear strength (MPa)
$E_x=200000$	$\nu_{xy}=0.29$	$G_{xy}=51277$	$X_t=2400, X_c=2250$
$E_y=14050$	$\nu_{xz}=0.29$	$G_{xz}=5127.7$	$Y_t=69, Y_c=350$
$E_z=14050$	$\nu_{yz}=0.6$	$G_{yz}=4390.6$	$S=87$

**Table 3-7 :CFRP mechanical properties [99] .**

**III.2.1.Results and discussion:**

The results of the FE investigation are described in the next section; each specimen was given a name: The first character in each specimen designation is the name of the tested beam, followed by the CFRP stiffening configuration (PS1 or PS2), and finally the CFRP profile thickness. For example, ‘A2-PS1-3’ is the cellular beam ‘A2’ reinforced with bonded CFRP profiles of 3mm in one side of the vulnerable regions. It should also be noted that the discussion of results was separated into two groups according to dimensions and structural behavior of strengthened beams: Group 01 comprises specimen A2 and specimen B2 while Group 2 includes specimens A5 and B5 .

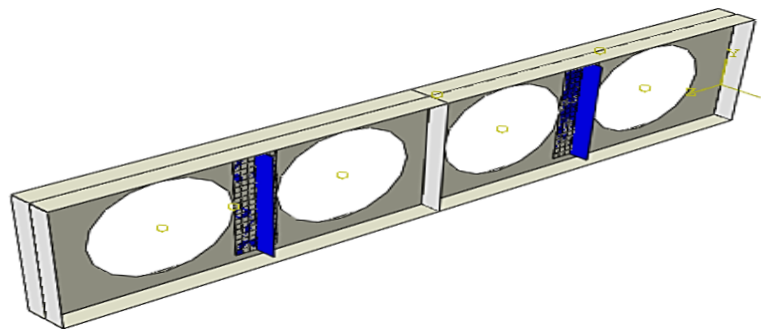


**Figure 3-17 :CFRP T section strengthening .**

**III.2.1.1.T section strengthening :**

The load-deflection curves of all FRP T section strengthened beams are plotted in **Figures (3-18 and 3-19 )** for groupe 1 specimens and **Figures (3-20 and 3-21)** for groupe 2 tested specimens . **Table 3-8** lists the ultimate load capacities of stiffened and unstiffened cases.

It can be seen that Group 1 strengthened specimens have demonstrated identical responses in all cases, this can clearly be shown in **Figure 3-18** and **Figure 3-19**, despite the fact that they all had significantly higher strength than control beams (around 47 % for A2 strengthened beams and around 32 % for B2 strengthened beams), the use of different profile thicknesses and strengthening configurations did not produced the desired difference in load enhancement, and the reached ultimate loads were close in all cases.

On the other hand, the percentage of ultimate load augmentation for Group 2 reinforced beams varied depending on the strengthening technique and the T section profile thickness ( **Table 3-8**) when compared to control beams A5 and B5, the strength gain ranged from 24% to 38 %



and 16% to 31 %, respectively. The ultimate load improved as the profile thickness increased. For all Group 2 scenarios, the PS2 arrangement outperformed the PS1 configuration in terms of strength . Due to the identical structural behaviour of Groupe 2 tested beams, the load-vertical displacement response of A5 and B5 reinforced beams were extremely comparable (**Figures 3-20 and 3-21**), the load curves for PS1 configuration with one side stiffening declined earlier than for PS2 configuration, indicating the earlier beam failure.

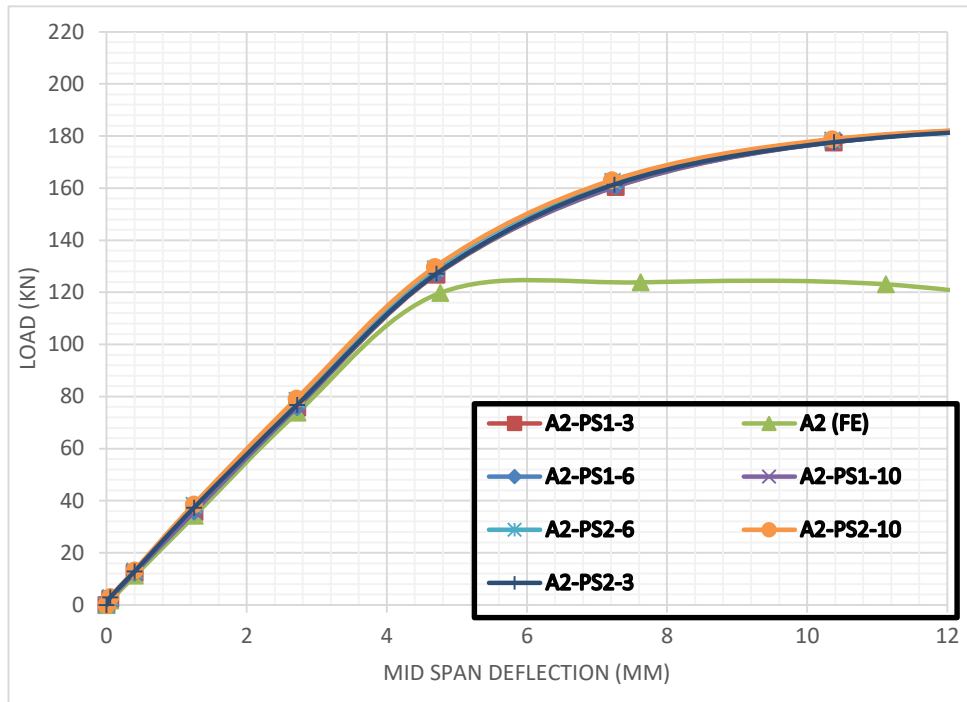


**Figure 3-18: Load -deflection curves of T section strengthening specimen A2 .**

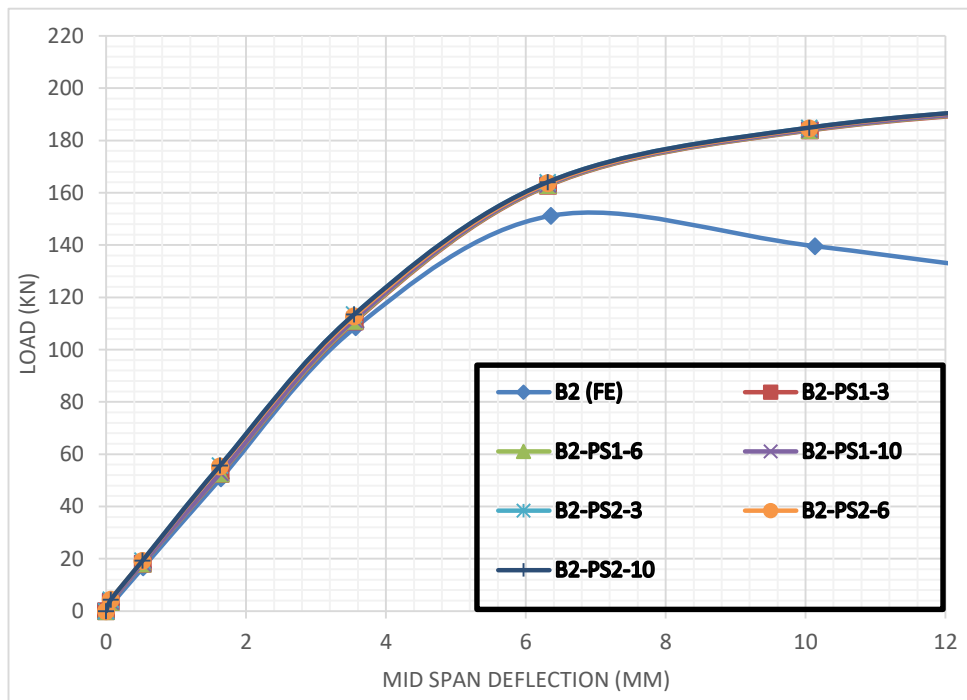


**Figure 3-19: Load -deflection curves of T section strengthening specimen B2.**

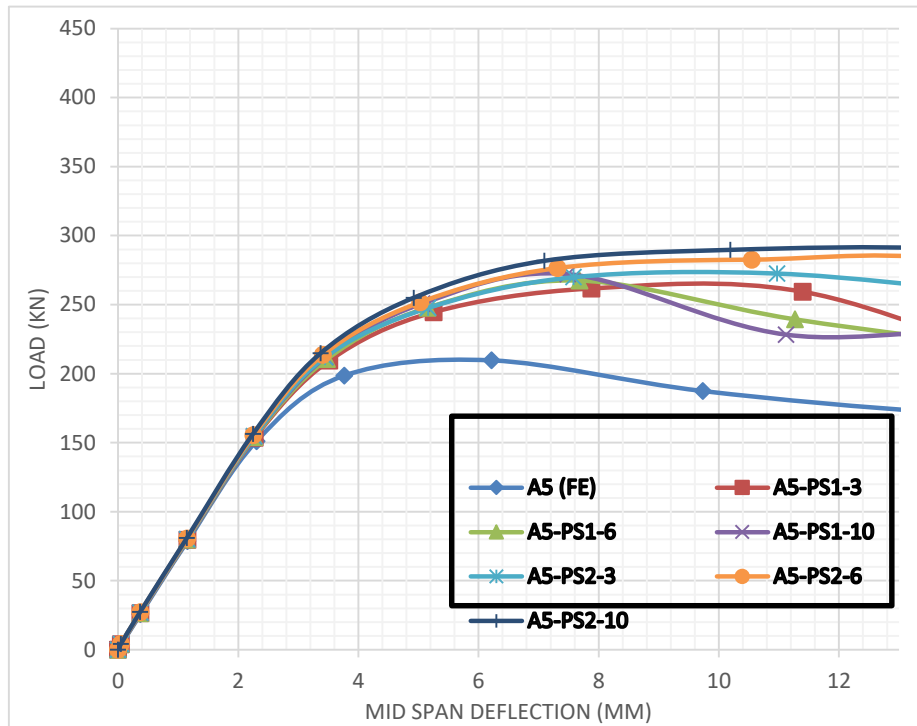


Figure 3-20: Load -deflection curves of T section strengthening specimen A5.

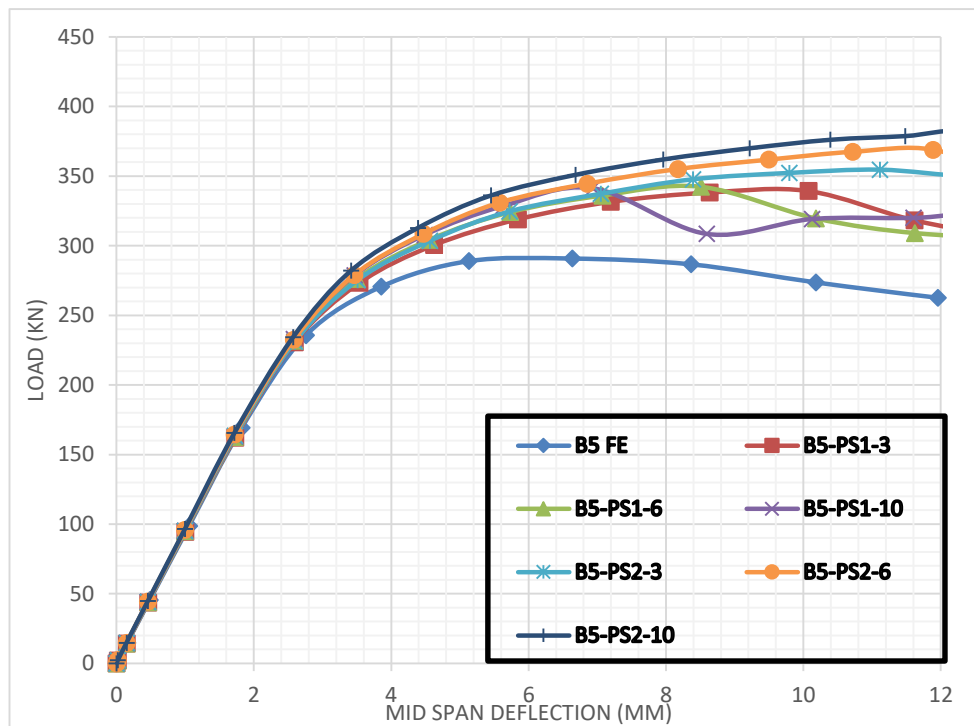
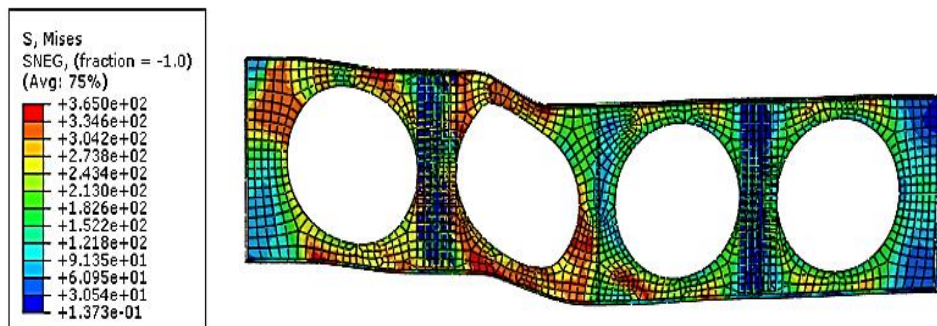


Figure 3-21: Load -deflection curves of T section strengthening specimen B5.

The bond behavior has been checked using the numerical output SDEG (stress degradation). For Group 1 tested beams debonding happened in all PS1 situations. However, the SDEG value did not approach 1 in any PS2 configuration (Table 3-9). This was explained by the

complement of adhesive layers facing each other's resistance [101]. It can also be noticed from **Table 3-9** that brittle debonding occurred in all cases of Group 2 beams which might be explained by the sudden buckling of the slender web post. Therefore, regarding to the bond behavior and the web post slenderness in all cases of strengthened beams, debonding was primarily influenced by the web post slenderness.

Different failure mode of Group 1 tested beams was observed. For A2 strengthened beams, the failure mode was changed to Vierendeel failure with slight debonding of T section profile for PS1 configuration (**Figure 3-22**). Although web post-buckling was not avoided for B2-PS1-3 and B2-PS1-6, a profile thickness of 10 mm (B2-PS1-10) was willing to alter the stress state of the beam and change the failure mode to Vierendeel failure which was also accompanied by slight profile debonding. As previously stated, the PS2 arrangement allowed the tested beams to fail via Vierendeel failure without debonding, confirming that using CFRP on both sides of the web post helps to prevent the bond separation failure mode. In contrast to the aforementioned Group 1 beams, all Group 2 strengthened beams failed by T section debonding due to an excessive web post-buckling (**Figure 3-24**), indicating that, unlike the aforementioned Group 1 beams, the pultruded T section stiffeners were unable to change the failure modes of Group 2 strengthened beams, the undesirable web post-buckling was only delayed to a higher load.



**Figure 3-22: Vierendeel failure mode for specimen : A2 -PS1-3.**

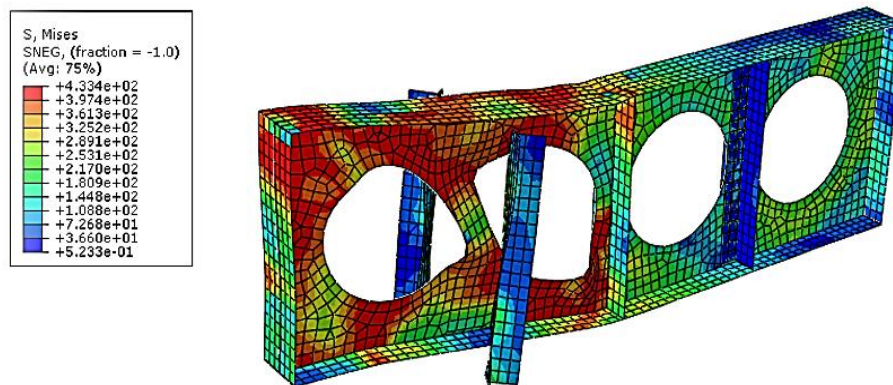


**Figure 3-23: Web post-buckling failure mode and profile debonding for specimen: A5-PS2-6**

<b>Spécimen</b>	<b><math>P_u</math> (KN)</b>	<b>Strength enhancement (%)</b>
A2	123.82	/
A2-PS1-3	182.58	47.45
A2-PS1-6	182.63	47.49
A2-PS1-10	182.67	47.52
A2-PS2-3	182.82	47.64
A2-PS2-6	183.12	47.89
A2-PS2-10	183.18	47.94
B2	151.18	/
B2-PS1-3	198.09	31.02
B2-PS1-6	199.00	31.22
B2-PS1-10	199.35	31.86
B2-PS2-3	199.58	32.01
B2-PS2-6	199.95	32.25
B2-PS2-10	200.29	32.48
A5	209.63	/
A5-PS1-3	261.71	24.84
A5-PS1-6	267.42	27.56
A5-PS1-10	272.11	29.80
A5-PS2-3	272.51	29.99
A5-PS2-6	282.59	34.80
A5-PS2-10	290.65	38.64
B5	290.77	/
B5-PS1-3	339.27	16.67
B5-PS1-6	342.31	17.72
B5-PS1-10	342.32	17.72
B5-PS2-3	354.61	21.95
B5-PS2-6	368.9	26.87
B5-PS2-10	381.75	31.28

**Table 3-8 :T section strengthening ultimate load enhancement .**

<b>Spécimen</b>	<b>Web post slendress</b>	<b>SDEG</b>	<b>Failure mode</b>
A2	102.84	/	WPB
A2-PS1-3	102.84	1	V+DEB
A2-PS1-6	102.84	1	V+DEB
A2-PS1-10	102.84	1	V+DEB
A2-PS2-3	102.84	0	V
A2-PS2-6	102.84	0	V
A2-PS2-10	102.84	0	V
B2	94.09	/	WPB
B2-PS1-3	94.09	1	WPB+DEB
B2-PS1-6	94.09	1	WPB+DEB
B2-PS1-10	94.09	1	V+DEB
B2-PS2-3	94.09	0	V
B2-PS2-6	94.09	0	V
B2-PS2-10	94.09	0	V
A5	75.50	/	WPB
A5-PS1-3	75.50	1	WPB+DEB
A5-PS1-6	75.50	1	WPB+DEB
A5-PS1-10	75.50	1	WPB+DEB
A5-PS2-3	75.50	1	WPB+DEB
A5-PS2-6	75.50	1	WPB+DEB
A5-PS2-10	75.50	1	WPB+DEB
B5	59.11	/	WPB
B5-PS1-3	59.11	1	WPB+DEB
B5-PS1-6	59.11	1	WPB+DEB
B5-PS1-10	59.11	1	WPB+DEB
B5-PS2-3	59.11	1	WPB+DEB
B5-PS2-6	59.11	1	WPB+DEB
B5-PS2-10	59.11	1	WPB+DEB

**Table 3-9 :T section strengthening bond behavior and failure mode.**

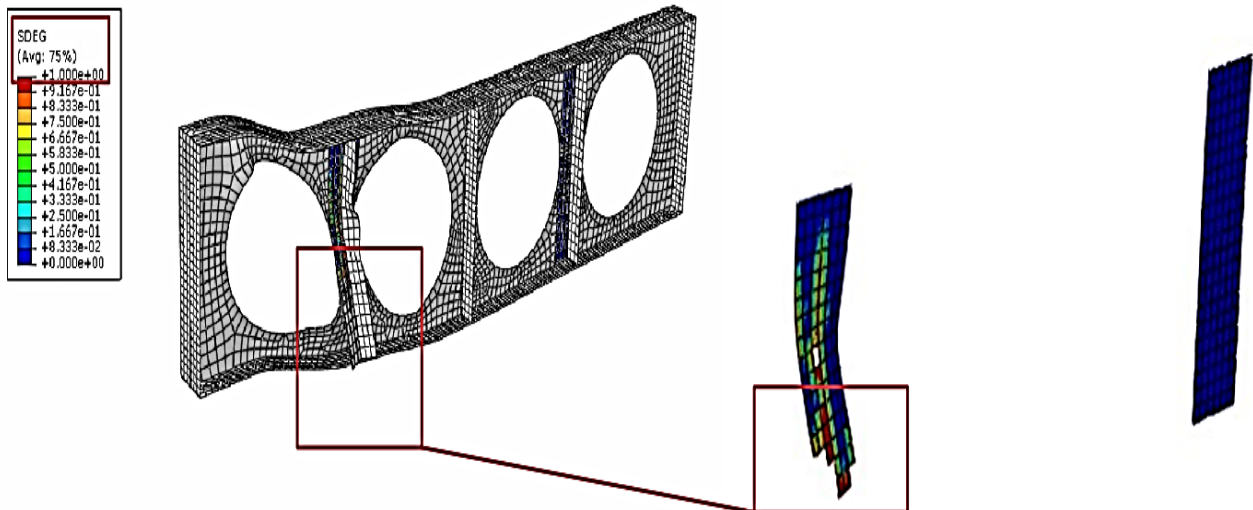


**Figure 3-24: Checking bond behavior using SDEG parameter and adhesive layer deletion for specimen : B2 -PS1-3.**

### III.2.1.2.U section strengthening :

As mentioned before with the T section profile, the strength improvement employing the U profile section for Groupe 1 reinforced beams was roughly 47 percent and 32 percent for all cases of A2 and B2 strengthened beams, respectively (**Table 3-10**) , The load level was the same as with the T section profile, but the U section shape had a slightly greater percentage of augmentation. Besides to that, the load-vertical displacement response for A2 and B2 strengthened beams was similar, and the strengthening technique and increased profile thickness had no effect on the strength enhancement (**Figure 3-25** and **Figure 3-26**).

Moreover, compared to the T section strengthening, very interesting results were achieved using the U section carbon profile to strength A5 and B5 specimens. According to the strengthening technique and U profile thickness, Group 2 strengthened beams showed an increase ranged from 26 % to 39 % and 20% to 34 % for A5 and B5 respectively (**Table 3-10**) ,( **Figure 3-27** and **Figure 3-28** ) , confirming that the additional strength and stiffness were based on the pultruded stiffener geometry which relies on the moment of inertia of the pultruded section for the out of plane resistance [101].it should also be mentioned that the load-displacement curves of PS1 configuration dropped sooner than PS2 configuration for Groupe 2 tested beams. bond behavior of Group 1 and Group 2 strengthened beams adopting U carbon PFRP was similar to T section strengthening. debonding occurred for PS1 configuration of Group 1 strengthened beams (**Figure 3-29**) and all Group 2 strengthened beams (**Table 3-11**).

It was observed that the failure mode was also similar to T section strengthening ,only B2-PS1-6 which failed by vierendeel failure mode and A5-PS2-10 which failed by top Flange buckling which was followed by a slight debonding, indicating that stress concentration and failure mode had shifted away from the reinforced zone. So, for both profile shapes, the PS2 configuration was the most effective technique in all circumstances, with 3mm profile thickness for group 1 and 10 mm profile thickness for group 2.

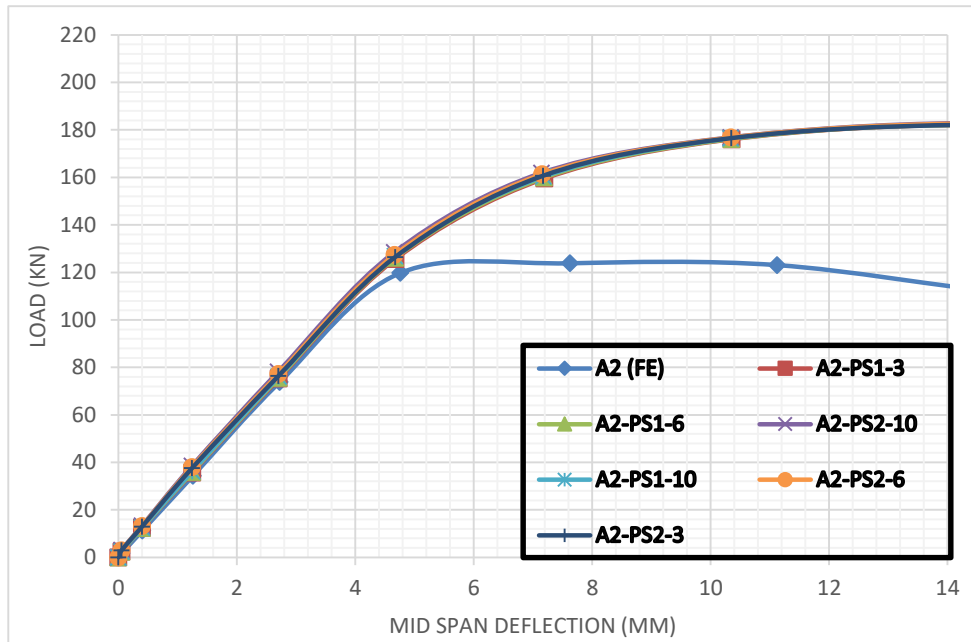


**Figure 3-25: Load -deflection curves of U section strengthening specimen A2 .**

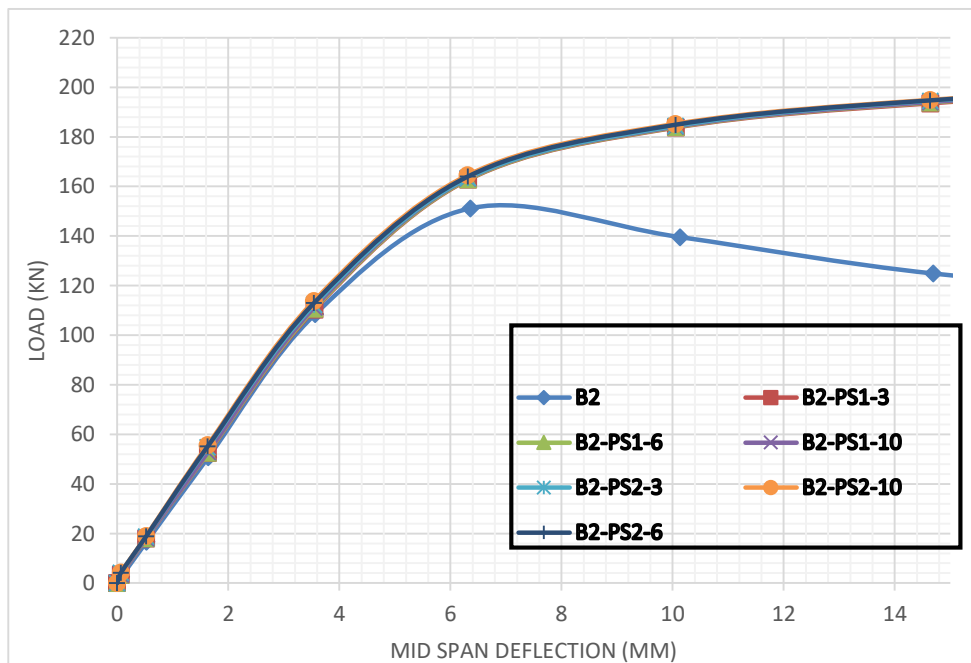


**Figure 3-26: Load -deflection curves of U section strengthening specimen B2 .**

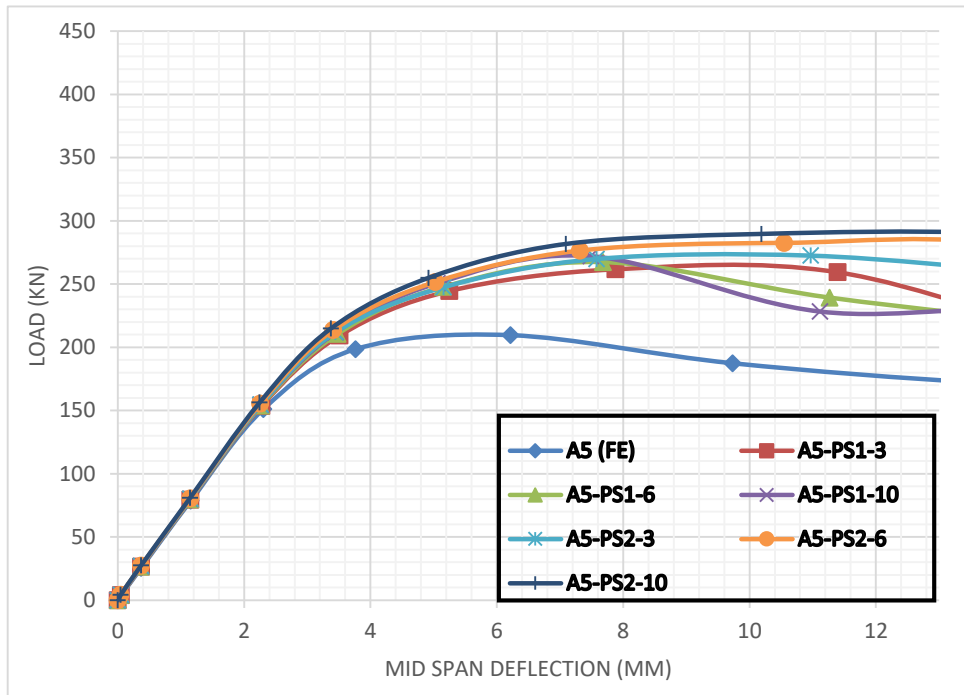


**Figure 3-27: Load -deflection curves of U section strengthening specimen A5 .**

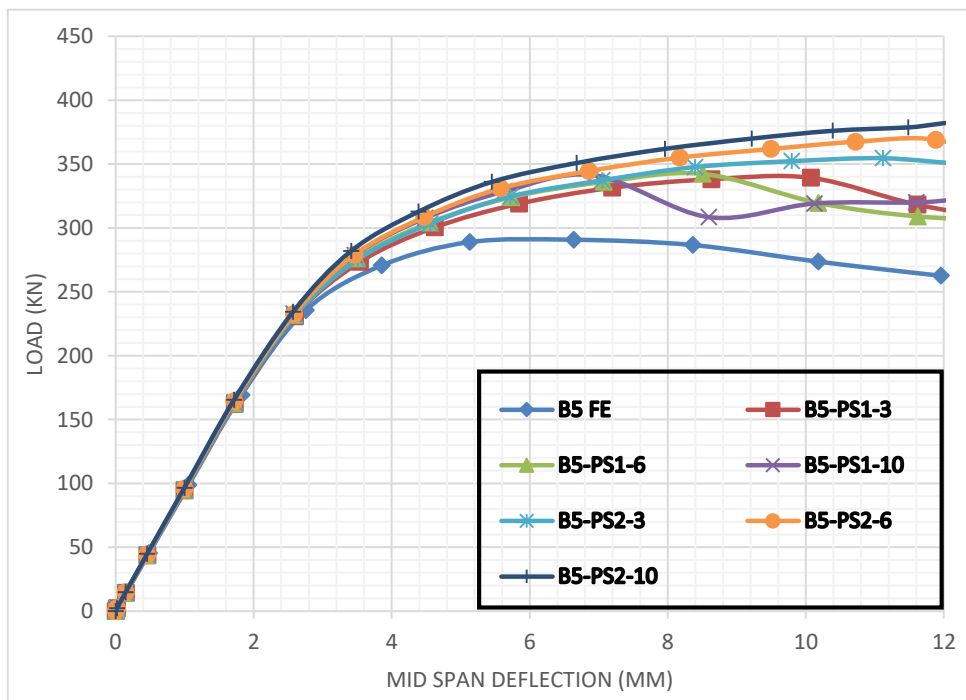


**Figure 3-28: Load -deflection curves of U section strengthening specimen B5 .**



Spécimen	$P_u$ (KN)	Strength enhancement (%)
A2	123.82	/
A2-PS1-3	182.67	47.52
A2-PS1-6	182.72	47.56
A2-PS1-10	182.79	47.62
A2-PS2-3	182.96	47.76
A2-PS2-6	183.16	47.92
A2-PS2-10	183.24	47.98
B2	151.18	/
B2-PS1-3	198.88	31.55
B2-PS1-6	199.24	31.78
B2-PS1-10	199.58	32.01
B2-PS2-3	199.96	32.26
B2-PS2-6	200.27	32.47
B2-PS2-10	200.38	32.54
A5	209.63	/
A5-PS1-3	265.19	26.50
A5-PS1-6	273.22	30.33
A5-PS1-10	278.62	32.91
A5-PS2-3	283.61	35.29
A5-PS2-6	292.17	39.37
A5-PS2-10	292.55	39.55
B5	290.77	/
B5-PS1-3	350.43	20.51
B5-PS1-6	350.85	20.66
B5-PS1-10	350.88	20.67
B5-PS2-3	376.57	29.50
B5-PS2-6	389.22	33.85
B5-PS2-10	391.26	34.55

**Table 3-10 :T section strengthening ultimate load enhancement .**

<b>Spécimen</b>	<b>Web post slendress</b>	<b>SDEG</b>	<b>Failure mode</b>
A2	102.84	/	WPB
A2-PS1-3	102.84	1	V+DEB
A2-PS1-6	102.84	1	V+DEB
A2-PS1-10	102.84	1	V+DEB
A2-PS2-3	102.84	0	V
A2-PS2-6	102.84	0	V
A2-PS2-10	102.84	0	V
B2	94.09	/	WPB
B2-PS1-3	94.09	1	WPB+DEB
B2-PS1-6	94.09	1	WPB+DEB
B2-PS1-10	94.09	1	V+DEB
B2-PS2-3	94.09	0	V
B2-PS2-6	94.09	0	V
B2-PS2-10	94.09	0	V
A5	75.50	/	WPB
A5-PS1-3	75.50	1	WPB+DEB
A5-PS1-6	75.50	1	WPB+DEB
A5-PS1-10	75.50	1	WPB+DEB
A5-PS2-3	75.50	1	WPB+DEB
A5-PS2-6	75.50	1	WPB+DEB
A5-PS2-10	75.50	1	TFY+DEB
B5	59.11	/	WPB
B5-PS1-3	59.11	1	WPB+DEB
B5-PS1-6	59.11	1	WPB+DEB
B5-PS1-10	59.11	1	WPB+DEB
B5-PS2-3	59.11	1	WPB+DEB
B5-PS2-6	59.11	1	WPB+DEB
B5-PS2-10	59.11	1	WPB+DEB

**Table 3-11 :T section strengthening bond behavior and failure mode.**

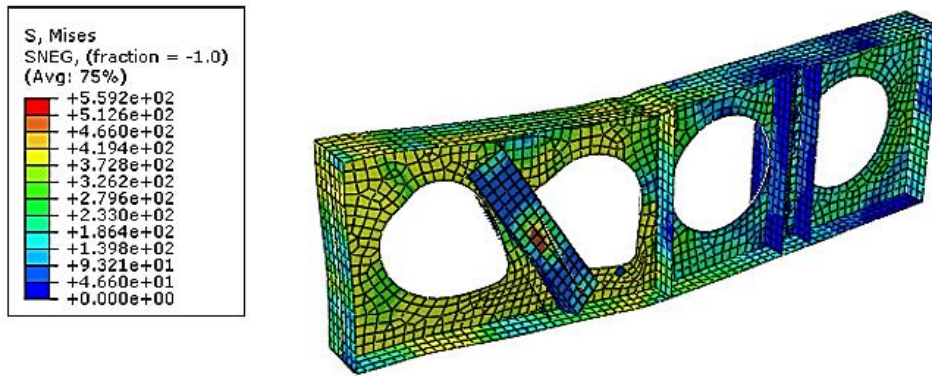


Figure 3-29: Pultruded CFRP U section debonding for specimen B2 -PS1-3.

### III.2.2. How the FRP process strengthening of cellular beam web posts works:

The fundamental idea behind the suggested approach is to use pultruded FRP profiles to improve the shear deficiency capability of cellular beam web posts. As a consequence of the preceding results after using different strengthening configuration and different section thicknesses, this stiffening approach is derived from the fact that the flexural rigidity,  $EI$ , of the added stiffener must be in an interval scale more than that of the reinforced steel web post.

Contrary to common FRP reinforcing procedures, which depend solely on the in-plane strength of composite fibers, this strengthening approach makes use of the out-of-plane rigidity of pultruded FRP elements. This implies that the flexural rigidity,  $EI$ , and geometric characteristics of the FRP section are the most critical parameters (Figure 3-30). So, we suggest that the usage of high modulus FRPs is not required for this strengthening strategy, despite the fact that most of published research, employing composite material for reinforcing steel structures recommended high modulus FRP.

In the next section the ability of low modulus pultruded GFRP profiles to reinforce web post buckling of cellular beams will be investigated.

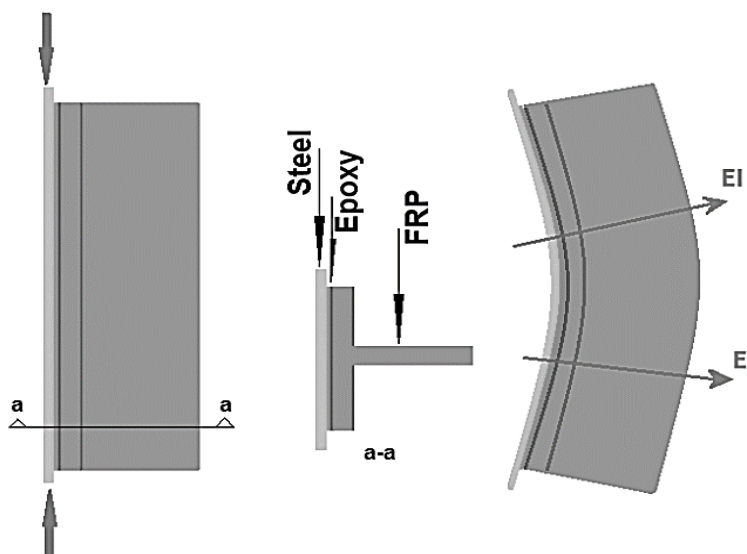


**Figure 3-30 : FRP pultruded element out-of-plane stiffness.**

**III.3.Strengthening web post buckling of cellular beams using GFRP :**

The previous obtained results encourage the investigation of low modulus glass fiber reinforced polymer to prevent the web post buckling of cellular beams .To keep the study program and findings discussion as simple as possible, only the cellular beam A2 was used. used previously will be strengthened now using Three type of GFRP pultruded profile sections : T section – U section –Angle section (**Figure 3-31**), bonded in the instability region by two types of adhesives . Three strengthening techniques will be conducted as in the previous section with CFRP (**Table 3-3**), and the optimum GFRP profile thickness will be investigated (3mm,6mm and 10mm) . Material properties of the adhesive and GFRP are detailed in **Table 3-12** and **Table 3-13**.The Discussion of Results will be in term of: horizontal displacement measured in point D1,D2,D3 and D4 as shown in **Figure 3-2** ,Ultimate load, failure mode, and bond behavior between steel and GFRP profile .

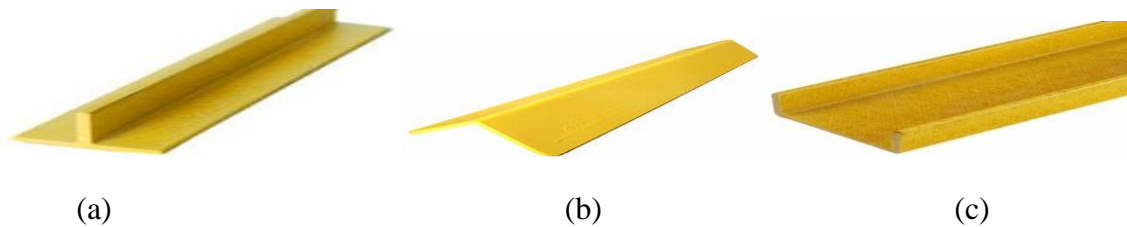


**Figure 3-31.Pultruded glass FRP profiles : (a) T section –(b) Angle section – (c) U section**

	<b>Elastic modulus (MPa)</b>	<b>Major Poisson’s ratio</b>	<b>Shear modulus (MPa)</b>
GFRP	$E_x = 21000$	$\nu_{xy}=0.26$	$G_{xy}=1520$
	$E_y = 7000$	$\nu_{xz}=0.26$	$G_{xz}=1320$
	$E_z = 7000$	$\nu_{yz}=0.30$	$G_{yz}=2630$

**Table 3-12 : GFRP mechanical properties [102].**

	<b>Elastic modulus (GPa)</b>	<b>Shear modulus (GPa)</b>	<b>Tensile strength (MPa)</b>
Adhesive 1	8	2.6	29.7
Adhesive 2	11.3	2.2	22.3

**Table 3-13: Mechanical properties of adhesives: Adhesive 1 [103]-Adhesive 2[100].**

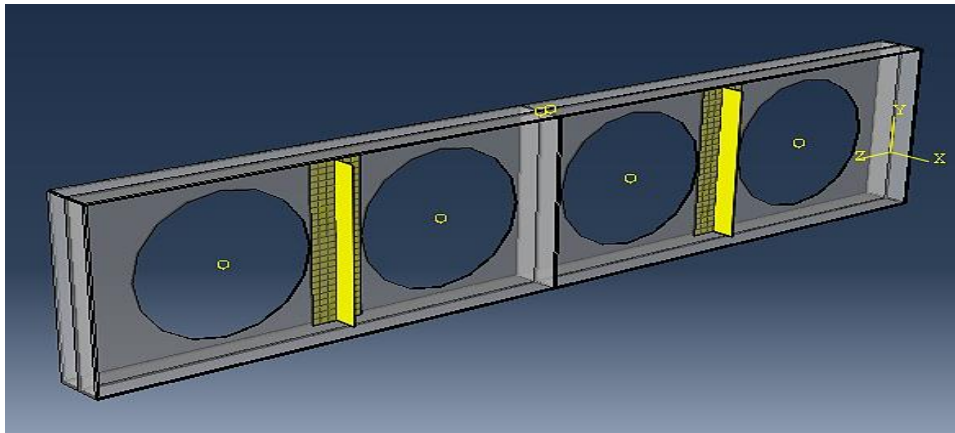


**Figure 3-32: GFRP T section strengthening .**

### **III.3.1.Results and Discussions:**

#### **III.3.1.1.Pultruded GFRP T section strengthening :**

Test results showed that ultimate load of glass FRP T section strengthened beams increased also with different percentages according to strengthening configuration as found previously with CFRP (**Table 3-14**) .Compared to the un-strengthened beam the ultimate load of PS1 strengthening arrangement beams were approximately 25% higher, However for PS2 and PS3 strengthened beams the ultimate load increased by approximately 47% (**Table 3-14**)(**Figure 3-33 To 3-37**) .In comparison to the earlier CFRP findings for PS1 layout, the beam revealed the same strength augmentation, the load climbed till 160 kN and fell rapidly, and the same yielding and maximum load was also seen for PS2 and PS3.

As previously discovered, increasing the thickness of GFRP pultruded T sections did not help the strength enhancement for PS2 and PS3 strengthening techniques; the ultimate load and load - vertical displacement response were very comparable; only PS1 strengthening was impacted by increasing the thickness of GFRP and CFRP profiles

On the other side according to the strengthening technique and GFRP thickness, it can be seen from (**Table 3-14**) that the application of glass FRP T section led to an improvement of the web post stiffness and a reduction of its horizontal displacements . In the first configuration PS1 for all GFRP thickness the horizontal displacement in points D1 and D2 were almost zero ,However in D3 and D4 points were reached 31.79 mm and 32.19 mm respectively due the web post-buckling which occurred far from the strengthened area .

Nevertheless ,in the second case of PS2 strengthening technique the horizontal displacement in D1, D2, D3 and D4 decreased proportionally with the increase of the GFRP thickness (**Table 3-14**) but the web post-buckling was not totally avoided which means that the use of this strengthening technique with an effective thickness of GFRP only delayed and reduced the horizontal displacement of the web post to a higher load.

Regarding to the PS3 strengthening configuration, no horizontal displacement was indicated for specimens strengthened with 2 mm and 3mm GFRP profile thickness (**Table 3-14**). This helps to understand the importance of strengthening the web on both sides using the most efficient proportion of GFRP thickness to web thickness.

The bond behavior has been checked using SDEG (stress degradation) which is explained above as the D parameter to calculate the adhesive damage. From **Table 3-14** it can be noticed that no debonding occurred for the strengthening configuration PS1, where the values of damage variable SDEG did not reach 1, this can be explained also by the occurrence of failure away from the strengthened area (**Figure 3-38**).

Debonding was occurred with PS2 configuration for both adhesive types **Table 3-14**, this can be proved by the SDEG and the end deletion of the adhesive layer for the majority of PS2 strengthened beams. However the adhesive layer of A3-PS2-3SI was totally deleted which means that the GFRP section is totally detached from the beam.

It can also be observed that no debonding was occurred for the cases of PS3 strengthening configuration with 2 mm GFRP thickness and the two types of the adhesives (A2-PS3-2S and A2-PS3-2SI). On the other hand for A2-PS3-3S and A2-PS3-3SI we found a different performance of bond behavior (**Table 3-14**), slight end debonding was observed with adhesive 2 despite the GFRP thickness and the strengthening technique was the same (**Figure 3-39**).

Although the strength and stiffness was enhanced for PS1 and PS2 strengthening techniques, the web post instability was not prevented and all tested beams failed by the web post-buckling accompanied by the end debonding of the T-section for PS2 configuration (**Table 3-14**). This was not the case with CFRP, when the failure mode was modified to vierendeel collapse mode. Using the PS3 strengthening technique with GFRP T section of 2mm and 3 mm the failure mode was changed from web post-buckling to Vierendeel failure which means that the web post is more stiffer and stable. Despite the proportion of GFRP needed is slightly more than the amount of CFRP, the strength restoration was almost identical.

	Beam	Adhésive	GFRP Thickness(mm)	Pu(kN)	D1(mm)	D2(mm)	D3(mm)	D4(mm)	SDEG	Failure mode
Control	A2	/	/	123,37	-38,54	46,7	3,4	1,32	/	WPB
PS1	A2-PS1-1S	Adhesive1	1	153.83	-0,63	2,85	-31,76	32,19	0	WPB
	A2-PS1-2S	Adhesive1	2	154.22	-0,38	2,59	-30,61	31,12	0	WPB
	A2-PS1-3S	Adhesive1	3	155.15	-0,42	2,53	-30,33	30,17	0	WPB
PS2	A2-PS2-1S	Adhesive1	1	182,28	-35,95	44,53	1,26	1,16	1	DB+WPB
	A2-PS2-1SI	Adhesive2	1	182,31	-36,96	43,95	-1,84	1,35	1	DB+WPB
	A2-PS2-2S	Adhesive1	2	182,26	-28,48	38,55	1,6	1.07	1	DB+WPB
	A2-PS2-2SI	Adhesive2	2	182,57	-28,52	36,07	-0,15	1.18	1	DB+WPB
	A3-PS2-3S	Adhesive1	3	182,54	-26,71	26,69	0,79	0,53	1	DB+WPB
	A3-PS2-3SI	Adhesive2	3	182,54	-26,54	26,44	0,84	0,48	1	DET+WPB
PS3	A2-PS3-1S	Adhesive1	1	183,78	-28,06	41,81	-2,05	2,1	1	DB+WPB
	A2-PS3-1SI	Adhesive2	1	183,77	-27,35	39,35	-2,15	2,01	1	DB+WPB
	A2-PS3-2S	Adhesive1	2	183,87	-4,01	8,11	-3,29	2,73	0	V
	A2-PS3-2SI	Adhesive2	2	183,83	-3,61	8,39	-2,93	2,84	0	V
	A2-PS3-3S	Adhesive1	3	183,85	-3,56	7,06	-1,2	1,66	0	V
	A2-PS3-3SI	Adhesive2	3	183,83	-3,54	7,47	-1,26	1,86	1	DB+V

**Table 3-14 :Results of all strengthened steel beams using T GFRP section.**

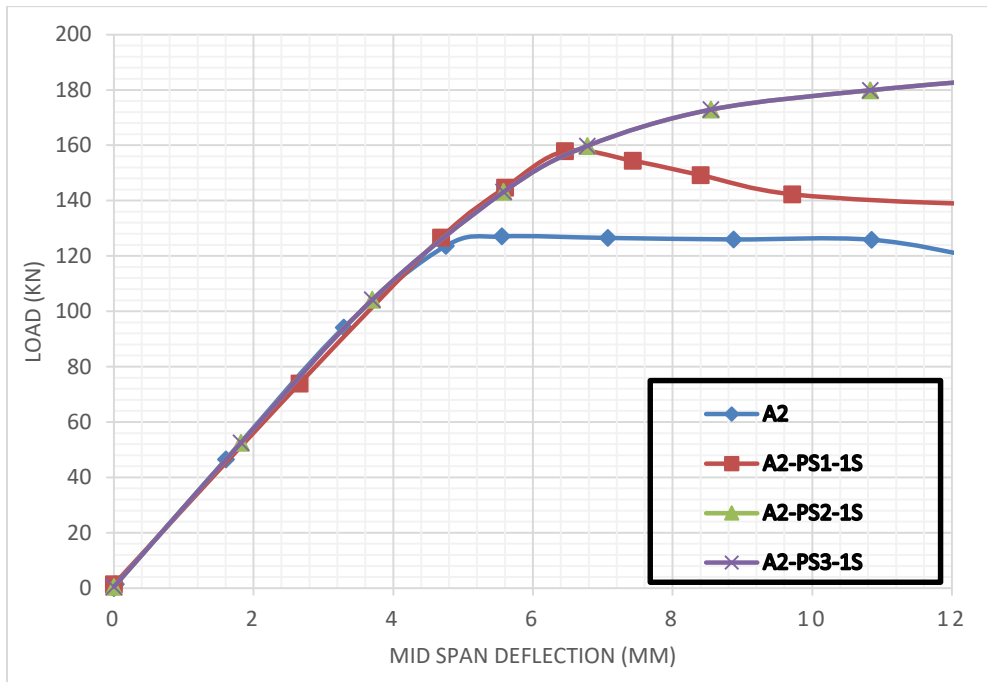


**Figure 3-33 : Load-deflection curves of PS1 strengthening configuration .**

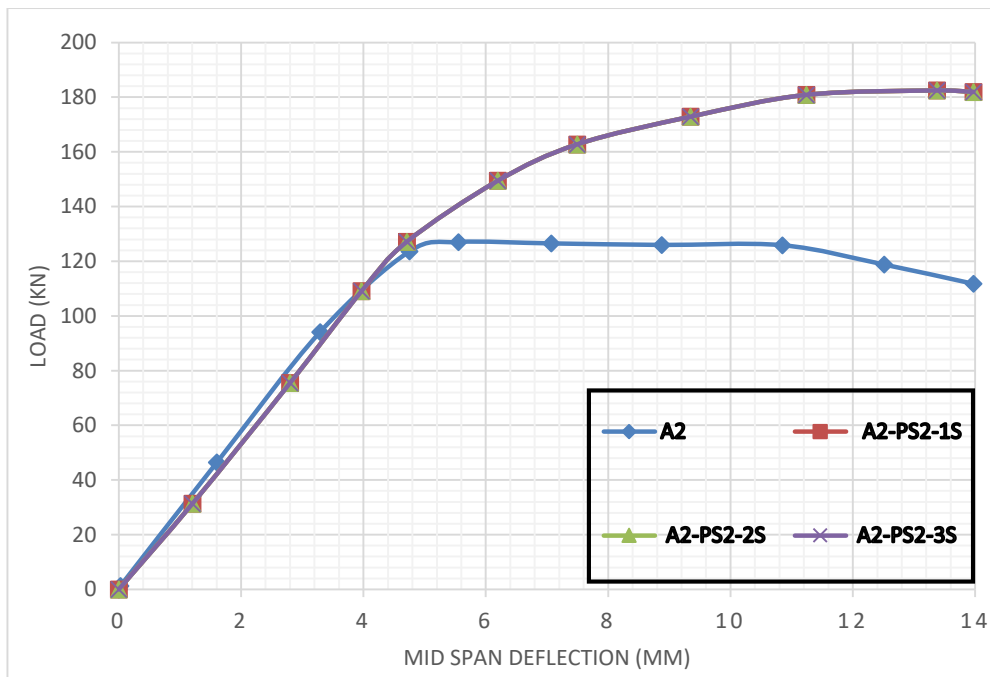


**Figure 3-34: Load-deflection curves of PS2 strengthening configuration using adhesive 1**



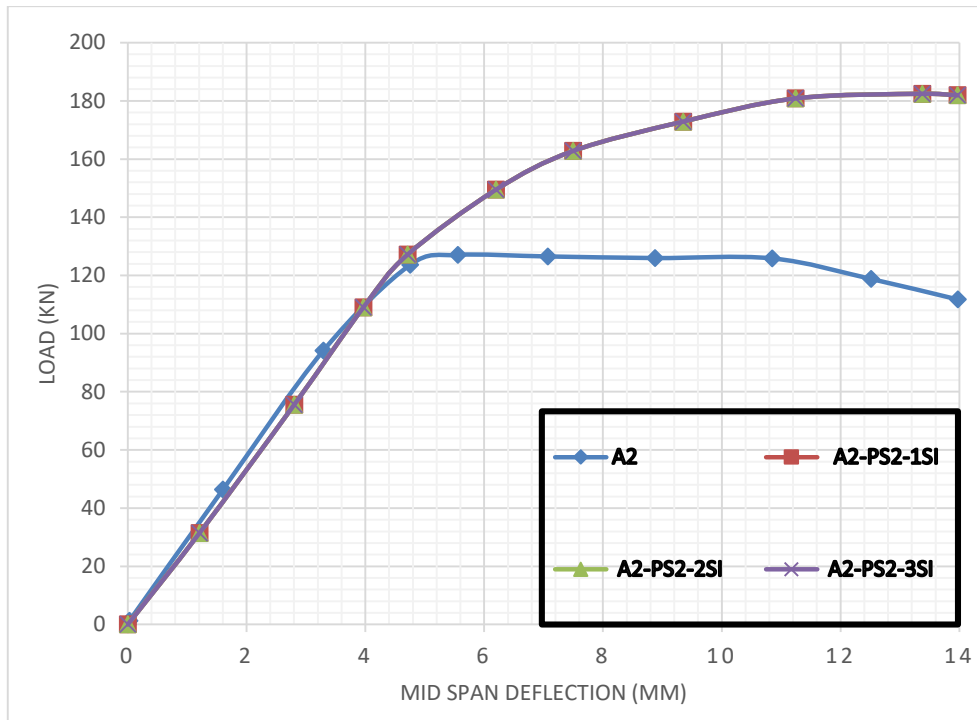


**Figure 3-35: Load-deflection curves of PS2 strengthening configuration using adhesive 2**

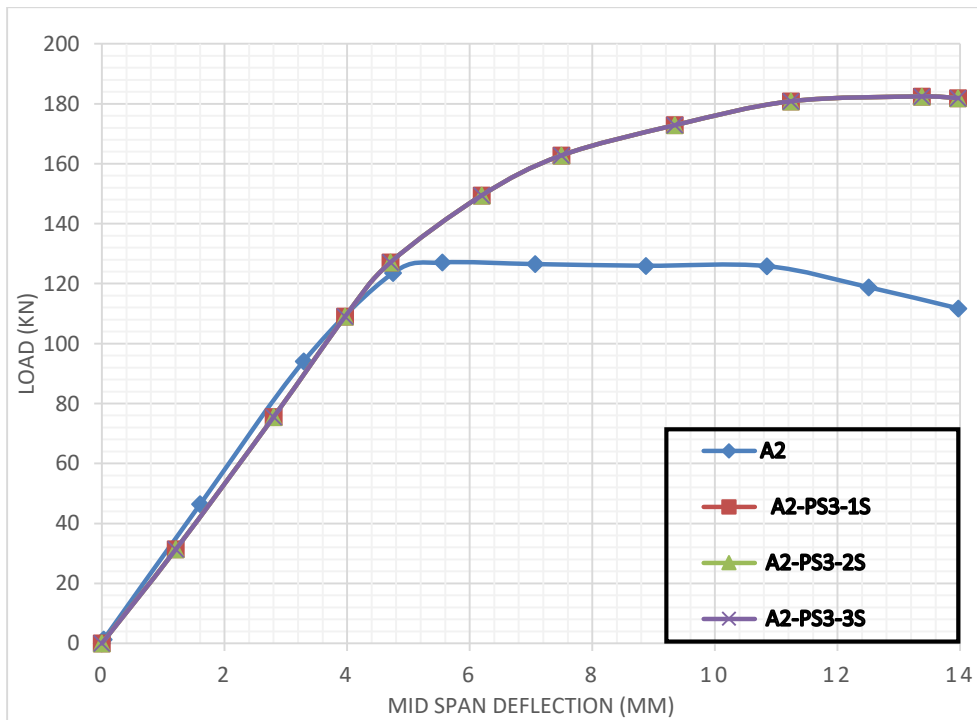


**Figure 3-36: Load-deflection curves of PS3 strengthening configuration using adhesive 1**

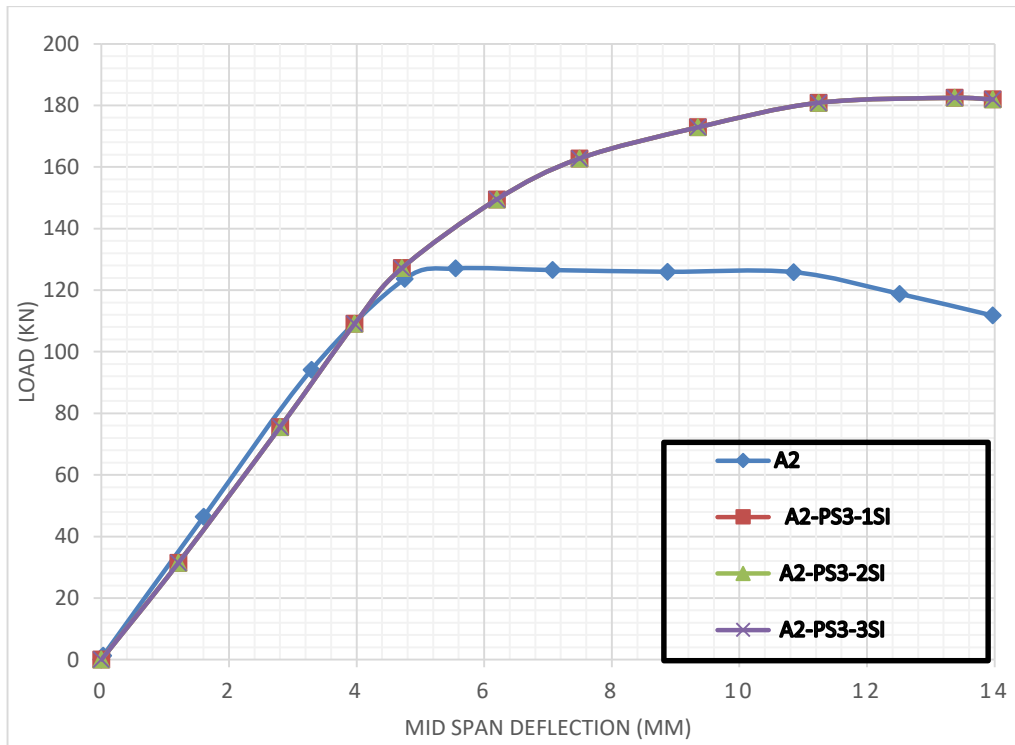


**Figure 3-37: Load-deflection curves of PS3 strengthening configuration using adhesive 2**

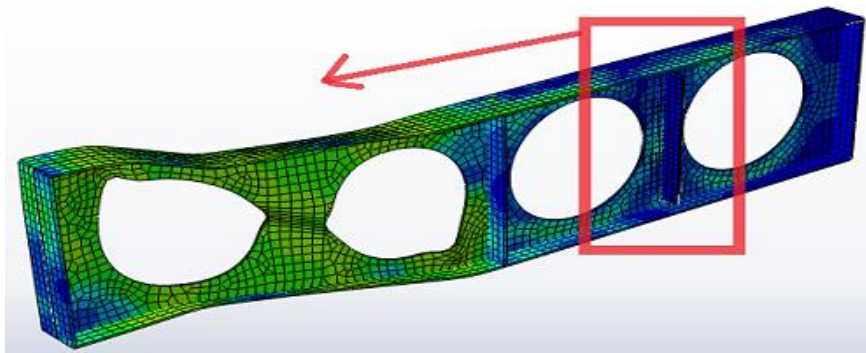


**Figure 3-38: Change of web post buckling position.**

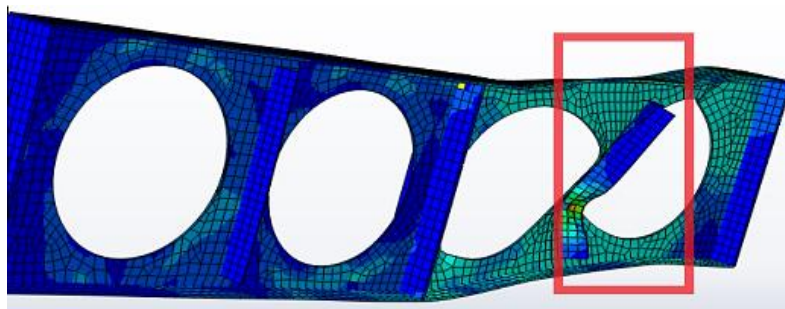


**Figure 3-39: End debonding of the GFRP T section.**

**III.3.1.2. Pultruded GFRP U section strengthening:**

In the same manner, the effectiveness of U shape GFRP pultruded section on strengthening web post instability of the cellular beam A2 will be investigated in this part.

All test results are summarized in **Table 3-15**. Compared to the control beam, an increase of approximately 26%, 48% and 49% on the ultimate load was observed for PS1, PS2 and PS3 strengthening techniques respectively. Because the identical strength enhancement had previously been observed with CFRP, it was not essential to plot the load deflection charts.

As commented previously the increasing of the U profile thickness did not provide a considerable strength enhancement among all tested beams, the ultimate load was nearly the same for every strengthening configurations (**Table 3-15**) having slightly superior performance for the U section, which has higher flexural stiffness than the T section.

Although PS1 strengthening configuration gives the same results found with GFRP T section, no lateral displacement was recorded for all tested beams strengthened with PS2 and PS3 techniques (**Table 6-15**). The U GFRP profile performed identically to the U CFRP profiles in terms of strength increase and rigidity, affirming the hypothesis that the out-of-plane capacity of pultruded parts is specified not only by the fiber type in the matrix, but also by the geometric features of the stiffener's cross section. Since the out-of-plane characteristics of the cross section provide enough resistance, it was observed that the failure happens at the junction.

As the failure was away from the strengthening area for PS1 strengthening configuration, it's obvious that the adhesive was not damaged and GFRP debonding did not happen. However, contrary to what was previously found with T section for all tested beams PS3 strengthening technique no debonding has occurred with adhesive 1 and adhesive 2 using U GFRP section this can be shown by the no deletion of adhesive layers and the damage variable SDEG in **Table 3-15**. Delamination has happened as a result of the PS2 reinforcing arrangement, and the adhesive connection has been damaged as a result of one side strengthening of a beam.

It's also clear that web post buckling was not observed for all beams tested with PS2 and PS3 strengthening technique and unlike the control beam, the strengthened web post of the beam showed no apparent buckling. Failure mode was changed to vierendeel failure which indicates the web post stability (**Figure 3-40**). As a consequence of the extremely intriguing findings obtained with the U shape pultruded GFRP profile with the same CFRP thickness proportion with web post thickness, the usage of another pultruded profile section was suggested.

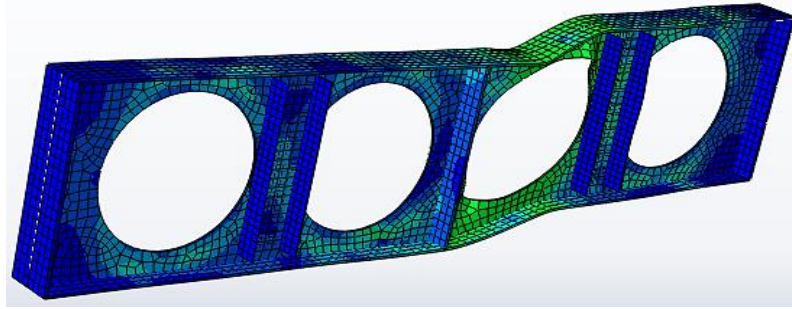


**Figure 3-40: Vierendeel failure of A2-PS2-1S.**

**VI.3.1.3. Pultruded GFRP Angle section strengthening :**

With the same strengthening techniques ,two GFRP opposite angle will be bonded to the web post as shown in **Figure 3-41** .From obtained results it can be reported that for PS1 ultimate load enhanced by approximately 26 % ,However PS2 and PS3 where nearly the same 47% (**Table 3-16**) . This was the same strength improvement percentage as previous pultruded sections .The specimen's behavior was comparable to what had earlier been seen.

Moreover, even for angle section the increase of the profile thickness did not produced the desired effect on the strength of the beam (**Table 3-16**) . This aided in determining the appropriate ratio of web post to profile thickness, after which any rise in profile thickness had no influence on the reinforced beam's strength enhancement.

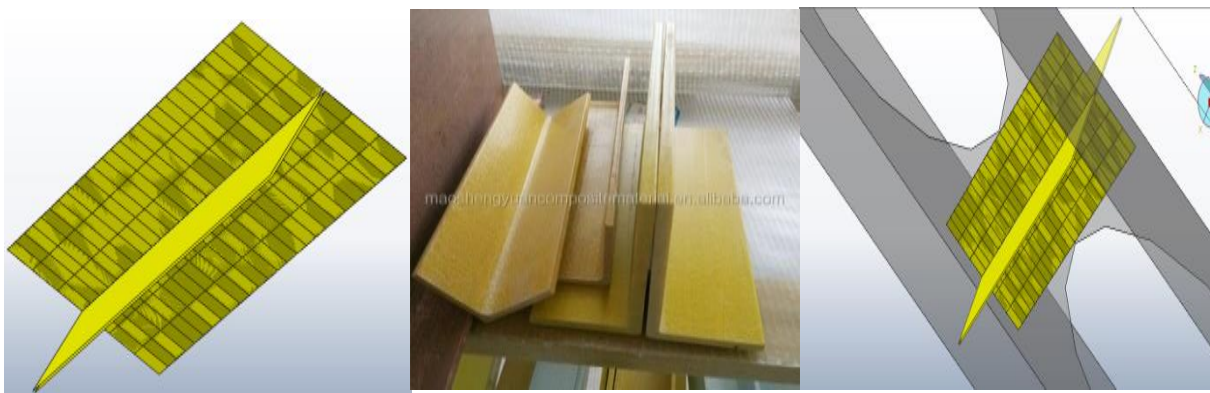


**Figure 3-41. Pultruded GFRP angle section strengthening technique.**

The corresponding results about the lateral displacement of angle sections strengthened beams seemed almost the same of U pultruded strengthening section with slight difference for A2-PS2-1S and A2-PS2-1SI,significant displacement was recorded in D1 and D2 (**Table 3-16**). The prediction of bond behavior using the validated FE approach indicate that débonding occurred with all tested beams of PS2 strengthening technique and the specimen A2-PS3-3SI (**Table 3-16**).The stability of the web post was reached for both PS3 and PS2 strengthening arrangement of 2mm and 3 mm GFRP thickness Table 8 ,the failure mode was changed to vierendeel failure .

	Beam	Adhésive	GFRP Thickness(mm)	Pu(Kn)	D1(mm)	D2(mm)	D3(mm)	D4(mm)	SDEG	Failure mode
Control	A2	/	/	123,37	-38,54	46,7	3,4	1,32	/	WPB
PS1	A2-PS1-1S	Adhesive1	1	153.87	-0,57	2,45	-32,45	33,02	0	WPB
	A2-PS1-2S	Adhesive1	2	154.25	-0,41	2,62	-30,78	31,22	0	WPB
	A2-PS1-3S	Adhesive1	3	155.11	-0,44	2,34	-31,05	30,11	0	WPB
PS2	A2-PS2-1S	Adhesive1	1	182,21	-3,88	4,42	-1,73	1,6	1	DEB+V
	A2-PS2-1SI	Adhesive2	1	182,21	-4,02	4,25	-1,68	1,72	1	DEB+V
	A2-PS2-2S	Adhesive1	2	182,31	-3,01	1,67	-0,15	0,27	1	DEB+V
	A2-PS2-2SI	Adhesive2	2	182,32	-2,89	1,62	-0,16	0,25	1	DEB+V
	A3-PS2-3S	Adhesive1	3	182,41	-2,92	1,18	-0,59	0,59	1	DEB+V
	A3-PS2-3SI	Adhesive2	3	182,4	-2,89	1,22	-0,62	0,57	1	DEB+V
PS3	A2-PS3-1S	Adhesive1	1	183,64	-4,3	5,9	-2,2	1,55	0	V
	A2-PS3-1SI	Adhesive2	1	183,66	-4,24	5,6	-2,29	1,41	0	V
	A2-PS3-2S	Adhesive1	2	183,61	-4,27	4,97	-0,05	0,52	0	V
	A2-PS3-2SI	Adhesive2	2	183,61	-4,23	4,89	-0,1	0,49	0	V
	A2-PS3-3S	Adhesive1	3	183,65	-4,19	4,25	-0,01	0,07	0	V
	A2-PS3-3SI	Adhesive2	3	183,64	-4,21	4,24	-0,05	0,085	0	V

**Table 3-15: Results of all strengthened steel beams using U GFRP section.**

	<b>Beam</b>	<b>Adhesive</b>	<b>GFRP Thickness(mm)</b>	<b>Pu(kN)</b>	<b>D1(mm)</b>	<b>D2(mm)</b>	<b>D3(mm)</b>	<b>D4(mm)</b>	<b>SDEG</b>	<b>Failure mode</b>
Control	A2	/	/	123,37	-38,54	46,70	3,4	1,32	/	WPB
PS1	A2-PS1-1S	Adhesive1	1	153.83	-0,62	2,39	-32,56	32,97	0	WPB
	A2-PS1-2S	Adhesive1	2	154.21	-0,43	2,71	-30,51	31,85	0	WPB
	A2-PS1-3S	Adhesive1	3	155.12	-0,47	2,56	-31,65	30,14	0	WPB
PS2	A2-PS2-1S	Adhesive1	1	183,2	-35,78	39,43	-2,46	1,4	1	DB+WPB
	A2-PS2-1SI	Adhesive2	1	183,2	-37,76	39,89	-2,15	1,37	1	DB+WPB
	A2-PS2-2S	Adhesive1	2	183,18	-3,48	12,54	-1,29	0,35	1	DB+V
	A2-PS2-2SI	Adhesive2	2	183,18	-4,66	13,31	-1,2	0,57	1	DB+V
	A3-PS2-3S	Adhesive1	3	183,15	-2,14	6,93	-0,79	1,26	1	DB+V
	A3-PS2-3SI	Adhesive2	3	183,16	-2,4	6,02	-0,85	1,29	1	DB+V
PS3	A2-PS3-1S	Adhesive1	1	183,57	-4,65	13,78	-3,49	4,35	0	V
	A2-PS3-1SI	Adhesive2	1	183,58	-4,32	13,88	-3,72	4,32	0	V
	A2-PS3-2S	Adhesive1	2	183,64	-3,85	5,92	-0,44	1,37	0	V
	A2-PS3-2SI	Adhesive2	2	183,64	-3,82	5,95	-0,51	1,35	0	V
	A2-PS3-3S	Adhesive1	3	183,67	-3,97	4,18	-0,58	0,25	0	V
	A2-PS3-3SI	Adhesive2	3	183,62	-3,92	4,21	-0,56	0,24	1	DB+V

**Table 3-16: Results of all strengthened steel beams using angle GFRP section.**

**VI.3.2. Process of GFRP stiffener breakdown at the adhesive interface:**

When only one stiffener is used in stiffening technique, the stiffeners are more prone to premature delamination. Since the adhesive layers that facing one another in a double stiffener attached case supplement the tension side that is vulnerable to failure with compressive stresses on the contrary direction, the presence of a supplementary stiffener on the other side of the web posts reduces early breakdowns.

There are two possible explanations for this behavior. First one is that attaching dual GFRP section opposite each other with the web post exposes the attaching adhesive's edges to compressive and tensile stresses on one face and tensile and compressive pressures over the other (**Figure 3-42**). It is well acknowledged that the tensile strength of adhesive is lower than its compressive strength, which results in greater extension [104]. As a consequence, even when the tension face of epoxy fails, the adhesive in compression will still be undamaged and in interaction with the web post and FRP section. The second explanation for the disparity in behavior among one and double stiffener specimens is that even the two-sided stiffener arrangement provides more strength and stiffness for the web post.

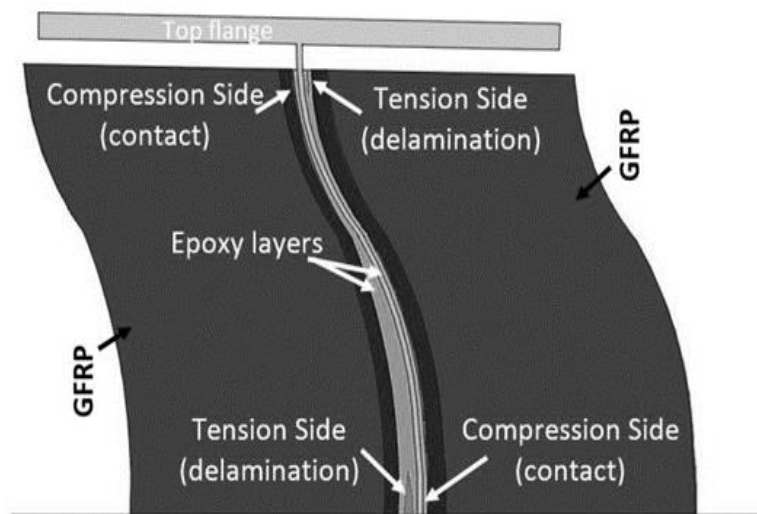


**Figure 3-42:GFRP stiffener degradation at the bonding contact**

To completely comprehend this novel proposed technique, more investigation of other criteria was required, such as the adequate bonding surface between web post and pultruded GFRP sections.



**III.3.3.Effect of different GFRP profile dimensions on bond behavior and strength enhancement:**

The cellular beam A2 used previously will be strengthened now with pultruded GFRP T sections of 3 mm thickness of different sizes .

All dimensions were fixed. only the width "B" altered to obtain an appropriate bonding surface as shown in **Table 3-17** and **Figure 3-44**. Because they both have the similar height, the contact surface ratio  $C_r$  of the GFRP portion can be described as the proportion of the GFRP section width "B" to the web post width ( $B/S_0$ ) (**Table 3-17**).

GFRP T sections were bonded on the two sides of web instability region (web post ). Using the prior strengthening configuration denoted as " PS1" and "PS2" .The T section profiles were bonded using " Adhesive 1" of the previous section ,in addition to that the mechanical properties of GFRP were the same of the prior section (**Table 3-12** and **Table 3-13**) .

The Discussion of Results will be in term of : peak load ,failure mode, horizontal displacement measured in point D1,D2,D3and D4 and bond behavior using the stress degradation SDEG of the adhesive.

As a result, the bending stiffness of the chosen GFRP section must achieve a minimum bending stiffness needs to the web post while maintaining appropriate bonding behavior between steel and GFRP.

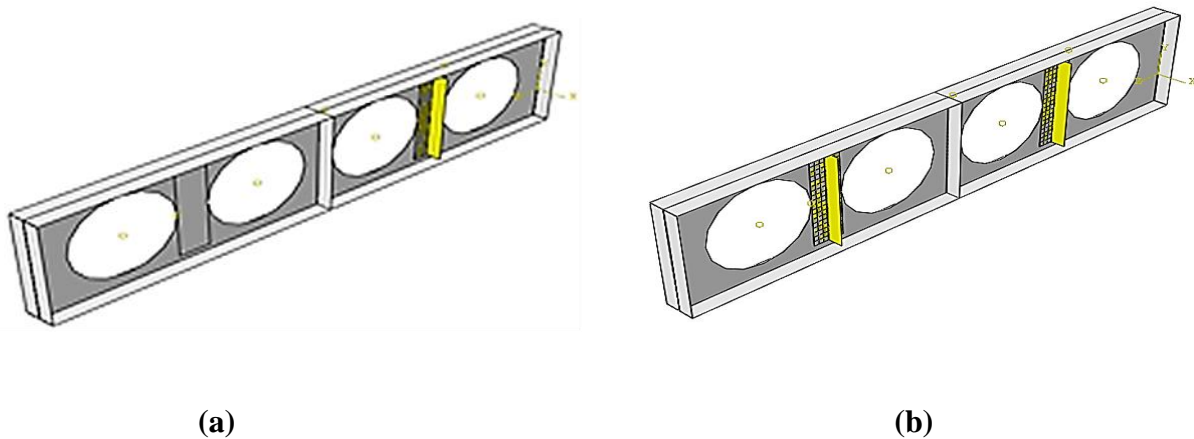


**Figure 3-43 : Strengthening arrangement :(a) PS1 – (b) PS2.**

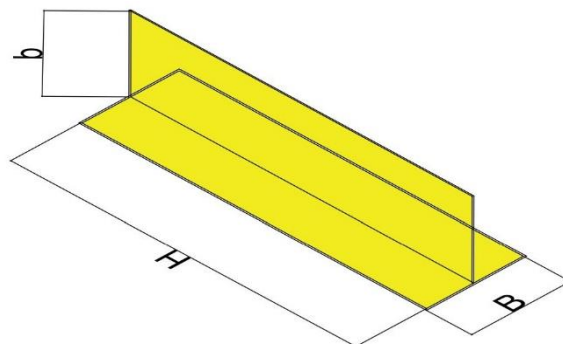


**Figure 3-44 : Pultruded GFRP T section dimensions .**



GFRP profile	H (mm)	B (mm)	b (mm)	$C_r$
G1	387	103	51	1
G2	387	85	51	0.82
G3	387	75	51	0.73
G4	387	70	51	0.68
G5	387	60	51	0.58
G6	387	50	51	0.48
G7	387	40	51	0.39

**Table 3-17 : Different GFRP T section dimensions.**

The designation of the tested specimen is the first symbol within every specimen identification, accompanied by the GFRP stiffener name and lastly the strengthening arrangement (PS1 or PS2). 'A2-G2-PS2,' for example, is the cellular beam 'A2' strengthened with GFRP T Section named G2 (**Table 3-17**) using PS 2 strengthening technique (Figure 6-44)

#### **VI.3.3.1.Results and discussion :**

Test results showed that ultimate load of glass FRP T section strengthened beams increased with different percentage according to strengthening configuration (**Table 3-18**) and not the GFRP T section dimensions . On the other side according to the strengthening technique, it can be seen form **Table 3-18** that the application of glass FRP T section led to an improvement of the web post stiffness and a reduction of its horizontal displacement.

In all cases of the first configuration PS1 the horizontal displacement in points D1 and D2 were almost zero ,However in D3 and D4 points were reached approximately the 31mm for both for all T section used dimensions .The bond behavior has been checked using the numerical input SDEG (stress degradation) which is explained above. So from **Table 3-19** it can be noticed that no debonding occurred for all cases of the strengthening configuration PS1 ,where the values of damage variable SDEG did not reached 1, this can be explained also by the occurrence of failure away from the strengthened area. Debonding was occurred on PS2 configuration with specimen A2-G7-PS2 . This help to understand the importance of strengthening with the effective profile dimension which provides the adequate bond surface ratio with the web post of cellular beams ,in this study it was found that using T section of bond surface equal to ( 0.49x web post surface ) (profile “G6”) present the most effective ratio with a an economic amount of material. Although the strength was enhanced in all cases of PS1 strengthening techniques ,the web post instability was not prevented and all tested beams failed by the web post buckling.

Specimens	Pu (kN)	D1(mm)	D2 (mm)	D3 (mm)	D4 (mm)
A2	123.37	-38,54	39.56	63,4	1,32
A2-G1-PS1	155.15	-0,42	2,53	-30,33	30,17
A2-G1-PS2	183,85	-3,56	7,06	-1,2	1,66
A2-G2-PS1	155.36	-0.46	2.67	-30.13	30,10
A2-G2-PS2	183.04	-3.48	6.87	-1.17	1,71
A2-G3-PS1	154.97	-0.43	2.62	-30.94	30,21
A2-G3-PS2	183.01	-3.52	6.99	-1.2	1,69
A2-G4-PS1	153.84	-0.41	2.49	-31.23	30.1
A2-G4-PS2	182.36	-3.49	6.73	-1.05	1,34
A2-G5-PS1	151.91	-0.46	2.37	-31.15	30.87
A2-G5-PS2	182.11	1.87	0.59	-1.12	1.59
A2-G6-PS2	183.06	-3.39	6.12	-1.08	1,40
A2-G7-PS2	177.85	-28.97	25.47	-1.02	1.62

**Table 3-18: Peak load and horizontal displacement findings.**

Using the PS2 strengthening technique different failure mode was observed according to the profiles dimension ,for specimens A2-G1-PS2 , A2-G2-PS2, A2-G3-PS2, A2-G4-PS2, A2-G5-PS2 and A2-G6-PS2 the failure mode was changed from web post buckling to Vierendeel failure mode which means that the web post is more stiffer and stable ( **Table 3-18** ) . The last specimen A2-G7-PS2 failed by web post buckling which occurred after the profile debonding (**Figure 3-45**).

Specimens	SDEG	Failure mode

A2	/	WPB
A2-G1-PS1	0	WPB
A2-G1-PS2	0	V
A2-G2-PS1	0	WPB
A2-G2-PS2	0	V
A2-G3-PS1	0	WPB
A2-G3-PS2	0	V
A2-G4-PS1	0	WPB
A2-G4-PS2	0	V
A2-G5-PS1	0	WPB
A2-G5-PS2	0	V
A2-G6-PS2	0	V
A2-G7-PS2	1	DEB+WPB

**Table 3-19: Bond behavior and failure mode.**

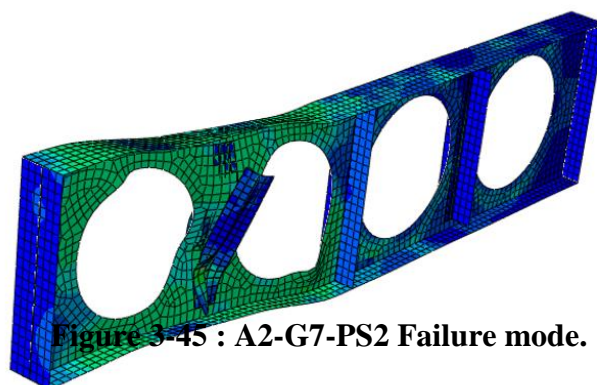


**Figure 3-45 : A2-G7-PS2 Failure mode.**

**III.3.3.2.Validation of results on other GFRP profile shape :**

These preceding results on strengthening web post buckling using GFRP T section profile encouraged to examine the use of GFRP U section in the same manner using PS2 strengthening configuration with the same adequate bond surface ratio obtained previously with A2-G6-PS2 (H = 387 ,B= 50 ,b = 51) and the same profile thickness (3mm) to investigate the effectiveness of U shape GFRP pultruded section on strengthening web post instability .



**Figure 3-46 :GFRP U section (H = 387 ,B= 50 ,b = 51).**

Results obtained using U section GFRP profile (named “G8”) are detailed in Figure 6-48: It can be reported that compared to A2-G7-PS2 the same strength enhancement and the same response was observed with A2 -G8-PS2 , This confirm the ability of Pultruded GFRP profiles to enhance the strength of steel beams .

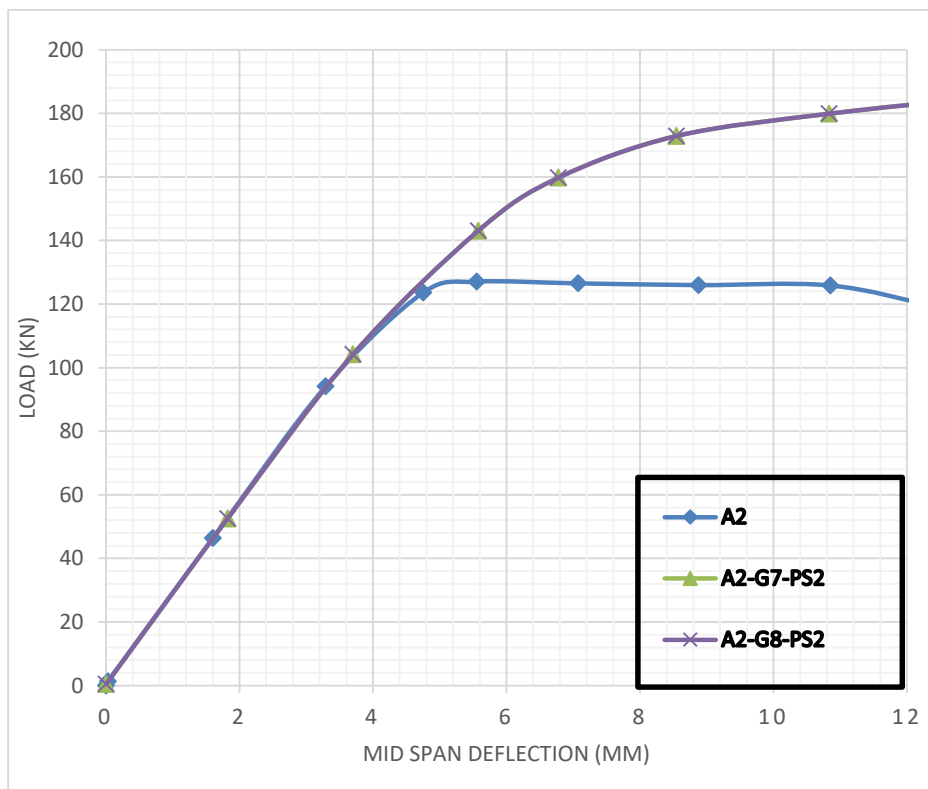


**Figure 3-47 :Load deflection curves of GFRP U validation .**

No horizontal displacement was also observed with A2-G8-PS2 , which indicate that web post buckling was not happened and failure mode was also changed to Vierendeel mechanism (Figure 6-49) . From the SDEG parameter debonding was not also occurred With A2-G8-PS2.

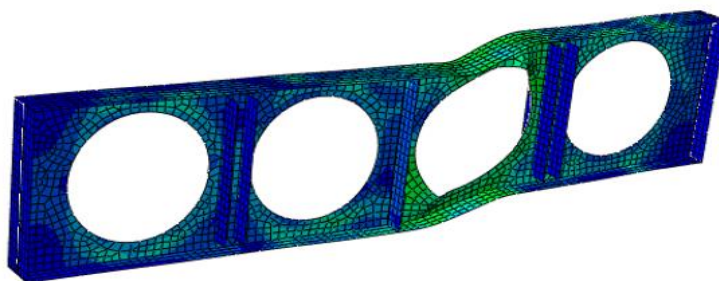


**Figure 3-48 : A2-G8-PS2 Failure mode.**

#### **III.4. Conclusion :**

The goal of this chapter was to discover a new practical strengthening method for web post-buckling failure mode in cellular beams using the most effective CFRP profile section form and configuration. The traditional steel stiffener approach necessitates welding, a proven and widely used procedure in the industry. Nevertheless, this raises well-known concerns including fatigue attributable to stress concentrations, the need for massive material and machinery in engineering application, and the need for qualified workers to execute the welding on situ, that can be difficult if major initial flaws occur. Composite materials, in contrast side, provide a lightweight product option for worksite processing, simplicity of installation, as well as less strict labor demands. The fundamental distinction among the two composites , this novel technique and bonded composite sheets, is how fiber strength is used. Pultruded composite portions used in this suggested technique rely mostly on geometrical features such as out-of-plane opposition, with a modest participation from fiber uniaxial resistance. Composite sheets, on the other hand, can only supply in-plane resistance in reinforcing situations since their out-of-plane influence is negligible. It was concluded that:

- Depending on the slenderness of the web post, this strengthening approach was able to avoid or delay web post-buckling to greater load in all situations.
- The effectiveness of this approach is largely dependent on the strengthening configuration and geometric properties of the CFRP profile, which offer an additional bending resistance to the web post.
- The evaluation of different GFRP stiffener combinations revealed that the double stiffener design is more efficient than the single arrangement, and all reinforced cellular beam web posts should be stiffened.
- The use of bonded stiffeners on one side of web posts causes the earlier debonding of CFRP profiles
- Debonding CFRP profiles has a significant influence on strength enhancement, especially for slender web posts.
- The U section profile's superior performance can be attributed to its flexural stiffness, which is an order of magnitude more than that of the CFRP T section profile.
- The proposed strengthening technique improved the beam stiffness, web post yielding, and web post-buckling capacity.

- This study presents a primary investigation on the ability of CFRP profiles to strengthen web post-buckling of cellular beams, further studies are in need as part on the ongoing research in this topic.
- Because the high modulus and tensile strength of FRP composites are not the most important factors in this technique of the pultruded FRP part, CFRP fibers can be replaced with less expensive composite such as GFRP .
- Both adhesives were effective in increasing the web post strength of reinforced cellular beams. These findings support the efficacy of the proposed approach.
- The contact area for the GFRP T section was the same as for the other GFRP profile shapes.
- Once successful bonding is set up, the GFRP size has no influence on load capacity improvement.

It should be highlighted that the small amount of research included in this study is insufficient to provide a comprehensive knowledge of this approach. As a result, more research is required for a better knowledge of important factor including FRP strengths and bonding area in order to optimize the reinforcement mechanism and generate a trustful design technique.

## **CHAPTER IV : STRENGTHENING STEEL BEAMS WITH SINGLE WEB OPENINGS USING FRP**

### **IV.1.Strengthening steel beams with single rectangular web openings using NM CFRP**

Based on previous experimental study results conducted by M Altaee [56] and detailed in the previous chapter on strengthening steel beams after the creation of single rectangular web hole on the web using high modulus CFRP and with the practical application limitations and the scarcity of research the aim of this section is to investigate the ability of normal modulus CFRP to reinforce this type of beams .Furthermore, the efficiency of NM CFRP reinforcing will be compared to the prior HM CFRP strengthening findings in order to gather more information and understand how the FRP system strengthening work with steel beams having single web opening and gather important recommendations . Once the composite FRP reinforcement mechanism of single rectangular web opening performance is completely understood, it can be applied in real applications and provide guidance for in site applications and project studies.

#### **IV.1.1.Model description and material properties:**

For more research credibility ,the previous experimental test conducted by M Altaee and al [56] used in the prior chapter to validate the numerical model is employed in this part to investigate the ability of NM CFRP to strengthen the same steel specimens used previously ,which consisted of simply supported 305x102x25 UKBs steel section beams with a 3 meter effective span. B0 is the basic solid specimen without a web opening, whereas B1-R0 and B2-R0 are CFRP reinforced specimens having individual rectangular web holes of 210 x 185mm in the mid span and shear regions, correspondingly (**Figure 4-1** and **Figure 4-2**). This size of the aperture was 0.75 of the specimen depth in length and 0.6 of the specimen beam height in depth.

It should be mentioned also that specimens B1-U0 and B2-U0 are the unstrengthened specimens having rectangular web openings in mid span and shear zone ,respectively . Specimens were loaded under a six-point flexure test to generate a uniformly distributed load and were laterally constrained in four sites along the beam span. Utilizing the same strengthening technique of bonding plates on the flanges and the web two types of normal modulus CFRP will be used with 167 MPA and 127 MPA elastic modulus in the fiber orientation , the other mechanical properties in other direction are detailed in **Table 4-1** and **Table 4-2** .bonded using the same epoxy glue used in the prior test to explore the bond behavior with NM CFRP which have a 1.5 GPa young's modulus and a tensile strength of 29 MPa. The bonding length was equal to 840 mm which is equivalent to four times the opening length .

As a basis, the CFRP width was chosen using the same functional proportion, CFRP width/flange and CFRP/web used in prior study .The numerical simulation details was the same used in the previous chapter for validation the proposed FE model.

The HM CFRP reinforcement arrangement utilized on the specimens in the previous research was likewise utilized here. In **Figure 4-1** and **Figure 4-2**, as well as **Table 4-1** and **Table 4-2** , all configurations, dimensions and CFRP material properties of tested specimens are given.

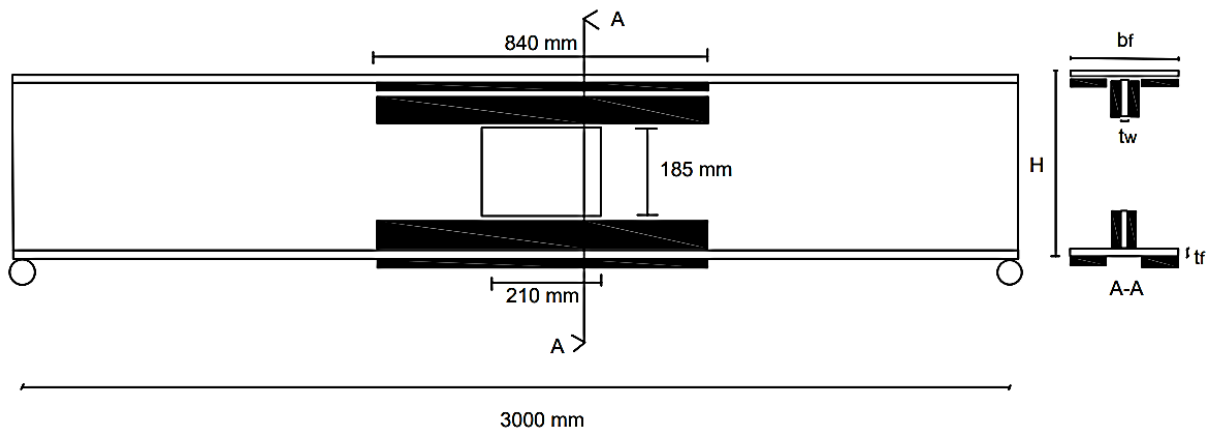


Figure 4-1 :Details and dimensions of HM CFRP strengthened specimen B1-R0.

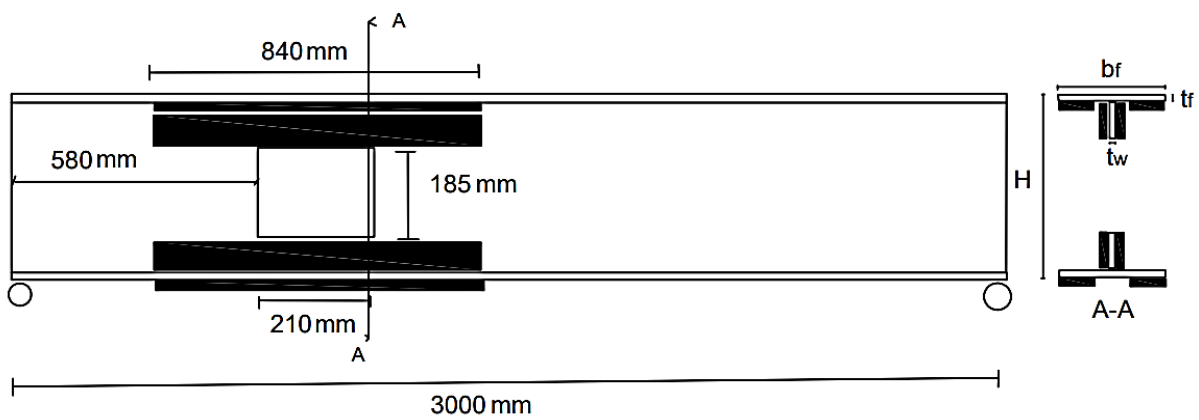


Figure 4-2 :Details and dimensions of HM CFRP strengthened specimen B2-R0.

$E_x(\text{MPa})$	$E_y(\text{MPa})$	$E_z(\text{MPa})$	$\nu_{xy}$	$\nu_{xz}$	$\nu_{yz}$	$G_{xy}(\text{MPa})$	$G_{xz}(\text{MPa})$	$G_{yz}(\text{MPa})$
127000	7400	7400	0.33	0.33	0.188	6900	6900	4300

Table 4-1 :Mechanical properties of NM CFRP (127 MPa)

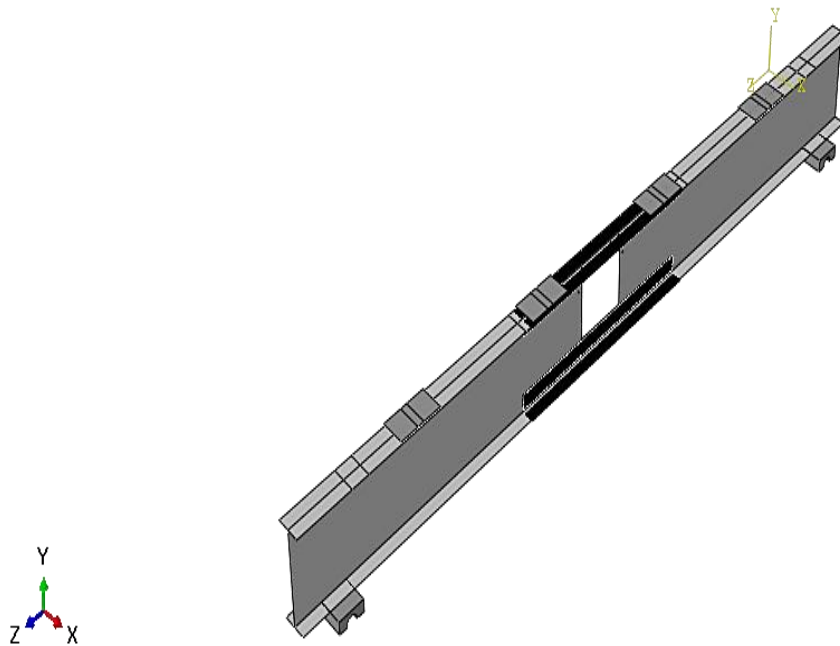
$E_x(\text{MPa})$	$E_y(\text{MPa})$	$E_z(\text{MPa})$	$\nu_{xy}$	$\nu_{xz}$	$\nu_{yz}$	$G_{xy}(\text{MPa})$	$G_{xz}(\text{MPa})$	$G_{yz}(\text{MPa})$
167000	10000	10000	0.0058	0.0058	0.3	25500	25500	3600

Table 4-2 :Mechanical properties of NM CFRP (167 MPa)

The findings of the FE study are discussed in the following section. Specimens reinforced using normal modulus carbon fiber plates (NM CFRP plate ) are named B1-R0-127 and B1-R0-167 which are specimen strengthened with NM CFRP of 127 GPa elastic modulus and 167 GPa



young's modulus respectively and B1-R0-200 is the specimen strengthened previously with high modulus CFRP of 200 GPa elastic modulus.



**Figure 4-3 : Normal modulus CFRP Strengthening model .**

#### **IV.1.2.Results and discussion :**

##### **IV.1.2.1.Mid span opening position :**

###### **IV.1.2.1.1.Strength enhancement and failure mode comparison:**

Normal modulus carbon fiber provided satisfactory findings when reinforcing rectangular opening in the flexure zone, the beam could retain its original capacities and offer nearly the same strength augmentation as high modulus CFRP strengthening. The strength enhancement with normal modulus CFRP of 167 GPa and 127 GPa was approximately 40 % in comparison to the unstrengthened specimen of mid span opening B1-U0 that was the same strength improvement with high modulus CFRP of the same plate thickness and length .

As a load deflection curves comparison between HM CFRP and the two NM CFRP reinforcements ,the load improvement was linear up to 444 kN ,above this load stage the plastic hinge creation occurred in the top flange close to the end of the CFRP plate and the maximum load capacity was measured at around 500 kN (**Figure 4-4**). Beyond this stage, the force fell substantially, allowing a phase of lateral displacement to begin (**Figure 4-5** and **Figure 4-6**). It should be noticed that the specimen reinforced with HM CFRP (B1-R0-200) had a quite stiffer elastic phase response. Furthermore, for a more cost-effective strategy, the NM CFRP plate thickness could be reduced since it delivers the same strength gain over the solid original beam as the HM CFRP .

The obtained findings confirm the ability of normal modulus CFRP to provide the same performance obtained with high modulus CFRP in terms of strength enhancement and failure

mode . In addition to that these results help to understand that this novel technique did not really require a high modulus CFRP or a young's modulus equal to that of steel material , Because the high cost of HM CFRP is a drawback in addition to the bonding behavior, the use of NM CFRP for strengthening steel beams with single rectangular openings, which was affirmed here, could be a solution for the economical matter . Furthermore, these findings contribute to research into other low modulus FRP materials in terms of strength enhancement and bond behavior.

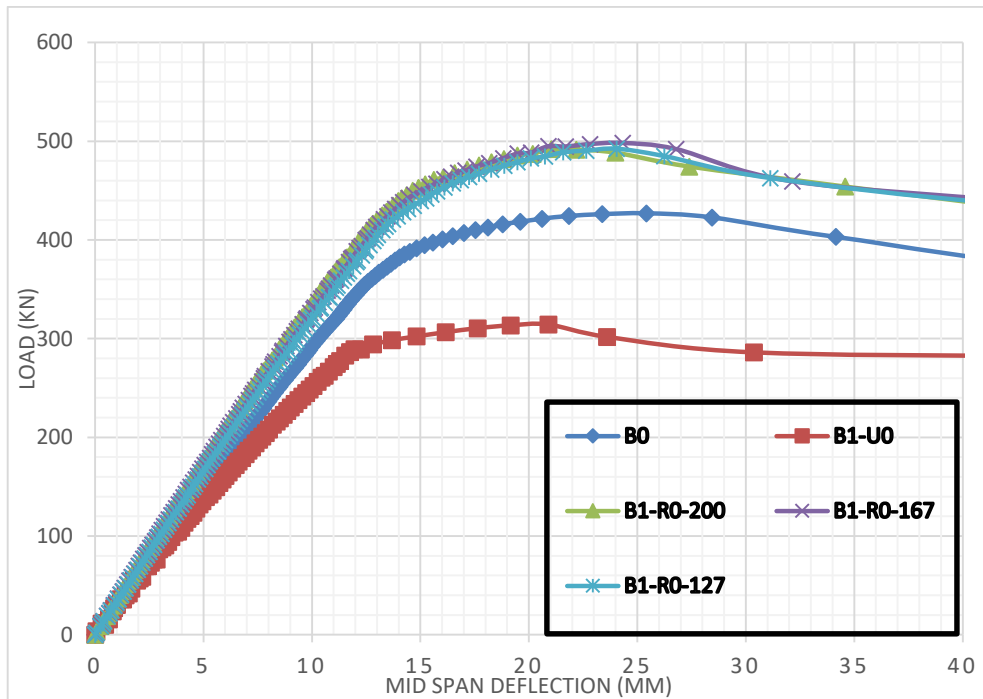


**Figure 4-4: Load-deflection curves of HM CFRP and NM CFRP strengthening .**

**IV.1.2.1.2. Bond behavior :**

As previously stated , the SDEG was employed to assess the adhesive's damage condition. If this variable for any part is identical to 1, it signifies there are no stresses and the component has fallen, and it will be eliminated and deleted.

For the tested specimens it was seen that the optimum value of this variable were found at the ends of the joints .The delamination of the CFRP initiated in the upper flange far away from the entrance. This can be confirmed by the adhesive layer deletion (Figure 7-7 and Figure 7-8). It should be noted also that the debonding was happened at around 460 kN of load for the two tested specimens B1-R0-127 and B1-R0-167 which was the same observation with high modulus CFRP (B1-R0-200) and confirm that the debonding was happened after the restoration of the load capacity of the solid original beam B0 .Besides to that the effective bonding length with high modulus CFRP which was equal to 840 mm was efficient with the two NM CFRP used in this test and the CFRP plate which was equal to four time the opening length was also useful to restore the load capacity of the specimens before debonding with a restricted debonding , Furthermore, reducing the NM CFRP plate thickness will have an effect on the bond behavior, and using a thinner CFRP plate can prevent or delay debonding [55].

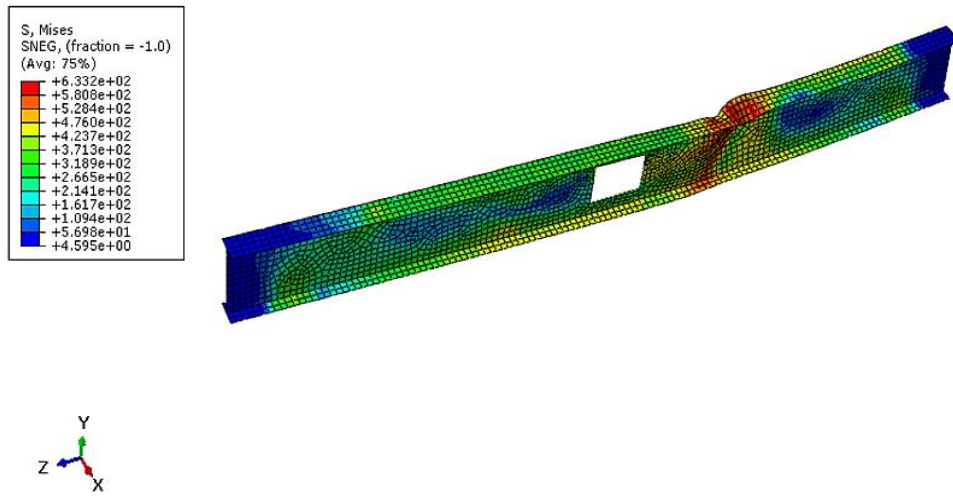


**Figure 4-5 : Failure mode of spécimen B1-R0-127.**

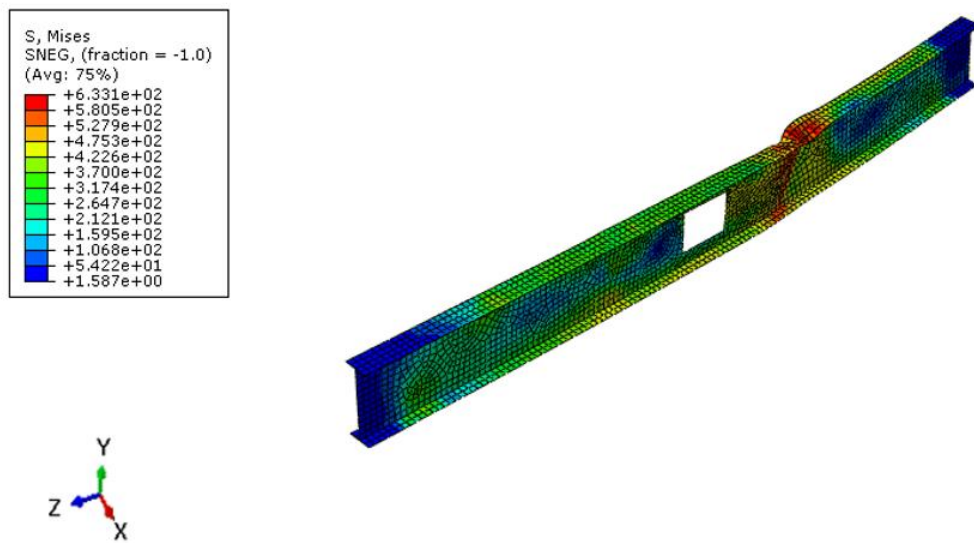


**Figure 4-6 : Failure mode of spécimen B1-R0-167.**

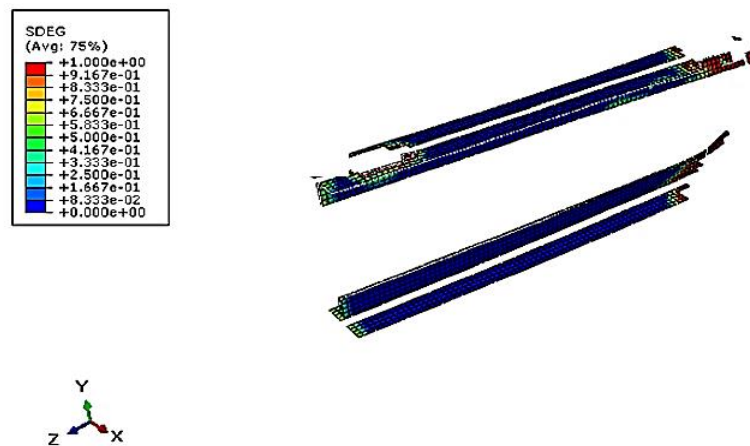


**Figure 4-7 : Adhesive damage parameter, SDEG at failure of specimen B1-R0-127.**

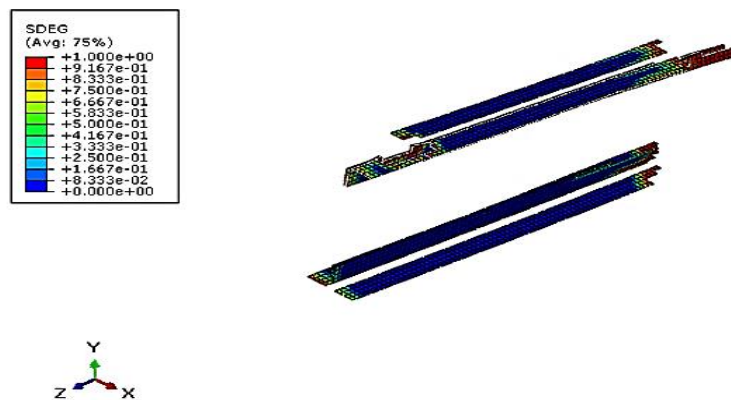


**Figure 4-8: Adhesive damage parameter, SDEG at failure of specimen B1-R0-167.**

#### **IV.1.2.1.3.CFRP plate strain dispersion :**

The FE modeling can provide a wealth of information about strain dispersion on the CFRP .It was chosen to obtain the strain distribution of CFEP plates in all tested specimens that could not be obtained from experiments as the previous experimental test with high modulus CFRP. **Figure 4-9** ,**Figure 4-10** and **Figure 4-11** presents the strain dispersion of CFRP plates at the maximum load ,it can clearly be seen that the maximum recorded CFRP plates strain was very close for the HM CFRP and the two NM CFRP ,despite that the comparison of these recorded maximum strains with the ultimate strain capacity of each CFRP type provided by the manufacturer was not in the same level. A tensile strain generated in the CFRP plates underneath the aperture, whereas a perfect compressive strain evolved mostly along CFRP plates upper the hole.

The utilization proportion, which indicate how hard the reinforcing plate is performing. For the high modulus CFRP the utilization ratio was only 18 % while for the two normal modulus CFRP was around 37 % . This confirm that there are no economic consideration in the previous study employing high modulus CFRP of 3 mm plate thicknesses besides to that the strength enhancement was above the solid original beam capacity which was not the required strength improvement .Even the two employed normal modulus CFRP in this study were lowly stressed despite that they were more stressed than the high modulus CFRP .This could imply that NM CFRP plate thickness could be decreased in many situations calibrating with the strength enhancement and the bond joint between steel and CFRP plate performance to achieve the best economic and secured configuration in term of CFRP type and thicknesses for practical applications. It should also be mentioned that the acquired strain findings are specific to the suggested CFRP design, in addition to the CFRP plate thickness and steel grade. The employment proportion of the CFRP and the optimal plate thickness might vary with other strengthening arrangements or steel grades.

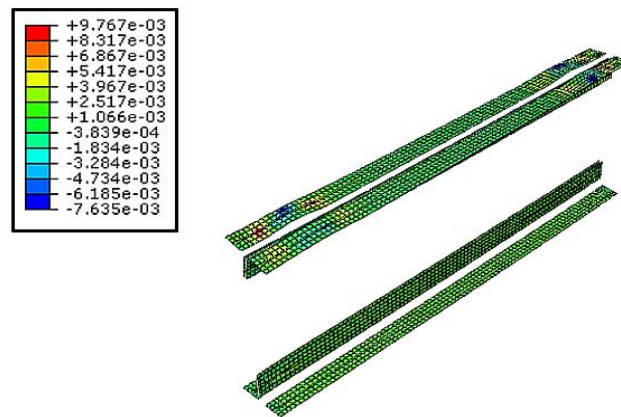


**Figure 4-9 : Strain distribution on high modulus CFRP plates at the peak load B1-R0 beam .**

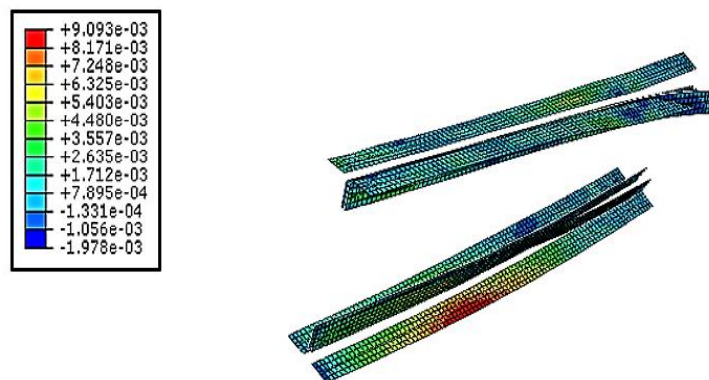


**Figure 4-10 : Strain distribution on normal modulus CFRP167 plates at the peak load B1-R0beam**

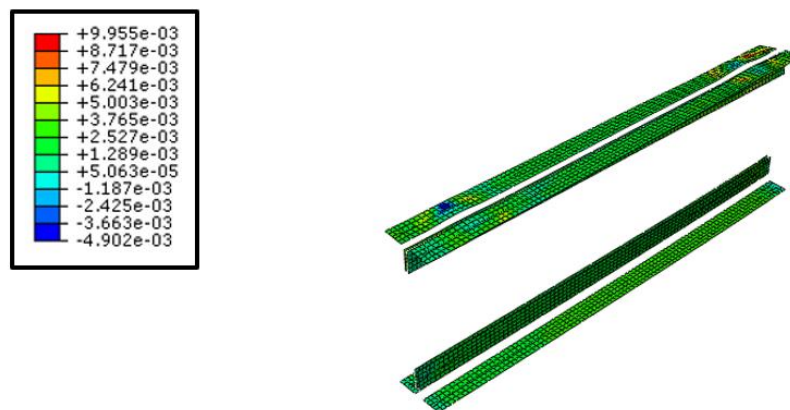


**Figure 4-11 : Strain distribution on normal modulus CFRP 127 plates at the peak load B1-R0 beam**

**IV.1.2.1.4. The optimum NM CFRP plate thickness in mid span :**

A parametric analysis was undertaken to determine the efficient thickness of CFRP due to the low exploitation percentage in normal modulus and high modulus CFRP examined specimens, which has been validated by the previous numerical findings.

In contrast to the previously explored 3mm NM CFRP thickness .1 and 2mm thicknesses were indeed investigated in order to determine the most appropriate thickness. It can be observed from **Figure 4-12** and **Figure 4-13** that using NM CFRP of 127 GPa and 167 GPa elastic modulus and 2mm plate thicknesses provided nearly the same strength increase as the previous 3 mm plate thickness has a quite lower stiffer reaction that is correlated to laminate stiffness while the use of 1 mm plate thicknesses provided an acceptable stiffness recovery with slight lower strength enhancement than the prior 3 mm and 2mm NM CFRP .

Raising the CFRP thickness results in a minor improvement in strength with a drop in beam ductility due to the debonding between steel and CFRP which occurs before the CFRP's maximum reinforcing capability, as a result, aside from the economic considerations, the adoption of 1 mm NM CFRP plate is justified. Regarding to the failure mode for the three adopted NM CFRP plates thicknesses specimens failed by top flange buckling accompanied by lateral torsional buckling (**Figure 4-14** and **Figure 4-15**).

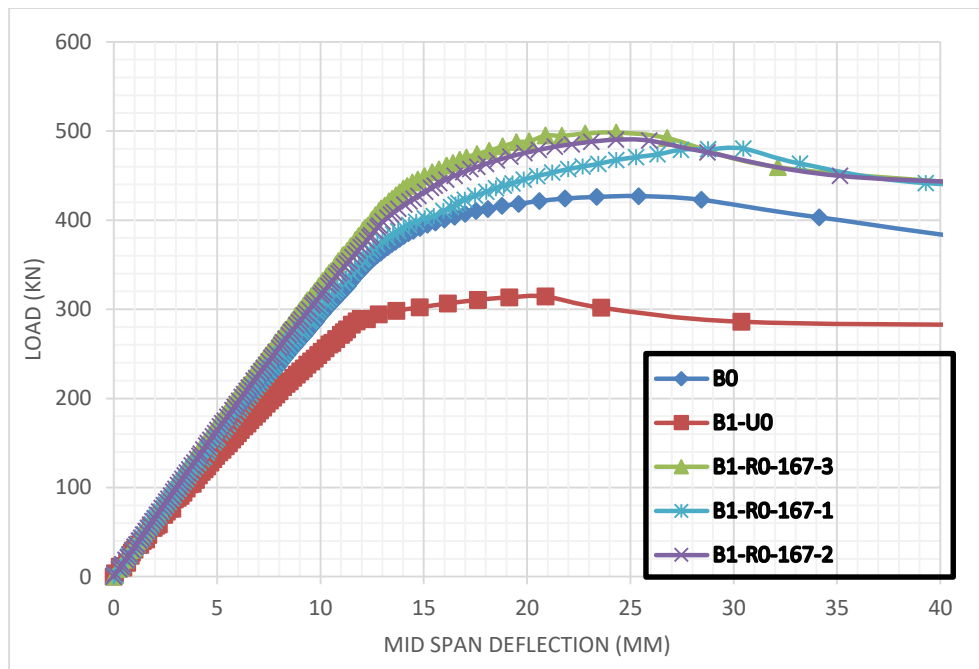


**Figure 4-12 : Load deflection curves of different NM CFRP 167 MPa plate thicknesses .**

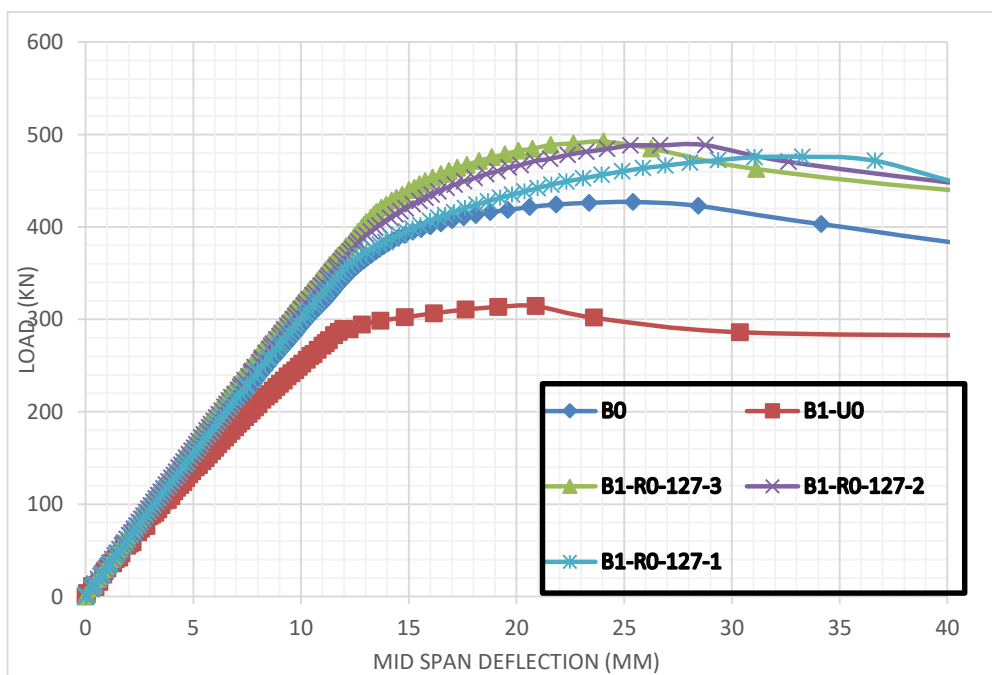


**Figure 4-13 : Load deflection curves of different NM CFRP 127 MPa plate thicknesses .**



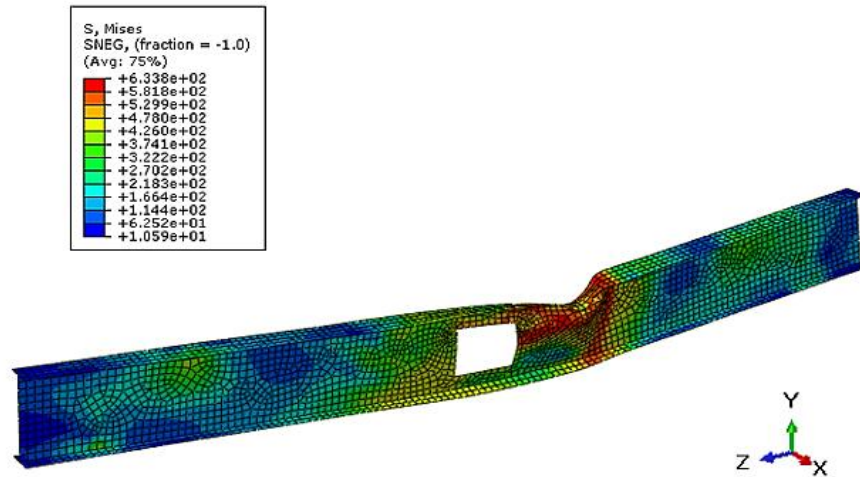


**Figure 4-14 : Failure mode of spécimen B1-R0-167-1.**

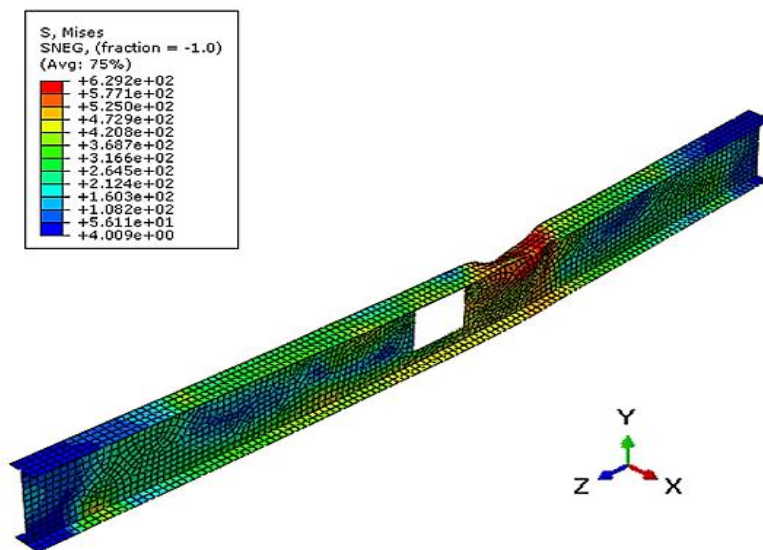


**Figure 4-15 : Failure mode of spécimen B1-R0-127-1**

**IV.1.2.2. Shear zone opening position :**

**IV.2.2.1. Strength enhancement and failure mode comparison :**

The insertion of two NM CFRP plates in specimens with shear zone opening resulted in a 21% improvement in strength and a stiffer reaction over the unreinforced beam B2-UO . This strength enhancement was close to the HM CFRP strengthening and confirm the strength recovery of the original beam B0 .

Specimens B2-R0-127 and B2-R0-167 similarly showed a linear trend up to 370 kN. Above this stress level, the commencement of plastic hinge development was in the upper flange at the



mid-span of the beam Figure . As a result, transverse buckling began at 400 kN of stress between the middle transverse supports. The force was maintained by the specimens until it reached 440kN, at this point it was lowered. Subsequently, caused by excessive horizontal distortion, a plastic behavior was observed under loading, as illustrated in **Figure 4-16**. This was not included in the previous experiment since it was halted as the stress dropped.

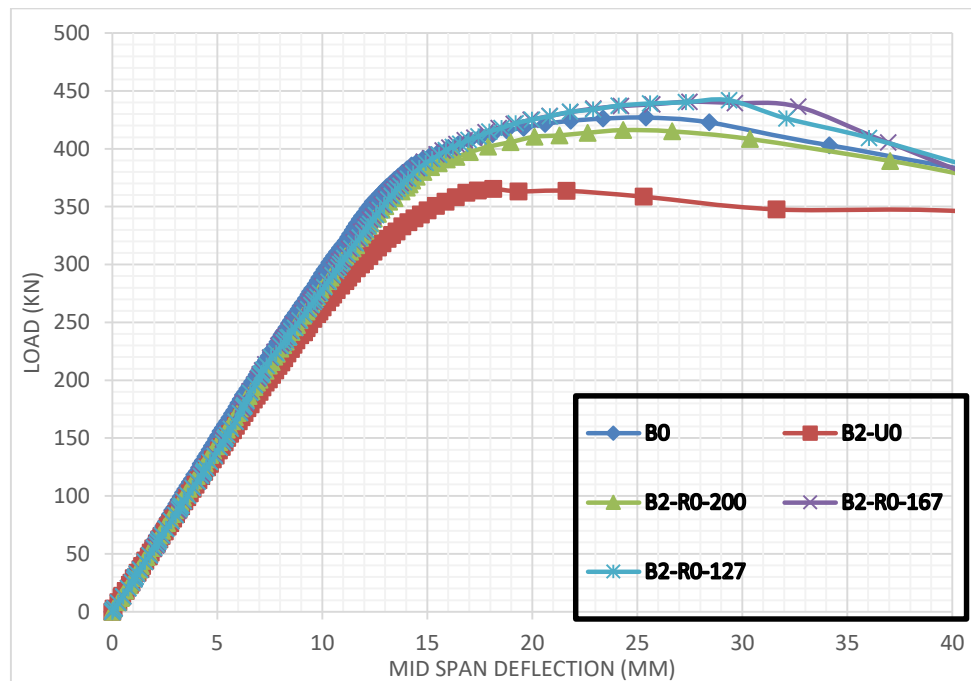


**Figure 4-16 : Load-deflection curves of shear zone HM and NM CFRP web opening strengthening .**

**IV.2.2.2. Bond behavior :**

For all shear zone strengthened specimens CFRP delamination did not happen since this failure occurred away from the reinforcement area (**Figure 4-17**) . It is apparent that no debonding has occurred in any of the bonded joints of tested beams and the adhesive was not harmed. This is evident from the damage parameter, SDEG, having values less than 1.0 .It is also worth noting that the highest values of this parameter were found near the junction extremities equal to  $9.188 e^{-1}$  and close to 1 (**Figure 4-17**) .Since there was no de-bonding type failure recorded for any tested specimens in the various circumstances it can be noted that the normal modulus CFRP provided the same bond performance as the previous high modulus CFRP and confirm the same effective bonding length ,any other addition in the bonding length will be useless .In addition to that the use of a high-modulus epoxy, provided complete shear transmission across CFRP and Steel .The successful bond is enough for completely mobilizing the section and developing full force transfer between steel and CFRP which explain the alteration of failure mode and the transfer of stress concentration from the corner of the opening in shear zone to the mid span in the upper flange of the beam .Bond failure with NM CFRP of the same thickness was not an issue in all reinforced beams that reached full composite action for both the steel beam and the CFRP reinforcing scheme, like it was in the test employing high modulus CFRP.

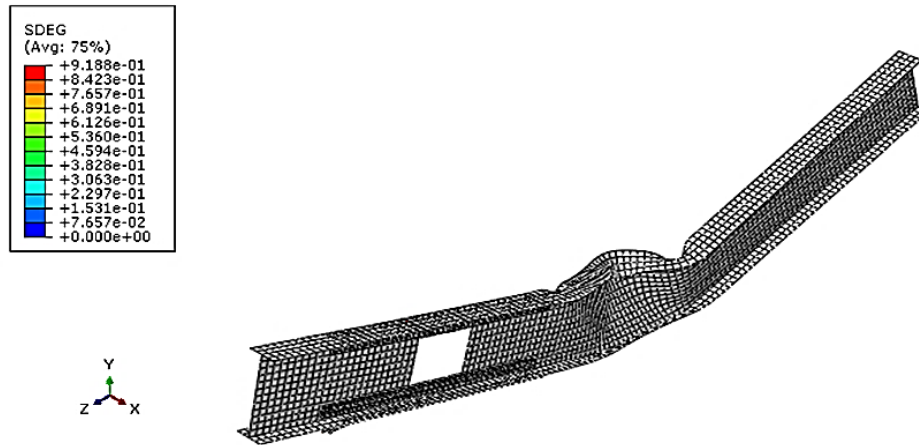


**Figure 4-17 : Bond behavior checking for NM CFRP strengthening .**

**IV.2.2.3.CFRP plate strain dispersion :**

Vierendeel action causes strain to be concentrated at the apertures' angles with tensile and compressive values. Besides to that, it was decided to measure the strain dispersion along the CFRP that was joined at the web and flange. The strain values on the NM CFRP were comparable to the HM CFRP, and the current peak CFRP plate strains were similar. It can be noted also that the ultimate strain values of the NM CFRP and HM CFRP were measured for plates joined at the web just below hole. It should also be noted that the highest recorded strain for HM CFRP 1610 micro strain (**Figure 4-20**), is around 13% of its ultimate strain ability, 12000 micro strain, indicating a poorer consumption percentage. In the other hand , for the two types of NM CFRP the maximum strain value corresponds to around 20 % of their maximum strain capacity, which present also a low utilization ratio (**Figure 4-18** and **Figure 4-19**) .Although being strained as the HM CFRP, the two NM CFRPs used in this investigation were little stressed. This might suggest that the thickness of NM CFRP plates could be reduced in various cases, depending also on the strength improvement and the bond junction between steel and CFRP plate.

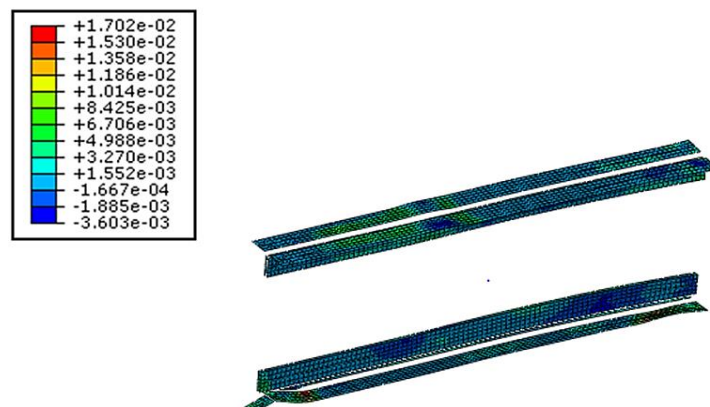


**Figure 4-18 : Strain distribution on normal modulus CFRP 167 plates at the peak load B2-R0 beam.**

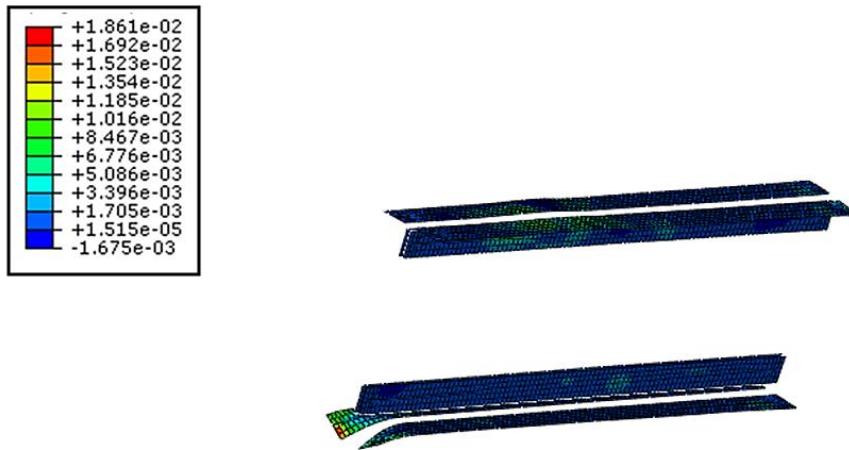


**Figure 4-19 : Strain distribution on normal modulus CFRP 127 plates at the peak load B2-R0 beam**

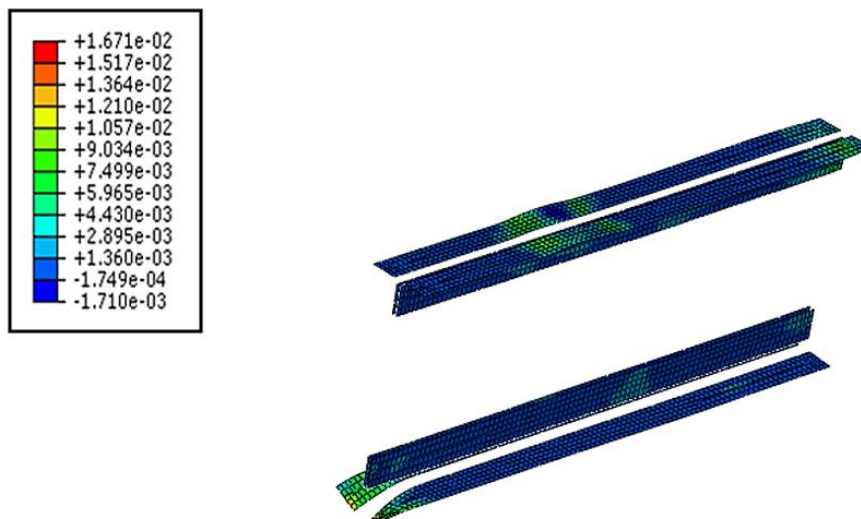


**Figure 4-20 : Strain distribution on normal modulus CFRP 200 plates at the peak load B2-R0 beam.**

**VII.2.2.4. The optimum NM CFRP plate thickness in shear zone :**

A parametric evaluation was carried out to determine the useful thickness of NM CFRP resulting in reduced CFRP usage ratios in the two specimens strengthened using NM CFRP which was corroborated by the numerical findings. A side from the previously examined 3mm CFRP thickness in shear zone , 1 and 2mm thicknesses were utilized for 127 kN and 167 kN elastic modulus of CFRP .

It can clearly be seen from **Figure 4-21** and **Figure 4-22** that 2mm plate thicknesses offered roughly the same strength gain as the preceding 3mm plate thickness for the two NM used CFRP . In the other hand the use of 1 mm provided the same strength enhancement as the previous 3mm thickness for 167 kN elastic modulus CFRP (**Figure 4-21**) despite the fact that it was slightly less stiffer in the elastic range. The utilization of 1 mm CFRP plates of 127 kN elastic modulus was not able to recover the strength of the solid original beam B0 and provided less stiffer response .Regarding the bond behavior ,In all of the situations, no de-bonding form failure has been documented for any of the tested specimens only specimen B2-R0-127-1 which failed by end debonding . Despite the failure mode of the tested specimens was top flange buckling accompanied by lateral torsional buckling far from the strengthened zone (**Figure 4-23**) only specimen B2-R0-127-1 which failed by Vierndeel failure mode (**Figure 4-24**).

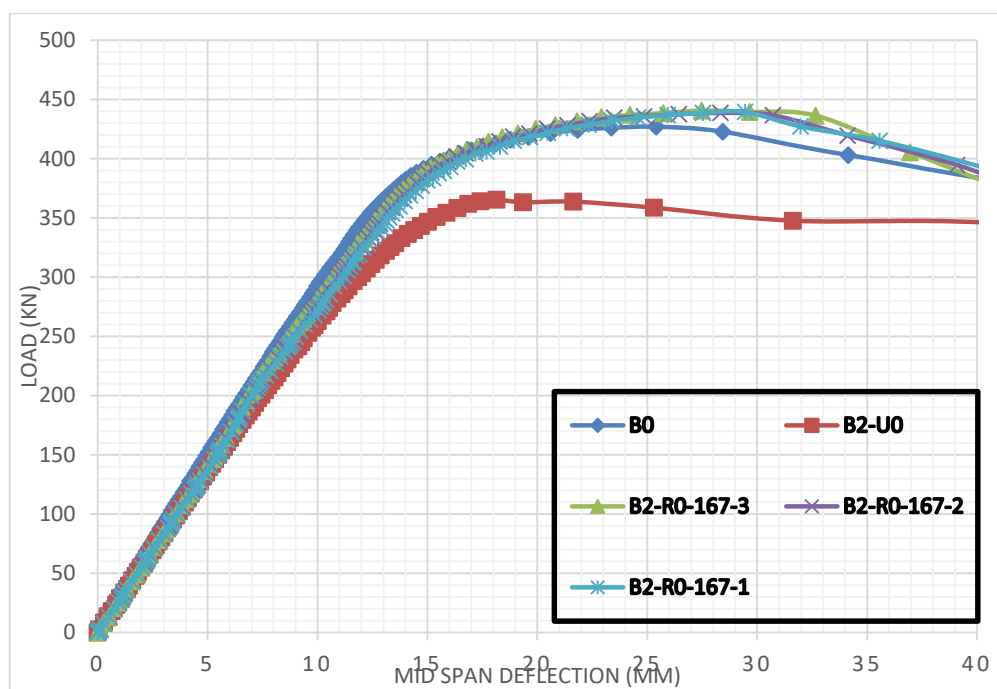


**Figure 4-21 : Load deflection curves of different NM CFRP 167 MPa plate thicknesses for shear zone opening position .**

According to these findings, the use of 1mm CFRP plate for NM CFRP with an elastic modulus < 150 MPa is not advised, despite the fact that the strength recovery was near to the original capacity of the beam. This failure mode causes brittle end debonding. The optimal thickness in the shear zone for NM CFRP of 167 MPa, on the other hand, was discovered to be 2 mm.

In terms of cost, more research is needed to evaluate the capabilities of other composites like GFRP to strengthen web apertures of steel beams , The first research on strengthening of steel beams with web holes employing GFRP will be carried out in the following section.

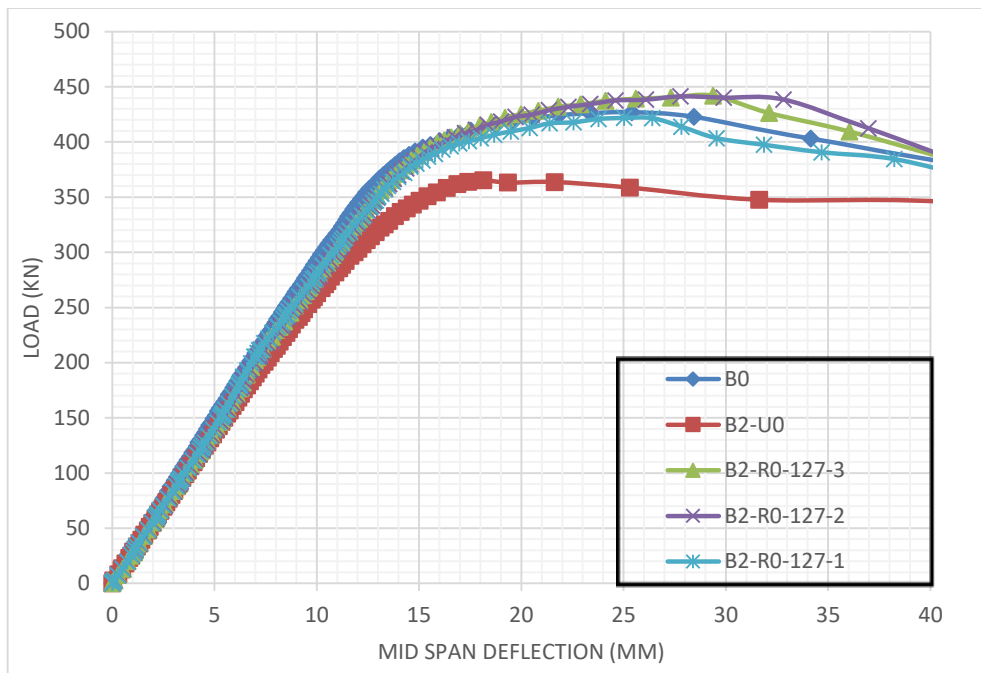


**Figure 4-22 : Load deflection curves of different NM CFRP 127 MPa plate thicknesses for shear zone opening position .**

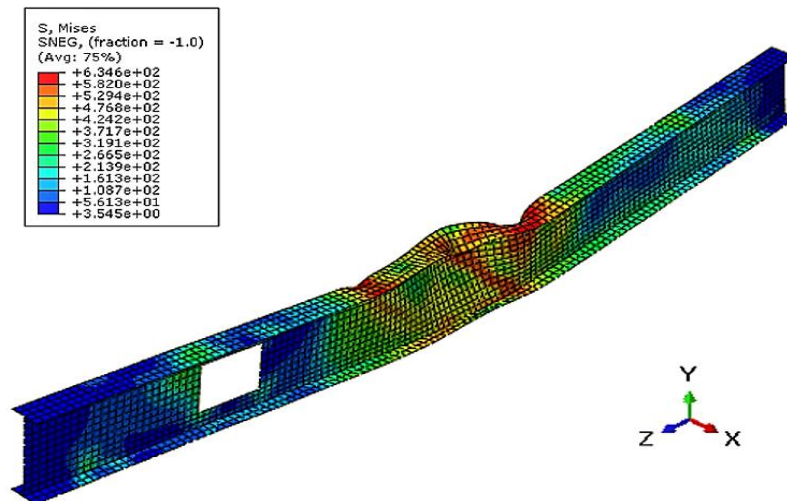


**Figure 4-23 : Failure mode of spécimen B2-R0-167-2.**

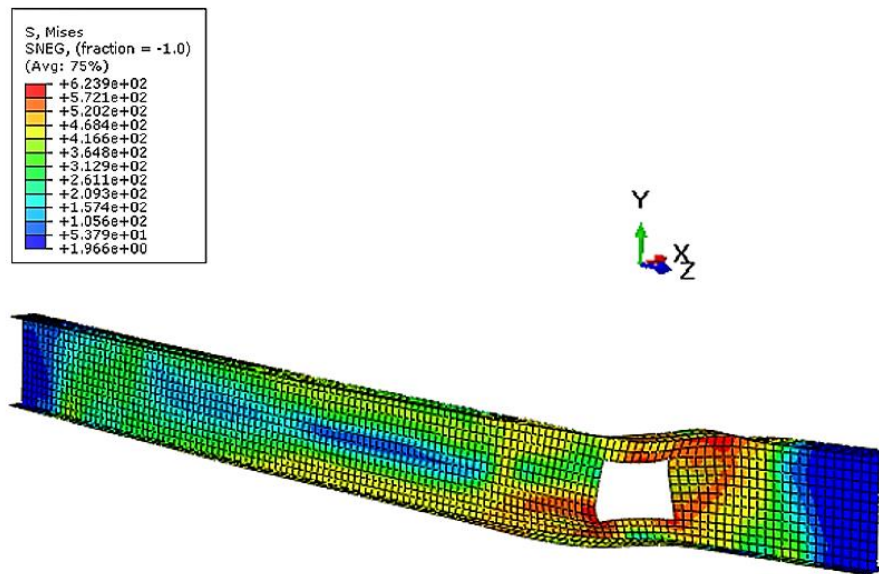


**Figure 4-24 : Failure mode of spécimen B2-R0-127-1.**

#### **IV.2.Strengthening steel beams with single rectangular web opening using GFRP:**

Because the use of FRP to reinforce steel beams with web openings is a new approach, there are currently no design guidelines or manuals available for the use in the building sector. More detailed investigations and other testing of various factors are required to offer enough information to make suggestions and fully comprehend the application of FRP strengthening of web aperture in current steel beams. The purpose of this section is to investigate the capacity of low modulus fibers to strengthen steel I beams with web openings under static loading.

Using the approved numerical simulation, the tested specimen B0 was reinforced using pultruded GFRP laminates following the creation of rectangular web apertures with the same opening sizes and locations as in the preceding sections.

The unstrengthened specimens with mid span and shear zone web openings were named B1-U0 and B2-U0, respectively as in the previous section. Four strengthening configurations were considered using pultruded GFRP plates and different GFRP profile shapes (U section–angle section–T section) (Figure 7-24) and (Table 7-3).

The GFRP elastic modulus was 18 GPa [25]. The adhesive and the bonding length were similar to the previous study. In addition, the influence of different GFRP laminate thicknesses was investigated.

The results will be discussed in regards to strength improvement, load-deflection response, failure mechanism, bond behavior, and will be compared to previous HM CFRP strengthening data.



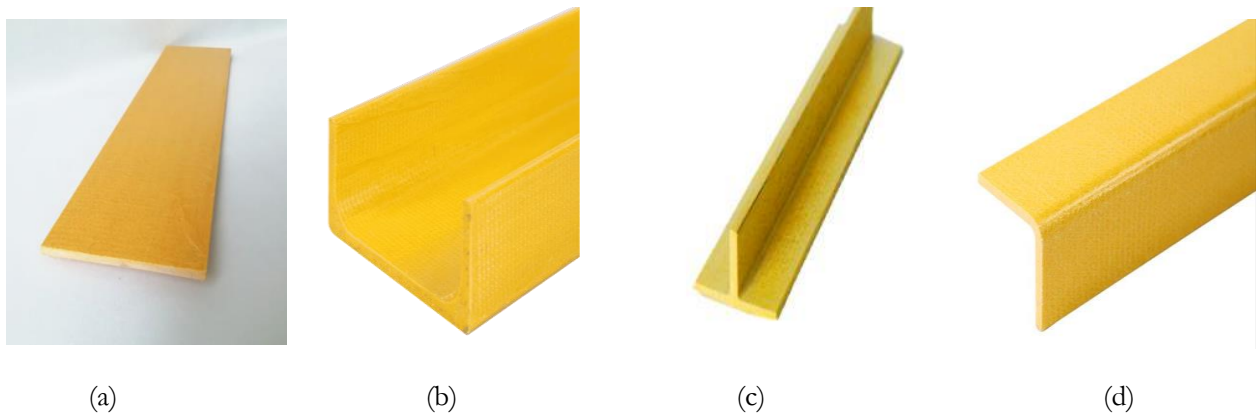


**Figure 4-25: Pultruded GFRP :(a) plate-(b) U section –(c) T section –(d) Angle section .**

R1	R2	R3	R4
GFRP plate.	U section GFRP.	Angle section GFRP	Combination of GFRP plate and GFRP T-section.

**Table 4-3 : The Proposed GFRP strengthening configurations .**

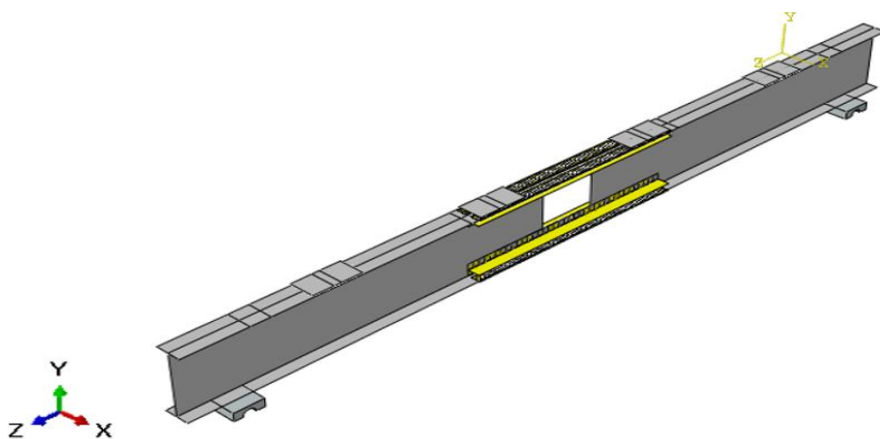


**Figure 4-26 : Strengthening specimen B1-U0 using (R4) GFRP technique .**

**IV.2.1.Results and discussion:**

The following section describes the findings of the FE study. Every tested specimen was labeled: The first letter in every case identification is the designation of the tested beam, accompanied by the GFRP strengthening arrangement (R0-R1-R2-R3-R4), and eventually the GFRP laminate thicknesses ( 3mm-6mm-10mm) .For example , " B1-R2-3" is the specimen B1 of mid span rectangular opening strengthened using R2 pattern with U GFRP sections of 3mm thicknesses .

**IV.2.1.1Mid span position results :****IV.2.1.1.1.GFRP laminates of 3mm thicknesses:**

The creation of a rectangular web opening in the mid span of the beam resulted in a strength decrease of 12 % compared to the initial beam B0, as shown by the load-deflection curve of specimen B1-U0 (**Figure 4-27**).

Due to the presence of various GFRP strengthening patterns, different percentages of the strength and stiffness restore was noted in comparisons to the unstrengthened specimen B1-U0. The specimen B1-R1-3 showed an increase of 25 % in the strength enhancement, while specimens B1-R2-3 and B1-R3-3 were improved by 19%. Despite the strength of the solid beam B0 was recovered using R1, R2 and R3 strengthening configurations, only the "R4" reinforcement technique was able to exhibit the same strength enhancement found using CFRP in the previous study (B1-R0) [56], which was around 37 % compared to B1-U0 and 20 % over the solid beam B0 . It was also observed that the stiffness of the original beam B0 was recovered in all cases of GFRP strengthened specimens, although it was not at the same level as the CFRP strengthened specimen B1-R0, which exhibited a stiffer response than the solid beam B0 (**Figure 4-27**). Specimens B1-R1-3, B1-R2-3, and B1-R3-3 demonstrated a very linear trend up to around 360 kN of load. While for specimen B1-R4-3 the yielding load was around 380 kN. Further than this stress level, the commencement of plastic hinge generation was in the mid span above the opening. As a consequence, lateral buckling was initiated in the beam's mid span (**Figure 4-28** and **Figure 4-29**).

This was not the same failure mode as CFRP plates . So it can be noted that the adoption of 3 mm GFRP laminates did not impact the stress state of the beam. Regarding the bond behavior, the adhesive damage can be predicted from the simulation analysis, employing the numerical output parameter SDEG, which represents the adhesive's damage progression. End debonding was started on the top flange of all GFRP reinforced specimens once the original force was attained. The SDEG parameter attained a value of 1, and the adhesive layer was deleted (**Figure 4-30**).



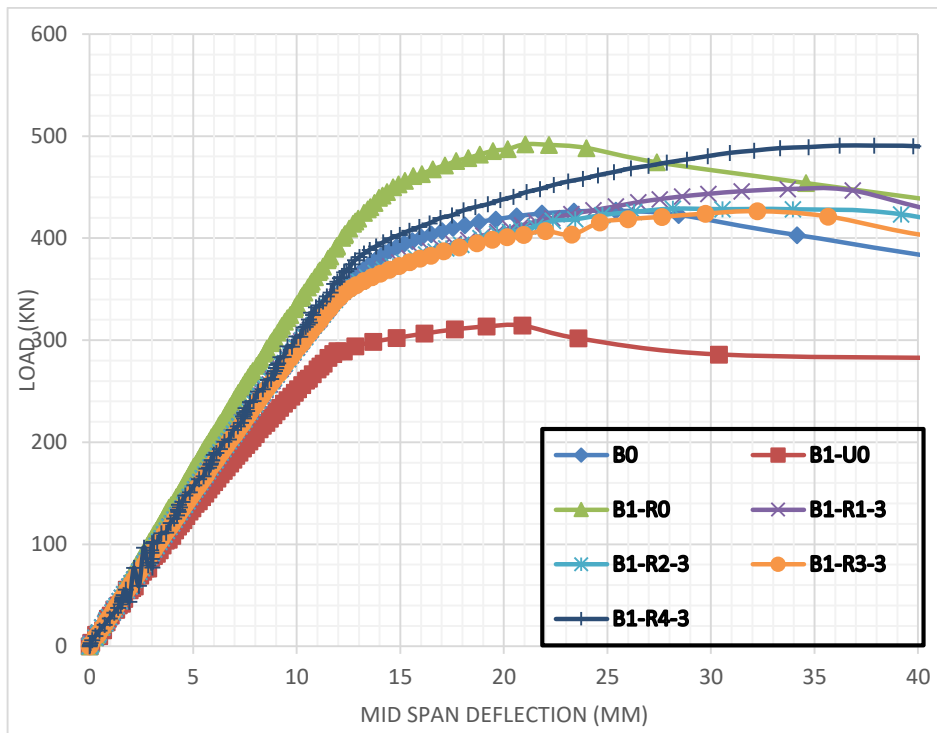


**Figure 4-27 : Load-deflection curves of 3mm GFRP laminates strengthening .**

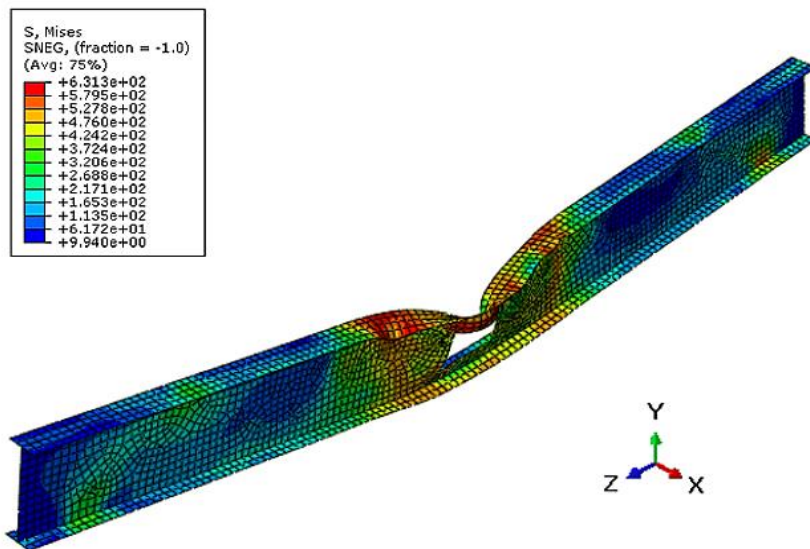


**Figure 4-28 :Mid span lateral buckling of specimen B1-R3-3 .**

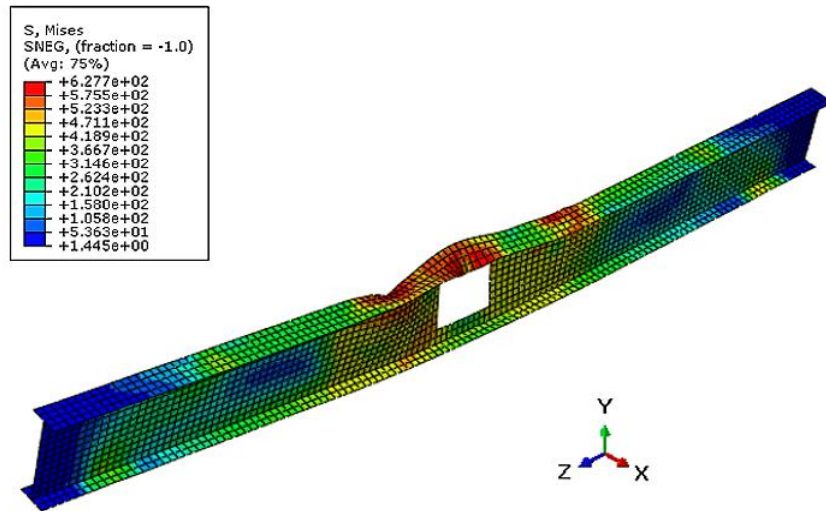


**Figure 4-29 : Mid span lateral buckling of specimen B1-R4-3 .**

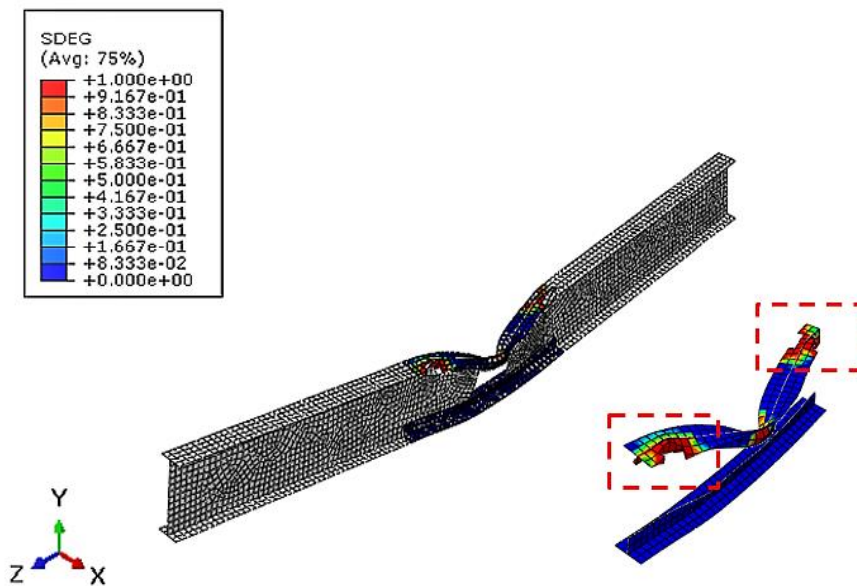


**Figure 4-30 : Bond behavior for specimen B1-R3-3.**

**IV.2.1.1.2.GFRP laminates of 6mm thicknesses:**

Increasing the thickness of the GFRP laminates to 6 mm allowed the reinforced specimens B1-R1-6, B1-R2-6, B1-R3-6, and B1-R4-6 to obtain a strength improvement percentage of 35%, 30%, 25%, and 43%, respectively, when compared to the unstrengthened beam B1-U0. As a result, all GFRP strengthened specimens with a thickness of 6 mm demonstrated a strength increase greater than the solid beam B0 (Figure 4-31) .

Besides that, the strength enhancement percentage of the ‘R1’ strengthening configuration with 6 mm plate thickness was comparable to 3 mm CFRP plate strengthening (specimen B1-R0). Furthermore, the ‘R4’ strengthening pattern with 6 mm GFRP laminates provided a significant improvement in strength more than of the prior CFRP strengthening approach. However, despite the fact that the stiffness of the original beam B0 was restored with all 6mm GFRP strengthening cases, the specimen B1-R0 is considerably stiffer (**Figure 4-31**) and increasing the GFRP laminate thicknesses to 6mm did not really affect the stiffness in comparison to GFRP laminates of 3 mm thickness. B1-R1-6 and B1-R4-6 specimens showed a linear trend up to 360 kN and 380 kN of load, respectively. Further than this level of stress, the top flange at the end of the GFRP laminates saw the commencement of plastic hinge development. As a response, lateral buckling occurred far from the strengthened area at the end of the bonded GFRP laminates (**Figure 4-32**). This was the same failure mechanism as in the prior experiment, with the CFRP reinforcing arrangement [56]. On the other hand, specimens B1-R2-6 and B1-R3-6 demonstrated a very line graph up to around 350 kN. Above this load level, the top flange at the mid-span of the beam began to develop plastic hinges. As a consequence, lateral buckling occurred in the mid span of the beam (**Figure 4-33**). So it should be stated that R2 and R3 strengthening designs with laminate thicknesses of 6 mm were unable to modify the failure mode of the examined specimens. In terms of bond behavior, end debonding of all GFRP reinforced specimens began at the top flange.

**Figure 4-34** and **Figure 4-35** shows that the SDEG indicator achieved a value of 1 at the adhesive end in specimens B1-R2-6 and B1-R3-6, confirming adhesive failure. As a result, the GFRP laminates were debonded there.

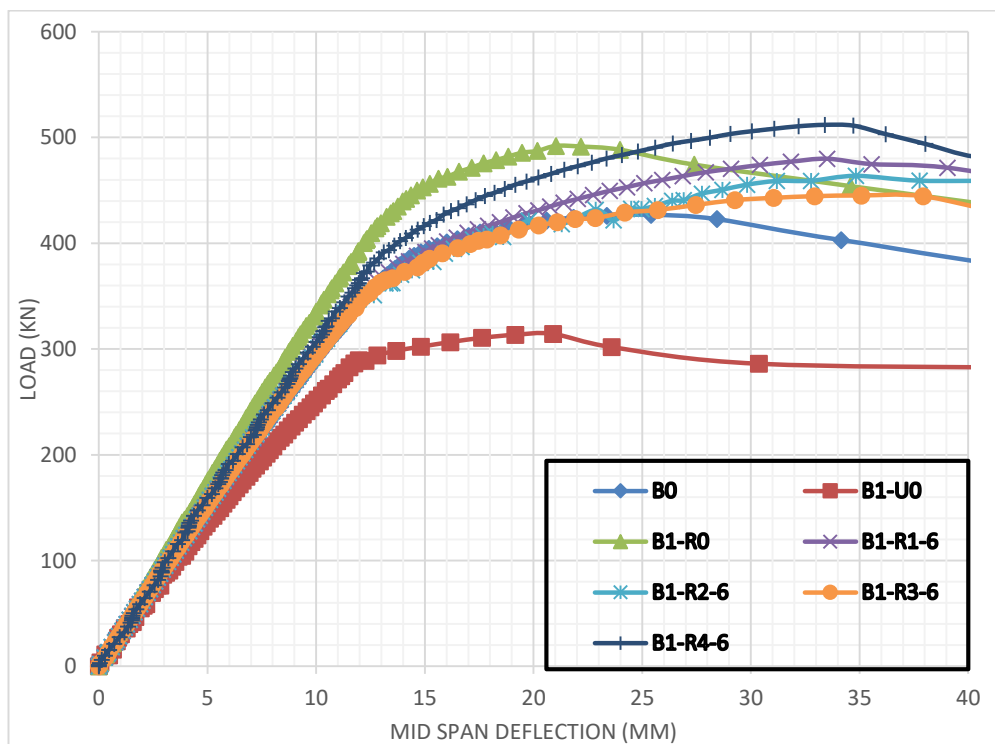


**Figure 4-31 : Load deflection curves of specimen B1-UO strengthened using 6 mm GFRP laminates thicknesses .**

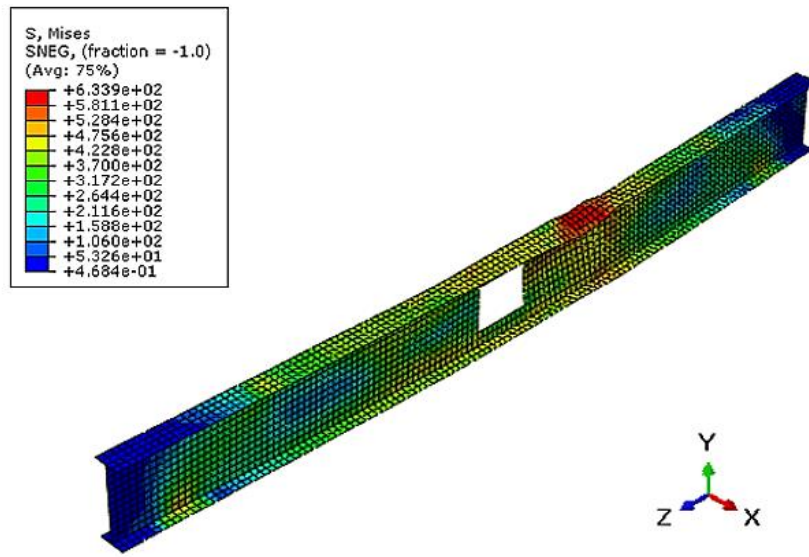


**Figure 4-32 : Failure mode of specimen B1-R4-6 .**

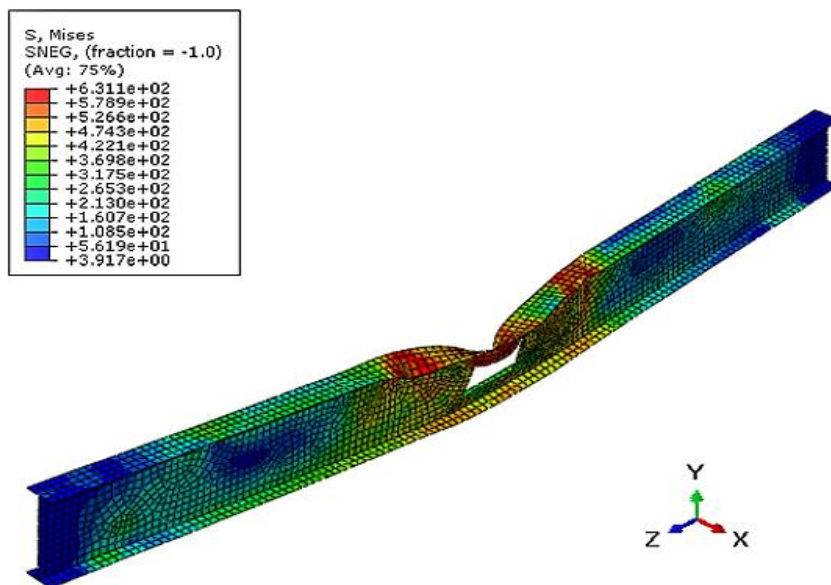


**Figure 4-33 : Failure mode of specimen B1-R3-6 .**

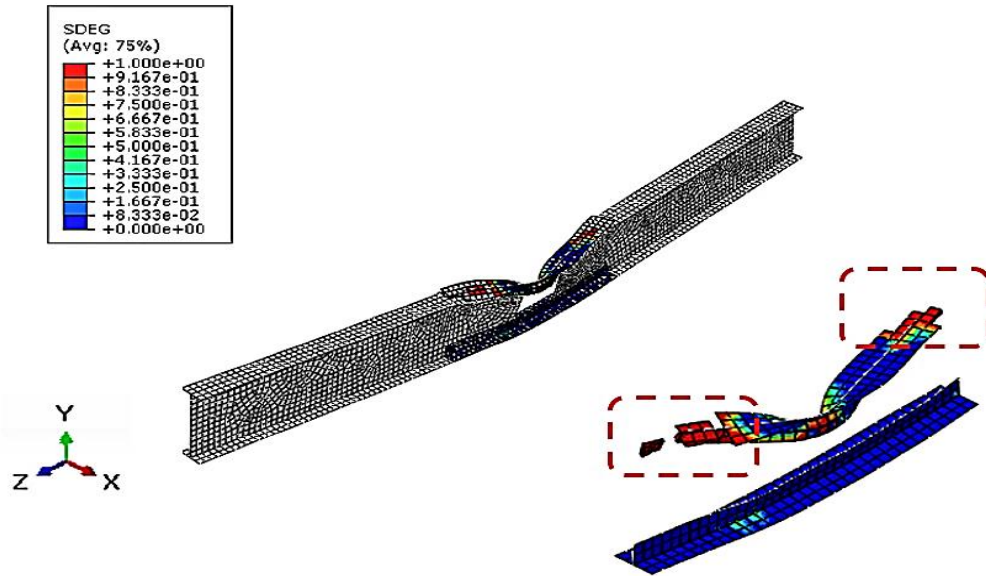


Figure 4-34 : Bond behavior of specimen B1-R2-6.

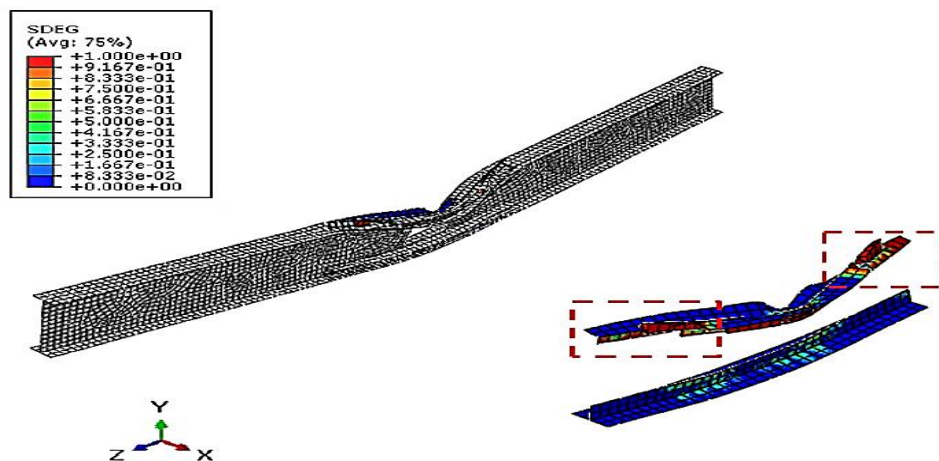


Figure 4-35: Bond behavior of specimen B1-R3-6.

#### IV.2.1.1.3. GFRP laminates of 10 mm thicknesses:

When the thicknesses of the GFRP laminates were increased to 10 mm, very intriguing results were observed. In contrast to B1-U0, specimens B1-R1-10, B1-R2-10, B1-R3-10, and B1-R4-10 improved in strength by 37 %, 33 %, 23 %, and 45 %, respectively (**Figure 4-36**). According to these numerical results, GFRP plates with a thickness of 10 mm ('R1') were able to achieve the same strength increase as CFRP plates with a thickness of 3 mm. Furthermore, utilizing the 'R4' configuration of 10 mm (B1-R4-10) revealed a 6% gain in strength over the prior CFRP strengthening with non-ductile response (**Figure 4-36**) Concerning stiffness, it is crucial to note that the original beam's stiffness was recovered using all strengthening patterns, with the 'R4' strengthening technique being the most comparable to the CFRP strengthening specimen (B1-

R0) (**Figure 4-36**). Specimens B1-R1-10, B1-R2-10, and B1-R3-10 showed a linear curve up to the yielding load, which was about 365 kN. whereas specimen B1-R4-10 had a yielding load of 405 kN.

Just above this load stage, the origins of plastic hinge initiation was observed at the end of the reinforcement zone . As a natural consequence, lateral buckling started at the end of GFRP laminates with top flange buckling for specimens B1-R1-10, B1-R2-10, and B1-R3-10 (**Figure 4-37**) , while for specimen B1-R4-10 lateral buckling was not seen. The beam failed only by top flange buckling (**Figure 4-38**).This can be explained by the flexural stiffness of the T-section GFRP profile, which was able to prevent the out of plane buckling .

Brittle end debonding was observed (**Figure 4-39**) particularly specimen B1-R3-10.This demonstrates the significance of adjusting bond performance and laminate thickness. It appears to be plausible, the strength of the reinforced specimens will increase as the thickness of the GFRP laminates increases. However, the need for strength restoration must be controlled with the ductility response of the reinforced section and the bond performance to avoid premature debonding.

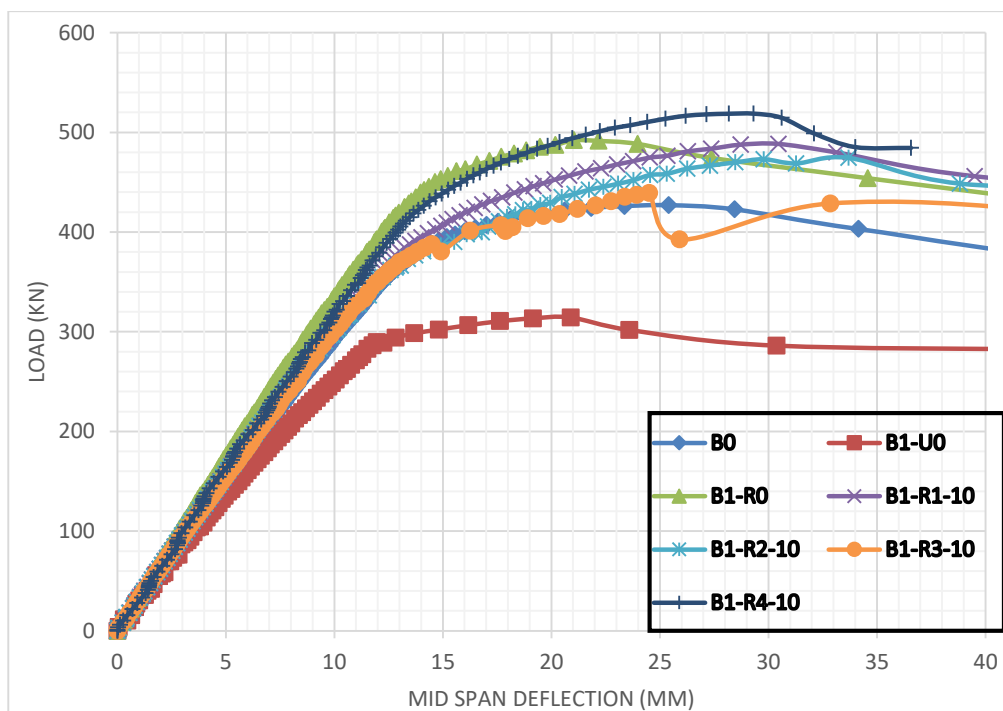


**Figure 4-36:Load deflection curves of specimen B1-UO strengthened using 10 mm GFRP laminates thicknesses.**



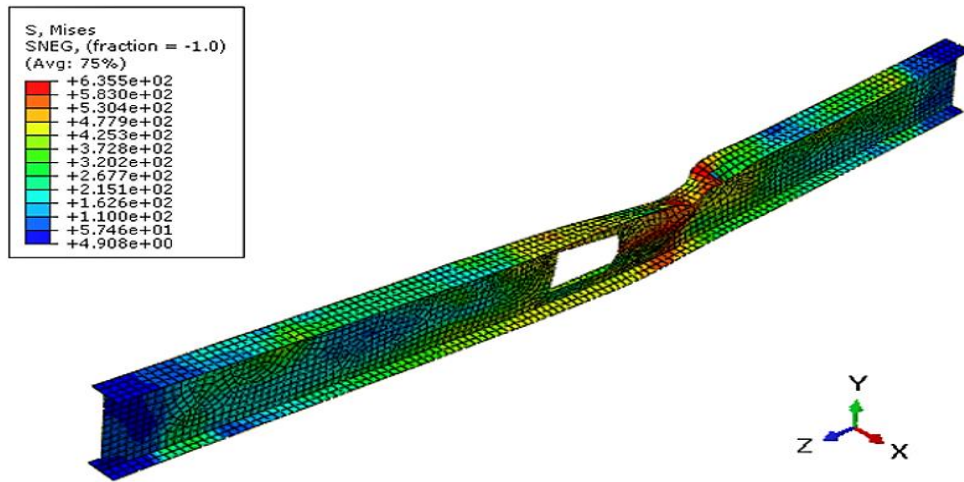


Figure 4-37: Failure mode of specimen B1-R1-10.

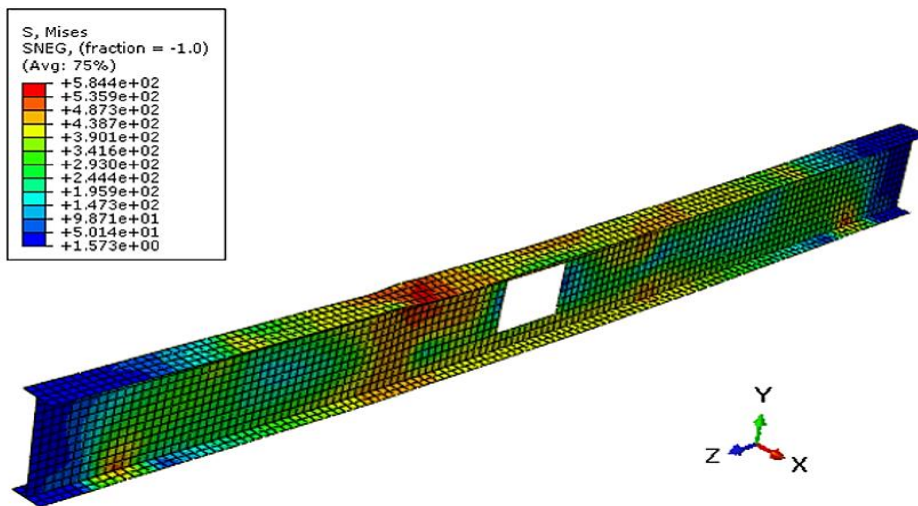


Figure 4-38: Failure mode of specimen B1-R4-10.

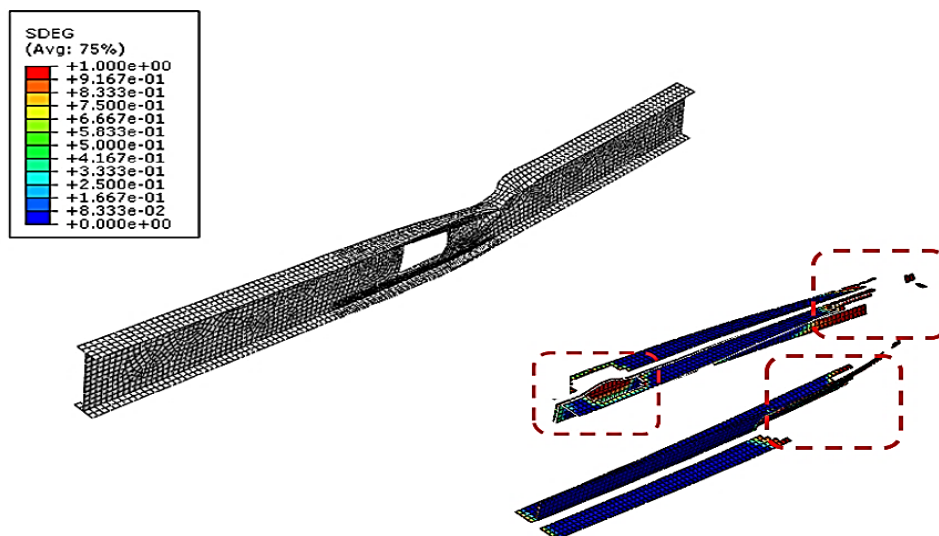


Figure 4-39: Bond behavior of specimen B1-R1-10.

**IV.2.1.2. Shear zone position results :****IV.2.1.2.1. GFRP laminates of 3mm thicknesses:**

The existence of a large rectangular perforation in the shear zone of the control specimen B0 reduced the beam's strength by 17%, as seen in **Figure 4-40**. The same GFRP reinforcement arrangement that was employed for the mid span aperture was applied here to push the perforated beam to regain its initial capacity.

**Figure 4-40** show the load-deflection curves of all GFRP reinforced beams. It can be seen that the percentage of strength enhancement in comparison to B2-U0 was 22 % ,32 % ,30 % and 35 % for specimens B2-R1-3 ,B2-R2-3 ,B2-R3-3 and B2-R4-3 respectively . Despite the fact that GFRP plates of 3 mm (B2-R1-3) did not exhibit the same strength enhancement as CFRP plates of 3 mm, all other reinforced specimens displayed a greater strength enhancement than the control beam and the CFRP strengthened specimen (B2-R0).

In addition, the stiffness of the initial beam was restored and it was extremely comparable for all strengthened specimens (**Figure 4-40**). Nevertheless, all beams displayed a linear rise up to the same yielding load, which was equal to 360 kN. The initiation of stress concentration was not in the same position.

For specimen B2-R4-3, the commencement of plastic hinge creation was in the top flange at the mid-span of the beam. As a response, lateral buckling occurred at the mid span between the central lateral support (**Figure 4-41**). In contrary specimens B2-R1-3, B2-R2-3 and B2-R3-3 failed by Vierendeel failure mode (**Figure 4-42**). Only specimen B2-R4-3, which used GFRP laminates with a thickness of 3 mm, was capable of influencing the stress status of the beam and demonstrating the same failure mechanism as before (HM CFRP strengthening) [56]. This emphasizes the need to select the most appropriate strengthening scheme.

Additionally, for specimen B1-R4-3, since the failure occurred outside of the strengthening region, GFRP debonding did not occur. While the SDEG clearly shows that debonding which was performed for specimens B1-R1-3, B1-R2-3, and B1-R3-3 (**Figure 4-43**).

**IV.2.1.2.2. GFRP laminates of 6mm thicknesses:**

The prior findings prompted an investigation into the usage of 6 mm GFRP laminates. The strength gain varied from 28% to 36% for the GFRP enhanced specimens (**Figure 4-44**).

The increase of GFRP laminates to 6 mm did not significantly boost the strength improvement in comparison to the previous 3 mm GFRP products. In terms of stiffness, all beams demonstrated remarkably similar stiffness to their original beam B0 when reinforcement was implemented.

Up to 360kN of load, all GFRP strengthened beams displayed a linear graph similar to the original and CFRP strengthened beams (B0 and B2-R0). Above this yielding load, the official start of plastic hinge development was in the top flange at the mid-span of all tested specimens. As a reaction, lateral buckling was seen in the specimens' mid span (**Figure 4-45**). However,



despite the fact that the failure mode of all reinforced specimens was outside the strengthened portion, the bond behavior varied. Debonding was detected for examples B2-R2-6 and B2-R3-6, which might be attributable to the lack of bonded GFRP laminates in the beams' bottom flanges (Figure 4-46).

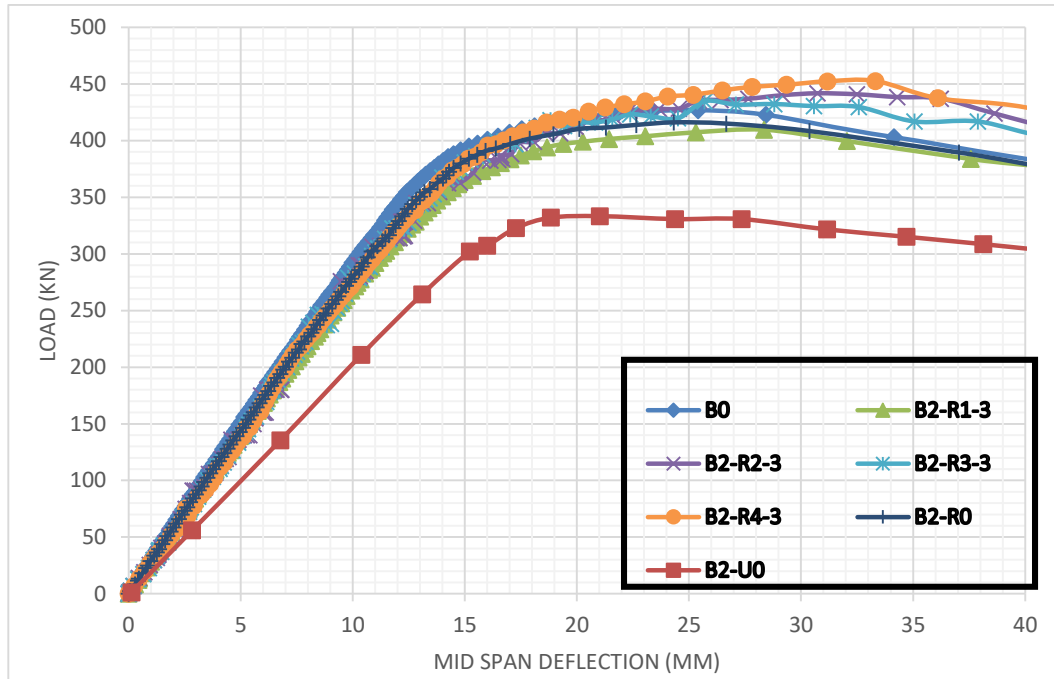


**Figure 4-40: Load deflection curves of specimen B2-UO strengthened using 3 mm GFRP laminates thicknesses.**

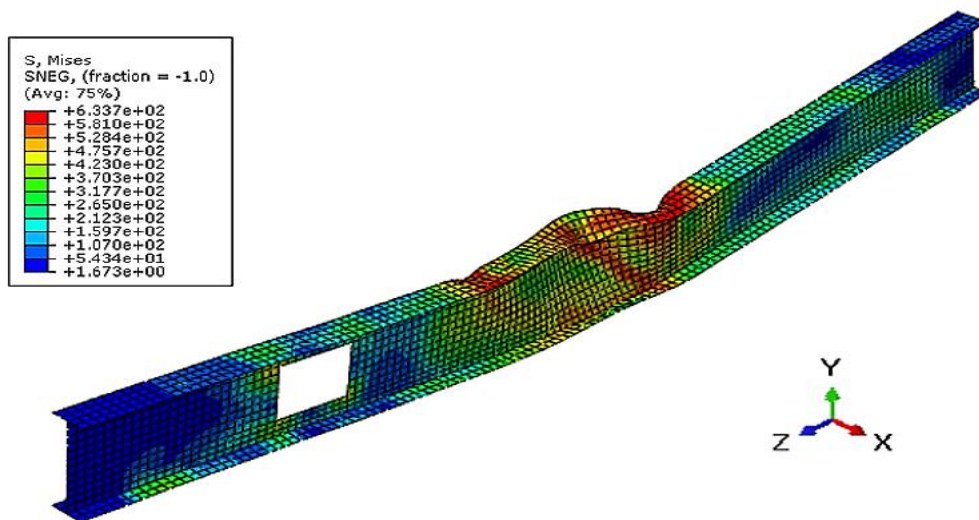


**Figure 4-41: Failure mode for specimen B2-R4-3.**

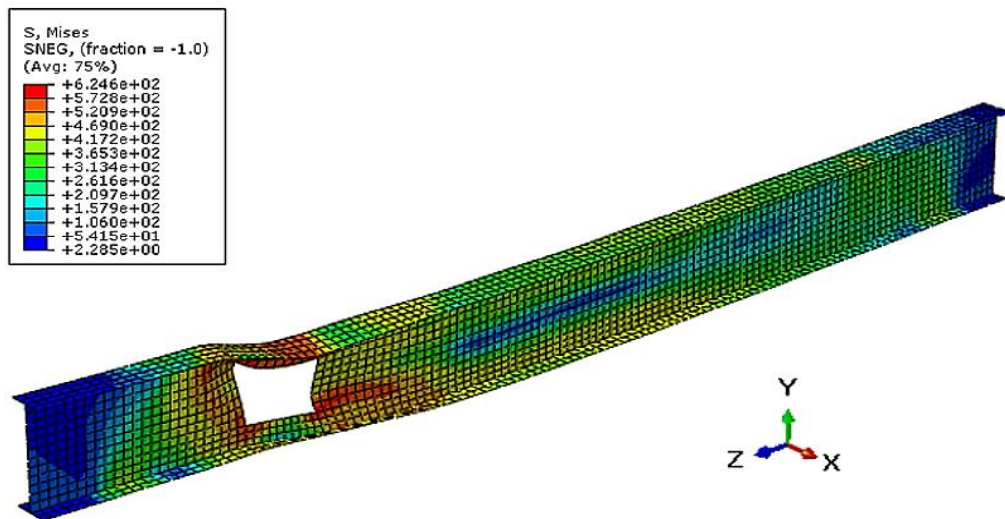


**Figure 4-42 : Failure mode for specimen B2-R2-3.**

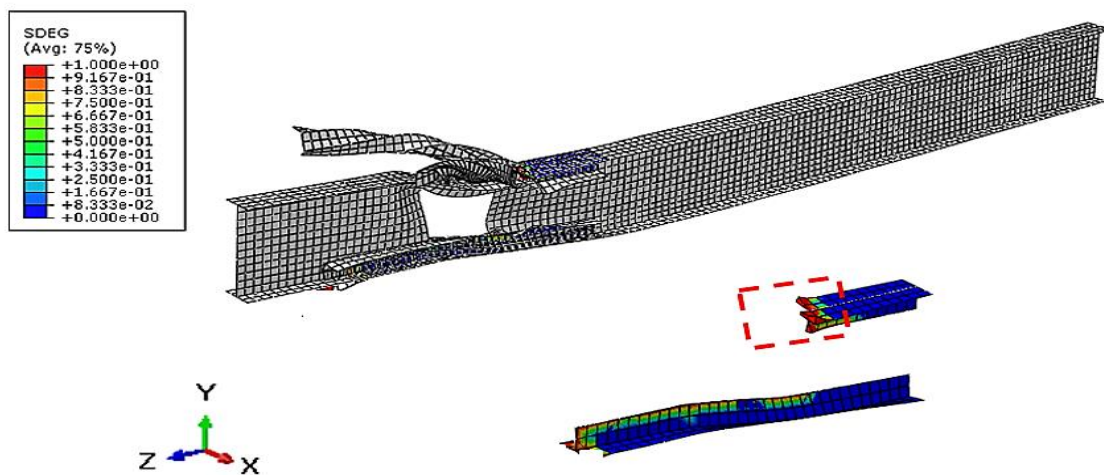


**Figure 4-43: Bond behavior for specimen B2-R2-3.**

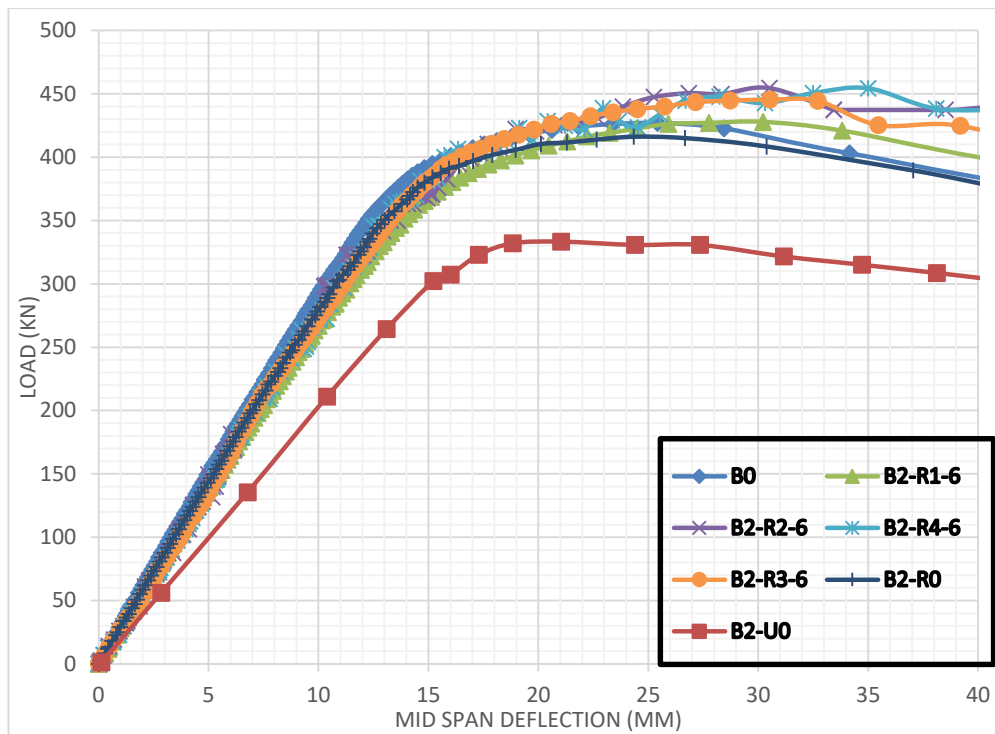


Figure 4-44: Load deflection curves of specimen B2-UO strengthened using 6 mm GFRP laminates thicknesses.

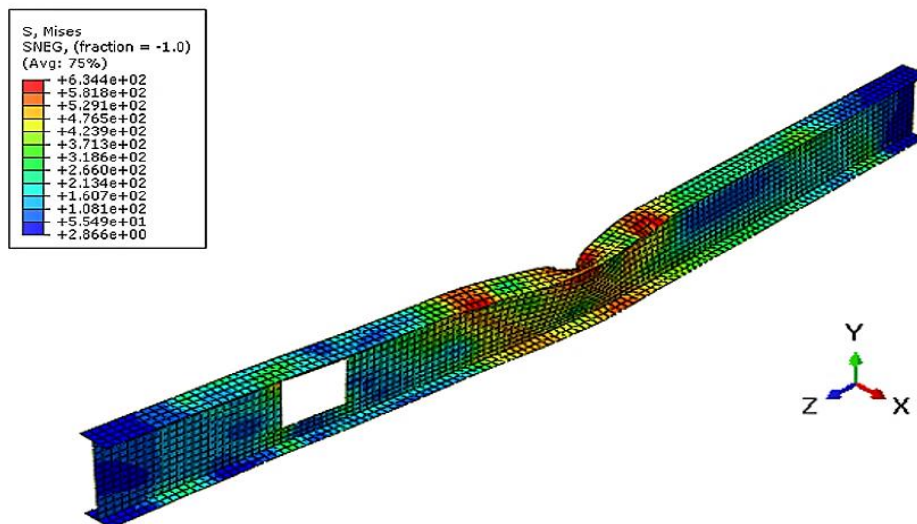
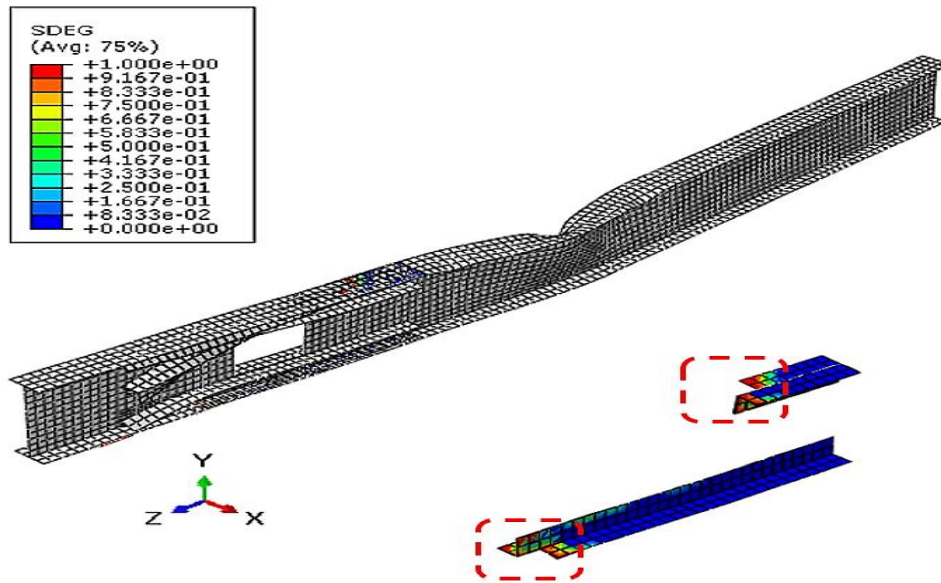


Figure 4-45: Failure mode for specimen B2-R2-6.



**Figure 4-46: Bond behavior for specimen B2-R2-6.**

#### **IV.2.1.2.3.GFRP laminates of 10 mm thicknesses:**

As previously reported, the strength gain attained with GFRP thickness increased to 10 mm ranged from 24% to 36% (**Figure 4-47**), which indicates that the strength of the initial beam was also restored. In the other hand these findings implies that the increase in GFRP laminate thickness seemed to have no influence on strength and stiffness improvement. This is explained by the premature debonding that occurs before the GFRP reinforcing ability is accomplished, which was the same observation in the previous study with HM CFRP [56].

In contrast to the mid span opening location, despite the fact that the augmentation of GFRP laminates to 10 mm did not produce the anticipated strength improvement, it was able to achieve better stiffness for all tested beams, particularly the 'R4' strengthening arrangement. The failure mode of specimens B2-R1-10 ,B2-R3-10 and B2-R4-10 was changed to mid span later torsional buckling (**Figure 4-48**),whereas B2-R2-10 failed by Vierndeel failure mode .In addition to that, debonding was observed with all GFRP strengthened specimens (**Figure 4-49**) .

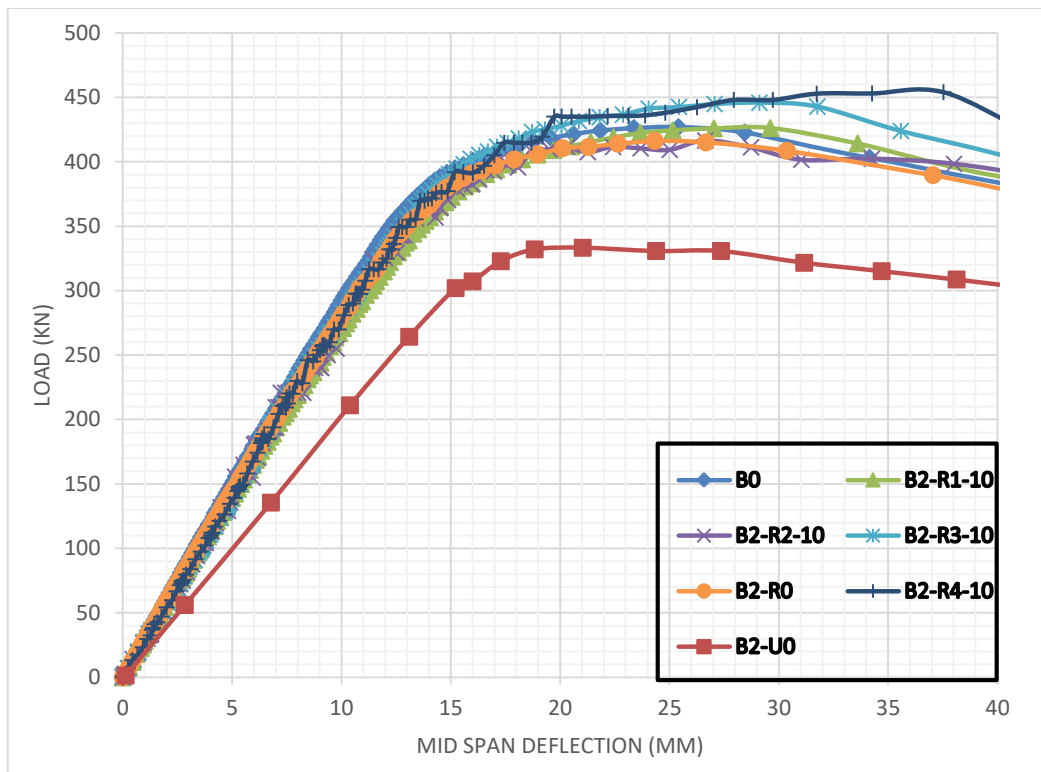


Figure 4-47 : Load deflection curves of specimen B2-UO strengthened using 10 mm GFRP laminates thicknesses.

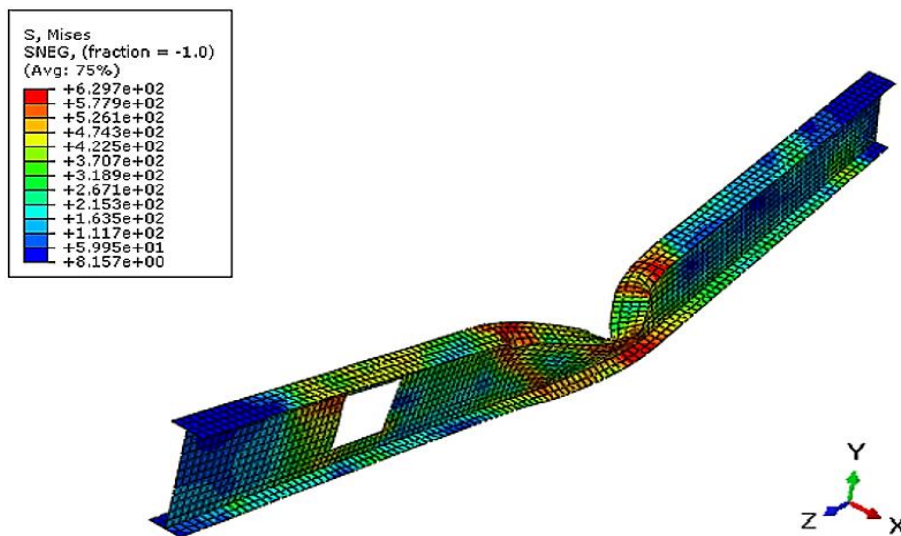
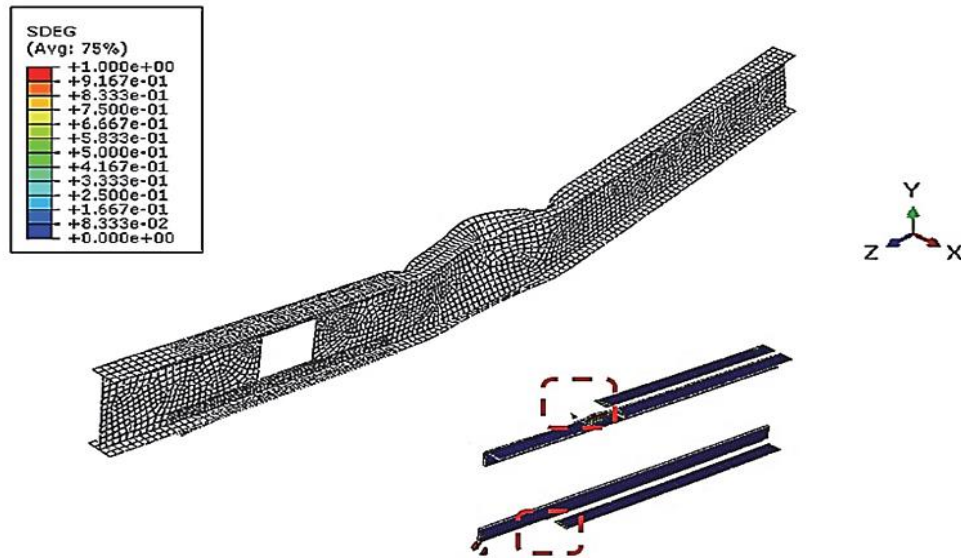


Figure 4-48 : Failure mode of specimen B2-R4-10.



**Figure 4-49 : Bond behavior for specimen B2-R1-10.**

#### **IV.2.2. Conclusion:**

In terms of economics, and based on previous results obtained on strengthening steel beams with web openings using HM CFRP and NM CFRP, the aim of this chapter was to investigate the ability of alternative composites such as GFRP to reinforce web openings in order to gather more information about the use of FRP composites to strengthen these types of beams and progress to a stage where guidelines can be established to support designers in their practical engineering and execution. It was determined that:

- Instead, to CFRP the GFRP strengthening technique proves to be an effective approach in practice for recovering the stiffness and strength of steel beams with rectangular web openings.
- This approach not only assisted to restoring the beam's capacity, but it also provided a boost of strength over to the original solid beam.
- In all situations, the reinforced beams had a stiffer reaction and a higher load-bearing capacity than the unreinforced specimens with web openings did.
- The most effective GFRP strengthening technique was the combination of pultruded GFRP T section and plates denoted "R4" in this study.
- The most efficient GFRP thickness for the two web opening positions along the span used in this research was 6 mm, which is equivalent to  $0.85 t_w$  . and  $t_f$ .
- The end debonding, which was noticed in the simulation for the majority of mid span and shear zone opening locations, happened after steel yielding and after the strength recovery.
- Using Araldite 420 epoxy adhesive, this strategy achieves full composite action between steel and GFRP.



- The failure location and mechanism of the strengthened beams were not always the same as in the control or the unstrengthened cases due to this approach of reinforcing.
- The bond length of the CFRP plate layout was suitable for GFRP reinforcing arrangements, particularly configurations "R1" and "R4".
- This finding suggests that GFRP is a suitable, practical and economic way of strengthening steel beams with web openings in comparison to the relatively expensive CFRP.

### **IV.3.Strengthening steel beam with different web opening shapes and dimensions using GFRP**

This study is yet in its initial stages, and further analysis is required to investigate numerous elements that may influence the performance of the suggested approach. There aren't any code regulations for FRP stiffening of web openings, and because of to the expense of conducting laboratory investigation, using the validated numerical model, and the GFRP reinforcing method that employs a combination of GFRP T sections and plates discovered to be the most effective in the preceding section, an investigation will be performed to provide adequate information for a comprehensive understanding of beam behavior and prove the technique's capacity when applied to another beam span and section size, as well as various aperture geometries with various sizes.

#### **IV.3.1.Case study :**

In the current investigation, the steel I-beam section is an IPE 400 with a clear span of 4 m (**Figure 4-50**), uniformly loaded which currently represents a common industrial floor beam. All web apertures are centered to the portions' mid-height in mid span and shear zone position close to the supports with dimensions ranging from 0.6 H to 1.5H, in which H denotes the depth section web. A series of five web openings of various geometries are investigated: Rectangular, trapezoidal, reversed trapezoidal, parallelogram and ellipse web opening . The opening aperture length which is the length of the tee-sections upper and lower the gaps, is the important dimensional factor in all of these aperture designs. The GFRP strengthening arrangement initially indicated in the preceding section, with a mixture of GFRP strips with 4 times the aperture length, will be applied below. The stress-strain curve for S355 steel is illustrated in **Figure 4-53**. Steel density was 7850 kg/m<sup>3</sup> and modulus of elasticity was 210 GPa.

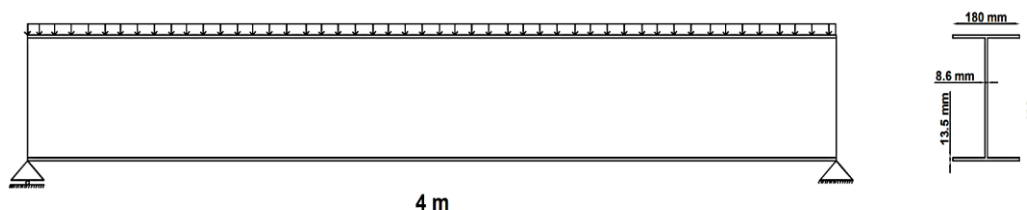


**Figure 4-50 : Details of tested specimen.**

The GFRP and adhesive material characteristics employed in this test were identical to the ones reported from the preceding section. **Figure 4-51** and **Tables 4-4** shows dimensions of the

aperture forms as well as the accompanying values of the opening length, which are stated below:

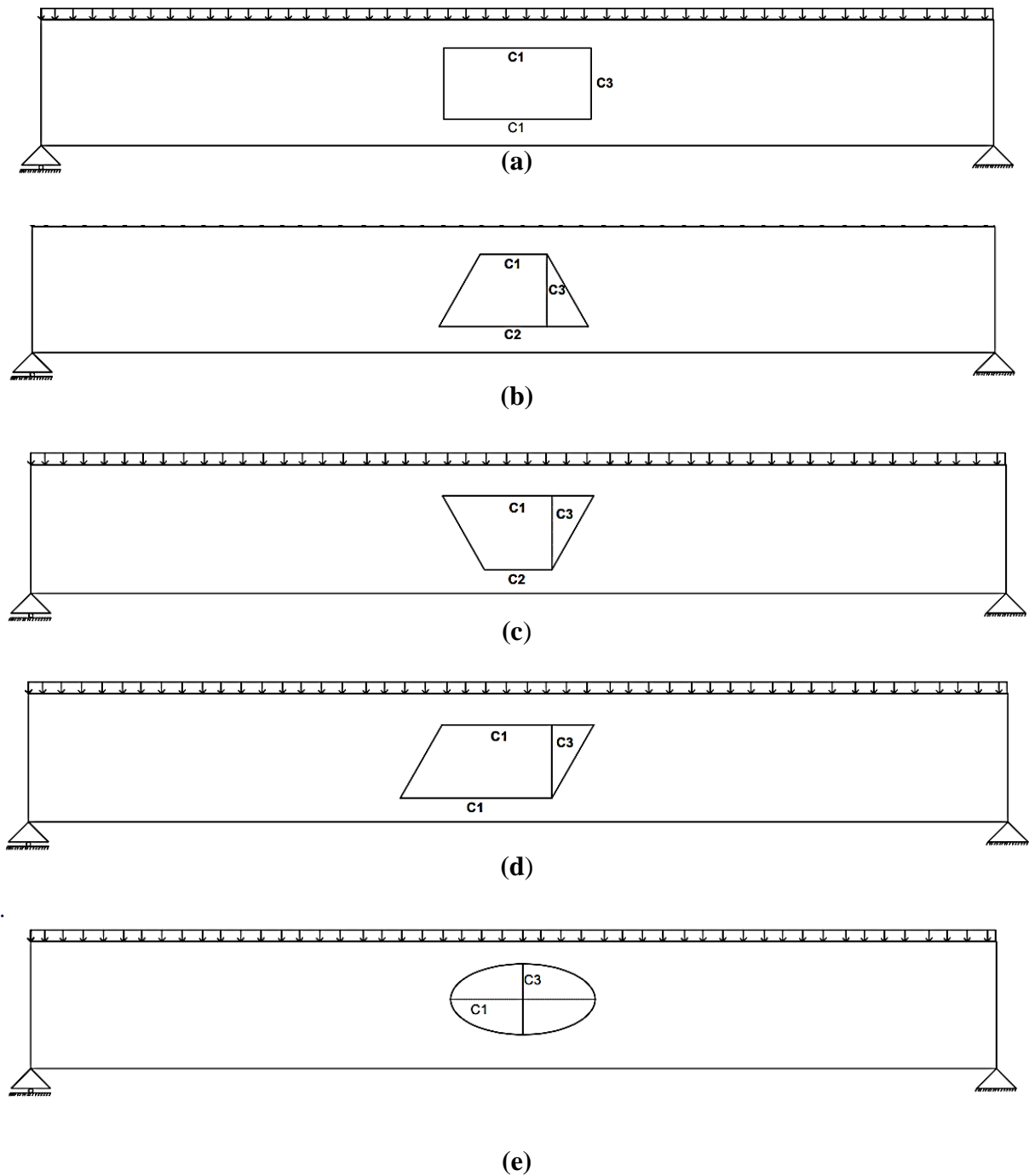


**Figure 4-51 : Web opening shapes used in this investigation and there dimensions.**



	Specimen	Dimensions		
Rectangular	U0-Rec-1	C1= 0.75H	/	C3=0.6H
	U0-Rec-2	C1= H	/	C3=0.6H
	U0-Rec-3	C1= 1.2H	/	C3=0.6H
	U0-Rec-4	C1= 1.5H	/	C3=0.6H
Trapezoidal	U1-Trap-1	C1= 0.6H	C2=H	C3=0.6H
	U1-Trap-2	C1= 0.75H	C2=1.2H	C3=0.6H
	U1-Trap-3	C1= H	C2=1.5H	C3=0.6H
Trapezoidal reversed	U2-Traprv-1	C1= H	C2=0.6H	C3=0.6H
	U2-Traprv-2	C1= 1.2H	C2=0.75H	C3=0.6H
	U2-Traprv-3	C1= 1.5H	C2=H	C3=0.6H
Parallelogram	U3-Parall-1	C1= 0.75H	/	C3=0.6H
	U3-Parall-2	C1= H	/	C3=0.6H
	U3-Parall-3	C1= 1.2H	/	C3=0.6H
elliptical	U4-Elli-1	C1=0.75H	/	C3=0.6H
	U4-Elli-2	C1=1.2H	/	C3=0.6H
	U4-Elli-3	C1=1.5H	/	C3=0.6H

**Table 4-4 : The different openings shapes dimensions in mid span position .**

	Specimen	Dimensions		
Rectangular	U0-SZRec-1	C1= 0.75H	/	C3=0.6H
	U0-SZRec-2	C1= H	/	C3=0.6H
	U0-SZRec-3	C1= 1.2H	/	C3=0.6H
	U0-SZRec-4	C1= 1.5H	/	C3=0.6H
Trapezoidal	U1-SZTrap-1	C1= 0.6H	C2=H	C3=0.6H
	U1-SZTrap-2	C1= 0.75H	C2=1.2H	C3=0.6H
	U1-SZTrap-3	C1= H	C2=1.5H	C3=0.6H
Trapezoidal reversed	U2-SZTraprv-1	C1= H	C2=0.6H	C3=0.6H
	U2-SZTraprv-2	C1= 1.2H	C2=0.75H	C3=0.6H
	U2-SZTraprv-3	C1= 1.5H	C2=H	C3=0.6H
Parallelogram	U3-SZParall-1	C1= 0.75H	/	C3=0.6H
	U3-SZParall-2	C1= H	/	C3=0.6H
	U3-SZParall-3	C1= 1.2H	/	C3=0.6H
elliptical	U4-SZElli-1	C1=0.75H	/	C3=0.6H
	U4-SZElli-2	C1=1.2H	/	C3=0.6H
	U4-SZElli-3	C1=1.5H	/	C3=0.6H

**Table 4-5 : The different openings shapes dimensions in shear zone position .**

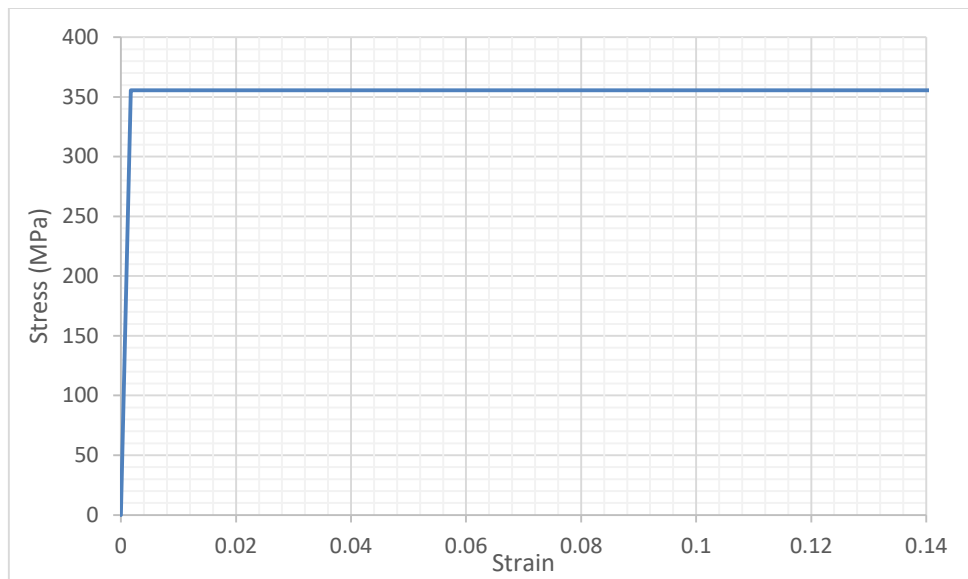


**Figure 4-52 : Steel stress-strain curve employed in the simulation.**

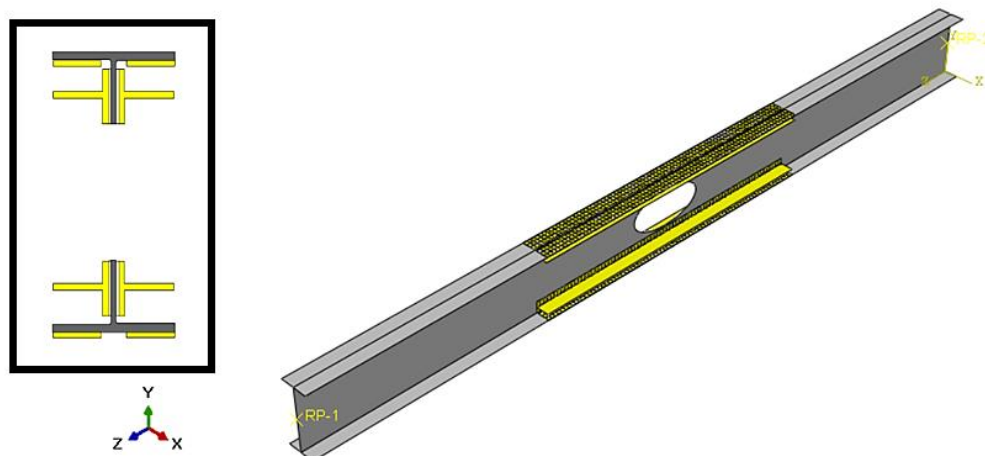


**Figure 4-53 : GFRP strengthening technique.**

#### **IV.3.1.1. Boundary conditions, material modelling and meshing:**

The material simulation was identical to that described in chapter II, with a shell element S4R representing GFRP and steel, while element COH3D8 representing the bonding substance. The load was distributed uniformly across the upper flange as fixed pressure for all tested specimens. Vertical restraints were added at the beam extremities to replicate the supporting boundary conditions using the MPC constraint function in ABAQUS, which covers the full cross section to avoid stress localization. Specimens were therefore horizontally constrained along the length to eliminate lateral torsional buckling (**Figure 4-54**). In these examples, the approved mesh outlined in Chapter II was employed by designating the amount of divisions for length, altitude, and wide of beams while maintaining identical divides/ sizes proportion.

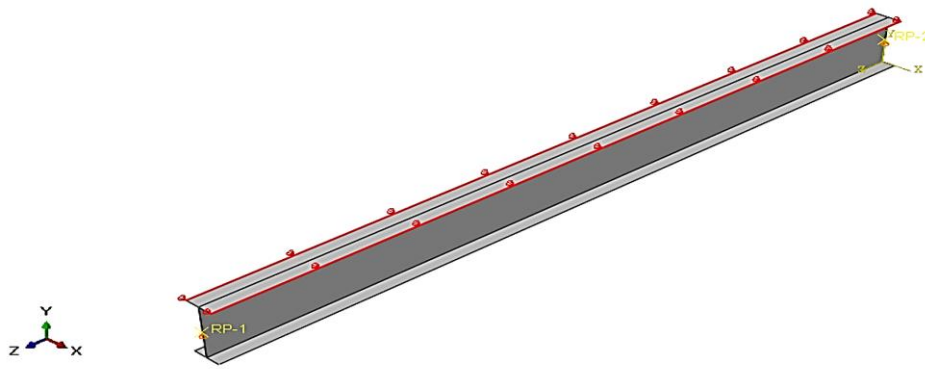


**Figure 4-54 : Boundary conditions.**

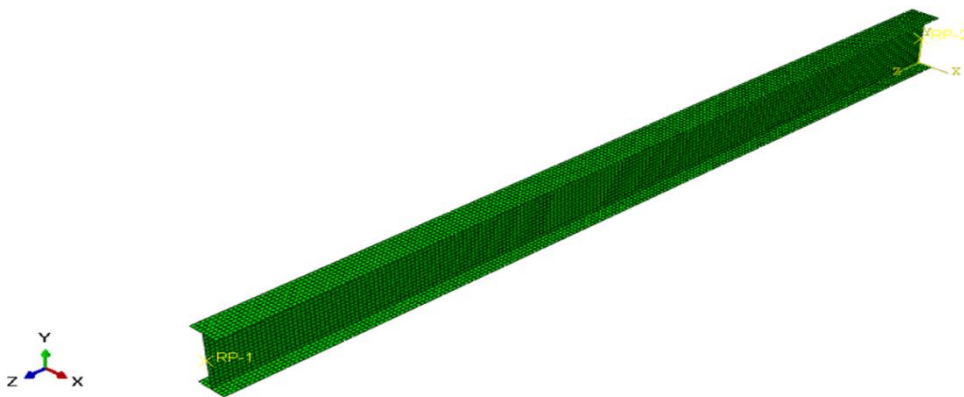


**Figure 4-55 : The chosen mesh distribution.**

### **IV.3.2.Results and discussion :**

#### **IV.3.2.1.Mid span position :**

##### **IV.3.2.1.1.Effect of web opening shape and size on steel beam performance and capacity:**

The numerical simulation was developed for various rectangular web opening dimensions which is the most often utilized web aperture in steel beams. **Figure 4-56** plots the imposed forces against the mid-span displacement curves produced using FE analysis. It is demonstrated that the load bearing capacity of the specimen reduces as the web opening length increases. The strength of specimens decreased by 14% ,15%,17% and 20 % for specimens U0-Rec-1 ,U0-Rec-2, U0-Rec-3 and U0-Rec-4 respectively . This confirms the influence of rectangular web opening size (opening length ) on steel beam structural performance and load carrying capability. The specimen U0-Rec-1, resulting in flexural failure attributable to decreased moment capacity (**Figure 4-57**) .In the other hand , specimens U0-Rec-2 ,U0-Rec-3 and U0-Rec-4 failed by flexural failure accompanied by top T section yielding (**Figure 4-57**).Due to the importance of web opening T section length, the transverse borders of the rectangular aperture are being irregular to generate a trapezoidal opening shape to examine the impact of aperture length on tension and compression tee-sections.

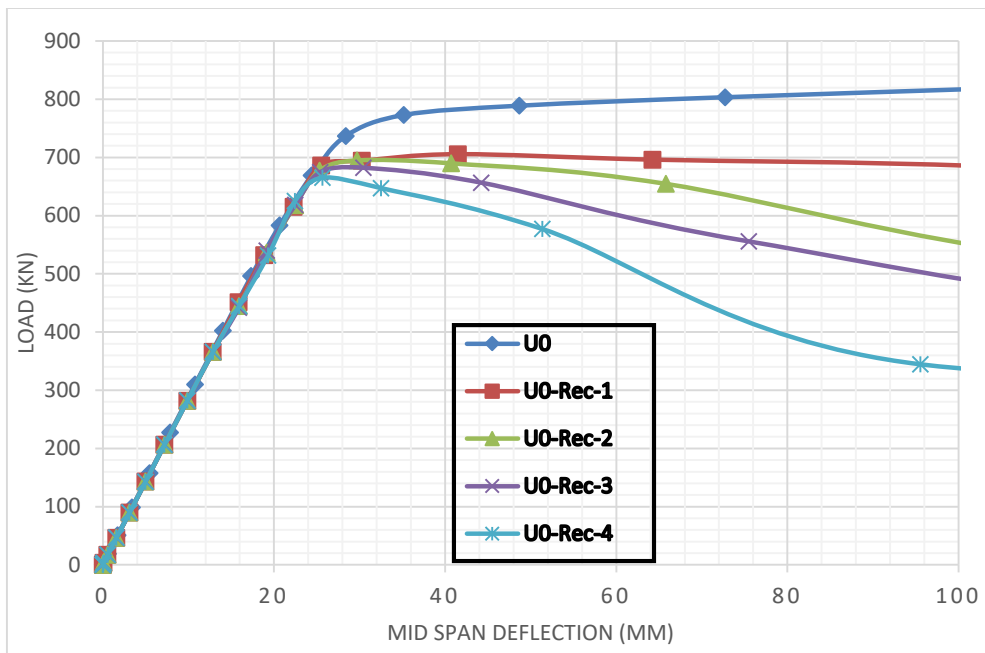


**Figure 4-56 : Load deflection curves of unstrengthened specimens with mid span rectangular web openings .**

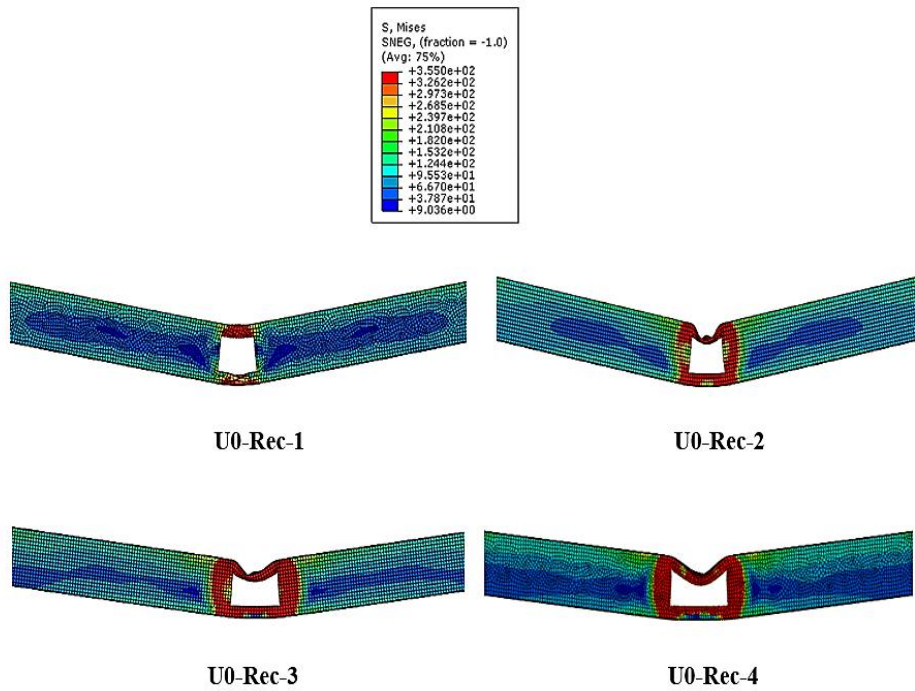


**Figure 4-57 : Failure mode of unstrengthened specimens with mid span rectangular web openings.**

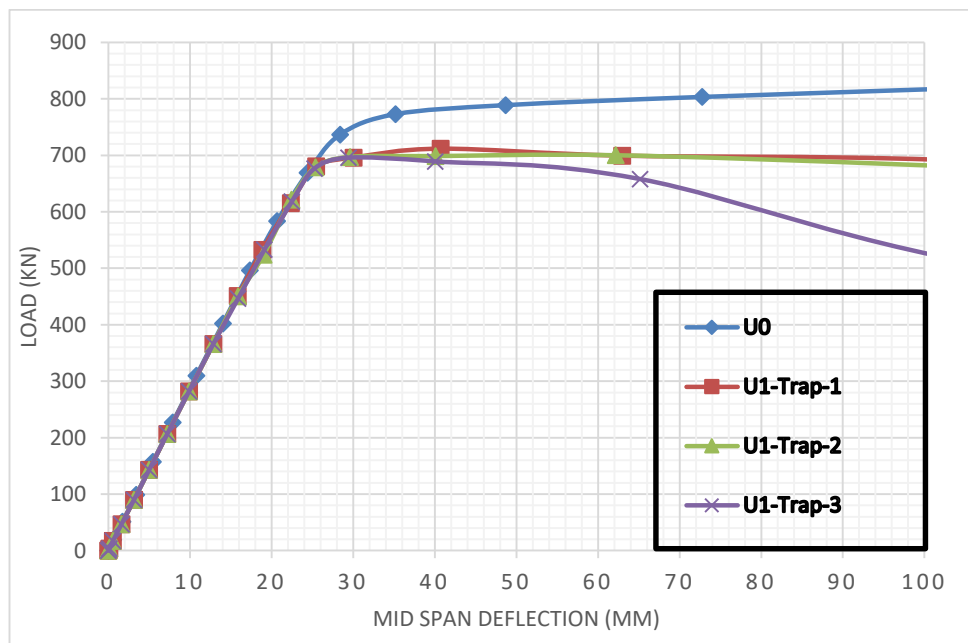


**Figure 4-58 : Load deflection curves of unstrengthened specimens with mid span trapezoidal web openings .**

**Figure 4-58** compares the load-deflection curves for specimens with trapezoidal holes and uneven size of compression and tension tee-sections. It can be shown that the load capacity of the structural member grows as the width of the compressive tee-section reduces, however the size of the trapezoidal web aperture in mid span position did not produce a large decrease in load carrying capabilities of the steel beam. Specimens U1-Trap-1 and U1-Trap-2 decreased by were closely 14% while for the strength decrease of specimen U1-Trap-3 was 15% . In comparison to rectangular openings, the effect of trapezoidal opening in strength decrease is smaller than the rectangular opening and the length of the compression tee-section has a larger impact in mid span placement. Specimens U1-trap-1 and U1-Trap-2 failed by flexural failure mode while specimen U1-Trap-3 failed by flexural failure accompanied by top flange yielding this signifies that the compression T section yields when it's length is equals to the height of the beam H.

Conversely, the load bearing capability of the specimen with a shorter tensile tee-section employing a reversed trapezoidal hole is plotted in **Figure 4-60** . The strength fell substantially as the compressive T section increased. The strength decreases for specimens U2-Traprv-1, U2-Traprv-2, and U2-Traprv-3 were 15%, 17%, and 20%, correspondingly. This was almost the same as the force drop with rectangular aperture, confirming the importance of compressive T section in the mid span position .Specimens failed by flexural failure accompanied by top flange T section yielding (**Figure 4-61**) .

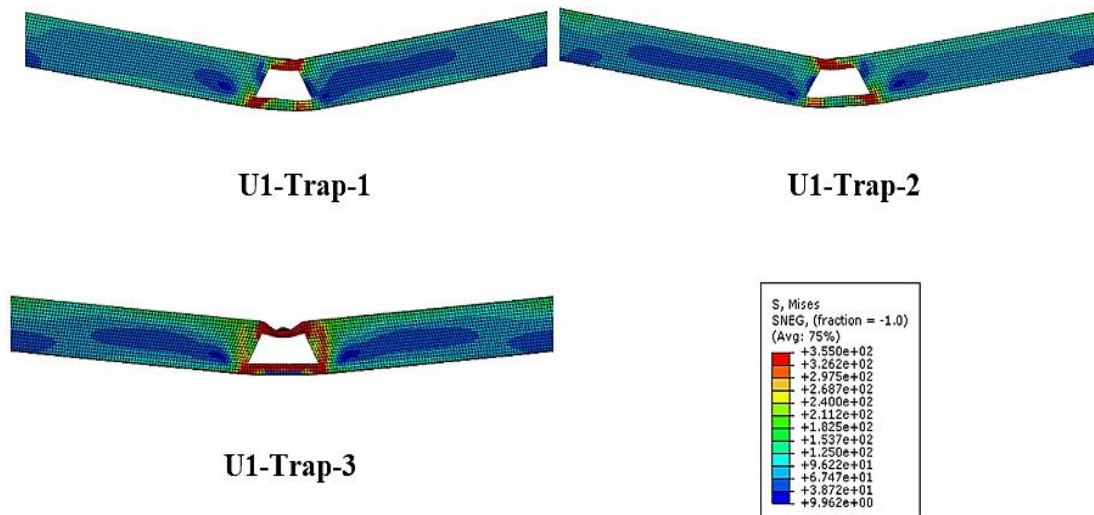


**Figure 4-59 : Failure mode of unstrengthened specimens with mid span Trapezoidal web openings.**

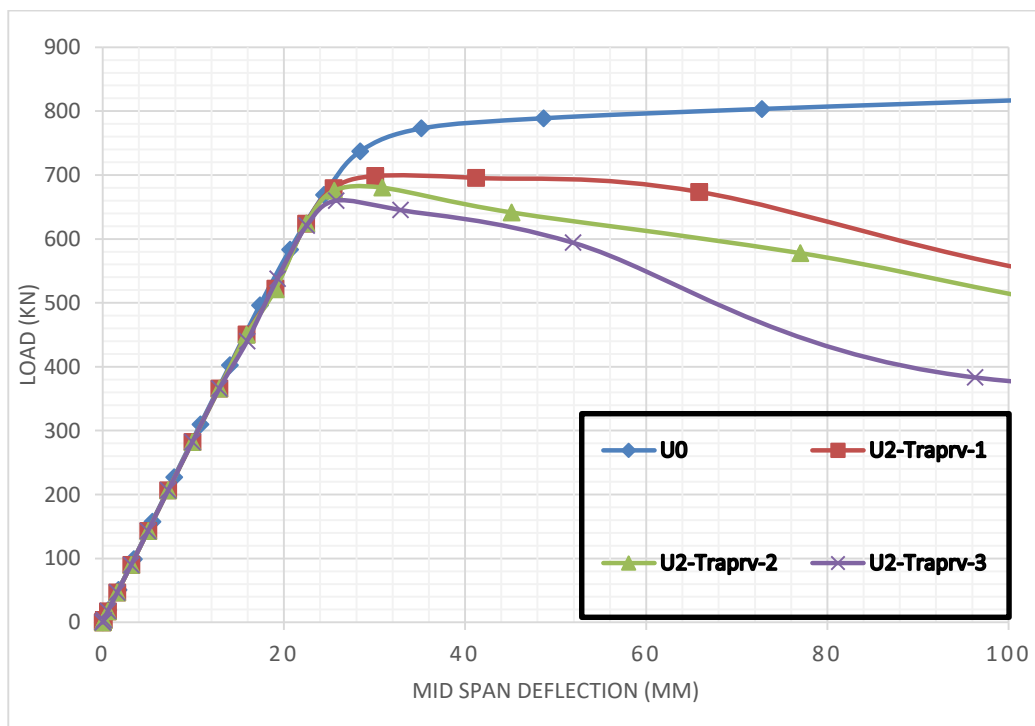


**Figure 4-60 : Load deflection curves of unstrengthened specimens with mid span reversed trapezoidal web openings .**

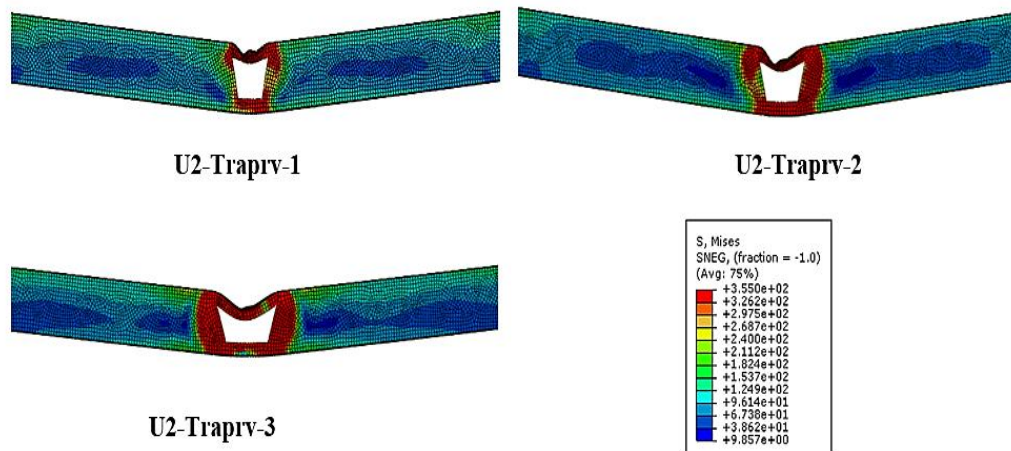


**Figure 4-61 : Failure mode of unstrengthened specimens with mid span reversed Trapezoidal web openings.**

Specimens having parallelogram web openings have the same structure as rectangular web holes, but their perpendicular edges are inclined. The introduction of parallelogram openings of various sizes in the mid span situation resulted in different decreases in specimen strength capacity. A decrease of 14% ,16% and 17% was noticed for specimens U3-Parall-1 , U3-Parall-2 and U3-Parall-3 . As can be observed, the load bearing capacity of parallelogram aperture specimens are roughly equal to those of rectangular aperture specimens for the identical opening dimensions (**Figure 4-62**) . This supports the notion that the opening length is the most essential component in assessing the structural response of perforated parts since it governs the amplitude of local solicitations operating on tee sections and the necessity to strengthen the T section above and below the opening. **Figure 4-63** also depicts the frequent failure scenario for beams with parallelogram holes.

Between the web aperture forms for beams investigated in this work, the elliptical web opening geometry which provides the smallest drop in load bearing capability . For all web opening diameters, the percentage of strength loss was roughly 14% (**Figure 4-64**).

In addition to that , Because of the stresses concentration at the corner of the rectangular hole, the load bearing capability of specimens is drastically reduced.

#### IV.3.2.1.2. Force mid-span deflection reaction :

As seen in the **Table 4-4**, the first character in each specimen characterization is the designation of the tested beam, followed by the web opening form, the number of the opening size according to **Table 4-4**, and finally the GFRP laminate thicknesses, for example "U0-Rec-1-3" is the specimen with rectangular opening with measurements of ( $C1=0.75H, C2=0.6H$ ) reinforced with GFRP laminate of 3 mm thickness.



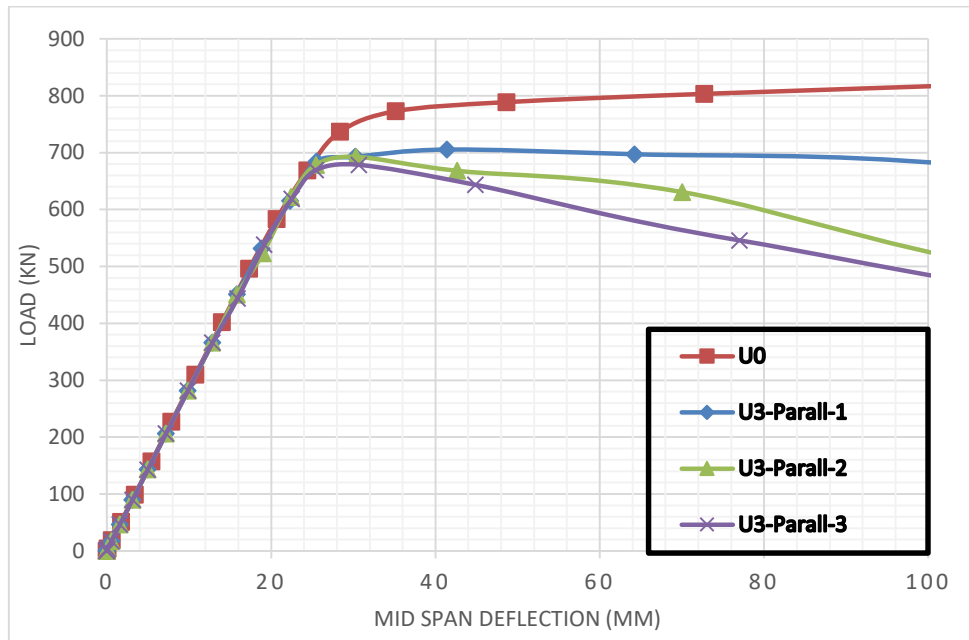
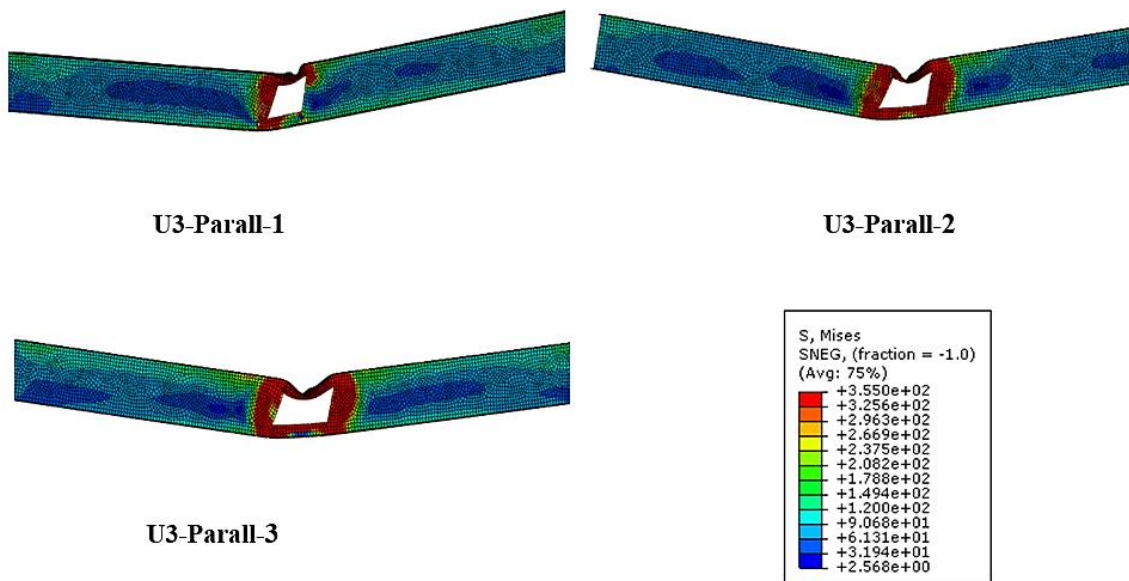
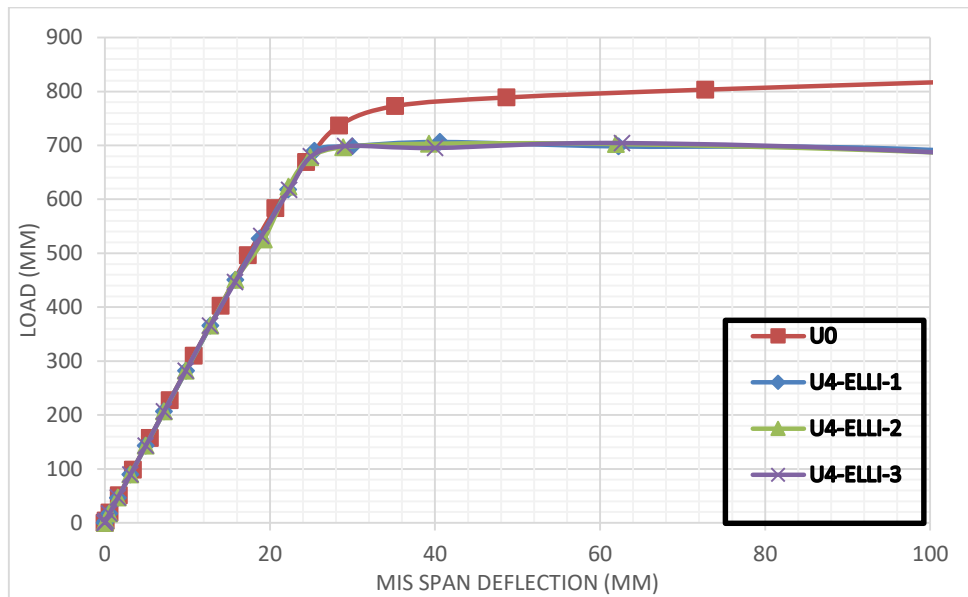


Figure 4-62 : Load deflection curves of unstrengthened specimens with mid span parallelogram web openings .





**Figure 4-63 : Failure mode of unstrengthened specimens with mid span Parallelogram web openings.**



**Figure 4-64 : Load deflection curves of unstrengthened specimens with mid span ellipsoidal web openings .**

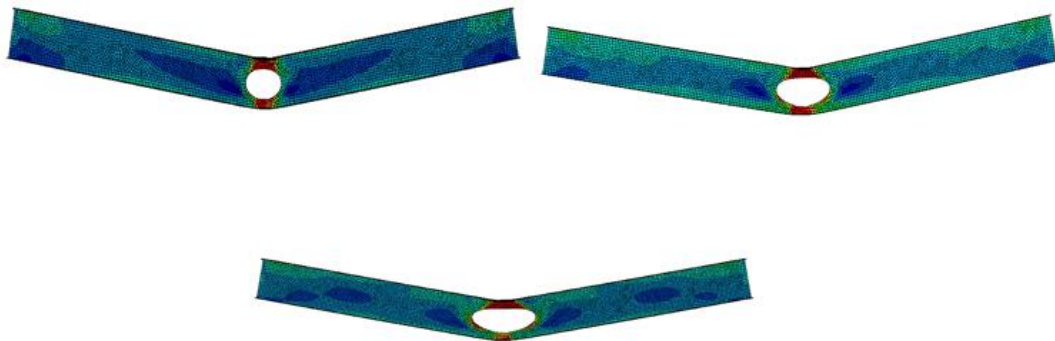


**Figure 4-65 : Failure mode of unstrengthened specimens with mid span ellipsoidal web openings.**

**Figures 4-66 to 4-69** illustrates the total load applied against mid-span deflection correlation for the specimens with mid span rectangular holes in the above said instances. To begin, the strength declined dramatically following the installation of a web opening at mid-span according to the opening size, as represented in **Figure 7-56** , whereas their capacity was largely restored following the proposed GFRP strengthening, with a different percentage of increase depending on the GFRP laminates thicknesses . The percentage of strength increase is shown in the **Table 4-6** below:

<b>GFRP thickness</b>	<b>U0-Rec-1</b>	<b>U0-Rec-2</b>	<b>U0-Rec-3</b>	<b>U0-Rec-4</b>
3 mm	17%	12%	9%	7%
6 mm	18%	26%	21%	16%
10 mm	19%	26%	30%	28%

**Table 4-6 : Strength enhancement percentage for specimens with rectangular opening .**

Using the proposed GFRP strengthening configuration, the GFRP laminates of 3mm thickness was effective for specimens U0-Rec-1 and U0-Rec-2 to recover the strength of the solid beam U0 despite the yielding load was not restored (**Figures 4-66 and 4-67**) . To persuade specimens U0-Rec-3 and specimen U0-Rec-4 to replenish their initial capacity the GFRP thickness was increased to 6 mm thickness .Although the ultimate load and the yielding load were increased for specimens U0-Rec-3 and the strength was achieved ,specimen U0-Rec-4 was not able to recover the strength of solid beam (**Figures 4-68 and 4-69**) .In the other hand the strength of specimens U0-Rec-1 and U0-Rec-2 enhanced slightly over the solid beam capacity despite the yielding load was not restored .The use of 10 mm GFRP laminates thicknesses helped the specimen to recover the yielding load and enhance the peak load over the solid beam .

Regarding to the trapezoidal opening in the mid span ,different strength enhancement was recorded according to the opening dimensions and the GFRP laminate thicknesses :

<b>GFRP thickness</b>	<b>U1-Trap-1</b>	<b>U1-Trap-2</b>	<b>U1-Trap-3</b>
3 mm	16%	18%	17%
6 mm	21%	22%	30%
10 mm	21%	26%	38%

**Table 4-7 : Strength enhancement percentage for specimens with trapezoidal opening .**

GFRP laminate thickness of 3 mm was effective to regain the original strength of instances U1-Trap-1 and U1-Trap-2, which displayed a near strength enhancement even though that the yielding load of the solid beam was not recovered (**Figures 4-70 and 4-71**). Furthermore to the 3mm GFRP thickness evaluated, the laminate thicknesses were raised to 6 mm. This thickness adjustment aided the evaluated specimens in regaining the beam performance and exhibiting a strength improvement over the basic beam and the yielding load was also restored (**Figures 4-70 and 4-71**) . The thickness was also then raised to 10 mm , **Table 4-7** shows that there were large gains in the force of examined cases, with lesser increases occurring with specimen U1-Trap-1.

It can also be observed that, like with the prior rectangular opening, increasing the GFRP laminate thickness to 10 mm was only beneficial for specimens with large web openings. The strength enhancement obtained with reinforced specimens having reversed trapezoidal web opening in the mid span are detailed in **Table 4-8** :

GFRP thickness	U2-Traprv-1	U2-Traprv-2	U2-Traprv-3
3 mm	13%	9%	7%
6 mm	21%	23%	18%
10 mm	23%	30%	36%

**Table 4-8 : Strength enhancement percentage for specimens with reversed trapezoidal opening .**

Compared to the trapezoidal opening the reversed trapezoidal web opening significantly decreased the capacity of solid beam which confirm the importance of compressive T section which must be strengthened . The installation of GFRP laminates of 3mm increased the beam's U2-Traprv-1 strength by 13% and demonstrated comparable performance to the solid beam U0, however specimens U2-Traprv-2 and U2-Traprv-3 failed to achieve the requisite strength gain (**Figures 4-73 to 4-75**) . As a consequence, increasing the thickness of the GFRP laminates to 6 mm assisted instances in restoring the original beam power, even though that the yielding load was not regained for specimens U2-Traprv-3-6 (**Figure 4-75**). Furthermore, the thickness of the GFRP laminates was elevated to 10 mm in order to obtain a strength improvement percentage ranging between 23% and 36% (**Table 4-8**), and the three tested prototypes were able to restore the initial strength and outperform the solid beam in terms of strength performance.

Despite the fact that the hole length of beams having parallelogram web openings is comparable to that of beams with rectangular web openings, it was chosen to investigate the sloped vertical sides of the aperture and the ideal GFRP laminate thicknesses required with this web opening architecture. As earlier established utilizing 6mm thick GFRP laminates, the strengthening process could only regain the original state using U3-Parall-1 with less stiffer response (**Figures 4-76 to 4-78**) . This prompted further investigation of the suggested approach utilizing 6 mm GFRP laminate thicknesses, which assisted the specimen U3-parall-2 in regaining its full beam capacity (**Figure 4-77**). On the other hand, extending the GFRP thickness to 10 mm was unavoidable in order to assist U3-Parall-3 to regain its structural capability (**Figure 4-78**)

GFRP thickness	U3-Parall-1	U3-Parall-2	U3-Parall-3
3 mm	13%	12%	9%
6 mm	18%	23%	11%
10 mm	19%	26%	21%

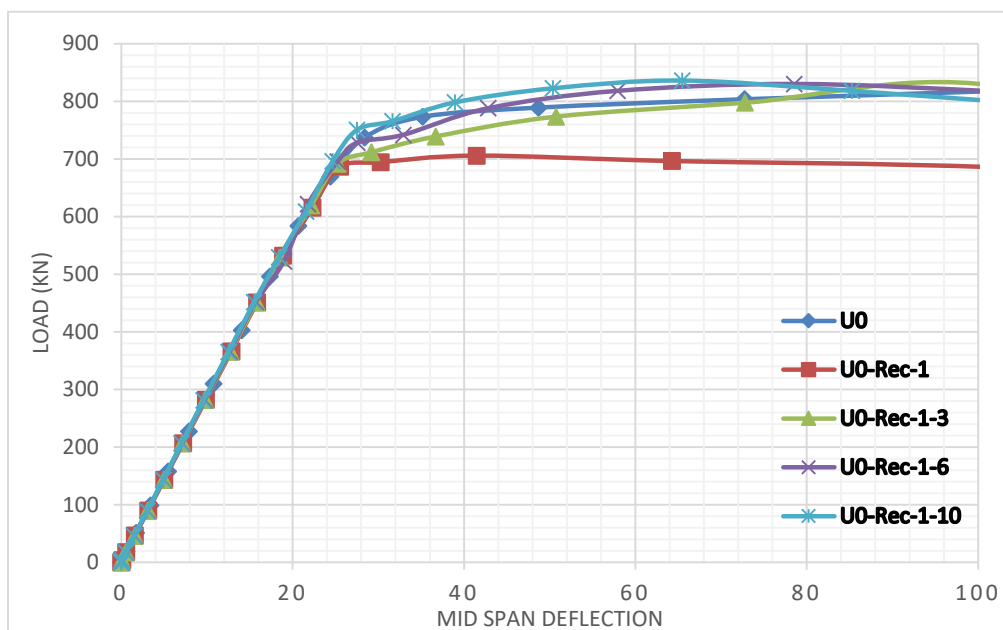
**Table 4-9 : Strength enhancement percentage for specimens with parallelogram opening.**

Considering that, it was discovered that perforated sections with elliptical web apertures of the selected dimensions did not result in a significant loss in load bearing capabilities. In this part, the influence of proportionate GFRP thickness on web opening size was also examined. The 3 mm GFRP laminates were able to rebuild the strength of the solid beam for the three examples

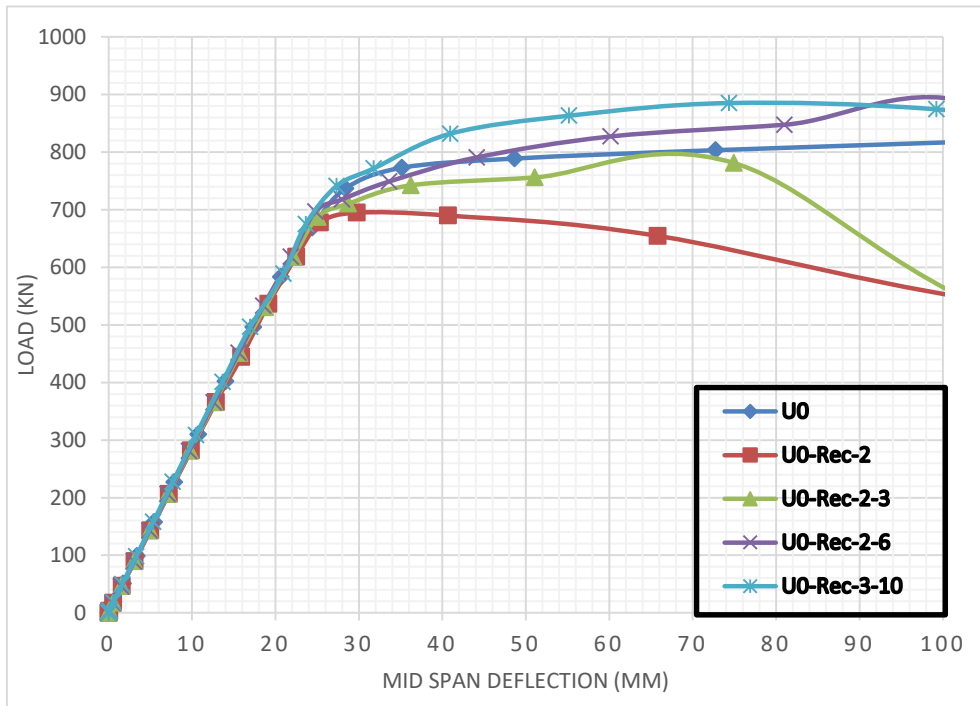
illustrated in **Figures 4-70 ,4-71 and 4-72**. Furthermore, increasing the GFRP thickness to 6mm and 10mm enhanced the beam's strength over the initial beam B0, demonstrating that the most proportionate GFRP thickness to the elliptical web aperture is 3mm.

GFRP thickness	U4-ELLI-1	U4-ELLI-2	U4-ELLI-3
3 mm	18%	19%	17%
6 mm	19%	26%	27%
10 mm	19%	26%	33%

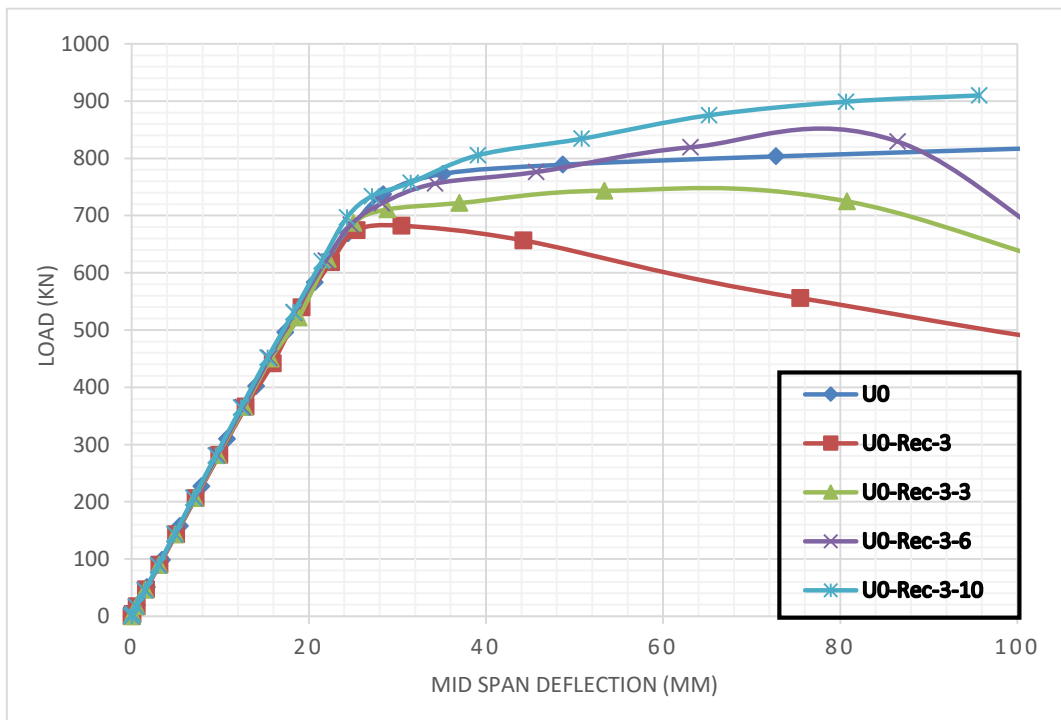
**Table 4-10 : Strength enhancement percentage for specimens with ellipsoidal opening.**



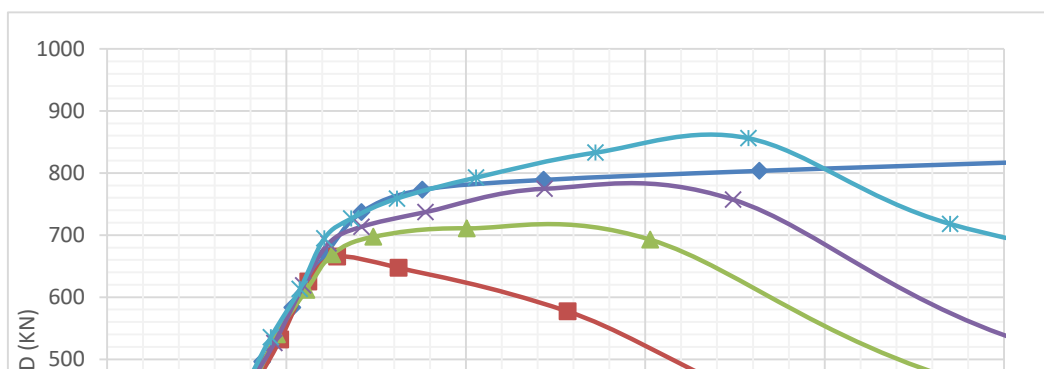
**Figure 4-66 : Load-mid span deflection curves for strengthened specimen U0-Rec-1.**



**Figure 4-67 : Load-mid span deflection curves for strengthened specimen U0-Rec-2.**



**Figure 4-68 : Load-mid span deflection curves for strengthened specimen U0-Rec-3.**



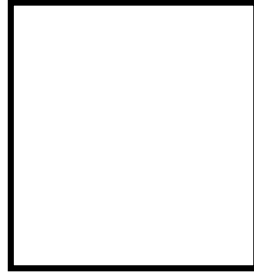


Figure 4-69 : Load-mid span deflection curves for strengthened specimen U0-Rec-4.

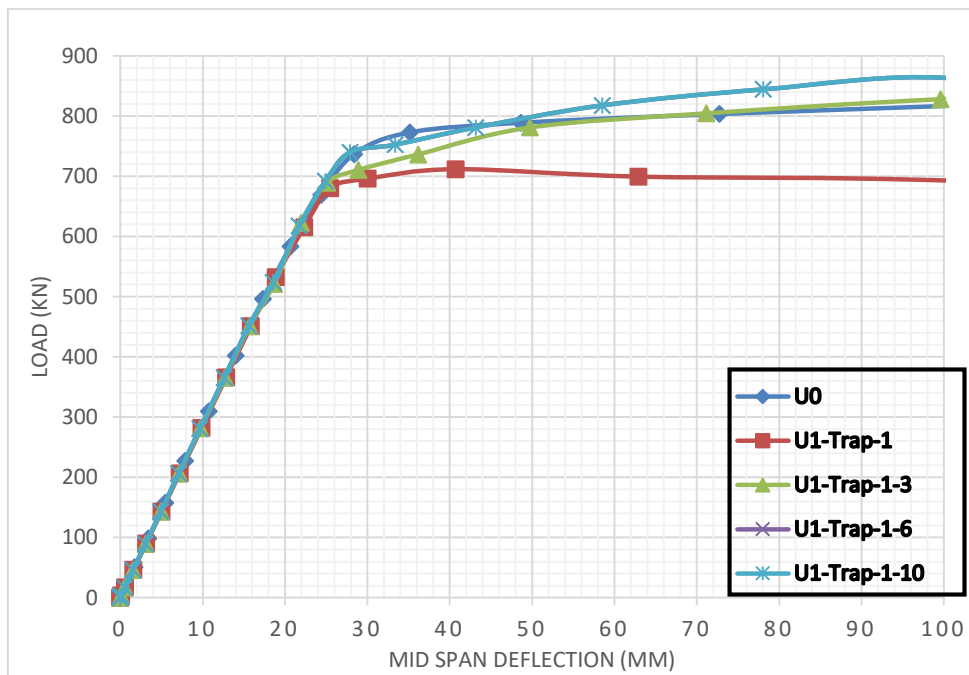
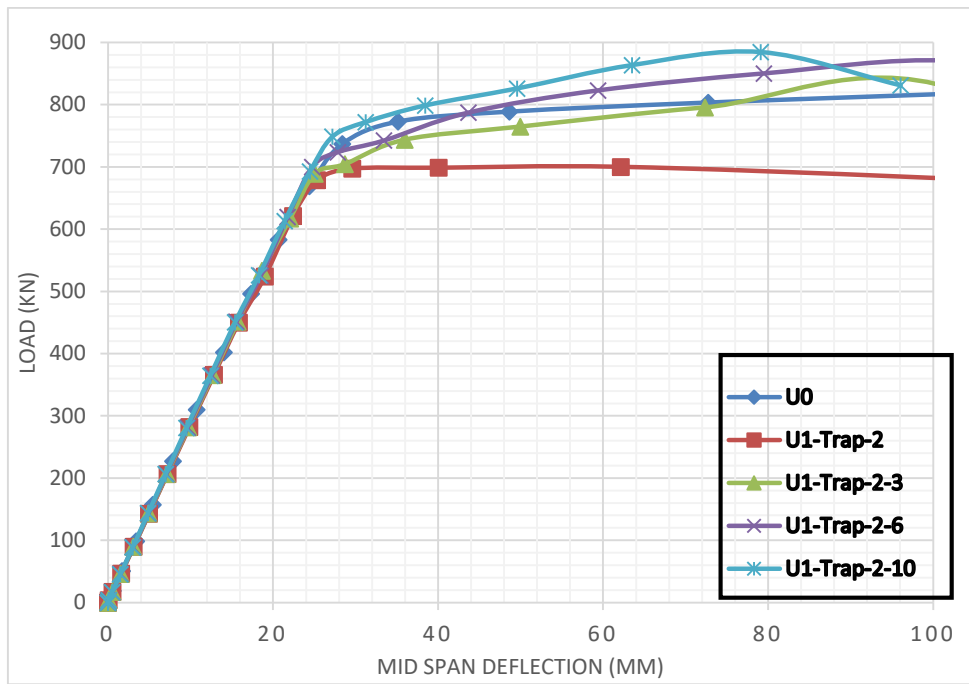
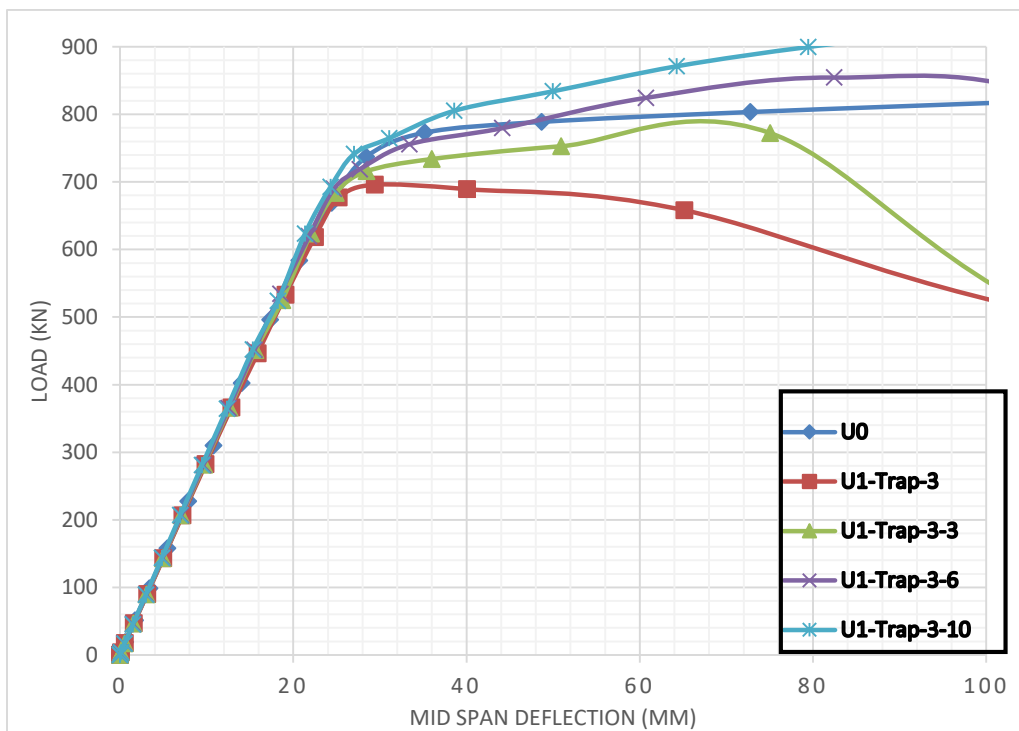


Figure 4-70 : Load-mid span deflection curves for strengthened specimen U1-Trap-1.



**Figure 4-71 : Load-mid span deflection curves for strengthened specimen U1-Trap-2.**



**Figure 4-72 : Load-mid span deflection curves for strengthened specimen U1-Trap-3.**

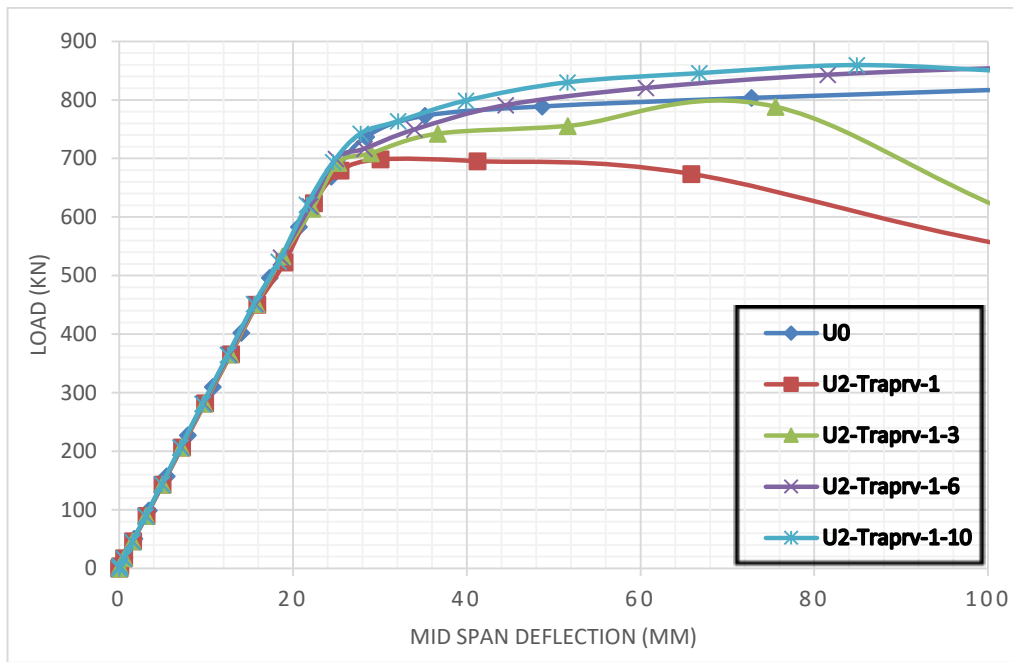


**Figure 4-73 : Load-mid span deflection curves for strengthened specimen U2-Traprv-1.**

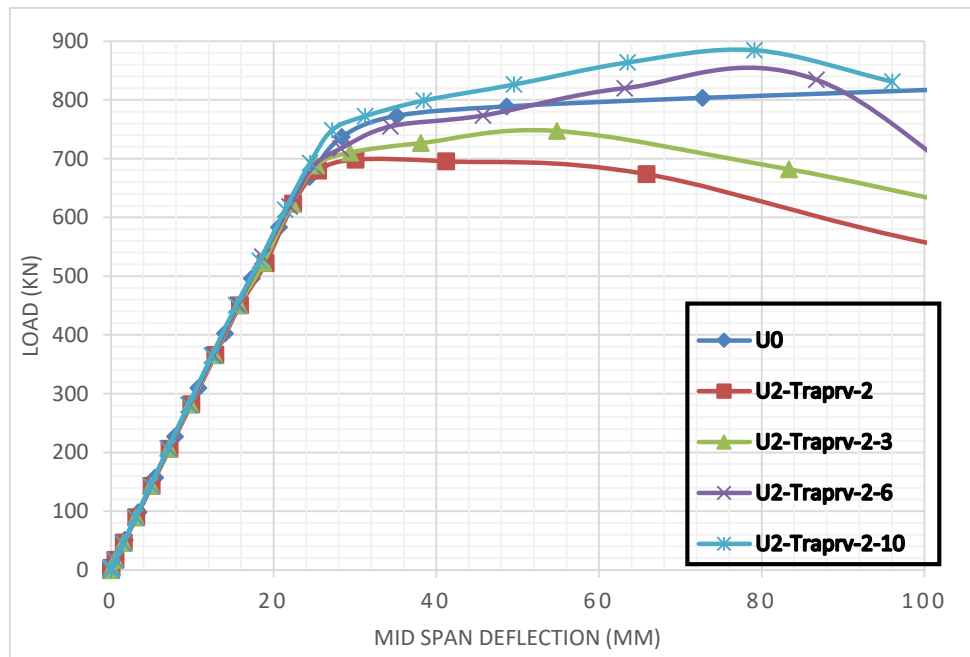


**Figure 4-74 : Load-mid span deflection curves for strengthened specimen U2-Traprv-2.**



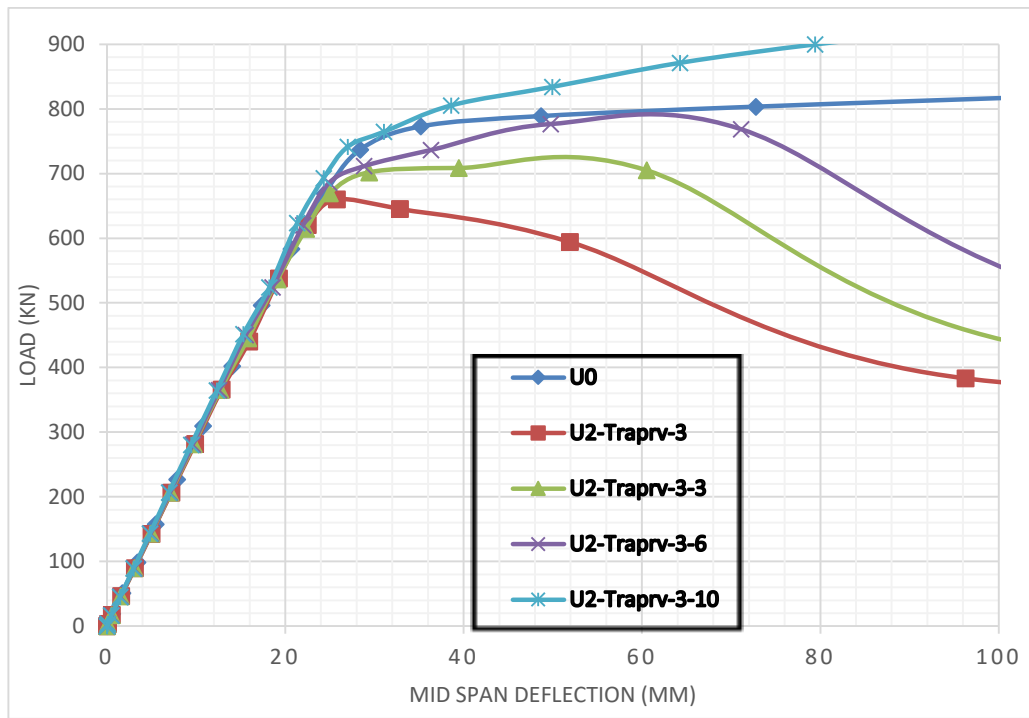


Figure 4-75 : Load-mid span deflection curves for strengthened specimen U2-Traprv-3.

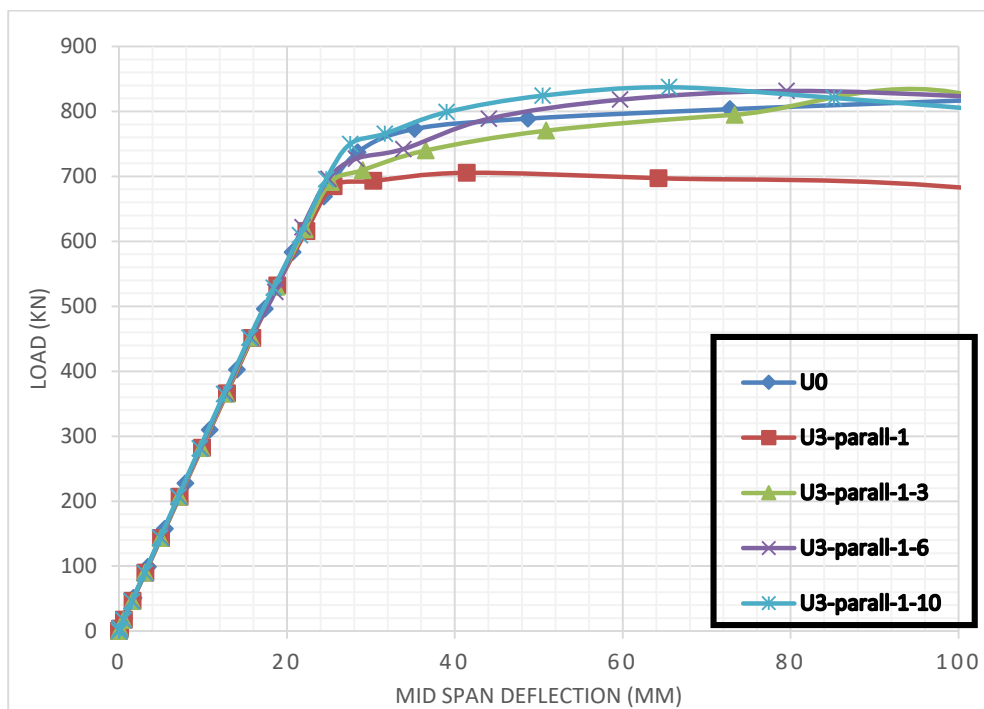
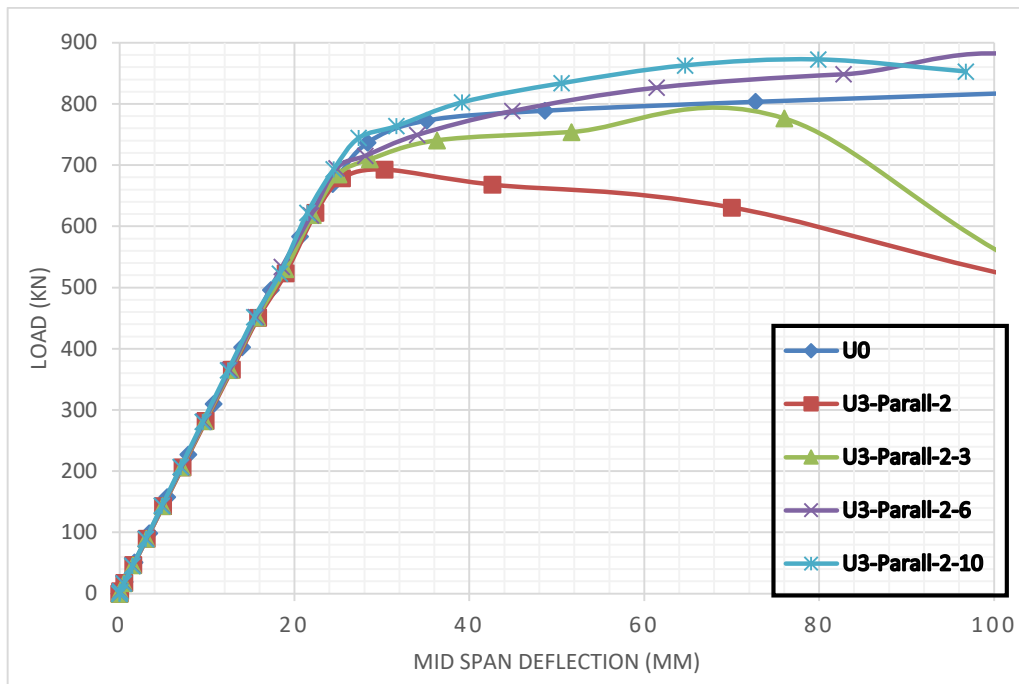
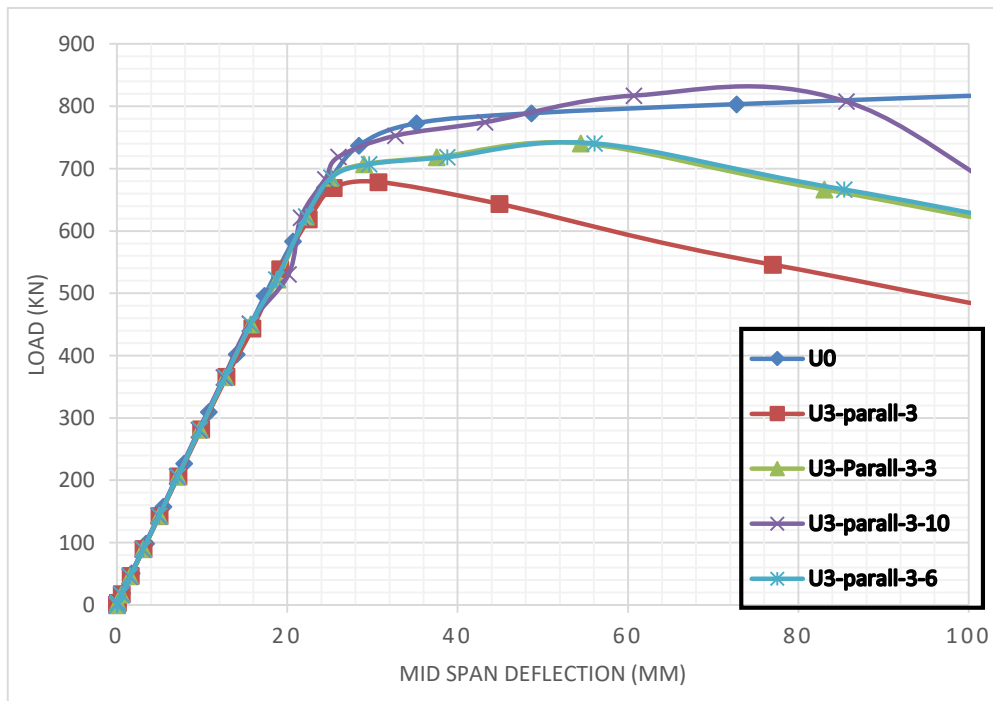


Figure 4-76 : Load-mid span deflection curves for strengthened specimen U3-Parall-1.



**Figure 4-77 : Load-mid span deflection curves for strengthened specimen U3-Parall-2.**



**Figure 7-78 : Load-mid span deflection curves for strengthened specimen U3-Parall-3.**

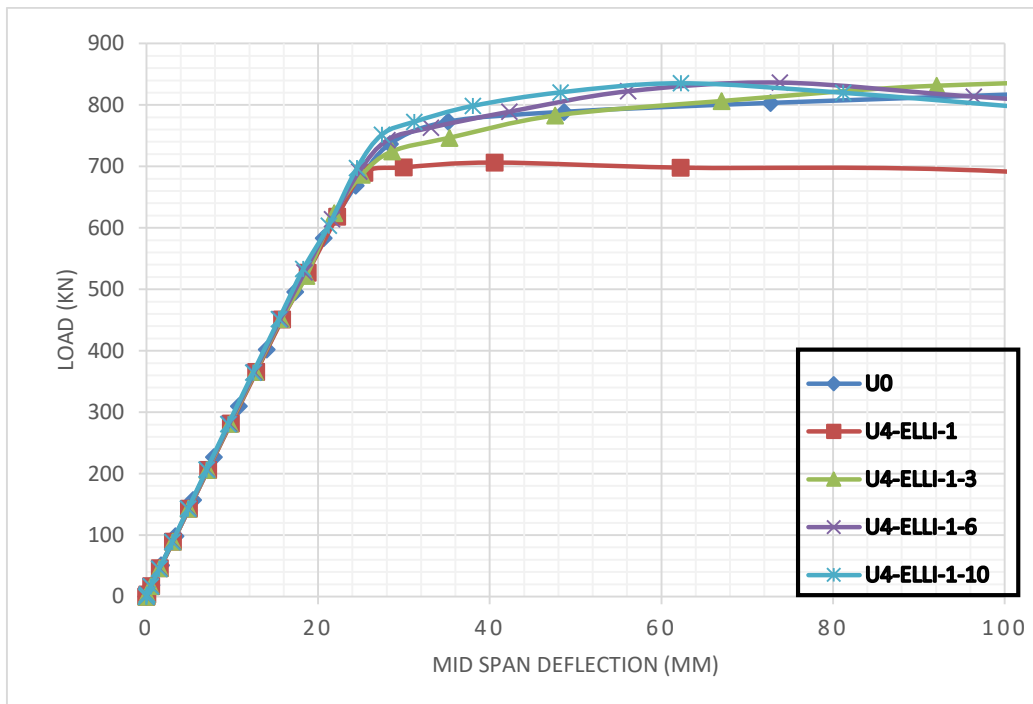


Figure 7-79 : Load-mid span deflection curves for strengthened specimen U4-Elli-1.

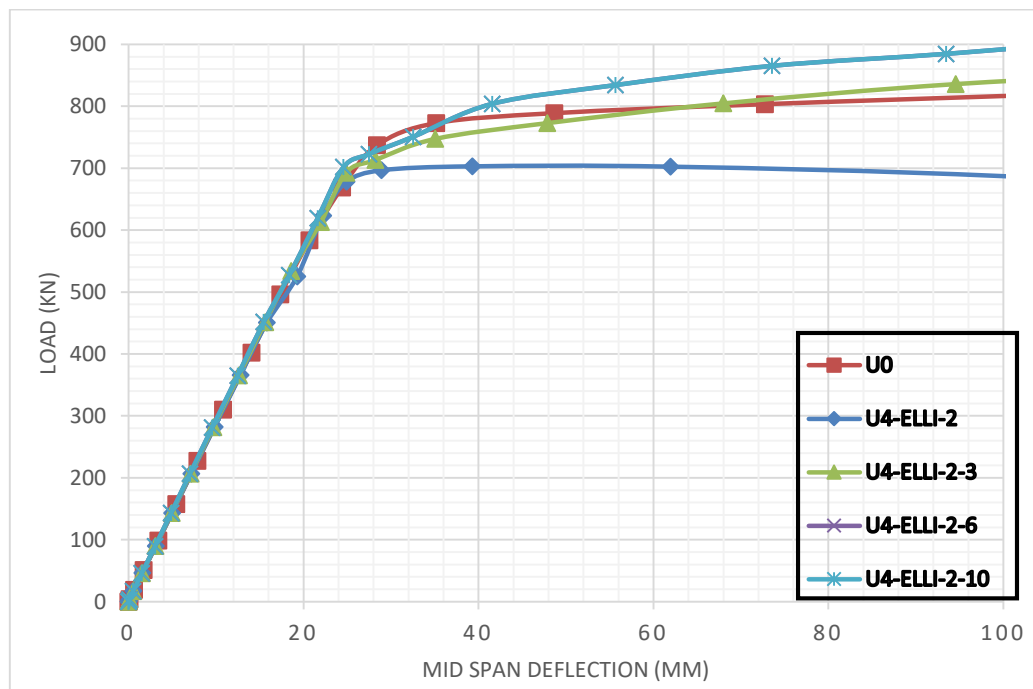
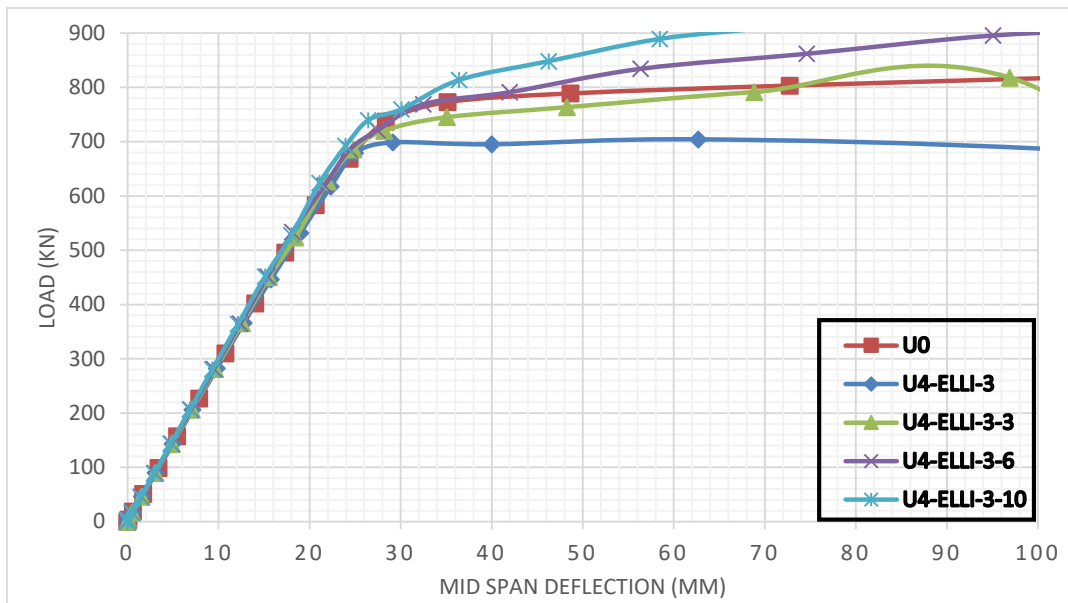


Figure 4-80 : Load-mid span deflection curves for strengthened specimen U4-Elli-2.



**Figure 7-81 : Load-mid span deflection curves for strengthened specimen U4-Elli-3.**

**IV.3.2.1.3. Adhesive degradation and failure mechanism:**

Initially, in terms of failure modes, since all of the beams were completely laterally restrained, none lateral torsional buckling was recorded as a type of failure. All of the unreinforced beams broke due to a standard flexural mechanism involving a plastic hinge develops at mid-span following upper flange yielding (Figures 4-59, 4-61, 4-63 and 4-65).

It can be noted that in terms of specimens with central rectangular web aperture, the most prevalent failure mode of this opening position sort is the buckling of T-section over the web hole accompanied by flexural failure. In contrast to reinforced beams, it can clearly be seen the plastic hinge creation at the extremities of the reinforcing process in specimens U0-Rec-1-6 and U0-Rec-1-10 (Figure 4-82). This demonstrates the ability of GFRP thicknesses of 6mm and 10 mm to modify the stress distribution of the beam and transfer stress concentrations away from the upper flange T section. Furthermore, for the remaining larger rectangular web openings, only specimens U0-Rec-2-10 and U0-Rec-3-10 failed by top flange buckling at the reinforcement laminates ends (Figure 4-82). This demonstrates that the additional thickness (10mm) is feasible with larger rectangular web openings, Most other specimens failed by top T section buckling, including those that were able to reinstate the initial force. It should also be highlighted that the rigidity of GFRP laminates with thickness augmentation resulted in a marked reduction in beam ductility.

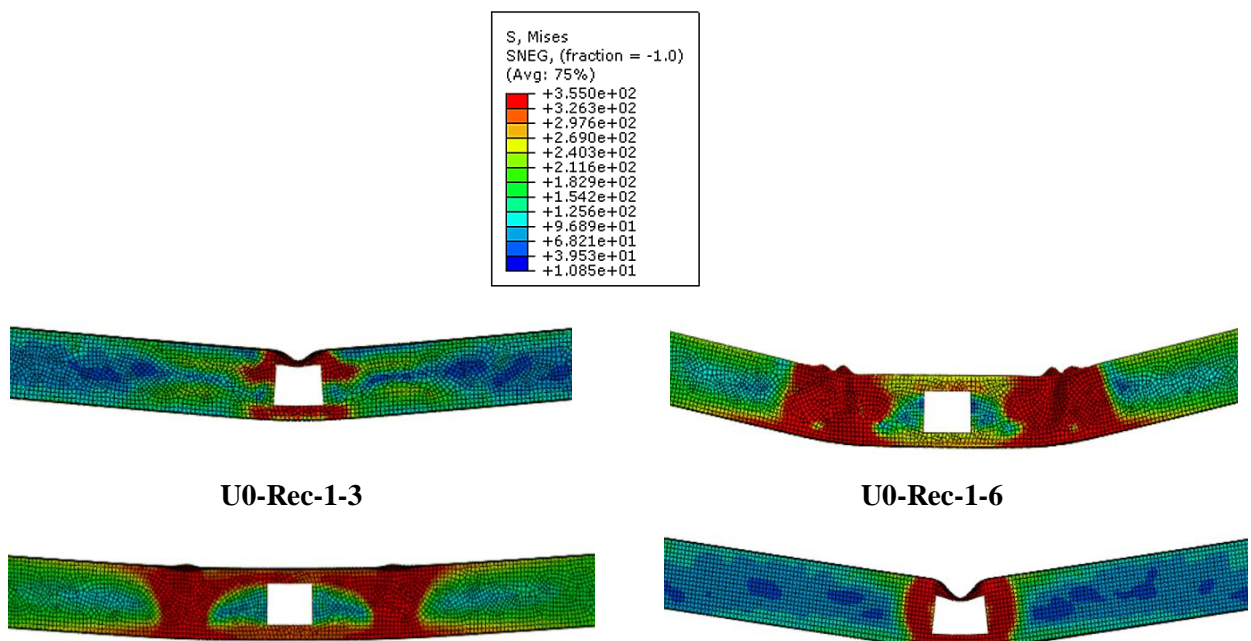
Unstrengthened specimens with trapezoidal apertures and variable tee-section lengths failed in diverse ways. Flexural failure was observed in specimens U1-Trap-1 and U1-Trap-2, whereas top T section buckling was detected with specimen U1-Trap-3 (Figure 4-83). This confirms that the compressive tee-section has a greater influence on the structural performance of the holed portions compared to other design variables of the web openings. Reinforced specimen U1-Trap-1 with the three proposed GFRP thicknesses failed by top flange buckling of at the extremities of the composite laminates and maximum stresses are transferred to the extremities

of the beam's half third length, when the whole depth of the structural element is moved, finally producing a plastic hinge (**Figure 4-83**). Specimen U1-Trap-2-3, on the other hand, failed due to top flange buckling above the hole, whereas specimens U1-Trap-2-6 and U1-Trap-2-10 failed due to flexural failure accompanied with a modest top flange buckling in the ends of GFRP composites. In addition, **Figure 4-83** depicts also the different damage scenario for U1-Trap-3-3 and U1-Trap-3-6, the 3 mm and 6 mm GFRP composites were unable to modify the failure mechanism of the large trapezoidal aperture, necessitating an increase in GFRP thickness to 10 mm in order to obtain flexural mechanism for specimen U1-Trap-3-10. This amount of local relieving stress corresponds to the degree of stiffness augmentation at the T-section caused by the addition of the GFRP thickness.

Similarly to the rectangular opening in the mid span, The trapezoidal aperture with a shorter tension tee-section and longer compressive tee-section, labelled as reversed trapeze failed by top T section buckling above the aperture coupled by flexural failure for the three tested specimens U2-Traprv-1, U2-Traprv-2, and U2-Traprv-3 (**Figure 4-61**). The GFRP strengthening approach was shown to be efficient for the first specimen U2-Traprv-1 utilizing 6 mm and 10 mm thicknesses, as shown in **Figure 4-84**. The failure mechanism was altered to flexural failure for specimens U2-Traprv-1-6 and U2-Traprv-10. Moreover, only the GFRP approach with laminates of 10 mm thickness was able to shift the stress distribution of the beam and switch the failure mechanism to flexural failure in the case of U2-Traprv-2-10 (**Figure 4-84**). However, despite the fact that the original load was obtained for specimen U2-Traprv-3 using 10 mm thickness GFRP, the reinforcement technique was unable to transform the failure mode of all specimens, which failed by top flange buckling over the hole as in the case of rectangular opening, confirming that compressive tee-section has a significantly larger impact on the structural reliability of the perforated sections. As mentioned before In the un-strengthened situation, buckling of the T-section leads to specimen weakness at load values that are often lower than those of the beam without holes. The unreinforced specimens with parallelogram opening failed also by top T section buckling as shown in **Figure 4-63**. Increasing the GFRP thickness to 6 mm and 10 mm for specimen U3-Parall-1-3 was enough to completely deploy the section and achieve full stress transmission, as repeatedly stated. Furthermore, only 10 mm GFRP thickness was adequate to avoid stress concentration in the T section above aperture in specimen U3-Parall-2 (**Figure 4-85**). It was also discovered that the suggested GFRP reinforcement strategy and the three GFRP thicknesses did not avoid T-section yielding accompanied by buckling upper of the aperture in specimen U3-Parall-3. Regardless of the fact that it has already been discovered that portions with elliptical web openings are the less influenced with the three different sizes, at aspects of failure mechanisms and deform path, perforated portions with transverse elliptical web apertures in mid span position perform similarly to regular web hole layouts, as shown in **Figures 4-65**. This is why it was discovered that the GFRP reinforced approach was capable of redistributing stress concentration in all instances except U4-Elli-3-10, which collapsed by top T section buckling. (**Figure 4-86**).

As previously stated in chapter II, the stress degradation variable was employed to assess the adhesive's degradation state. It illustrated the bond quality of steel and GFRP with various web opening shapes and sizes. To begin the bond performance results discussion, keep in mind that

the load was fixed in this chapter ( as a dead load in a steel-framed structure) indicating that, some of the reinforced specimens with a stiffer reaction could not be strained until failure. It's worth mentioned that debonding has been seen in all of the bonded joints of specimens with rectangular holes. Due to the considerable length of the aperture and the incapacity of 3 mm and 6 mm GFRP thicknesses to offer greater stiffness to the T section, delamination began at the mid span above the web aperture for specimens U0-Rec-3-3, U0-Rec-3-6, U0-Rec-4-3, and U0-Rec-4-6 , on the other hand, specimens U0-Rec-1-6, U0-Rec-1-10, U0-Rec-2-10, and U0-Rec-3-10 failed by slight end debonding in the top adhesive layer caused by flange buckling (**Figure 4-87**); this delamination can be avoided by expanding the length of GFRP laminates until the first third of the span, which is not required because this minor delamination occurred after steel plasticization. Regarding to the trapezoidal opening debonding did not occurred for specimens U1-Trap-1-3 ,U1-Trap-1-6 ,U1-Trap-2-10 ,U1-Trap-3-10 despite the SDEG was close to 1 (Figure 7-88) . Bond failure occurred in the large trapezoidal web openings of examples U1-Trap-3-3 and U1-Trap-3-6 due to top T section buckling. In addition to strength decrease ,it has been revealed that trapezoidal web openings, particularly U1-Trap-1, result in higher bond efficiency in comparison to rectangular opening. For the reversed trapezoidal opening only specimens U2-Traprv-1-6 and U2-Traprv-1-10 were strengthened without bond failure as can be seen in **Figure 4-89** . The considerable length of the compressive T section was the cause of debonding in all other specimens with reversed trapezoidal openings as well as large rectangular openings. In view of the bond behavior of GFRP and steel beams with parallelogram holes, it was discovered that debonding happened with all reinforced specimens and the SDEG parameter reached the value of 1 while in the other hand no debonding has been happened in any of the glued junctions of the most beams with elliptical web apertures except specimen U0-Elli-3-3 .In general, the adoption of a bond length equal to four times the opening length provided a successful bond behavior because even junctions who failed by debonding in certain cases took place after steel plasticization we'll see with strength development to advertise the ideal GFRP laminate thickness of every opening shape and dimensions in the mid span position.





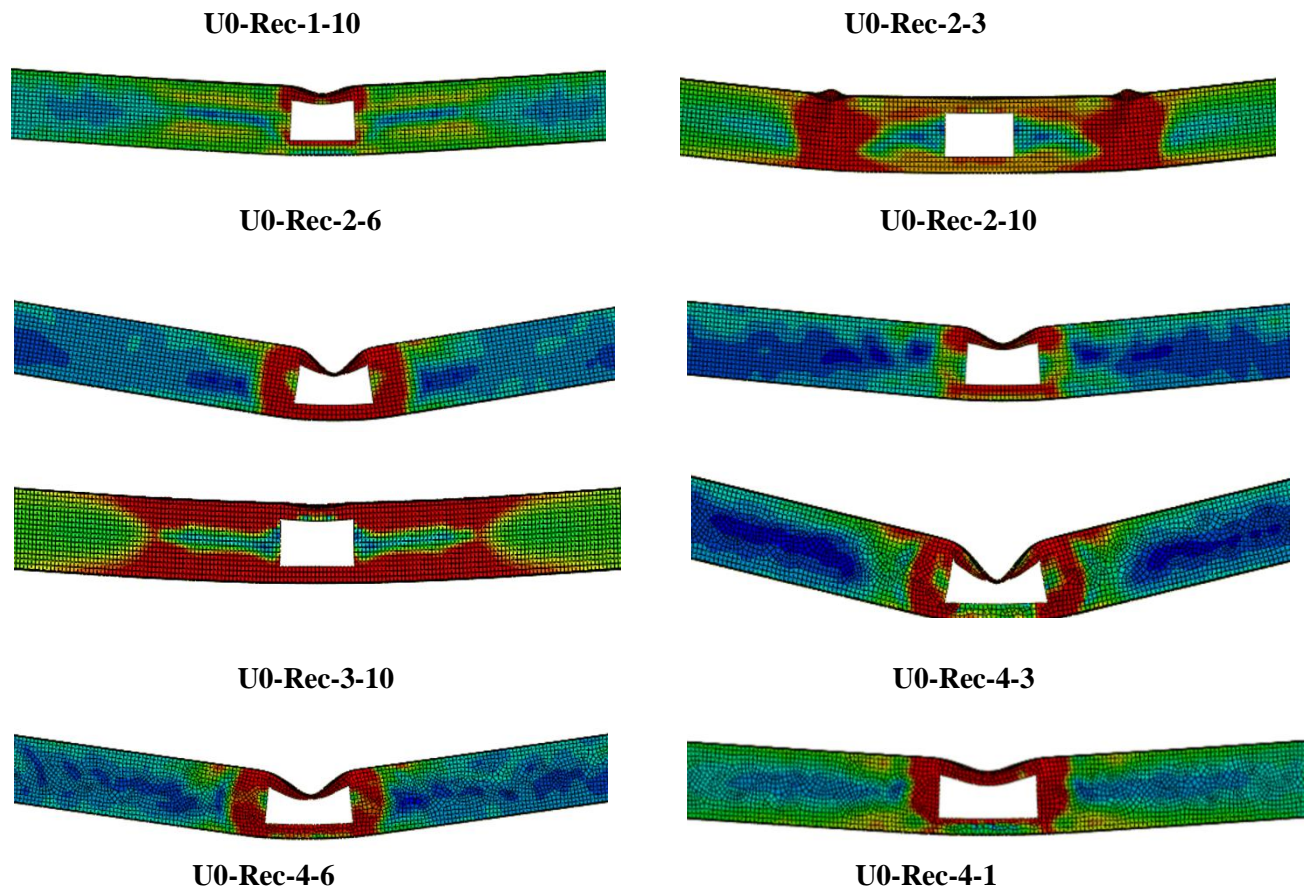
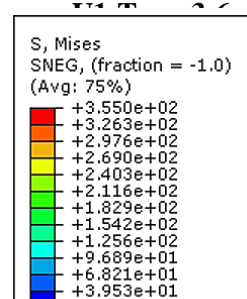
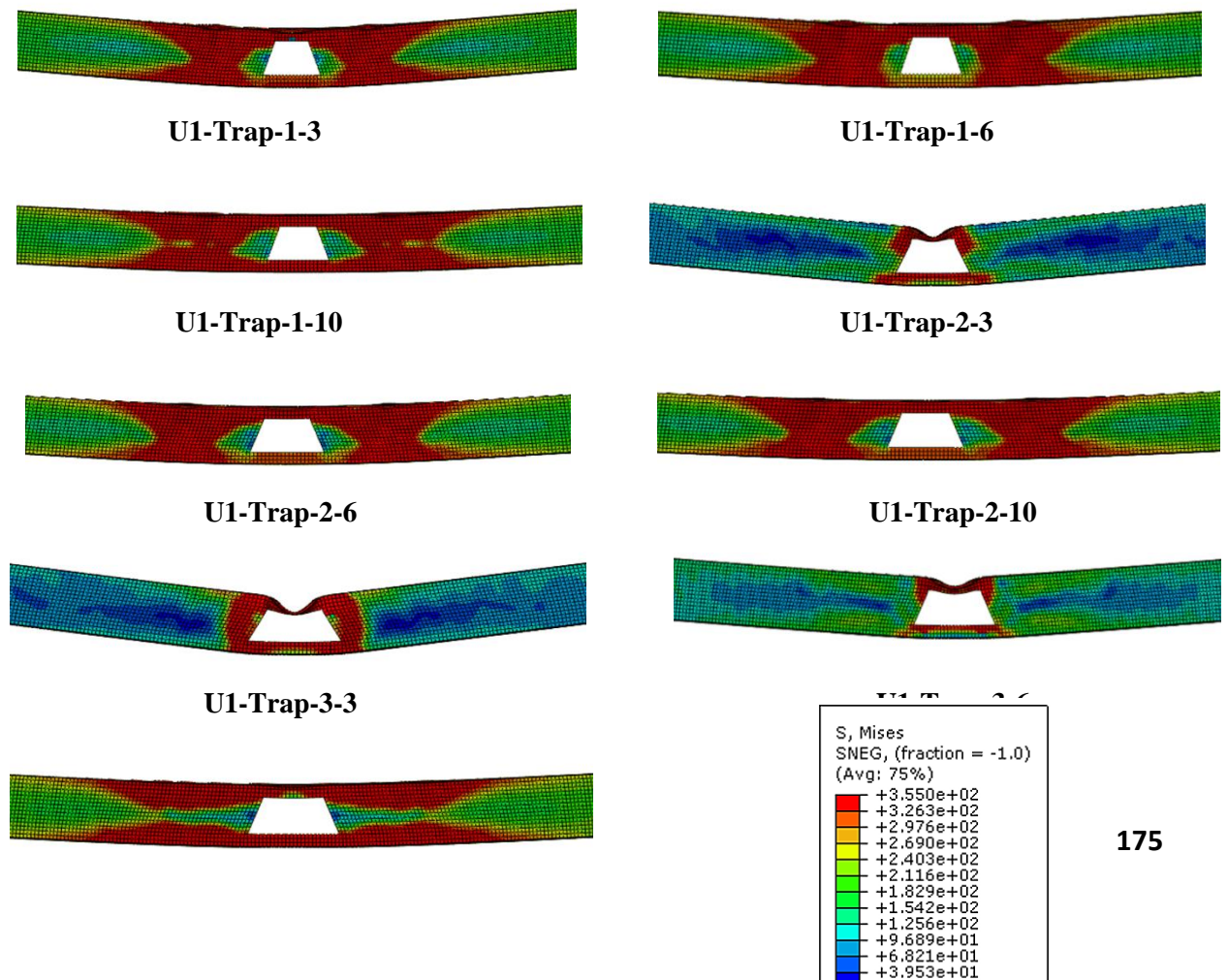
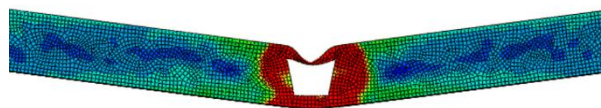


Figure 4-82 :Failure mode of strengthened specimens with mid span rectangular opening .



U1-Trap-3-10

Figure 4-83 : Failure mode of strengthened specimens with mid span trapezoidal opening .



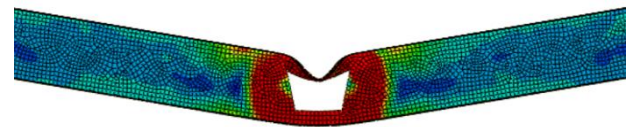
U2-Traprv-1-3



U2-Traprv-1-6



U2-Traprv-1-10



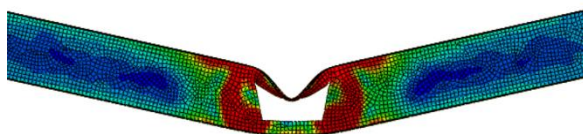
U2-Traprv-2-3



U2-Traprv-2-6



U2-Traprv-2-10



U2-Traprv-3-3



U2-Traprv-3-6



U2-Traprv-3-10

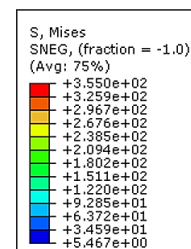
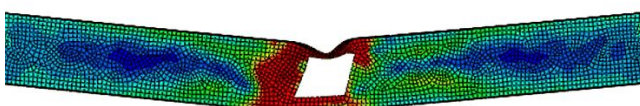


Figure 4-84 : Failure mode of strengthened specimens with mid span reversed trapezoidal opening .





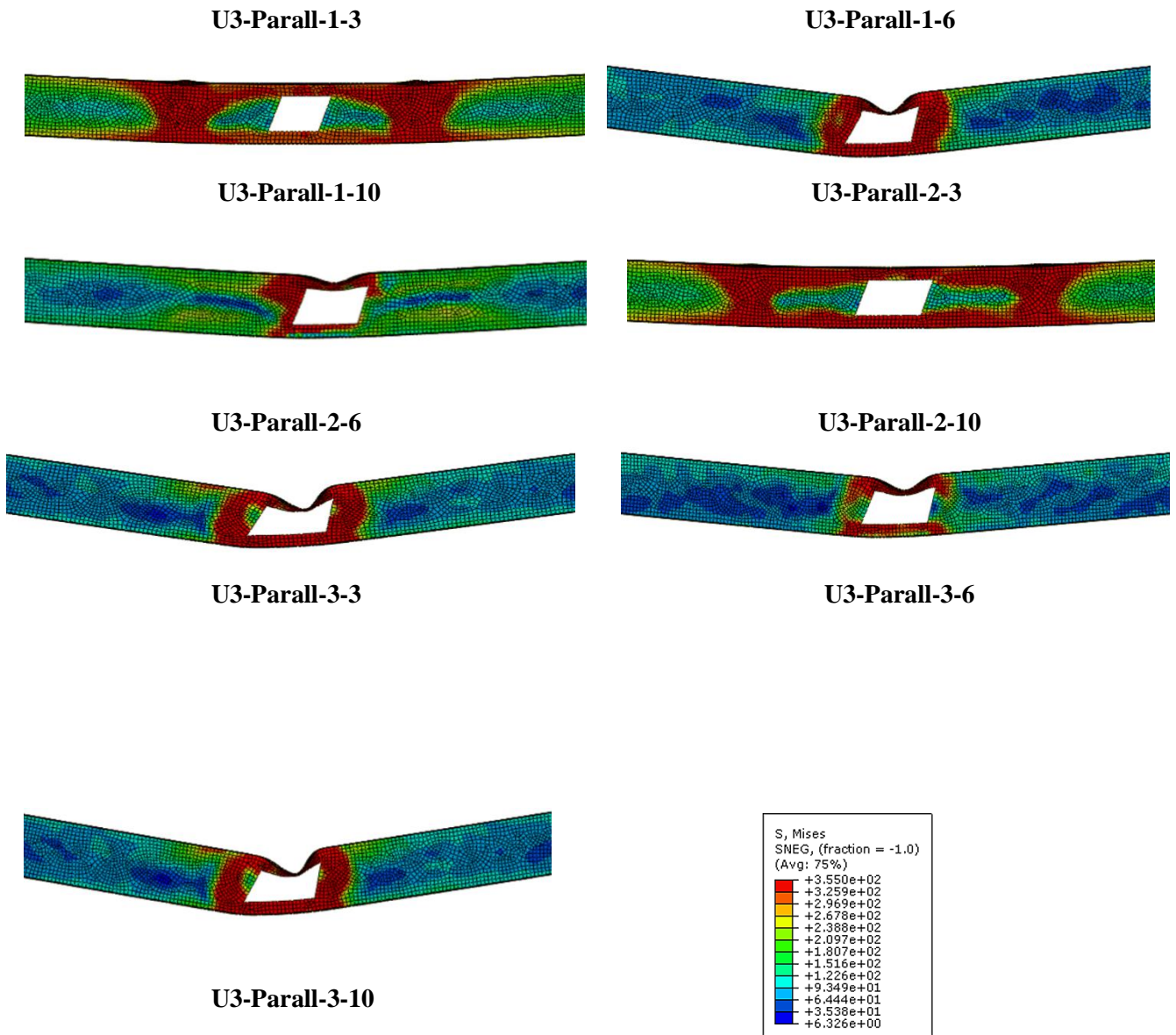
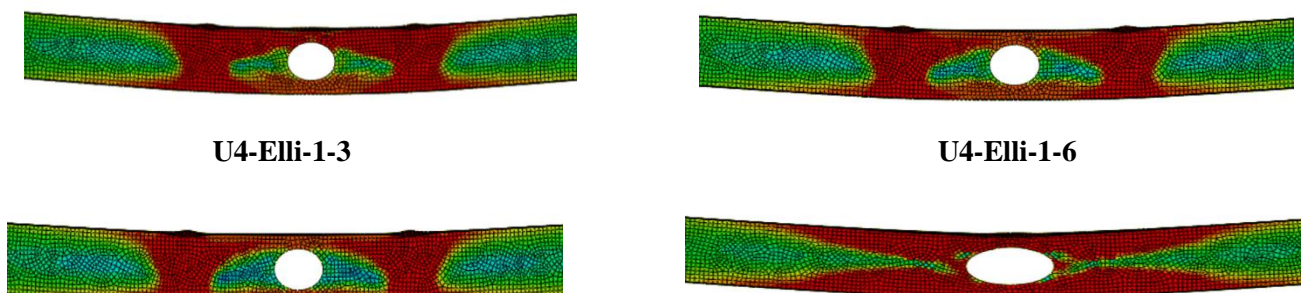


Figure 4-85 : Failure mode of strengthened specimens with mid span parallelogram opening .



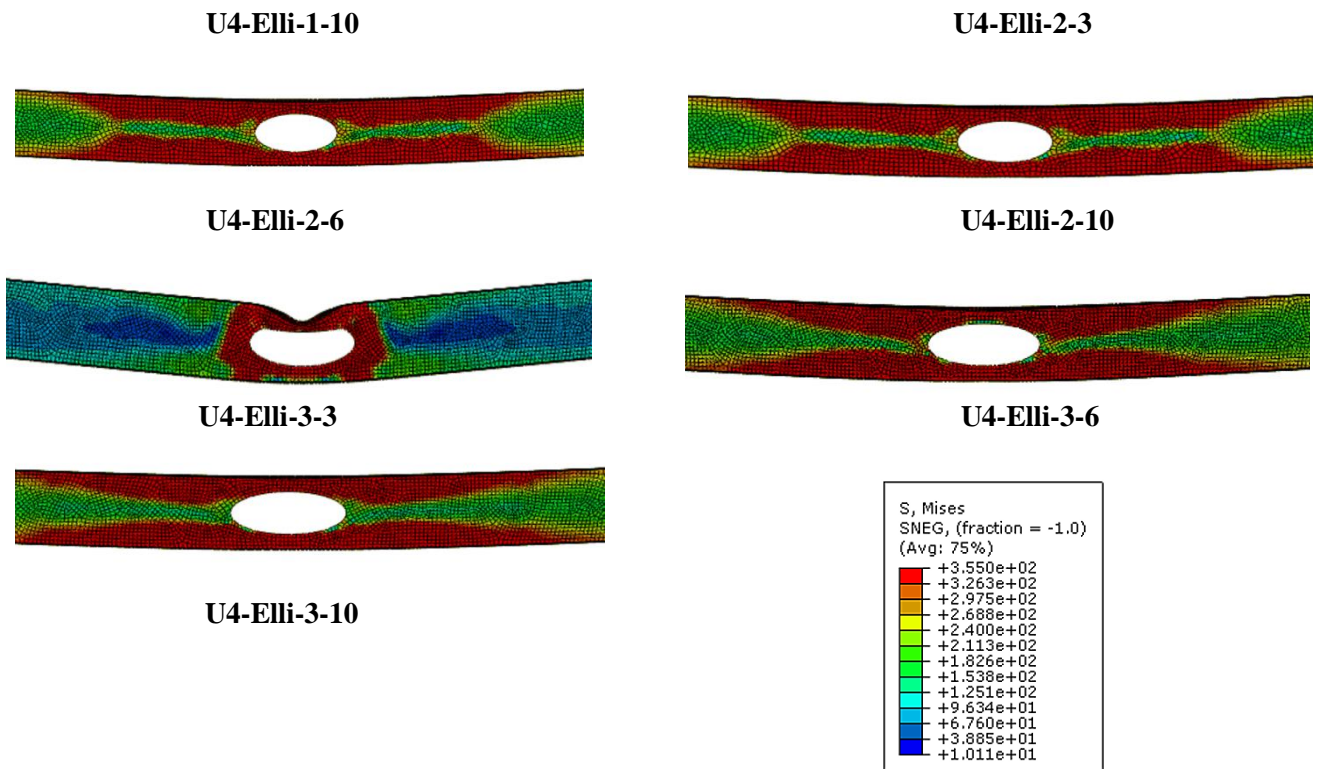


Figure 4-86 : Failure mode of strengthened specimens with mid span ellipsoidal opening

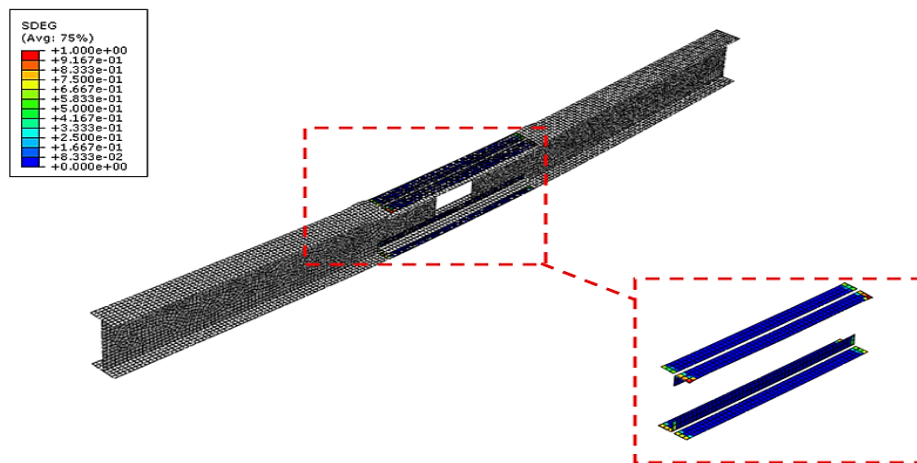
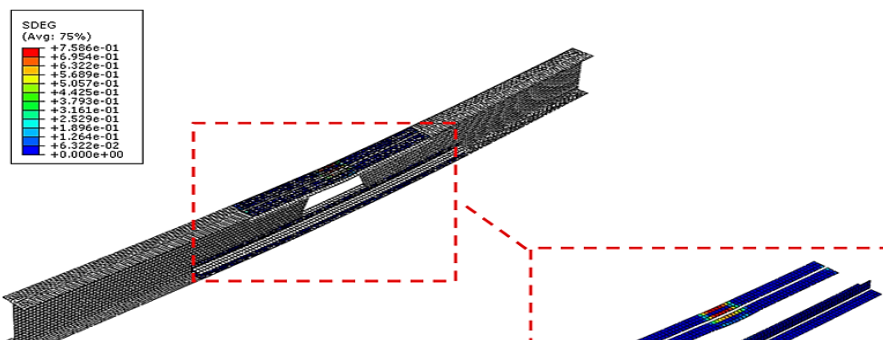
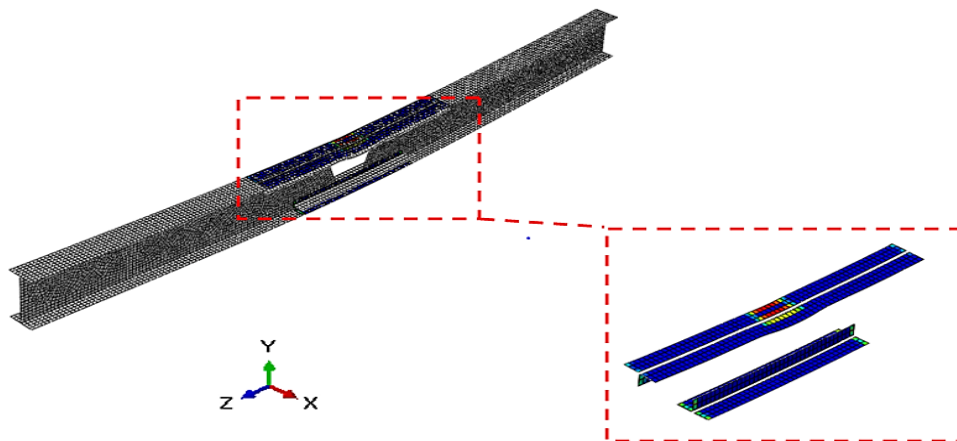


Figure 4-87 :Bond behavior for specimen U0-Rec-1-10.



**Figure 4-88 :Bond behavior for specimen U0-Trap-1-3.**



**Figure 4-89 :Bond behavior for specimen U2-Traprv-1-6.**

#### **IV.3.1.2. Shear zone position :**

##### **IV.3.1.2.1. Effect of web opening shape and size on steel beam performance and capacity:**

To comprehend the impacts of web aperture dimensions and shapes on structural behavior in shear zones, it is necessary to connect the load bearing capability of holed portions to the local concurrent moments and forces operating on the tee-sections upper and lower the web aperture.

When the findings of the beam with rectangular apertures are compared to the earlier findings in mid span position, it is clear that the load bearing ability of the beams has been greatly decreased due to the stress concentration at the edge of the rectangular hole. The load bearing ability of a rectangular web aperture decreases as the opening size grows (**Figure 4-90**). The strength decreased by 20% ,33%, 40% and 45% for specimens U0-SZRec-1, U0-SZRec-2 , U0-SZRec-3 and U0-SZRec-4 respectively .In addition, as seen in **Figures 4-91**, the Vierendeel failure is the most typical breakdown.

Load limits of holed parts are predicted to be inversely related to web apertures with similar depth values but varying length values. **Figure 4-93** depict the load-deflection curves for specimens with trapezoidal apertures.

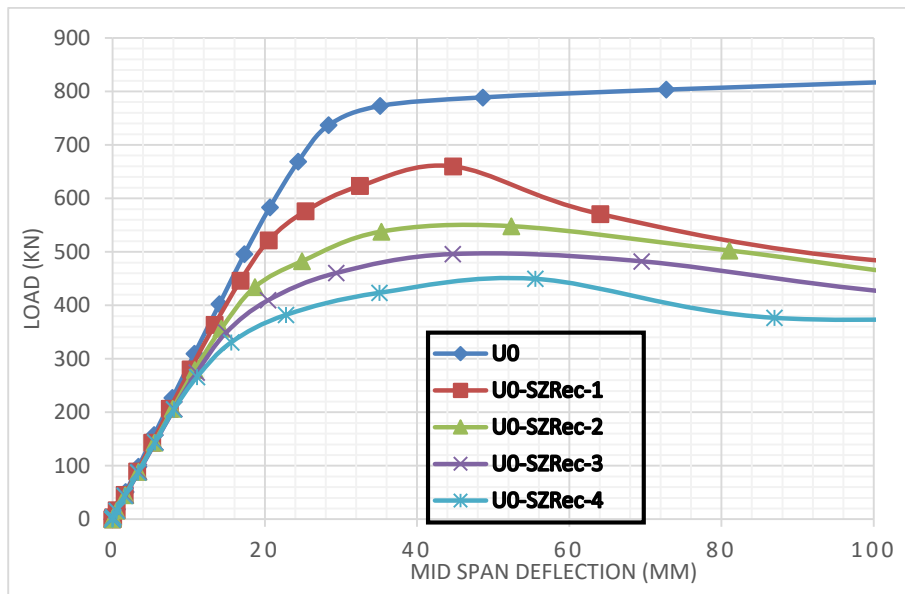


**Figure 4-90 : Load deflection curves of unstrengthened specimens with shear zone rectangular web openings .**

The load-bearing capacity of the structural member grows as the compression tee-section length reduces, however the size of the trapezoidal web aperture generates various reductions in load carrying capabilities. The strength decreased by 25 % ,26% and 34% for specimens U1-SZTrap-1 ,U1-SZTrap-2 and U1-SZTrap-3. The Vierendeel mechanism, which is primarily impacted by the size of the web apertures at the upper and bottom tee-sections, was found to be the general failure mechanism for all specimens with trapezoidal web openings in shear zones of varying sizes (**Figure 4-94**). Likewise, as illustrated in **Figure 4-93**, the load bearing capacity of the beam with shorter distance of tension tee-section adopting reversed trapezoidal opening the strength of the solid beam decreased by 17% ,24% and 33% for specimens U2-SZTraprv-1 ,U2-SZTraprv-2 and U2-SZTraprv-3

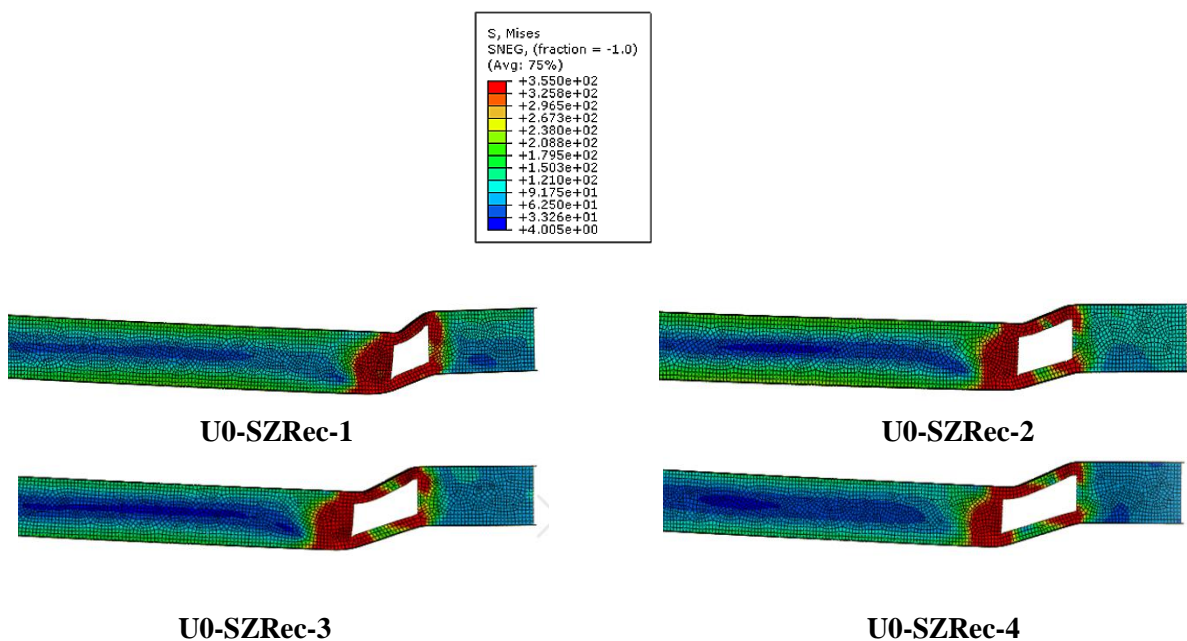


**Figure 7-91 : Failure mode of unstrengthened specimens with shear zone rectangular web opening.**

It can also be observed the vierendeel failure mechanism for the three specimens with reversed trapezoidal opening (**Figure 7-95**). It should be mentioned these specimens lost by vierendeel mechanism with load bearing capacity less than that of trapezoidal aperture due to greater length of compressive T section , formed by the production of multiple plastic hinges at crucial points of the holed portions under moment and shear .

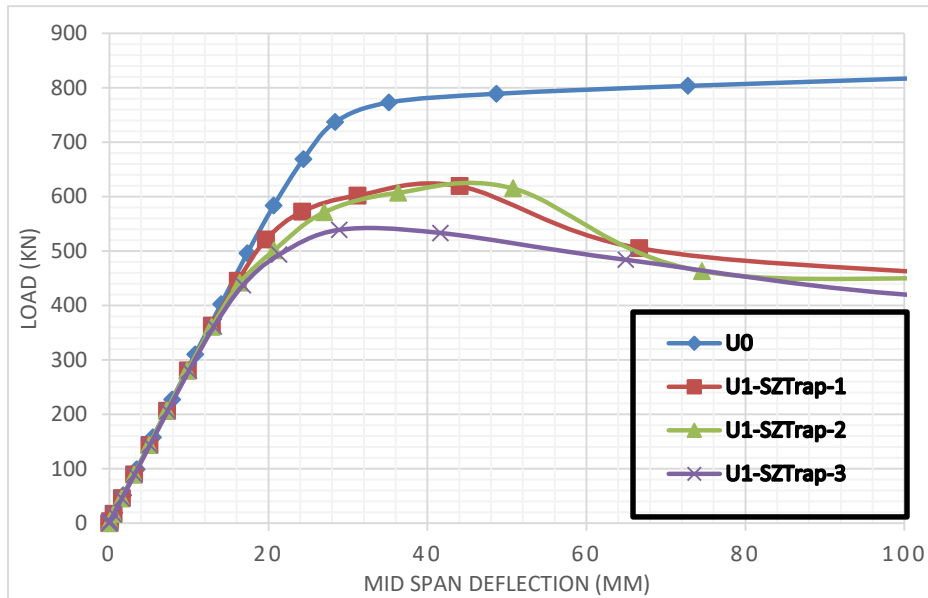


**Figure 4-92 : Load deflection curves of unstrengthened specimens with shear zone trapezoidal web opening.**

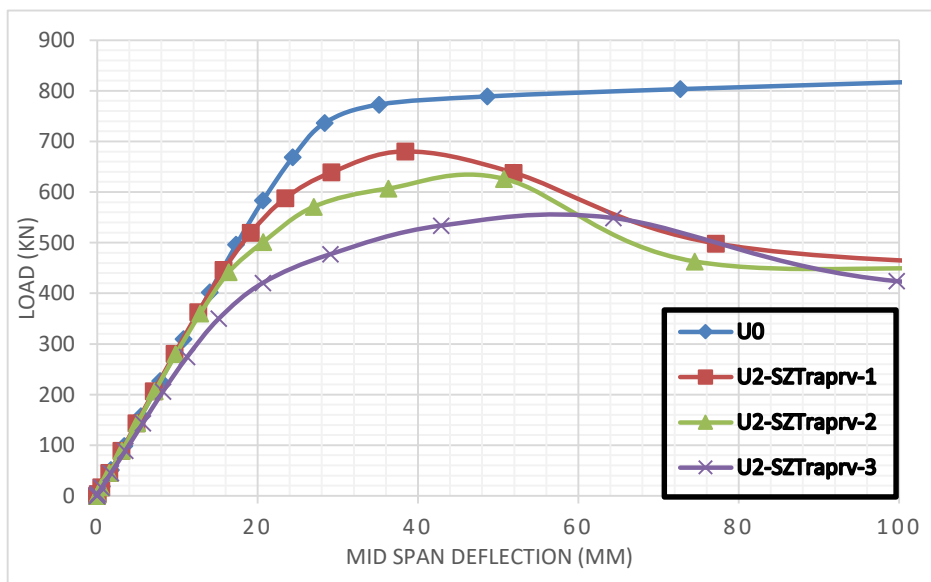


**Figure 4-93 : Load deflection curves of unstrengthened specimens with shear zone reversed trapezoidal web opening.**





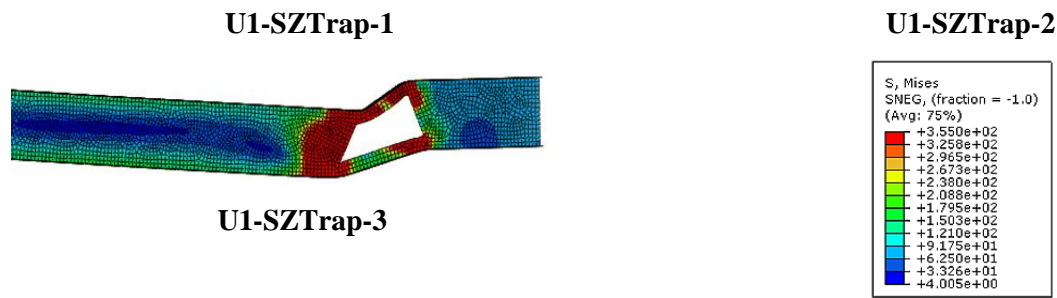


**Figure 4-94: Failure mode of unstrengthened specimens with shear zone trapezoidal web opening.**

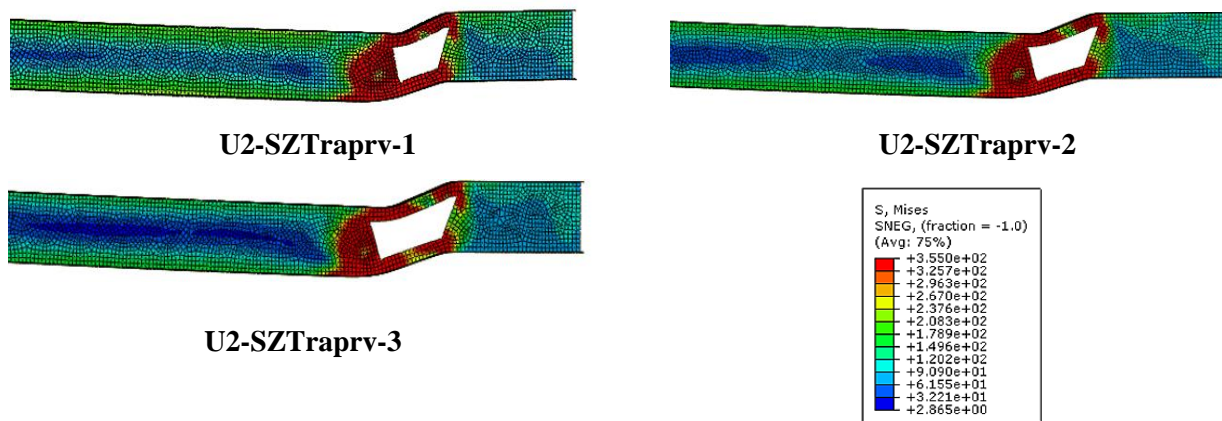


**Figure 4-95: Failure mode of unstrengthened specimens with shear zone reversed trapezoidal web opening.**

For equivalent open sizes, the load bearing capacities of parallelogram aperture specimens are roughly similar to those of rectangular hole beams (**Figure 4-96**). The Load decreased by 22% , 36 % and 41% for specimens U3-SZParall-1 , U3-SZParall-2 and U3-SZParall-3 . **Figure 4-97** further indicates that the frequent type of failure for parallelogram aperture in shear zone is the vierendeel phenomenon, which is identical to beams having rectangular web apertures. This supports the idea that in the shear zone, the key aperture length is the essential element in assessing the structural response of holed portions and regulates the level of local vierendeel forces operating on the tee sections. The conséquences of vierendeel réactions are substantial since the ellipses get a longer opening width. As the load bearing capacity is affected by the size of the web opening it was found that

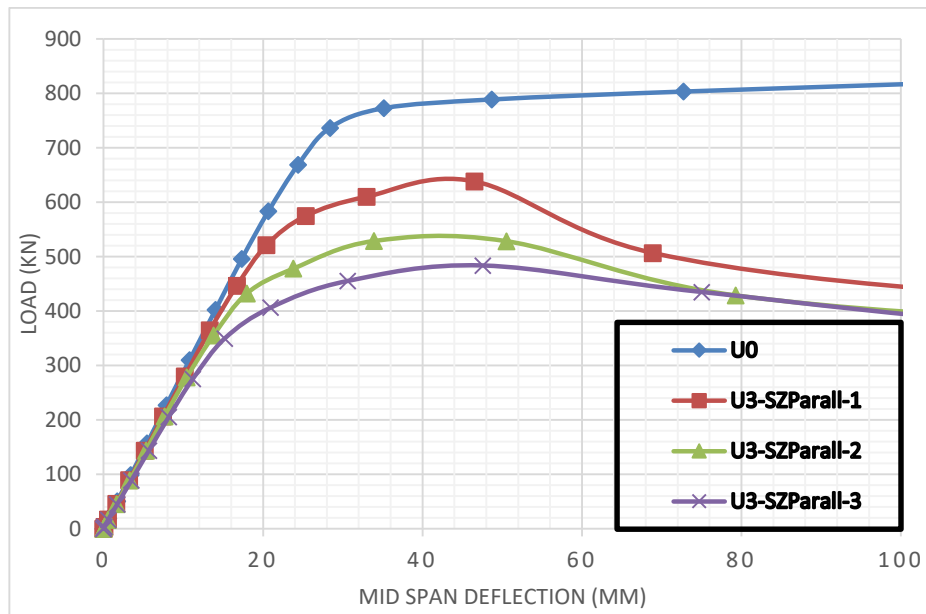


Figure 4-96 : Load deflection curves of unstrengthened specimens with shear zone parallelogram web opening.

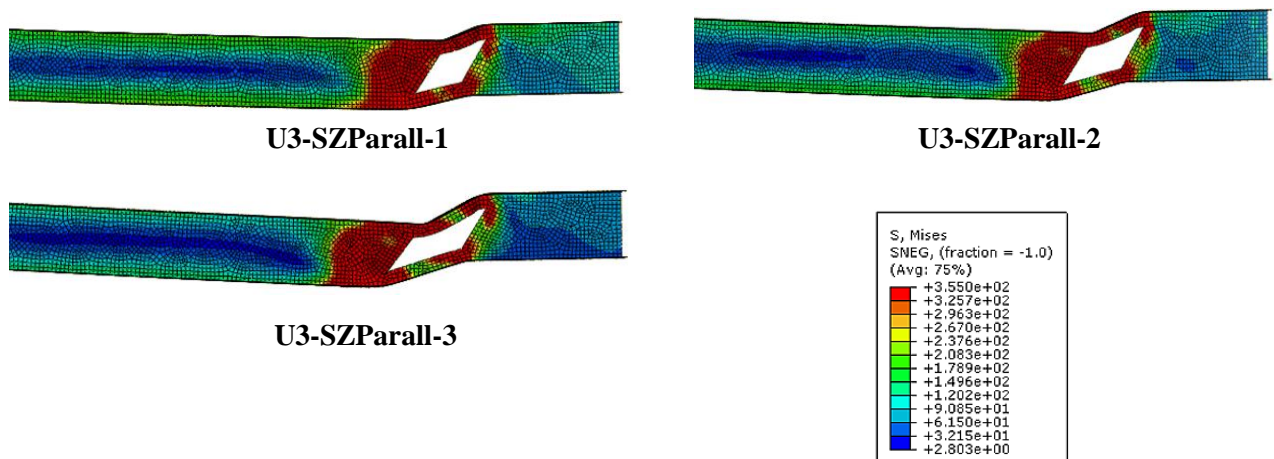


Figure 7-97: Failure mode of unstrengthened specimens with shear zone parallelogram web opening.

the initial beam strength fell by 4%, 8%, and 18% for specimens U4-SZelli-1, U4-SZelli-2, and U4-SZelli-3, respectively (Figure 4-98). Due to the important extension of larger web openings, in addition to the architecture of web opening shapes, a diverse combination of pressures acts on the upper and lower tee-sections, among the three examined specimens U4-SZelli-1 failed also by flexural failure while U4-SZelli-2 and U4-SZelli-3 failed by vierendeel mechanism (Figure 4-99) .

It is clear that the Vierendeel phenomenon is the most prevalent type of failure for beams having rectangular, trapezoidal, parallelogram, and wide elliptical web holes. The suggested GFRP strengthening approach will now be tested on various aperture sizes and shapes to determine the most efficient GFRP thickness for each scenario



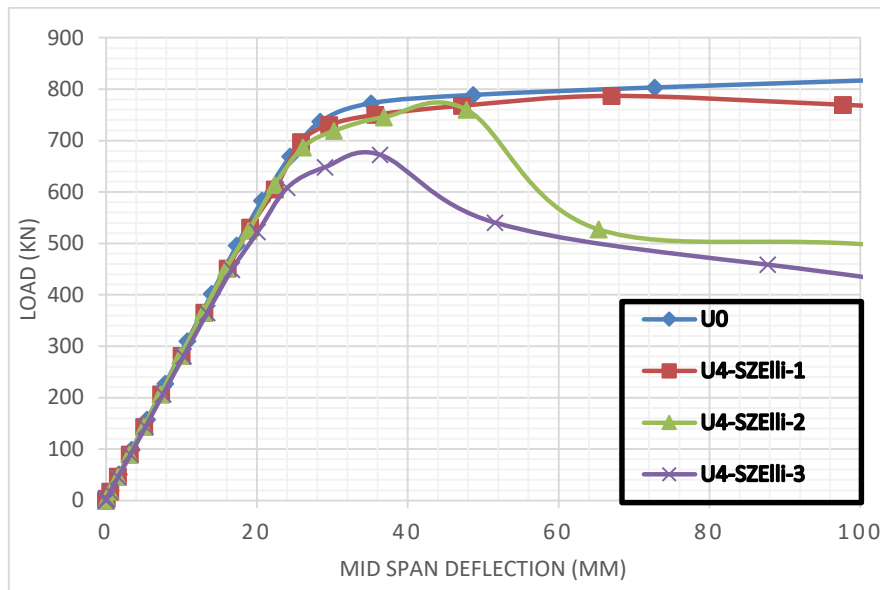


Figure 4-98 : Load deflection curves of unstrengthened specimens with shear zone ellipsoidal web opening.

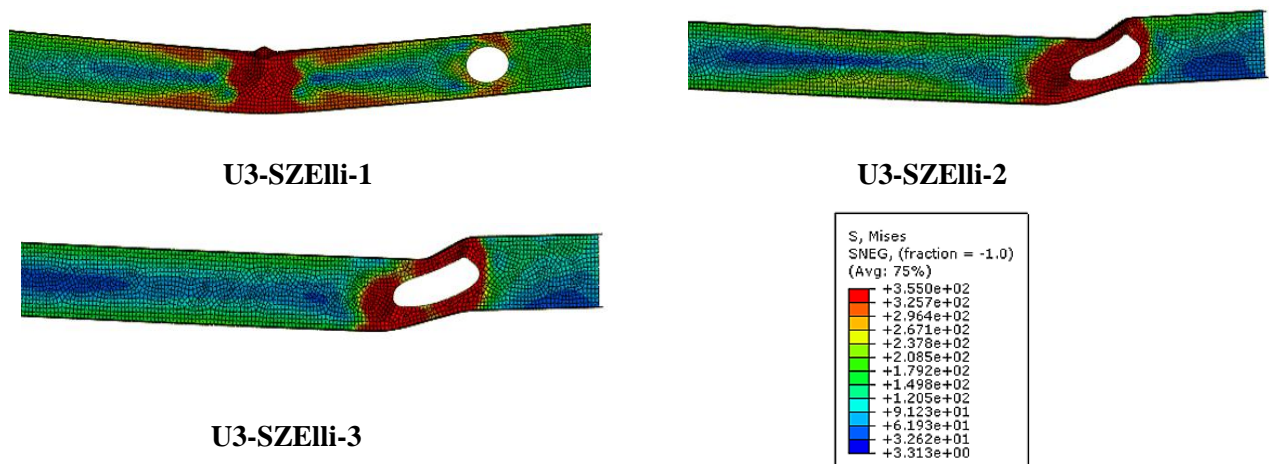


Figure 4-99: Failure mode of unstrengthened specimens with shear zone ellipsoidal web opening.

#### IV.3.1.2.2. Force mid-span deflection reaction :

The very worst situation for web openings is the presence of a big rectangular aperture in the shear location. This subsection attempts to determine the optimal reinforcing procedure for this beam in order to restore its full ability.

As illustrated in **Figure 4-100** and **Table 4-11**, the capacity of specimen U0-SZRec-1 rose by 17 % ,18% and 19% of their initial capacity using GFRP laminate thicknesses of 3mm ,6mm and 10mm correspondingly . In the other hand ,the maximum load achieved with specimen U0-SZRec-2 was 34 % ,42 % and 43% of the initial beam strength using the three proposed GFRP thicknesses (**Table 7-11**) . Furthermore, the strength of specimens U0-SZRec-3-3, U0-SZRec-3-6, and U0-SZRec-3-10 was increased by 38%, 57% and 58%, respectively, when compared

to the unreinforced beam U0-SZRec-3 (**Figure 4-102**). The last tested specimen with rectangular opening U0-SZRec-4 showed an increase of 28 %, 49 % and 60 % in strength using 3mm ,6mm and 10 mm GFRP Thickness laminates (**Figure 4-103**) .

From these findings with the exception of the first specimen U0-SZRec-1, the capacity of the original beam was not recovered and the percentage of strength enhancement increases with the GFRP thickness increase.

GFRP thickness	U0-SZRec-1	U0-SZRec-2	U0-SZRec-3	U0-SZRec-4
3 mm	17 %	34 %	38 %	28 %
6 mm	18 %	42 %	57 %	49 %
10 mm	19 %	43 %	58 %	60 %

**Table 4-11: Strength enhancement percentage for specimens with rectangular opening.**

This strength enhancement may propose further increase in GFRP laminate thickness, however the variation in strength enhancement was not substantial between 6 mm and 10 mm GFRP except for specimen U0-SZRec-4, and any other increase in GFRP thickness will result in early debonding as previously mentioned. Considering these findings, employing large rectangular openings in the shear zone in specimens is not advised.

The strength of the trapezoidal opening increased by 24% for specimen U1-SZTrap-1-3 as well as 26% for specimens U1-SZTrap-1-6 and U1-SZTrap-1-10 (**Figure 4-104**). The strength improvement percentages for specimens U1-SZTrap-2-3, U1-SZTrap-2-6, and U1-SZTrap-2-10 were 28%, 45%, and 46%, respectively (**Figure 7-105** and **Table 7-12**). The strength augmentation for specimens U1-SZTrap-3-3, U1-SZTrap-3-6, and U1-SZTrap-3-10, on the opposite side, was 25%, 47%, and 52%, correspondingly (**Figure 4-106** and **Table 4-12**). It should be noted that despite the fact that specimen U1-SZTrap-1-10 was quite near, the reinforcing procedure was unable to restore the original strength of the solid beam. Furthermore, except for specimen U1-SZTrap-3, increasing GFRP thickness had little effect on strength improvement. The results obtained for reversed trapezoidal opening in shear zone are detailed in **Figures 4-107 to 4-109** and **Table 4-13** . Specimen U2-SZTraprv-1-3 grew in strength by 14%, whereas specimens U2-SZTraprv-1-6 and U2-SZTraprv-1-10 rose by 15%.

GFRP thickness	U1-SZTrap-1	U1-SZTrap-2	U1-SZTrap-3
3 mm	24%	27%	26%
6 mm	26%	46%	47%
10 mm	26%	46%	52%

**Table 4-12: Strength enhancement percentage for specimens with trapezoidal opening.**

Furthermore, The strength of specimen U2-SZTraprv-2-3 rose by 22%, whilst that of specimens U2-SZTraprv-2-6 and U2-SZTraprv-2-10 jumped by 46%. The three GFRP laminate thicknesses provided a strength enhancement of 26%, 47% and 52 % for the three tested specimens (**Table 4-12** ). As previously indicated, the GFRP thickness increase had no effect

on the specimen with the biggest aperture dimension. Regardless of the fact that U2-SZTraprv-1 and U2-SZTraprv-2 performed quite similarly and close to initial beam, the previous strength was not totally restored (**Figure 4-107** and **Figure 4-108** ).

**Table 4-13: Strength enhancement percentage for specimens with reversed trapezoidal opening.**

Regarding to the parallelogram opening in shear zone position it can be seen in **Table 4-14** and

GFRP thickness	U2-SZTraprv-1	U2-SZTraprv-2	U2-SZTraprv-3
3 mm	14%	22%	23%
6 mm	15%	25%	33%
10 mm	15%	25%	42%

**Figure 4-110** that the strength increased by 20 % for specimen U3-SZParall-1-3 and 22% for specimens U3-SZParall-1-6 and U3-SZParall-1-10 . Similarly, specimen U3-SZParall-2 demonstrated a 32% increase in strength with 3 mm GFRP thickness and a 47% boost with 6 mm GFRP thickness (**Figure 4-111**) .It was also observed that specimen U3-SZParall-3 exhibited a strength improvement of 35% , 51% and 62% with GFRP thicknesses of 3mm ,6mm and 10 mm (**Figure 4-112**). The similar observation can be made about the growth in strength development as GFRP thickness, and the starting force of the solid beam was not totally restored. Interesting results were obtained with elliptical web opening in shear zone ,no strength enhancement was found for specimen U2-SZElli-1 using the three proposed GFRP laminates thicknesses (**Table 4-15**).

GFRP thickness	U2-SZParall-1	U2-SZParall-2	U2-SZParall-3
3 mm	20%	32%	35%
6 mm	22%	47%	51%
10 mm	22%	47%	62%

**Table 4-14: Strength enhancement percentage for specimens with parallelogram opening.**

Additionally, just a really modest increase in peak load was found for specimen U2-SZElli-2 utilizing the three recommended GFRP thicknesses ranging from 3% to 5% (**Figure 4-114**). The strength of specimen U2-SZElli-3-3, in contrast , was boosted by 7%, while specimens U2-SZElli-3-6 and U2-SZElli-3-10 were elevated by 14% (**Table 4-15**).

GFRP thickness	U2-SZElli-1	U2-SZElli-2	U2-SZElli-3
3 mm	0%	3%	7%
6 mm	0%	4%	14%
10 mm	0%	5%	14%

**Table 4-14: Strength enhancement percentage for specimens with ellipsoidal opening**

The percentage of force enhancement differed from a specimen to another according to web opening shape ,dimension and GFRP laminate thickness .This backs up the assertion that the

vital aperture length in shear zone location is the most essential aspect in assessing the structural performance of holed portions since it affects the amount of local Vierendeel stresses operating on tee portions. The GFRP thickness expansion had no effect on the reinforcement for rectangular, trapezoidal, reversed trapezoidal, and parallelogram web apertures for the two initial opening dimensions in every case . This is explained by the effective composite component to flange and web of steel; any other increase will not result in an enhancement in strength. On the contrary way, with the final recommended dimension, the strength increased as the GFRP thickness rose, which may be explained by the effective GFRP thickness which was not achieved . Concerning the elliptical web opening, it was discovered that the envisaged GFRP technique had no effect on the strength of the beam for the first tested specimen U4-SZelli-1, which will be revealed by the flexural failure occurring far from the reinforced region and because the stress concentration was in the mid span, neither cooperation for the shear zone GFRP strengthening was indicated (**Figure 4-113**).

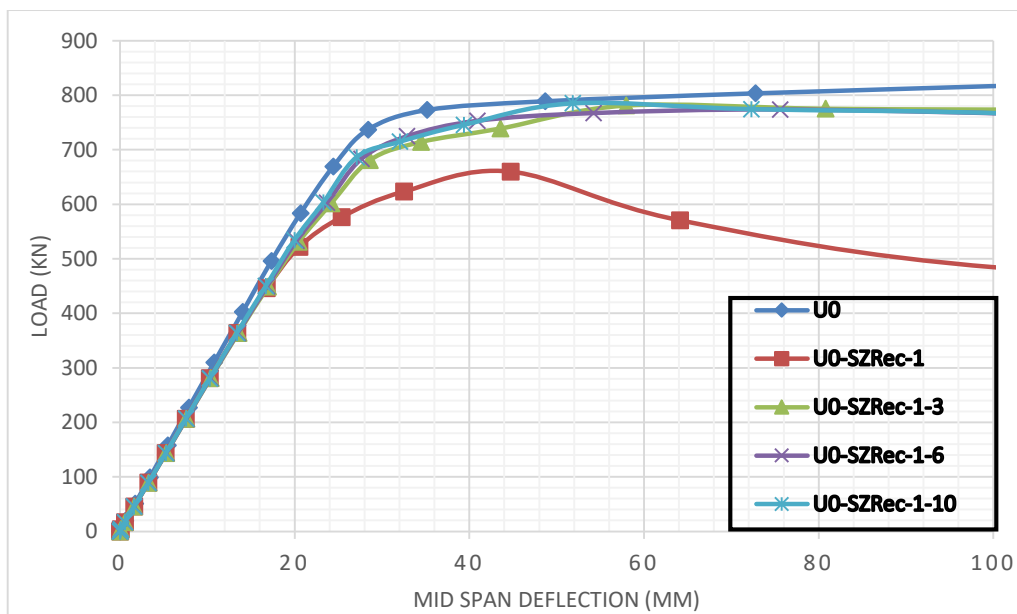


**Figure 4-100 : Load-mid span deflection curves for strengthened specimen U0-SZRec-1.**

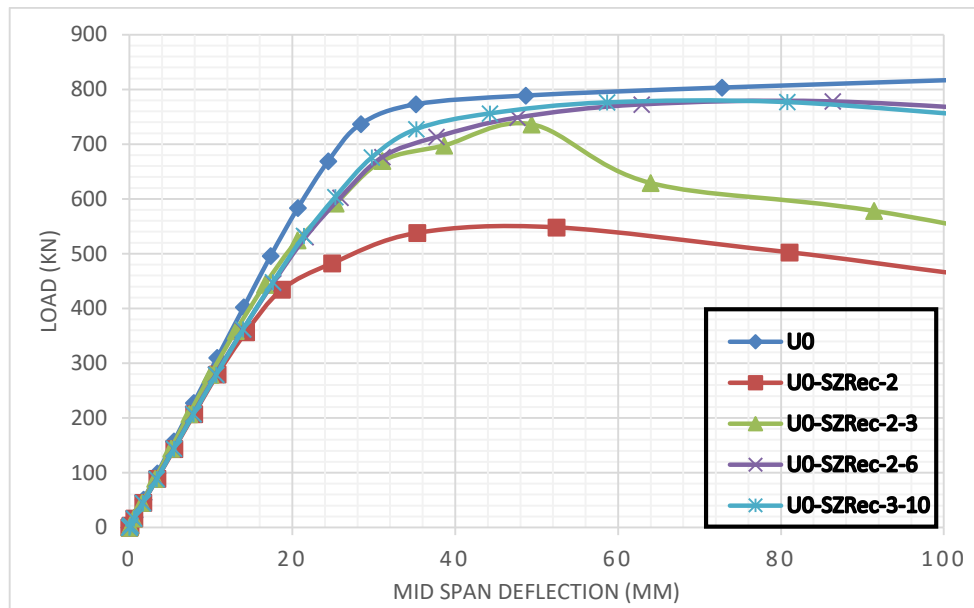


Figure 4-101 : Load-mid span deflection curves for strengthened specimen U0-SZRec-2.

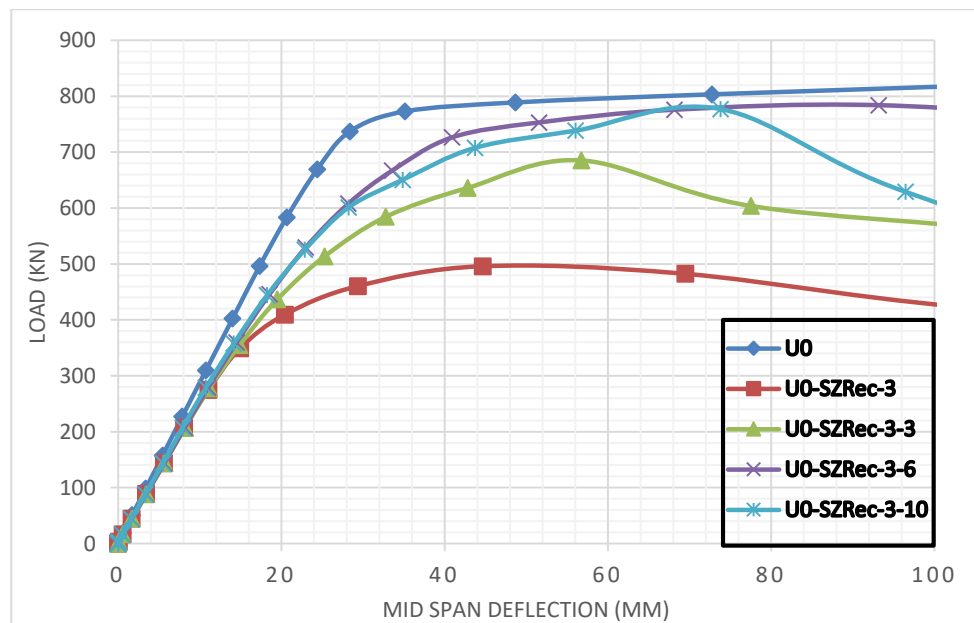


Figure 4-102 : Load-mid span deflection curves for strengthened specimen U0-SZRec-3.

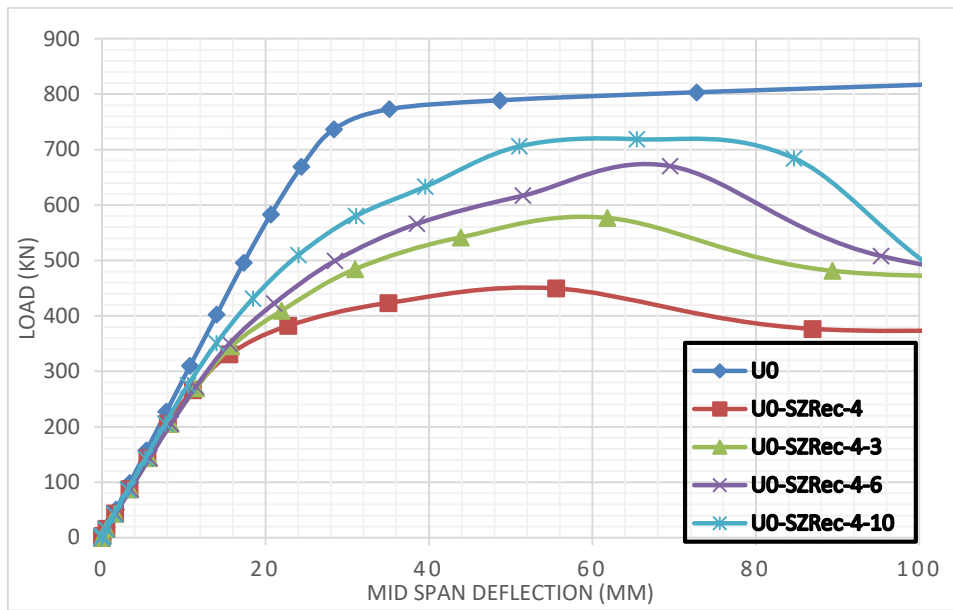


Figure 4-103 : Load-mid span deflection curves for strengthened specimen U0-SZRec-4.

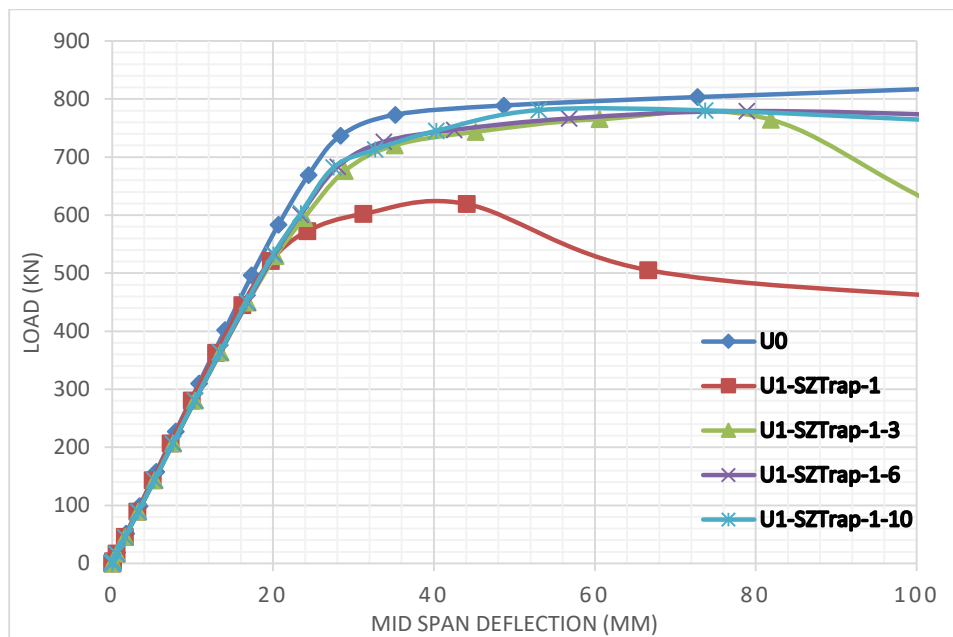


Figure 4-104 : Load-mid span deflection curves for strengthened specimen U1-SZTrap-1

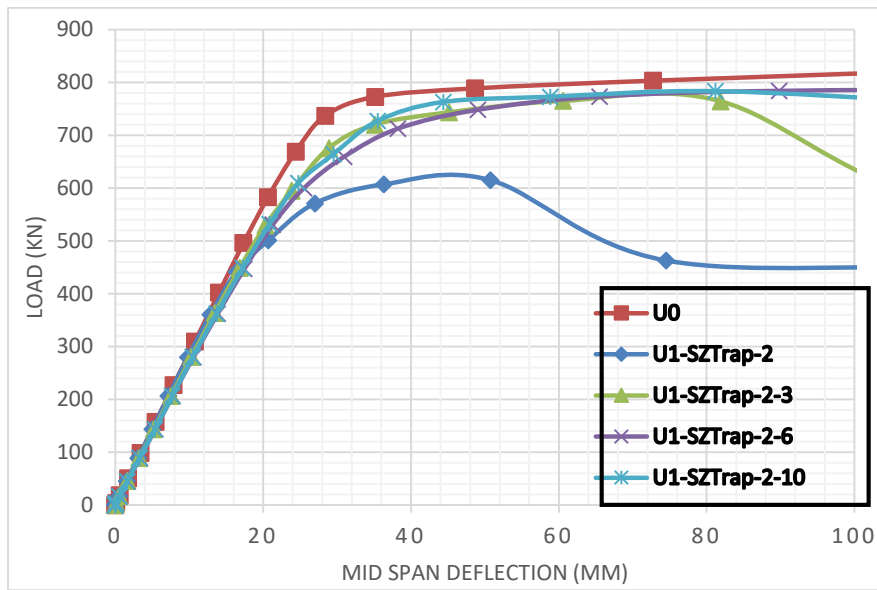


Figure 4-105 : Load-mid span deflection curves for strengthened specimen U1-SZTrap-2

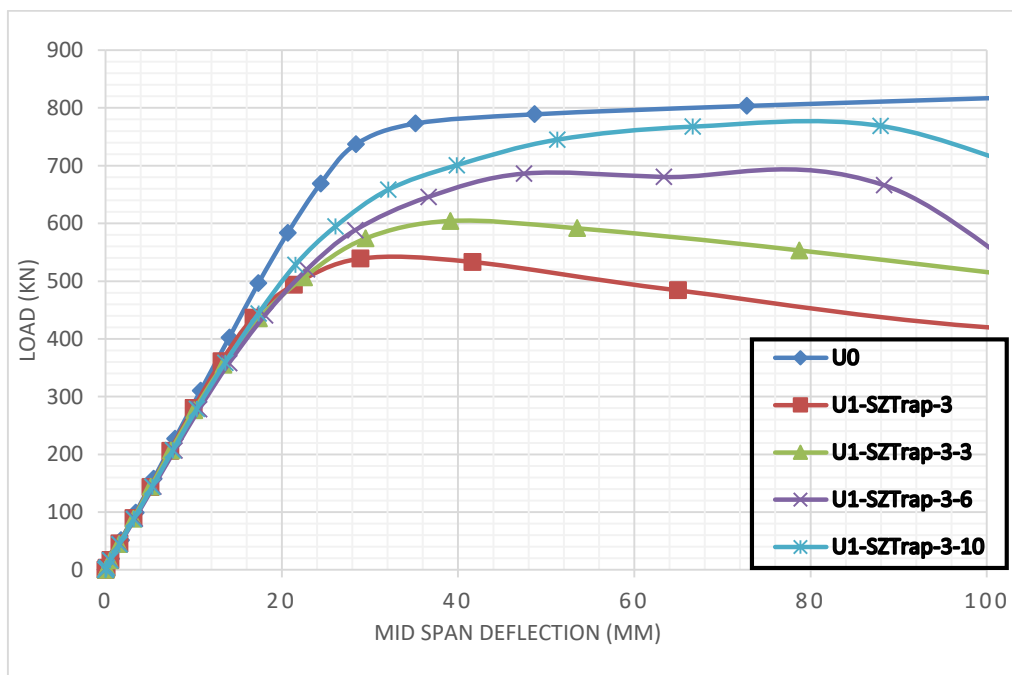
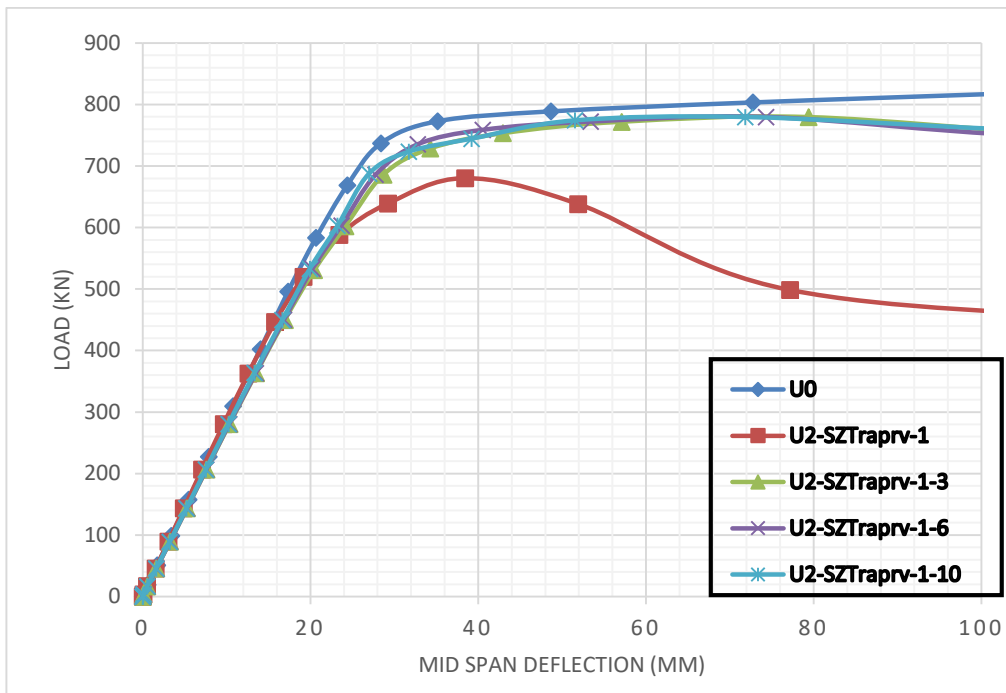
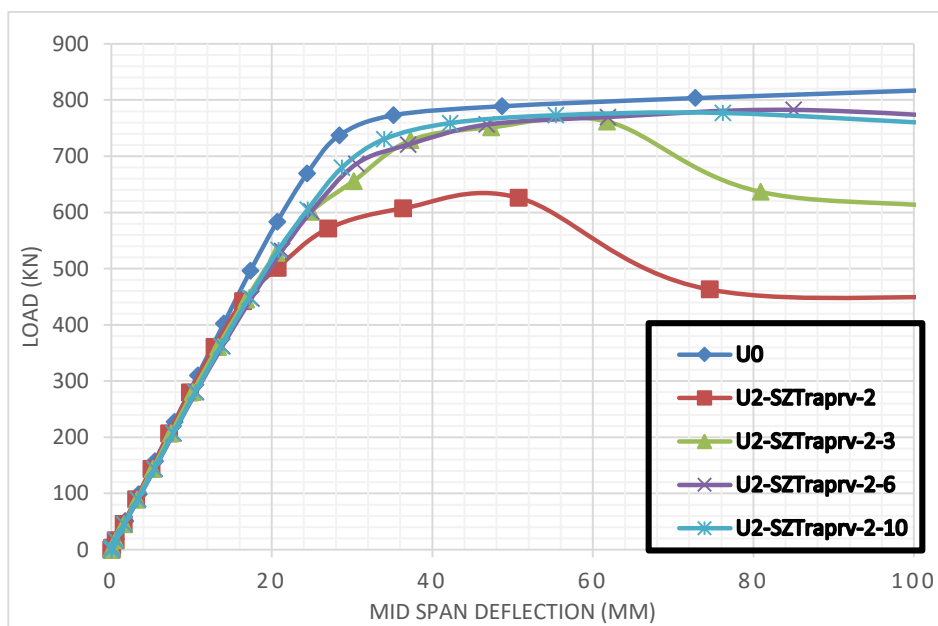


Figure 4-106 : Load-mid span deflection curves for strengthened specimen U1-SZTrap-3





**Figure 4-107 : Load-mid span deflection curves for strengthened specimen U1-SZTraprv-1**



**Figure 4-108 : Load-mid span deflection curves for strengthened specimen U1-SZTraprv-2**

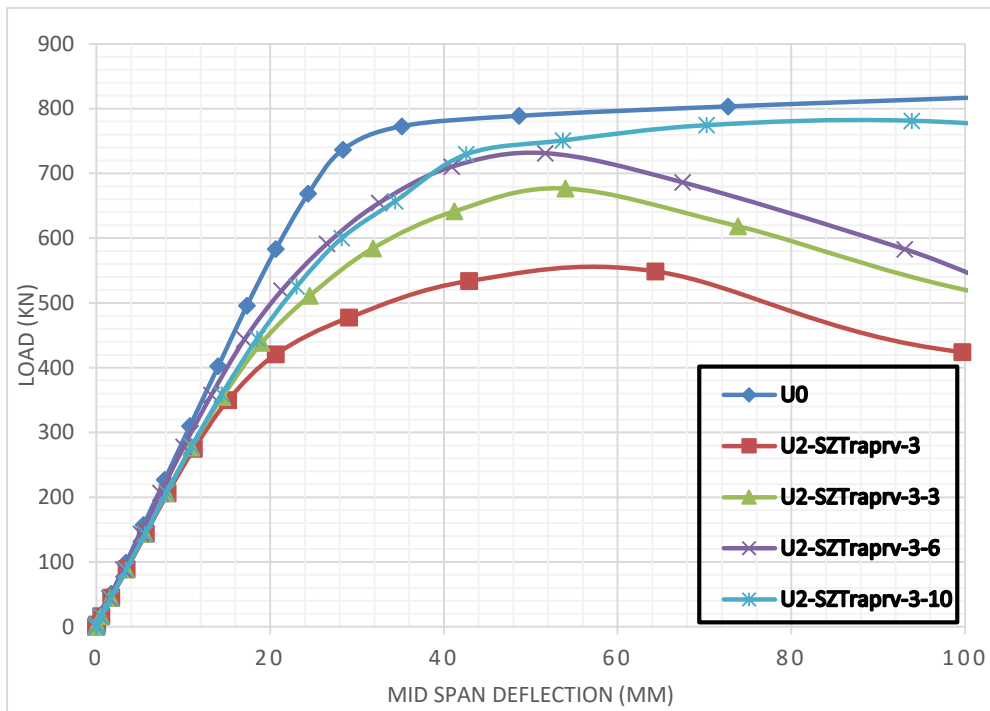


Figure 4-109 : Load-mid span deflection curves for strengthened specimen U1-SZTraprv-3

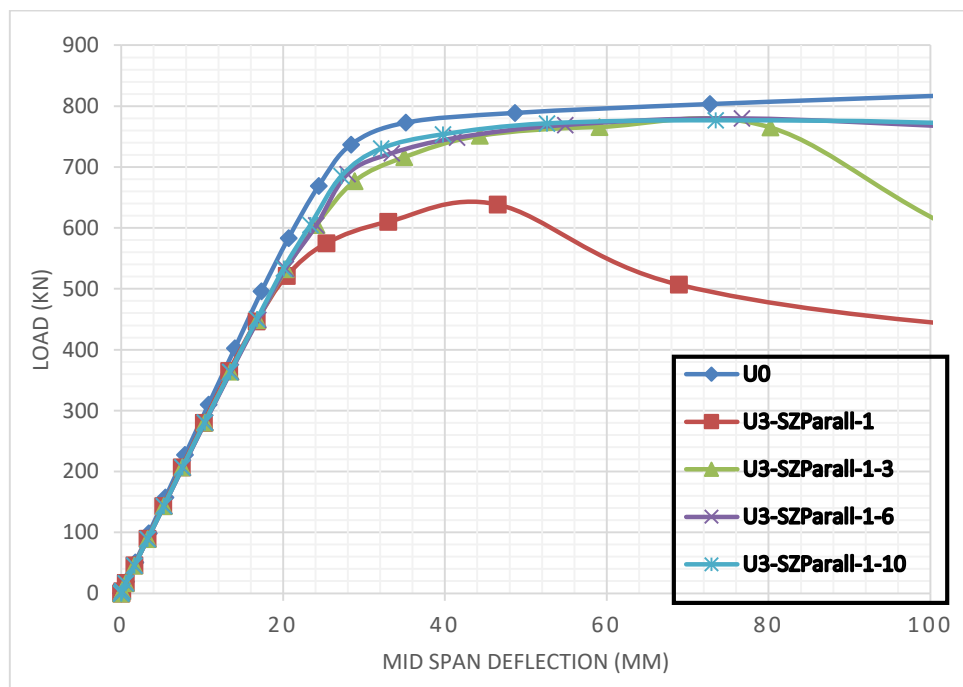


Figure 4-110 : Load-mid span deflection curves for strengthened specimen U3-SZParall-1.

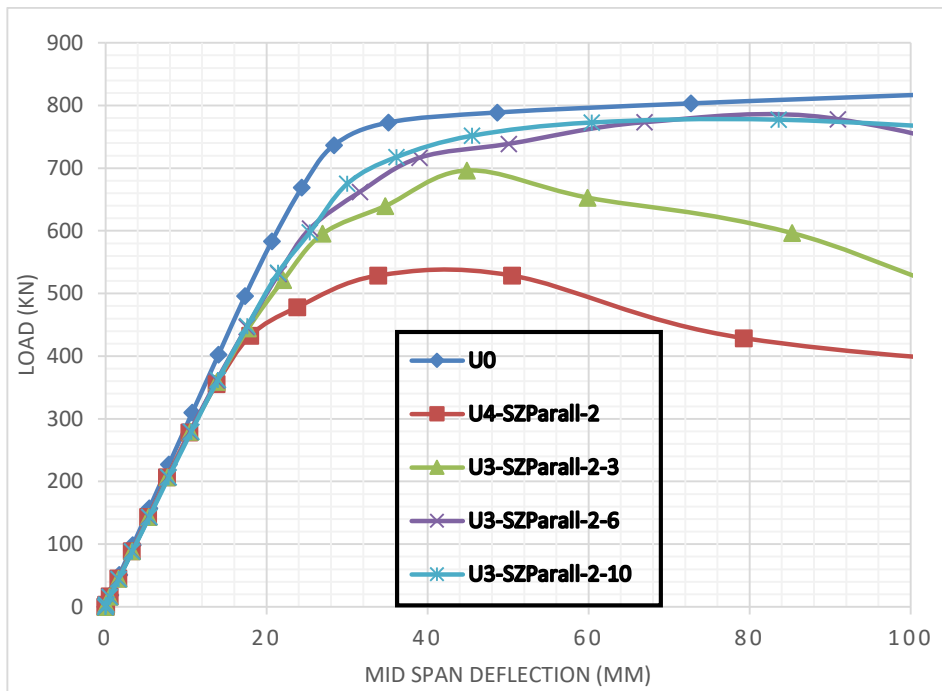


Figure 4-111 : Load-mid span deflection curves for strengthened specimen U3-SZParall-2.

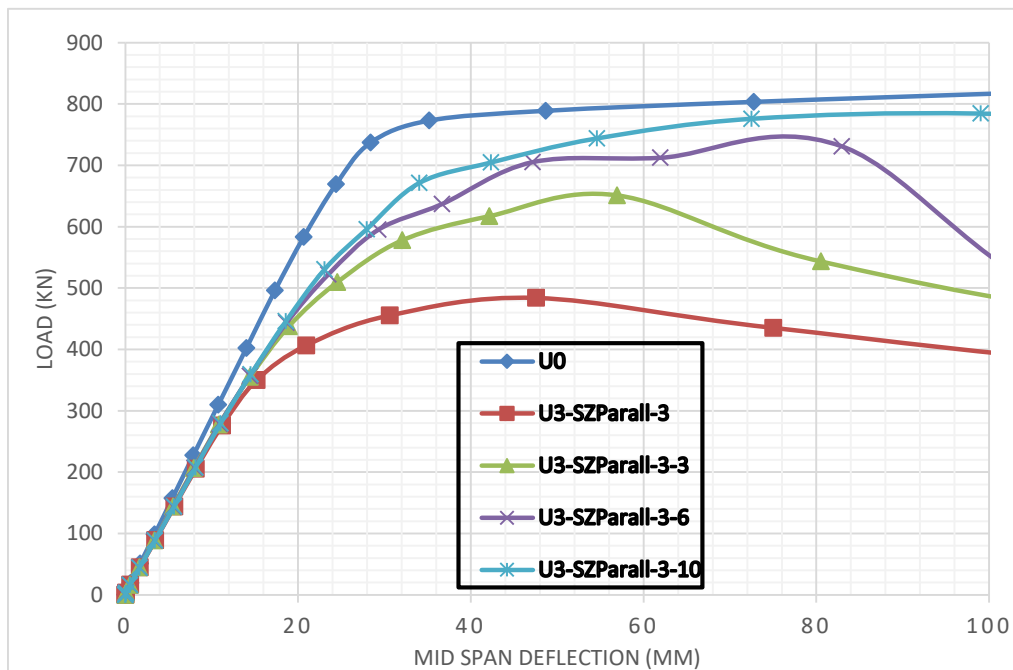


Figure 4-112 : Load-mid span deflection curves for strengthened specimen U3-SZParall-3.

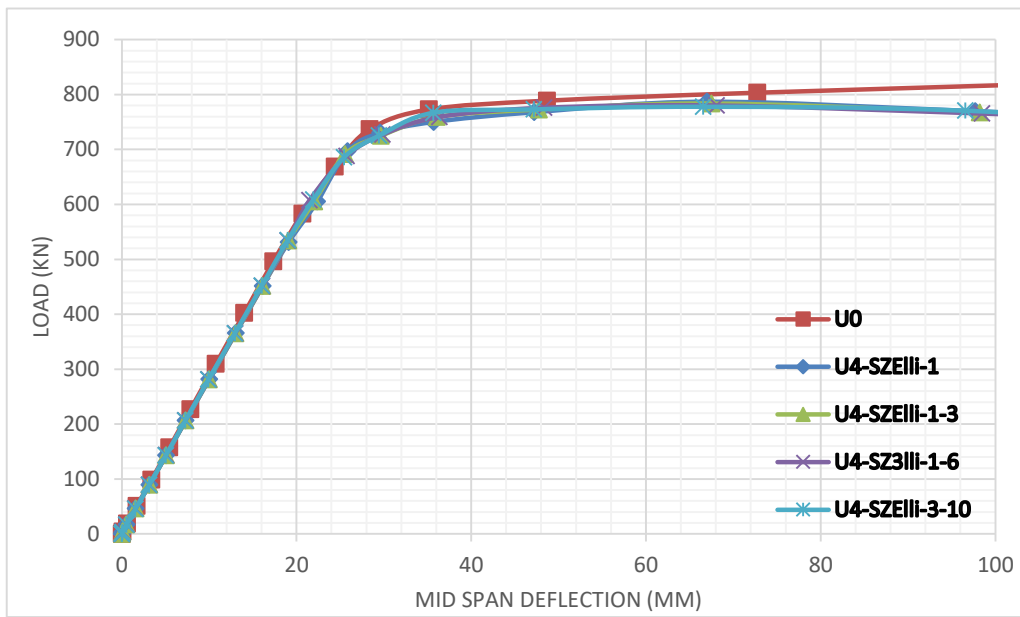


Figure 4-113 : Load-mid span deflection curves for strengthened specimen U4-SZelli-1

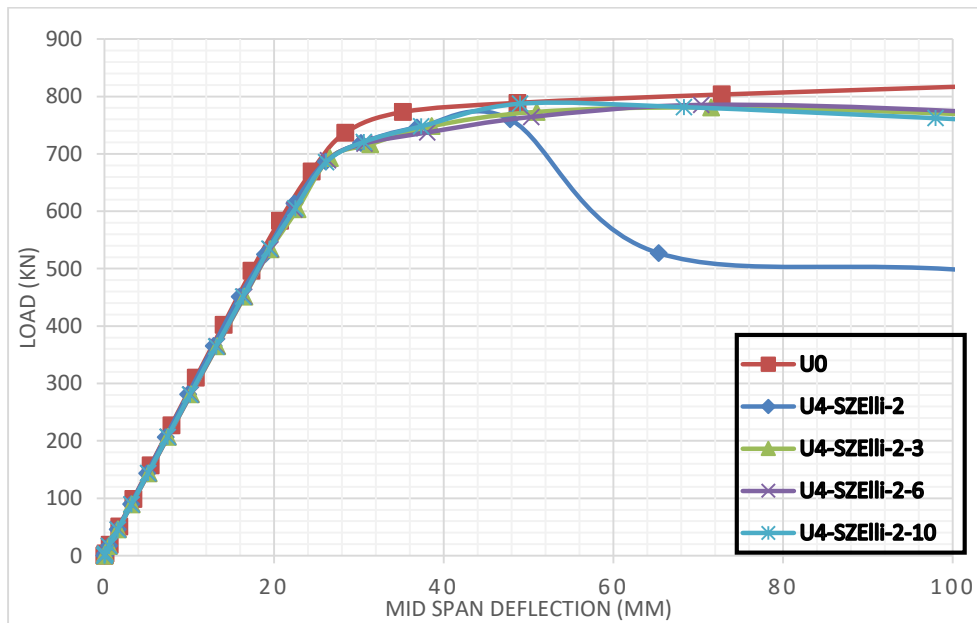
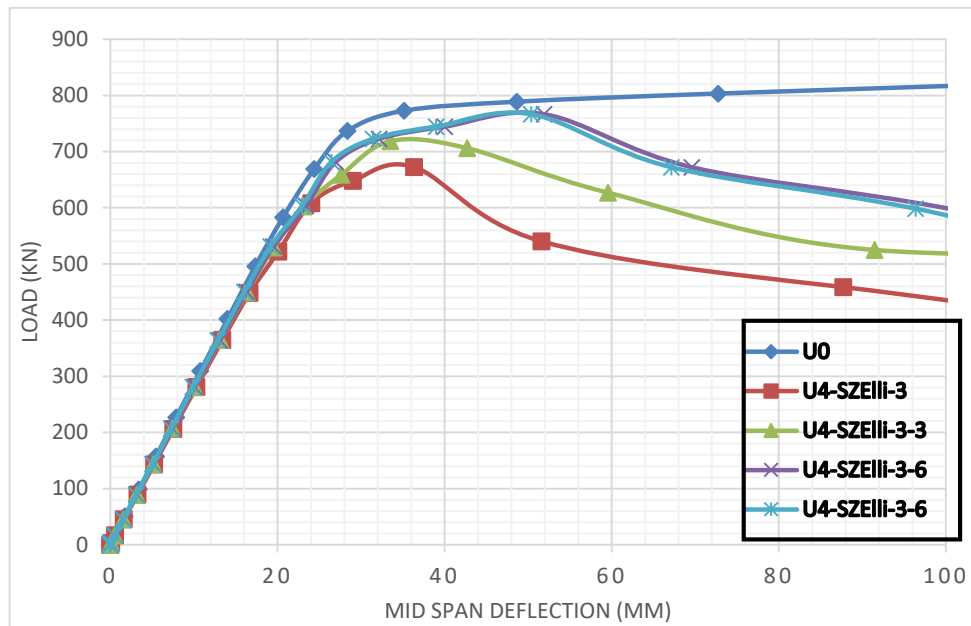


Figure 4-114 : Load-mid span deflection curves for strengthened specimen U4-SZelli-2



**Figure 4-115 : Load-mid span deflection curves for strengthened specimen U4-SZELI-3.**

**IV.3.1.2.2. Adhesive degradation and failure mechanism:**

The Vierendeel mechanism is clearly the most prevalent failure mechanism for beams with rectangular, Trapezoidal, elliptical and parallelogram holes. The essential size of the web holes at the upper and bottom tee sections governs the Vierendeel process.

As previously discovered The rectangular web opening shape had the highest drop in load bearing capability among the web opening forms for specimens evaluated in this research. The Vierendeel mechanism for all examined measurements was the type of failure of unreinforced specimens with rectangular web openings in shear zone. The first reinforced prototype U0-SZRec-1 failed by flexural failure mode with three GFRP thicknesses (3mm, 6mm, and 10mm) (**Figure 4-116**), confirming the observations reported in the previous chapter using another profile section; the suggested approach was able to change the stress state. To offer stronger response in the T sections above and below the aperture, the second dimension of the rectangular opening in specimen U0-SZRec-2 necessitated thickening the GFRP to 6mm. Only specimens U0-SZRec-2-6 and U0-SZRec-2-10 failed through typical flexural failure and evaded the vierendeel mechanism, as shown in **Figure 4-116**. In the U0-SZRec-3 specimen strengthened case, two distinct failure modes were observed .The GFRP suggested methodology was incapable to resist the vierendeel failure in specimens U0-SZRec-3-3 and U0-SZRec-3-6, and therefore GFRP thickness was increased to 10 mm to collect flexural failure as specimen U0-SZRec-3-10 (**Figure 4-116**). Gravest case scenario for a web aperture is the final rectangular opening proposed dimension with a wide region in the shear zone. The GFRP proposed pattern were not able to modify the stress state of tested specimens ,U0-SZRec-4-3 ,U0-SZRec-4-6 and U0-SZRec-4-10 failed by vierendeel failure ( **Figure 4-116** ) .

The location of the web hole in an unreinforced steel I-beam is recommended to be distant form shear zones, that induce the vierendeel action to operate all over the hole. Under uniform loads,

this phenomenon significantly reduces beam rigidity, strength, it also dominates the failure mechanism. This issue improves with larger holes.

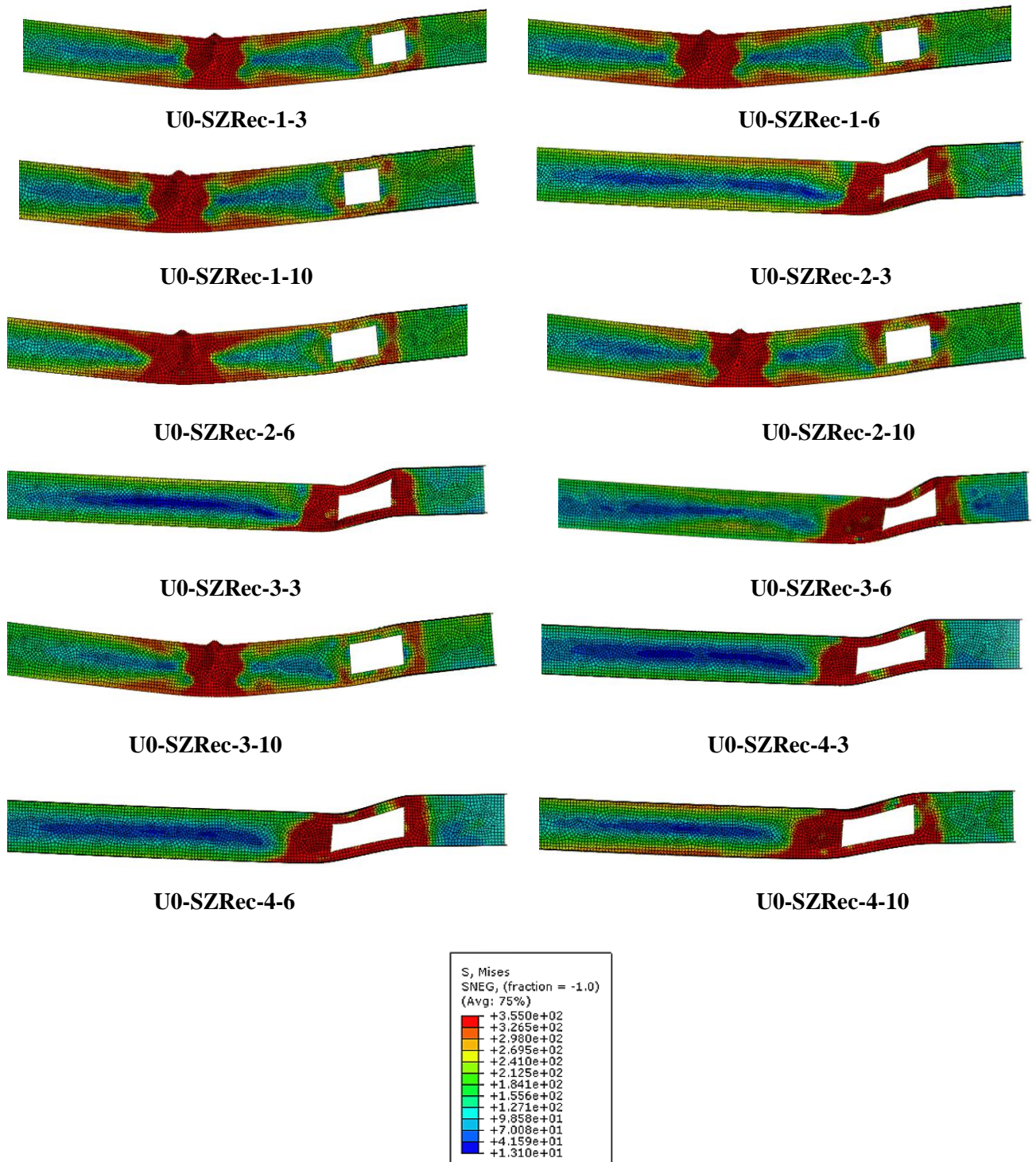


**Figure 4-116 :Failure mode of strengthened specimens with shear zone rectangular opening**



Similar to the rectangular opening unreinforced specimens having trapezoidal opening in shear zone failed by vierendeel mechanism with the three proposed dimensions . The effect of the GFRP reinforcement was clear in **Figure 4-117** , for the first specimen U1-SZTrap-1 it was found that the minimum recommended GFRP thickness to rigidify T sections below and above the opening was the 6 mm .Specimens U1-SZTrap-1-6 and U1-SZTrap-1-10 failed by flexural failure mode. Similarly, utilizing the 6 mm and 10 mm GFRP patterns, the T sections upper and lower the aperture in specimen U1-SZTrap-2 were able to transmit the flow of stresses from the aperture corners to the top flange in mid span of the beam (**Figure 4-117**) . To acquire a better grasp of the suggested reinforcement system's possible size impacts and application limitation, another large dimension was proposed in shear zone needed to be reinforced . It can clearly be seen in **Figure 4-117** that specimens U1-SZTrap-3-3 ,U1-SZTrap-3-6 and U1-SZTrap-3-10 failed by vierendeel mechanism . These findings indicate that Since the vierendeel process limits the beam achievement for all aperture dimensions by raising the essential opening length and producing trapezoidal opening with length  $L= 1.5 H$ , employing big trapezoidal openings in shear zone is not suggested for beams exposed to uniform force.

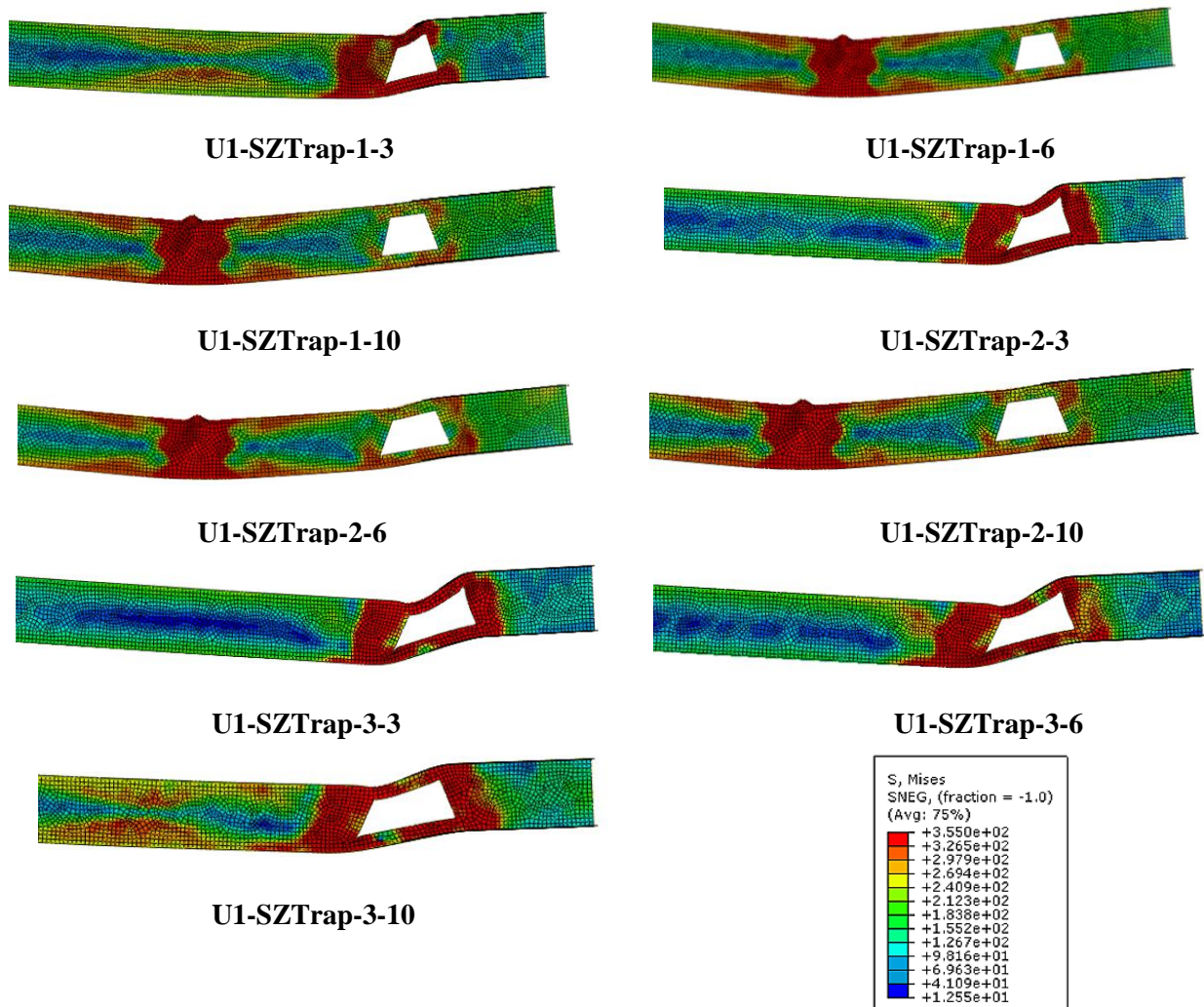


**Figure 4-117 :Failure mode of strengthened specimens with shear zone trapezoidal opening**



Meantime, the vierendeel failure mechanism was seen in unstrengthened specimens with reversed trapezoidal openings, as illustrated in **Figure 4-95**. Using the three proposed GFRP thicknesses, the failure mode for specimen U2-SZTraprv-1 was changed to flexural failure, while specimens U2-SZTraprv-1-3, U2-SZTraprv-1-6, and U2-SZTraprv-1-10 failed by flexural failure and the stress concentration was relocated away from the opening (**Figure 4-118**). Nonetheless, in comparison to the prior specimen with trapezoidal aperture U1-SZTrap-1, the optimal thickness to be determined will not be the same based on the discovered failure mode, the 3 mm was successful in changing the stress condition for the reversed trapezoidal opening of the first dimension (U1-SZTrap-1) while, previously, it was discovered that 6 mm GFRP thickness was acceptable for trapezoidal openings. Specimen U2-SZTraprv-2 failed by vierendeel failure mode with GFRP thickness of 3 mm, whereas specimens U2-SZTraprv-2-6 and U2-SZTraprv-2-10 failed by flexural failure mode offered the same performances in terms of failure mechanism as the previously tested specimen with the trapezoidal opening of identical sizes (U1-SZTrap-2) (**Figure 4-118**). Regarding to the case of specimen with the largest reversed trapezoidal dimension with specimen U2-SZTraprv-3, It was found that the vierendeel failure mode is the most prevalent with the three proposed GFRP thicknesses. **Figure 4-118** depicts the damaged morphologies and failure mechanisms for reinforced specimen with reversed trapezoidal apertures using of various GFRP laminate thicknesses.

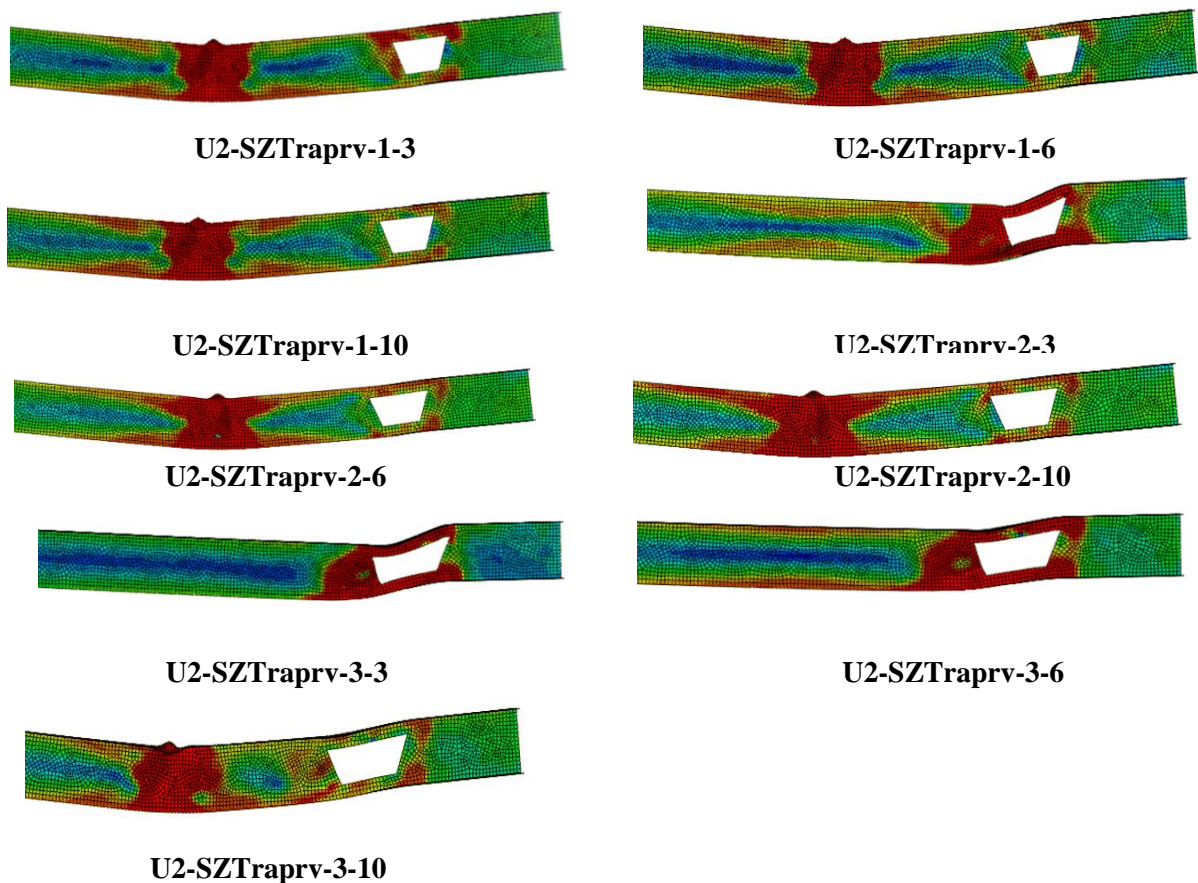


**Figure 4-118 :Failure mode of strengthened specimens with shear zone reversed trapezoidal opening .**



openings while for unreinforced specimens it was found that specimen U4-SZelli-1 failed by flexural failure and both specimens U4-SZelli-2 and U4-SZelli-3 failed by vierendeel failure. With a baseline suggested GFRP thickness of 3mm, the reinforcing GFRP system was able to switch the failure mechanism of U4-SZelli-2 to flexural failure. In the case of specimen U4-SZelli-3, it was discovered that increasing the GFRP thickness to 10 mm was required by a desire to impact the stress distribution of the beam and strengthen the opening section.

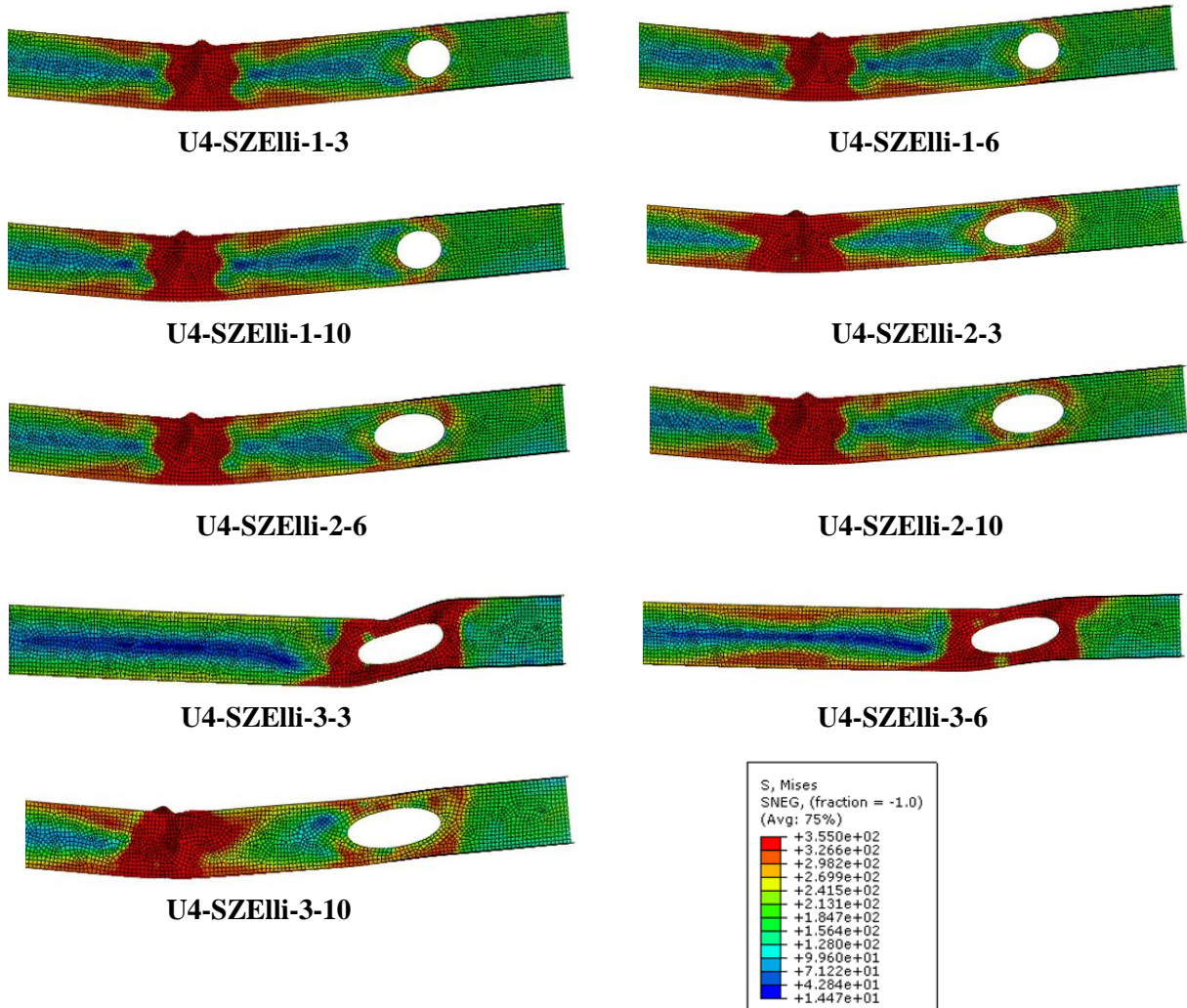


**Figure 4-120 :Failure mode of strengthened specimens with shear zone elliptical opening**

The bond behavior has been checked firstly for rectangular opening shape of different dimensions . It can be noted that no delamination was detected for the first dimension employed in the previous chapter, demonstrating that complete composite functionality combining steel and GFRP would be attained since the failure mode proceeds far from the reinforcing composites and out from the opening (**Figure 4-121**). Regarding to specimen U0-SZRec-2, debonding occurred with 3 mm GFRP laminates owing to the vierendeel mechanism, clearly demonstrated by the deletion of the adhesive layer, as illustrated in **Figure 4-122**. In the other hand, debonding did not occurred for specimens U0-SZRec-2-6 and U0-SEZRec-2-10. It was also determined that debonding occurred for specimens U0-SZRec-3-3 and U0-SZRec-3-6, both of which failed via the vierendeel failure mechanism; however, specimen U0-SZRec-3-



10, which failed by flexural failure, demonstrated successful bond behavior. The debonding occurred with all U0-SZRec-4 reinforced specimens, the SDEG was equal to 1 with the three used GFRP thicknesses. The Bond behavior of trapezoidal opening was identical to that of rectangular opening shape except specimen U1-SZTrap-3, the SDEG variable achieved the 1 value with the three GFRP thicknesses. In the other hand, the bond behavior of specimens having reversed trapezoidal opening also was similar to trapezoidal opening the debonding was happened with the large opening dimension (U2-SZTraprv-3) and the three GFRP thicknesses (**Figure 4-123**). Debonding occurred with specimens U3-SZParall-1-3, U3-SZParall-2-3, U3-SZParall-2-6, U3-SZParall-3-3, and U3-SZParall-3-6 with parallelogram holes. Despite the fact that the bonding length was effective in these circumstances, debonding happened, which could be justified by the occurrence of the vierendeel failure mode and the insufficient GFRP thickness, which did not shifted the failure mode of specimens.

No debonding was observed for specimens with elliptical web openings except specimen U4-Elli-3 which failed also by vierendeel mechanism.

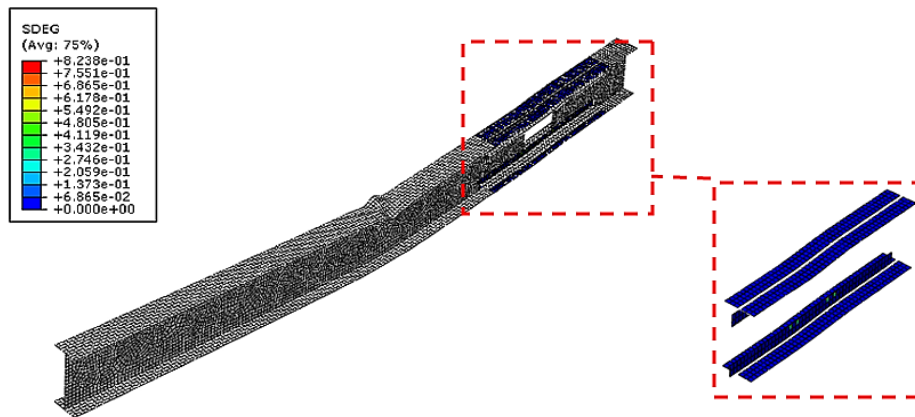


**Figure 4-121 :Bond behavior for specimen U0-SZRec-1-3 .**

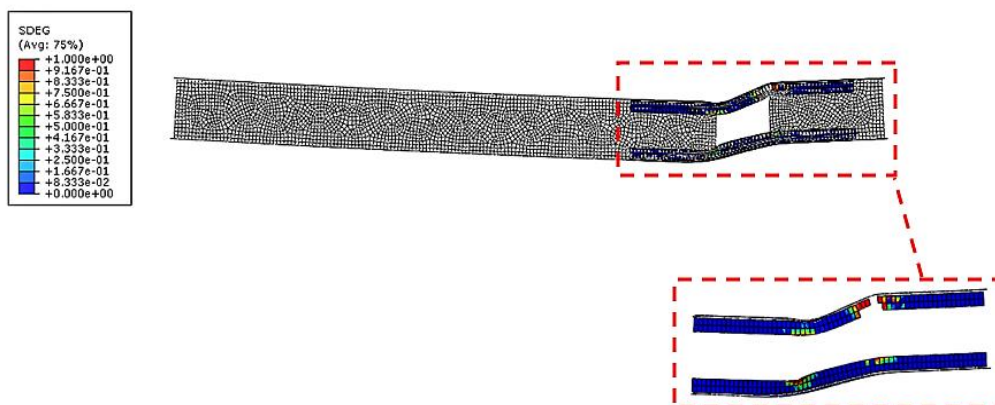


**Figure 4-122 :Bond behavior for specimen U0-SZRec-2-3 .**

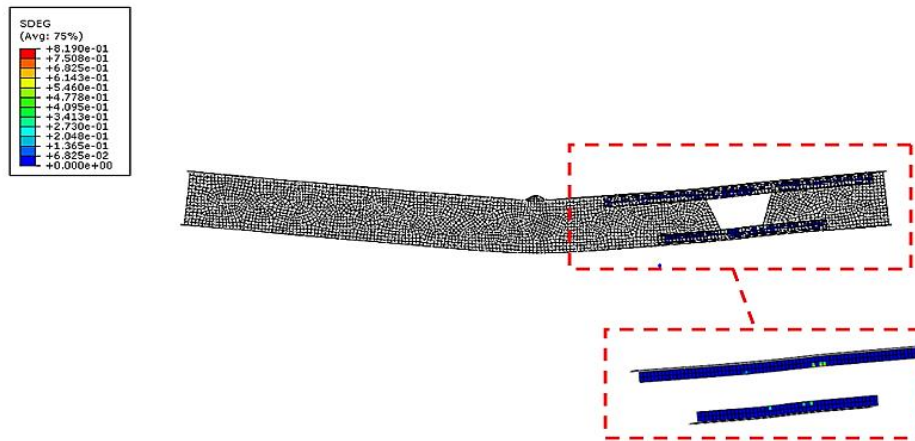


**Figure 4-123: Bond behavior for specimen U2-SZTraprv-1-3**

### **IV.3.3. Conclusion:**

The specifics and findings of an inquiry into the usage of glass fiber reinforced polymer (GFRP) composites to reinforce steel members following the insertion of web holes were reported in this section. The goal of this project was to create an effective CFRP strengthening configuration that could regain the strength and rigidity of steel beams after web apertures were added. The validated model was implemented to study the most beneficial discovered GFRP arrangement, to reinforce steel beam with various opening shapes and sizes in order to determine the ideal GFRP thickness and get a better knowledge of the proposed GFRP reinforcement technique possible size impacts and application constraints. The study's results can be summarised as follows:

- The GFRP-reinforcement approach can be used to restore the rigidity and strength of specimen with variable aperture geometries and reasonable sizes, whether in the mid-span or at the beam extremities in high shear locations.
- The location of the web hole in unreinforced steel I-beam is recommended to be far from shear zones, that induce the vierendeel mechanism to operate around the aperture. This mechanism significantly reduces beam strength, rigidity and ductility, and it also dominates the failure mechanism. This issue worsens with wider holes.
- Because of the substantial difference in rigidity between the reinforced section and the steel web and flange, stress concentration happened in the borders of the GFRP laminates.
- The use of Composite materials having low modulus of elasticity, like as GFRP, minimised ductility degradation and the stress distribution created at the extremities of the GFRP plates.
- Using GFRP, more reinforcement thickness is needed in the flexure region above and below the aperture to regain the initial force, in comparison to CFRP plates with normal and high modulus of elasticity, also the additional thickness is appropriate with reasonable opening sizes in shear zone.
- The preceding found findings are the appropriate GFRP laminate thicknesses for both locations and varied aperture shape and dimensions

---

## General Conclusion

The intention of this research is to aim at the possibility of employing externally bonded fiber reinforced polymer composites as an appropriate alternative means of reinforcing web holes in steel flexural parts. To attain this goal, the study documented in this thesis used a numerical inquiry. The impact of reinforcement schemes was examined utilizing non-linear finite element method in order to identify the most functionally effective design for empowering web post instability in cellular beams and reinforcing steel beams after the realization of single web opening in various positions.

The shear capability of web posts in cellular beams with Fiber Reinforced Polymer stiffeners is not specified by any regulation. The strength improvement was estimated using the current code while supposing that there would only be welded steel stiffeners. In contrary with the standard procedure used in the majority of FRP strengthening deployments in this study, the FRP laminates were glued to thin-webbed cellular beams in an arrangement that lends significantly to the web post's out-of-plane rigidity than its in-plane force. The geometry and reinforcing method of the FRP were the two factors affecting the out-of-plane rigidity. This indicates that it is feasible to employ low modulus FRP composites instead of the higher costly polymers as the GFRP stiffener. This achieved results needed a concentrated study to attempt the several aspects that could impact the effectiveness of the suggested approach, including:

- The proportion of the fiber reinforced polymer stiffener's out-of-plane geometrical qualities to its properties of materials.
- The design arrangement of glass FRP stiffener.
- Mechanical characteristics of the glue employed to attach the GFRP stiffener and their effects.
- The region of interaction in both the web post and the GFRP stiffener.
- The initial mechanism in which the unstrengthened and reinforced cellular beam failed.

This procedure, that could be accepted above conventional welding stiffening because its effectiveness, was capable of delaying or avoid the web post buckling mechanism based on the slenderness of web posts in cellular beams and using low cost FRP material type.

---

Furthermore, according to earlier experimental studies from scientific literature on reinforcing steel beams employing HM CFRP with the inclusion of a single rectangular web aperture in mid span and shear location.

Due to the previous experimental research's poor usage percentage of HM CFRP, using the validated numerical model, the same reinforcing technique was examined utilizing two different types of NM CFRP and various plate thicknesses. Regardless of the fact that the usage ratio for NM CFRP has improved, it was discovered that the ratio is still low when compared to the plate's maximum strain capacity.

In order to save costs, it was chosen to look into alternate composite materials like GFRP's capacity for strengthening web openings. Investigations were conducted on four suggested GFRP designs utilizing plates and sections. Most effectively, GFRP T sections and plates were bonded to the web and the flanges above and below the apertures, respectively.

The suggested GFRP technique was then used to strengthen different opening shapes and dimensions. To comprehend the possible consequences of dimensions, geometry and the validity of the suggested reinforcing approach. For every opening shape, dimension, and position, the ideal GFRP laminate thicknesses were identified. Additionally, the suggested reinforcement technique for GFRP can be utilized as an alternative to the widely employed method of reinforcement using stiffeners made of welded stiffeners, because the fiberglass reinforcement method has shown to be efficient for all of the various web beam shapes, aperture situations, and reinforcing arrangements taken into consideration in this thesis.



---

## References

- [1] LAWSON,R,M Design of openings in the webs of composite beams (P068),SCI/CIRIA ,1987 .
- [2] LAWSON ,R,M. CHUNG,K,F and PRICE , A.M. Tests on composite beams with large web openings to justify existing design methods ,The structural engineer ,VOL 70 ,N 1, 7 January 1992.
- [3] ENV 1993 -1-1 :1992 /A2 :1998 Eurocode 3 :part 1.1 – Amendement A2, CEN ,1998 .
- [4] Darwin ,D . Design of steel and composite beams with web openings .Steel design guide Series 2 .American institute of steel construction ,1990 .
- [5]P.K.K.LEE . Structures in the new millennium ,proceeding of the fourth international Kerensky conference on structures in the new millennium //3-5 September 1997.Department of civil& structural Engineering .The university Hong Kong.
- [6] Kerdal, D. &Nethercot, D.A., 1984. Failure modes for castellated beams. Journal of Constructional Steel Research, 4(4), pp.295–315.
- [7] Trorac, A.A., and Cooke, B.R. 1959. "An Experimental Investigation of open-Web Beams". Welding Research Council Bulletin, New York, Series No. 47, pp 1-10.
- [8] Halleux, P. 1967. "Limit Analysis of Castellated Steel Beams". Acier-Stahi-Steel, 32:3, 133-144.
- [9] Sherbourne, A. and Van Oostrom, J. (1972). "Plastic analysis of castellated beams— I interaction of moment, shear and axial force." Computers & Structures, 2(1): 79-109.
- [10] PattamadPanedpojaman, ThaksinThepchatri, SuchartLimkatanyu. (2014). "Novel design equations for shear strength of local web-post buckling in cellular beams". Thin Walled Structures, 76, 92–104
- [11] Aminian, P., Niroomand, H., Gandomi, A. H., Alavi, A. H. and Arab Esmaeili, M. (2013). "New design equations for assessment of load carrying capacity of castellated steel beams: a machine learning approach." Neural Computing and Applications, 23(1): 119-131.
- [12] Redwood, R.G. and Mccutcheon, J.O. (1968) Beam Tests with Unreinforced Web Openings. Journal of the Structural Division, 94, 1-17.
- [13] Wang, P., Wang, X. and Ma, N. (2014). "Vertical shear buckling capacity of web posts in castellated steel beams with fillet corner hexagonal web openings." Engineering Structures, 75: 315-326.
- [14 ]Jan Ravinger,PetronelaLascekova. (January 1988). Ultimate load behavior of thin-walled girders with circular holes
- [15] Menkulasi, F., Moen, C., Eatherton, M. and Kuruppuarachchi, D. (2015). "Investigation of Stiffener Requirements in Castellated Beams." Structural Stability Research Council Annual Stability Conference SSRC.
- [16] B. Kim, L. Li, and A. Edmonds, "Analytical Solutions of Lateral–Torsional Buckling of Castellated Beams, International Journal of Structural Stability and Dynamics," vol. 16, no. 8, pp. 1-16, 2016.
- [17] Hossein Showkati (2008),Lateral-torsional buckling of castellated beams,Iranian Journal of Science and Technology Transaction B: Engineering 32(2):153-156.
- [18] Morkhade, S. G. and Gupta, L.M. (2015). "An experimental and parametric study on steel beams with web openings." International journal of advanced structural engineering, Springer, 7(3):249-260.
- [19] Soltani et.al., 2012 . " Nonlinear FE analysis of the ultimate behavior of steel castellated beams". Journal of Constructional Steel Research 70, pp. 101–114.

- 
- [20] Zaarour, W.J. & Redwood, R., 1996. Web buckling in thin webbed castellated beams. *Journal of structural engineering*, 122(8), pp.860–866.
- [21] Kerdal D, Nethercot D (1984), Failure modes for castellated beams, *J Constr steel Res* (4) :295-315
- [22] Liu, T.C.H. & Chung, K.F., 2003. Steel beams with large web openings of various shapes and sizes: Finite element investigation. *Journal of Constructional Steel Research*, 59(9), pp.1159–1176.
- [23] Congdon, J. G. and Redwood, R.G. “Plastic behavior of beams with reinforced holes”, *Journal of the Structural Division, ASCE*, Vol. 96, No. ST9, Proc. Paper 7561, September 1970, pp.1933-1956.
- [24] Cooper P. B. and Snell R. R. “Tests on beams with reinforced web openings”, *Journal of the Structural Division* 1972; 98- ST3: 612-632.
- [25] Lupien R. and Redwood R. G. “Steel beams with web openings reinforced on one side”, *The National Research Council of Canada, Can. J. Civ. Eng.* 1978; 5: 451-461.
- [26] Redwood R. G. and Cho SH. “Design of steel and composite beams with web openings”, *J. construction steel* 1993; 25:23-41.
- [27] Prakash B. D., Gupta L. M., Pachpor P. D., and Deshpande N. V. “Strengthening of steel beam around rectangular web openings”, *International Journal of Engineering Science and Technology (IJEST)* 2011, ISSN: 0975-5462, Vol.3 No.2:1130-1136.
- [28] V Thevendran and N E Shanmugam, “Lateral Buckling of Doubly Symmetric Beams Containing Openings”, *J. Eng. Mech.*, 1991, pp 1427-1441.
- [29] Hayder Wafi Ali Al-Thabhwawee Muslim Abdul-Ameer Al-Kannoon Improving Behavior of Castellated Beam by Adding Spacer Plat and Steel Rings *Journal of University of Babylon, Engineering Sciences*, Vol.(26), No.(4): 2018.
- [30] HayderWafi Ali Al-Thabhwawee; Strengthening Circular Holes in Web of Steel I-Beams. *Journal of Babylon University/Engineering Sciences/ No.(2)/ Vol.(25): 2017.*
- [31] Konstantinos Daniel Tsavdaridis n , Grigorios Galiatsatos . Assessment of cellular beams with transverse stiffeners and closely spaced web openings. *Thin-Walled Structures*.
- [32] Fattouh M. F. Shaker and Mahmoud Shahat . Strengthening of web opening in non-compact steel girders .*IOSR Journal of Mechanical and Civil Engineering (IOSR-JMCE)*.
- [33] Morkhade S. G., Gupta L. M. (2015b). Analysis of steel I-beams with rectangular web openings: experimental and finite element investigation. *Engineering Structures & Technologies*, 7(1):13-23.
- [34] Cyril Thomas ABaskar K, (2018) ,Strengthening of thin-webbed castellated beam using CFRP, *International Journal for Computational Methods in Engineering Science and Mechanics* ,10.1080/15502287.2018.1534153.
- [35] Zhao, X. L., and Zhang, L. (2007). "State-of-the-art review on FRP strengthened steel structures," *Engineering structures*, Vol. 29, No. 8, pp. 1808-1823.
- [36] Johnson, T. Johnson, T.(2020). Understanding CFRP Composites. *ThoughtCo,thoughtco.com / understanding-cfrp-composites-820393.*
- [37] Peiris, N.A., 2011. Steel beams strengthened with ultra-high modulus CFRP laminates, *University of Kentucky*.
- [38] Miller, T.C. et al., 2001. Strengthening of a steel bridge girder using CFRP plates. *Journal of Bridge Engineering*, 6(6), pp.514–522.

- 
- [39] Hollaway, L.C. & Cadei, J., 2002. Progress in the technique of upgrading metallic structures with advanced polymer composites. *Progress in Structural Engineering and Materials*, 4(2), pp.131–148.
- [40] Ding Ke-wei & Zhang Xu-ping . Comparative Research on Reinforcement and Repairing Effect of The Steel Girder with CFRP and GFRP . Anhui Province National Natural Science Foundation through grant .
- [41] Mosallam, A., 2007. Structural evaluation and construction of fiber-reinforced polymer composites strengthening systems for the Sauvie Island Bridge. *Journal of Composites for Construction*, 11(2), pp.236–249.
- [42] Miller, T.C. et al., 2001. Strengthening of a steel bridge girder using CFRP plates. *Journal of Bridge Engineering*, 6(6), pp.514–522.
- [43] Tavakkolizadeh, M. and Saadatmanesh, H. “Repair of damaged steel-concrete composite girders using carbon fiber-reinforced polymer sheets,” *Journal of 50 Composites for Construction*, American Society of Civil Engineers, Reston, VA 20191-4400, United States, Vol. 7, No. 4, 2003, pp. 311-322.
- [44] Al-saidy, A.H., Klaiber, F.W. & Wipf, T.J., 2004. Repair of steel composite beams with carbon fiber-reinforced polymer plates. *Composite for Construction*.
- [45] Colombi, P. & Poggi, C., 2006. An experimental, analytical and numerical study of the static behavior of steel beams reinforced by pultruded CFRP strips. In *Composites Part B: Engineering*. pp. 64–73.
- [46] Galal, K., Seif El Din, H. M., and Tirca, L. (2012). "Flexural Performance of Steel Girders Retrofitted Using CFRP Materials." *Journal of Composites for Construction*, 16(3), 265- 276.
- [47] Narmashiri, K., Jumaat, M. Z., and Sulong, N. H. R. (2010). "Shear strengthening of steel I beams by using CFRP strips." *Scientific Research and Essays*, 5(16), 2155-2168.
- [48] Photiou, N., Hollaway, L.C. & Chryssanthopoulos, M.K., 2004. Strengthening Of An Artificially Degraded Steel Beam Utilizing A Carbon/Glass Composite System. In *Advanced Polymer Composites for Structural Applications in Construction: ACIC 2004*. pp. 274–283.
- [49] Vatonec, M., Kelley, P. L., Brainerd, M. L. and Kivela, J.B., 2002. Post strengthening of steel members with CFRP. presented at the International Conference SAMPE 2002, (California, USA).
- [50] Zhao, X.L. & Al-Mahaidi, R., 2008. Web buckling of light steel beams strengthened with CFRP subjected to end-bearing forces. *Thin Walled Structures*, 47, pp.1029– 1036.
- [51] Islam, S.M.Z. & Young, B., 2013. Strengthening of ferritic stainless steel tubular structural members using FRP subjected to Two-Flange-Loading. *Thin-Walled Structures*, 62, pp.179–190.
- [52] Fawzia, S.; Al-Mahaidi, R.; Zhao, X. L.; and Rizkalla, S. “Strengthening of circular hollow steel tubular sections using high modulus CFRP sheets, ” *Construction and Building Materials*, Elsevier Ltd, Oxford, OX5 1GB, United Kingdom, Vol. 21, No. 4, 2007, pp. 839-845.
- [53] AL-Khafaji, A. G. A., & AL-Abbas, B. H. (2016). Numerical Study on the Effect of openings in Steel IPE Beams Strengthened By CFRP Plates. 14(4), 213–227.
- [54] Mustafa, S., Fathy, E., & Rizk, M. (2017). Adequate CFRP length for strengthening steel beams with web opening. March 2017.

- 
- [55] Deng, J., & Lee, M. M. K. (2007). Behavior under static loading of metallic beams reinforced with a bonded CFRP plate. *Composite Structures*, 78(2), 232–242.
- [56] Altaee, M. J., Cunningham, L. S., & Gillie, M. (2017). Experimental investigation of CFRP-strengthened steel beams with web openings. *Journal of Constructional Steel Research*, 138, 750–760.
- [57] Hamood, M., Abdulsahib, W., & Abdullah, A. (2018). The effectiveness of CFRP strengthening of steel plate girders with web opening subjected to shear. *MATEC Web of Conferences*, 162, 1–8.
- [58] Mustafa, S. A. A., Fathy, E., & Rizk, M. S. (2020). Fiber-reinforced polymer plates for strengthening web opening in steel I-beams under cyclic loading. *Advances in Structural Engineering*, 23(2), 348–359.
- [59] Altaee, M., Cunningham, L. S., & Gillie, M. (2019). Practical Application of CFRP Strengthening to Steel Floor Beams with Web Openings: A numerical Investigation. *Journal of Constructional Steel Research*, 155, 395–408.
- [60] Kadhim, M. A., Abdulsahib, W. S., & Ali, A. A. (2020). CFRP strengthening of steel plate girders with web openings subjected to shear and bending. *IOP Conference Series: Materials Science and Engineering*, 737(1).
- [61] Ezzat, M., Elsabaawy, M., & Eltaly, B. (2021). Structural Performance of Strengthened Steel Girders with Web Openings under Shear Forces. *ERJ. Engineering Research Journal*, 44(2), 175–188.
- [62] El Damatty, A.A. and Abushagur, M. (2003). "Testing and modeling of shear and peel behavior for bonded steel/FRP connections", *Thin-Walled Structures*, 41(11), 987-1003.
- [63] Baldan, A. (2004). "Adhesively-bonded joints and repairs in metallic alloys, polymers and composite materials: Adhesives, adhesion theories and surface pretreatment", *Journal of Materials Science*, 39(1), 1-49.
- [64] Schnerch, D., Dawood, M., Rizkalla, S. and Sumner, E. (2007). "Proposed design guidelines for strengthening of steel bridges with FRP materials", *Construction and Building Materials*, 21(5), 1001-1010.
- [65] Packham, D.E. (2003). "Surface energy, surface topography and adhesion", *International Journal of Adhesion and Adhesives*, 23(6), 437-448.
- [66] Rosen, S.L. (1993). *Fundamental Principles of Polymeric Materials*, John Wiley and Sons.
- [67] Lavaste, V., Watts, J.F., Chehimi, M.M. and Lowe, C. (2000). "Surface characterization of components used in coil coating primers", *International Journal of Adhesion and Adhesives*, 20(1), 1-10.
- [68] Holloway, L.C. and Teng, J.G. (2008). *Strengthening and Rehabilitation of Civil Infrastructures Using Fibre-Reinforced Polymer (FRP) Composites*, Woodhead Publishing Limited, England.
- [69] Harris, A.F. and Beevers, A. (1999). "The effects of grit-blasting on surface properties for adhesion", *International Journal of Adhesion and Adhesives*, 19(6), 445-452.
- [70] Allan, R.C., Bird, J. and Clarke, J.D. (1988). "Use of adhesives in repair of cracks in ship structures", *Materials Science and Technology*, 4(10), 853-859.
- [71] Cadei, J.M.C., Stratford, T.J., Holloway, L.C. and Duckett, W.G. (2004). *Strengthening Metallic Structures Using Externally Bonded Fiber-Reinforced Polymers*, C595, CIRIA, London.

- 
- [72] Sallam, H.E.M., Ahmad, S.S.E., Badawy, A.A.M. and Mamdouh, W. (2006). "Evaluation of steel I-beams strengthened by various plating methods", *Advances in Structural Engineering*, 9(4), 535-544.
- [73] Silvestre, N., Young, B. and Camotim, D. (2008). "Non-linear behavior and load-carrying capacity of CFRP-strengthened lipped channel steel columns", *Engineering Structures*, 30(10), 2613-2630.
- [74] Xia, S.H. and Teng, J.G. (2005). "Behavior of FRP-to-steel bonded joints", *Proceedings, International Symposium on Bond Behavior of FRP in Structures (BBFS 2005)*, Hong Kong, China.
- [75] Chen, J.F. and Teng, J.G. (2001). "Anchorage strength models for FRP and steel plates bonded to concrete", *Journal of Structural Engineering*, 127(7), 784-791.
- [76] Bocciarelli, M. (2009). "Response of statically determined steel beams reinforced by CFRP plates in the elastic-plastic regime", *Engineering Structures*, 31(4), 956-967.
- [77] Hart-Smith, L.J. (1981). *Development in Adhesives-2*, Applied Science Publishing, London.
- [78] Volkersen, O. (1938). "Die nietkraftverteilung in zugbeanspruchten Nietverbindungen mit konstanten laschenquerschnitten", *Luftfahrtforschung* 15, 41-47, (In German).
- [79] Yuan, H., Teng, J.G., Seracino, R., Wu, Z.S. and Yao, J. (2004). "Full-range behavior of FRP-to-concrete bonded joints", *Engineering Structures*, 26(5), 553-565.
- [80] Zhang, L. and Teng, J.G. (2010). "Finite element prediction of interfacial stresses in structural members bonded with a thin plate", *Engineering Structures*, 32, 459-471.
- [81] Lu, X.Z., Teng, J.G., Ye, L.P. and Jiang, J.J. (2005). "Bond-slip models for FRP sheets/plates bonded to concrete", *Engineering Structures*, 27(6), 920-937.
- [82] Yao, J., Teng, J.G. and Chen, J.F. (2005a). "Experimental study on FRP-to-concrete bonded joints", *Composites Part B: Engineering*, 36(2), 99-113.
- [83] NANGALLAGE DILUM FERNANDO (2010), BOND BEHAVIOUR AND DEBONDING FAILURES IN CFRP-STRENGTHENED STEEL MEMBERS. A Thesis Submitted in Partial Fulfilment of the Requirements for the Degree of Doctor of Philosophy
- [84] ABAQUS, 2013. Theory Manual, User Manual and Example Manual Version 6., Dassault Systemes Simulia Corp.
- [85] Daniel and O. Ishai, *Engineering Mechanics of Composite Materials* (Oxford University Press, New York, 1994).
- [86] Dassault Système, Abaqus documentation, Retrieved May 28, 2018
- [87] S. Tsai and E. Wu, A general theory of strength for anisotropic materials, *Journal of Composite Materials* 5, 58 (1971).
- [88] Z. Hashin, Failure criteria for unidirectional fiber composites, *Journal of Applied Mechanics* 41, 329 (1979).
- [89] Linghoff, D., Haghani, R. & Al-Emrani, M., 2009. Carbon-fiber composites for strengthening steel structures. *Thin Walled Structures*, 47, pp.1048-1058.

- 
- [90] Lay, G. and Smith, R.D. (1965). "Role of strain hardening in plastic design", *Journal of Structural Division*, ST3, 25-43.
- [91] Pi, Y.L. and Trahair, N.S. (1994). "Inelastic bending and torsion of steel I-beams", *Journal of Structural Engineering*, 120(12 ), 3397-3417.
- [92] Byfield, M.P. and Dhanalakshmi, M. (2002). "Analysis of strain hardening in steel beams using mill tests", *Proceedings of the Third International Conference on Advances in Steel Structures*, Hong Kong SAR, China PRC. December. 139-146.
- [93] Byfield, M.P., Davies, J.M. and Dhanalakshmi, M. (2005). "Calculation of the strain hardening behavior of steel structures based on mill tests", *Journal of Constructional Steel Research*, Vol. 61, 133-150.
- [94] Okeil, A.M., Bingol, Y. & Ferdous, M.R., 2009. Novel Technique for Inhibiting Buckling of Thin-Walled Steel Structures Using Pultruded Glass FRP Sections. *Journal of Composites for Construction*, 13, pp.547–557.
- [95] Grilo, L.F., Fakury, R.H., Castro e Silva, A.L.R. de., Veríssimo, G. de S. (2018). Design procedure for the web-post buckling of steel cellular beams, *J. Constr. Steel Res.*, 148, pp. 525–541, DOI: 10.1016/j.jcsr.2018.06.020.
- [96] W.B. Vieira, Numerical-Experimental Study of the s Web-post Buckling in the Castellated Steel Beams, PhD; Thesis (in Portuguese) Federal University of Viçosa, Brazil, 2015.
- [97] Narmashiri, K., Ramli Sulong, N.H. & Jumaat, M.Z., 2012. Failure analysis and structural behavior of CFRP strengthened steel I-beams. *Construction and Building Materials*, 30, pp.1–9.
- [98] Bowden, F.P. & Tabor, D., 2001. *The friction and lubrication of solids*, Oxford university press.
- [99] Abdullah, A.M., 2010. *Analysis of Repaired/Strengthened R.C. Structures Using Composite Materials : Punching Shear*. University of Manchester.
- [100] Zeng, J.-J., Gao, W.-Y., Liu, F. (2018). Interfacial behavior and debonding failures of full-scale CFRP-strengthened H section steel beams, *Compos. Struct.*, 201, pp. 540–552, DOI: 10.1016/j.compstruct.2018.06.045.
- [101] Ulger, T., A.M. Okeil. (2016). *LSU Digital Commons Strengthening Shear Deficient Thin-Walled Steel Beams by Bonding Pultruded GFRP Sections*
- [102] Amer M. Ibrahim . Mohammed Sh. Mahmood. *Finite Element Modeling of Reinforced Concrete Beams Strengthened with FRP Laminates*. *European Journal of Scientific Research* ISSN 1450-216X Vol.30 No.4 (2009), pp.526-541

---

[103] Altaee, M., Cunningham, L. & Gillie, M.. 2016. CFRP Strengthening of Steel Beams with Web Openings. In Proceedings of Structural Faults & Repair 2016: 16th International Conference. Edinburgh, p. 1754.

[104] Fiedler, B., Hojo, M., Ochiai, S., Schulte, K., Ando, M. (2001). "Failure behavior of an epoxy matrix under different kinds of static loading." *Composites Science and Technology*, 61(11), 1615-1624.